Unnatural Amino Acids as Novel Probes for Ultrafast 2D-IR Spectroscopy of Proteins

Towards Real-Time Investigation of Biomolecular Dynamics and Vibrational Energy Flow

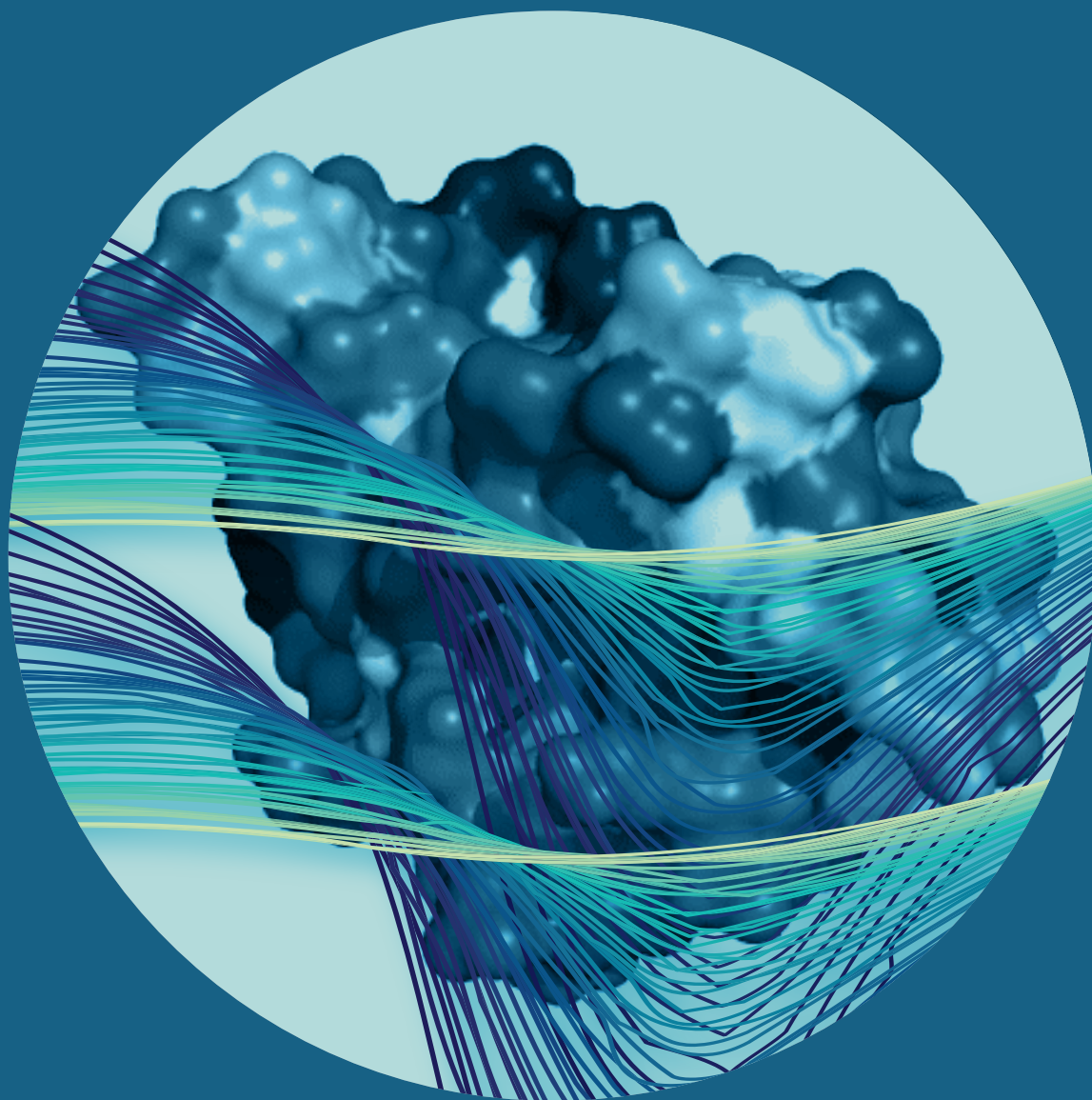**Henrike Müller-Werkmeister, 2014**

Unnatural Amino Acids as Novel Probes for Ultrafast 2D-IR Spectroscopy of Proteins

Towards Real-Time Investigation of Biomolecular Dynamics and Vibrational Energy Flow

Dissertation zur Erlangung
des Doktorgrades der Naturwissenschaften

vorgelegt beim Fachbereich Physik
der Johann Wolfgang Goethe-Universität
in Frankfurt am Main

von

Henrike Müller-Werkmeister

aus Hannover

Frankfurt 2014
(D 30)

vom Fachbereich Physik der
Johann Wolfgang Goethe-Universität als Dissertation angenommen.

Dekan:
Prof. Dr. René Reifarth

Gutachter:
Prof. Dr. Jens Bredenbeck
Prof. Dr. Harald Schwalbe

Datum der Disputation: 28. April 2015

We all like to congregate at boundary conditions.
Where land meets water. Where earth meets air.
Where body meets mind. Where space meets time.
We like to be on one side, and look at the other.

Douglas Adams
The Hitchhiker's Guide to the Galaxy

Abstract

Ultrafast protein dynamics are of particular interest for understanding the molecular basis of biochemical function. 2D-IR spectroscopy is a method to study molecular dynamics starting in the subpicosecond regime. But the application of 2D-IR to investigate protein dynamics with high spatial resolution is currently limited to few biological systems with intrinsic chromophores. Spectral congestion, the contribution of many similar oscillators to the same signals, makes it difficult to draw conclusions about local structural dynamics in most other proteins.

The aim of this thesis is to extend the application of 2D-IR spectroscopy to a wider range of proteins by introducing unnatural amino acids (UAAs) with azide or nitrile groups as site-specific vibrational probes, which absorb in the free spectral window between 1800–3000 cm^{-1} by using methods from chemical biology.

Part I introduces the methodology 2D-IR (Chapter 1) and the PDZ domain, a protein system of interest (Chapter 2). The PDZ domain is an interesting model system to study because a transfer pathway with energy flow on a few picosecond time scale has been predicted by MD simulations. This pathway is comprised of coupled amino acid residues and believed to be connected to intra domain long-range communication and thus allostery. The development of experimental tools to directly track the predicted ultrafast anisotropic heat transfer in PDZ defines a major goal of this thesis and is an ideal test case to demonstrate the application potential of UAAs as site-specific labels for 2D-IR.

Part II introduces the characteristics of the tested UAAs before their application as novel vibrational probes. Chapter 3 gives an overview of different methods for site-specific incorporation of amino acids with functionalized side chains into proteins. It focuses on supplementation based incorporation (SPI) and suppression-based approaches (SCS) such as artificial genetic code expansion. Some of the incorporated amino acids carry azides and nitriles in their side chains, which are strong IR active groups. Chapter 4 presents a full experimental characterization by FTIR, DFT, broadband IR, 2D-IR and two color 2D-IR of four azide- and nitrile-containing aliphatic and aromatic amino acids. Azidohomoalanine (Aha), which can be incorporated into proteins as methionine surrogate, is identified as favorable candidate for applications in proteins.

Part III applies Aha to the study of local microenvironment and conformational dynamics in PDZ. In Chapter 5 six mutants of PDZ are investigated on how the azide vibration can be employed as a qualitative monitor for local hydrophobicity by comparing FTIR spectra to structural data available. The results presented here show that it is indeed possible to use Aha for monitoring the local microenvironment and even conformational changes induced by ligand binding can be observed. This is the first experimental indication for the existence of the allosteric mechanism discussed.

Chapter 6 discusses 2D-IR measurements of two of the six PDZ mutants. 2D-IR spectra of the azide moiety of Aha in PDZ Ile327Aha and PDZ Ala390Aha have been recorded to validate the capability of monitoring ultrafast equilibrium dynamics using a site-specific probe. The mutant with Aha located in the binding pocket (PDZ Ile327Aha) was then chosen to investigate the influence of ligand binding on the line shape of the 2D-IR spectra, giving insight into the structural dynamics of ligand binding in PDZ on the level of hydrogen bonds on a picosecond time scale.

Part IV of this thesis explores the applicability of UAAs to real-time studies of vibrational energy transfer. Chapter 7 focuses on vibrational energy transfer (VET) in the single amino acid Azidophenylalanine (N3P). N3P in its boc-protected form (with an additional peptide bond in the system) was investigated using two-color 2D-IR. All cross peaks between the azide vibration and other marker modes could be recorded. The data show that it is possible to directly track vibrational energy flow through the system from the injection point at the proximal azide group to all other functional groups. The transfer times are shown to be distance dependent and reflect spatial proximity of functional groups. Comparing the results to DFT calculations demonstrates that this experimentally derived information of spatial proximity can be used for unambiguous spectral assignment in the N3P model system.

In larger systems like the PDZ domain this experimental approach fails because of spectral congestion. It is not possible to inject and track vibrational energy in a site specific fashion. Chapter 8 presents a VET pair of amino acids, Azulenylalanine as a donor and Aha as acceptor, that are spectrally separated from the native protein bands. Azulene converts the energy of a visible photon into vibrational energy efficiently and within 1 ps and Aha monitors VET by a change of its azide absorption band. Application in model peptides demonstrate the performance of the VET pair over a distance comparable to the size of the PDZ domain as well as in aqueous solution, which is a key prerequisite for the application in proteins. This is the first experimental tool dedicated to study directional biological energy flow on picosecond time scales which is applicable in proteins.

In Chapter 9 this VET pair is incorporated into a protein-ligand complex of the PDZ domain to study the proposed energy transfer pathway. First successful measurements are presented, after several experimental difficulties were encountered and overcome. The measured signal was still to small to serve as direct evidence of the proposed energy pathway. Thus a lot of work remains to finally solve the addressed long-standing question in biophysics on pathways for energy flow and allosteric communication in PDZ.

Publications and Presentations

This thesis is based on the following manuscripts (published, submitted and in preparation). The results have been presented at several conferences, both as oral presentations and poster presentations.

Publications

1. **H. M. Müller-Werkmeister**, Y.-L. Li, E.-L. W. Lerch, D. Bigourd, J. Bredenbeck,
Ultrafast Hopping from Band to Band: Assigning Infrared spectra based on vibrational energy transfer, Angewandte Chemie International Edition, **2013**, 52 (24), 6214–6217
doi: 10.1002/anie.201209916

2. **H. M. Müller-Werkmeister**, J. Bredenbeck,
A donor-acceptor pair for the real-time study of energy flow in proteins, Phys. Chem. Chem. Phys., **2014**, 16, 3261-3266
doi: 10.1039/C3CP54760D

3. L. J.G.W. van Wilderen, D. Kern-Michler, **H. M. Müller-Werkmeister**, J. Bredenbeck,
Vibrational dynamics and solvatochromism of the label SCN in various solvents and hemoglobin by time dependent IR and 2D-IR spectroscopy, Phys. Chem. Chem. Phys., **2014**, 16, 19643-19653
doi: 10.1039/C4CP01498G

4. **H. M. Müller-Werkmeister**, M. Essig, P. Durkin, N. Budisa, J. Bredenbeck,
Towards the direct measurement of vibrational energy flow in proteins, in: Ultrafast Phenomena XIX, Springer Series in Physics, **2014**, *in press*,
doi:10.1364/UP.2014.10.Thu.D.6

5. **H. M. Müller-Werkmeister**, K. B. Eberl, M. Essig, S. Eger, A. Marx, J. Bredenbeck,
FTIR spectroscopy of azidohomoalanine-labeled PDZ3 from PSD-95: Site-specific probing of local environment and ligand-induced long range interaction, submitted

6. **H. M. Müller-Werkmeister**, Y. - L. Li, E. - L. W. Lerch, D. Bigourd, J. Bredenbeck,
Azide- and Nitrile derivitized artificial amino acids for the application in 2D-IR of proteins, in preparation

7. A. T. Messmer, K. Nienhaus, Y.-L. Li, **H. M. Müller-Werkmeister**, D. Bigourd, G. U. Nienhaus, J. Bredenbeck
Investigating the speed limit of functional protein dynamics in equilibrium - a temperature dependent 2D-IR study, in preparation

8. **H. M. Müller-Werkmeister**, J. Bredenbeck,
2D-IR spectroscopic investigation of protein dynamics and ligand binding in PDZ3 using azidohomalanine as vibrational probe, in preparation

Oral Presentations at Conferences

1. **H. M. Müller-Werkmeister**, M. Essig, P. Durkin, N. Budisa, J. Bredenbeck
   Towards the direct measurement of vibrational energy flow in proteins,
   contributed talk, session *Excited State Dynamics* at Ultrafast Phenomena XIX, Okinawa, Japan,
   July **2014**

2. **H. M. Müller-Werkmeister**, K. B. Eberl, M. Essig, J. Bredenbeck
   FTIR and Femtosecond 2D-IR Spectroscopy of Azidohomoalanine-Labeled PDZ3 from PSD-95: Site-Specific Probing of Ultrafast Dynamics and Electrostatics in Proteins,
   contributed talk, session *Protein Dynamics* at 57th Annual Meeting of the Biophysical Society,
   Philadelphia, US, February **2013**
   abstract: Biophysical Journal, **2013** 104 (2), 29a,doi:10.1016/j.bpj.2012.11.199

3. **H. M. Müller-Werkmeister**, J. Bredenbeck,
   How to measure vibrational energy flow in proteins?,
   German Conference of Women in Physics, Freiburg, Germany, October **2012**

4. **H. M. Müller-Werkmeister**, Y.-L. Li, E.-B. W. Lerch, A. Messmer, D. Bigourd, S. Eger, A. Marx, J. Bredenbeck,
   Vibrational energy flow in artificial amino acids investigated by 2C-2D-IR spectroscopy,
   75th Spring meeting of the German Physical Society, Dresden, Germany, March **2011**

5. **H. M. Müller-Werkmeister**, Y.-L. Li, E.-B. W. Lerch, A. Messmer, D. Bigourd, S. Eger, A. Marx, J. Bredenbeck,
   Vibrational energy flow in artificial amino acids,
   Graduate student symposium: Research in Molecular & Cell Biological Sciences, Frankfurt,
   Germany, October **2010**

6. **H. M. Müller-Werkmeister**, Y.-L. Li, E.-B. W. Lerch, A. Messmer, D. Bigourd, S. Eger, A. Marx, J. Bredenbeck,
   Vibrational energy flow in artificial amino acids investigated by two-colour 2D-IR spectroscopy,
   contributed talk, First International Conference on Ultrafast Structural Dynamics, Lausanne,
   Switzerland, June **2010**

Poster Presentations at Conferences

1. **H. M. Müller-Werkmeister**, J. Bredenbeck,
   Artificial Amino Acids as site-specific probes for ultrafast dynamics in proteins, presented at
   Molecules, Light and Life, Manfred-Eigen-Nachwuchswissenschaftlergespräche, Jena, Germany, November **2012**

2. L. Blankenburg, J. Bredenbeck, K. Eberl, M. Essig, D. Kern-Michler, **H. M. Müller-Werkmeister**,
   Infrared spectroscopy & Artificial amino acids: a great couple for protein biophysics, presented
   at German Conference of Women in Physics, Freiburg, Germany, October **2012**

3. **H. M. Müller-Werkmeister**, J. Bredenbeck,
   Artificial Amino Acids as site-specific probes for ultrafast dynamics in proteins, presented
   at CMDS 2012 (6th International conference on Coherent Multidimensional spectroscopy),
   Berlin, Germany, July **2012**

4. **H. M. Müller-Werkmeister**, J. Bredenbeck,
   Artificial amino acids for the real time study of vibrational energy transfer in proteins by ultrafast spectroscopy, presented at Bunsentagung, Leipzig, Germany, May **2012**

5. **H. M. Müller-Werkmeister**, J. Bredenbeck,
   A co-translationally insertable donor-acceptor pair for the real time study of vibrational energy transfer in proteins, presented at 56th Biophysical Society Meeting, San Diego, US, February **2012**
   abstract:Biophysical Journal, **2012** 102 (3), 591a, doi:10.1016/j.bpj.2011.11.3221

6. **H. M. Müller-Werkmeister**, J. Bredenbeck,
   A co-translationally insertable donor-acceptor pair for the real time study of vibrational energy transfer in proteins, presented at UCP'11 (International Workshop on Ultrafast Chemical Physics), Glasgow, UK, December **2011**

7. **H. M. Müller-Werkmeister**, J. Bredenbeck,
   A co-translationally insertable donor-acceptor pair for the real time study of vibrational energy transfer in proteins, presented at presented at German Conference of Women in Physics, Saarbrücken, Germany, November **2011**

8. **H. M. Müller-Werkmeister**, Y.-L. Li, E.-B. W. Lerch, D. Bigourd, S. Eger, A. Marx, J. Bredenbeck,
   Artificial amino acids as versatile tools for 2D-IR studies of proteins, presented at TRVS XV (Fifthteenth International Conference on Time-Resolved Vibrational Spectroscopy), Monte Verita, Ascona, Switzerland, June **2011**

9. A.T. Messmer, Y.L. Li, **H. M. Müller-Werkmeister**, D. Bigourd, K. Nienhaus, G.U. Nienhaus, and J. Bredenbeck,
   Investigating the speed limit of functional protein dynamics in equilibrium, presented at First International Conference on Ultrafast Structural Dynamics, Lausanne, Switzerland, June **2010**

10. **H. M. Müller-Werkmeister**, Y.-L. Li, E.-B. W. Lerch, A. Messmer, D. Bigourd, S. Eger, A. Marx, J. Bredenbeck,
    Investigating the distance dependence of energy transfer times between vibrational modes with two-colour 2D-IR spectroscopy, presented at Bunsentagung, Bielefeld Germany, May **2010**

11. **H. M. Müller-Werkmeister**, Y.-L. Li, E.-B. W. Lerch, A. Messmer, D. Bigourd, S. Eger, A. Marx, J. Bredenbeck,
    Distance dependent energy transfer times in azido- and nitrile-labeled amino acids by time resolved two-colour two-dimensional infrared-spectroscopy (2C2D-IR), presented at International Bunsen Discussion Meeting, Leipzig, Germany, September **2009**

12. A.T. Messmer, Y.L. Li, **H. M. Müller-Werkmeister**, D. Bigourd, K. Nienhaus, G.U. Nienhaus, and J. Bredenbeck,
    Investigating the speed limit of functional protein dynamics in equilibrium, presented at International Bunsen Discussion Meeting, Leipzig, Germany, September **2009**

Contents

Motivation

Protein dynamics cover many orders of magnitude in time, from femtoseconds (~10^{-15} s) to hours and days [1, 2, 3]. Only a few hundred amino acids in chain length built complex and dynamic high-performance machines, such as myoglobin [4] involved in oxygen transport, or photo receptors like rhodopsin [5] and photoactive yellow protein [6] or a modular protein domain, as the PDZ domain investigated in this thesis [7, 8, 9, 10]. All those have a size of only few nanometers; the protein world is one billion times (10^{-9}) smaller than the macroscopic world. Is it surprising then that the fastest dynamics in proteins are happening on a timescale one billion times shorter than fast processes in the macroscopic world?

The timescale of protein dynamics starts in the subpicosecond range with the initial steps of chemical or biochemical reactions within less than 100 fs (~10^{-15} s to 10^{-13} s) [1, 2, 3, 5, 11, 12]. However, when biologists and biochemists think of proteins, at first static colorful three-dimensional structures come to mind - images of conformational states provided by methods such as X-ray crystallography, NMR spectroscopy or high-resolution cryoelectron microscopy [13, 14, 15].

For a full understanding of protein function and biochemical mechanisms three-dimensional static structures are highly important yet not sufficient. As the physicist Richard Feynman said: "Everything that living things do can be understood in terms of the jiggling and wiggling of atoms", [16] which holds true for all biological matter including proteins. Ligands are bound and unbound, hydrogen bonds are built and broken, side chains are rotating or chromophores are isomerising and all overall all functional groups move with the energy of kT. Therefore proteins are comprising a complex molecular dance and are not at all the static objects known from textbook images but highly dynamic machines, their dynamics covering a wide timescale. These diverse fluctuations are essential to drive the proteins' function determining biology on molecular level. However, the details remain subject to intensive experimental and theoretical studies.

The ultrafast processes in proteins can be described in great detail by quantum, semi-classical and classical molecular dynamics modeling approaches [17, 18, 19, 20]. Additionally many different experimental approaches have been developed to study protein dynamics with different time-resolutions, both in the steady-state or under non-equilibrium conditions. First steps towards experimental investigation of protein dynamics were already made in the 40s [21], the invention of stop-flow measurements gave access to non-equilibrium processes in the sub second or millisecond region. Much faster times scale are nowadays accessible with different technological approaches. NMR experiments can detect picosecond equilibrium dynamics indirectly, using relaxation methods [22, 23, 24, 25, 26, 27, 28, 29] or millisecond dynamics in real-time experiments [27, 30]. Time-resolved crystallography approaches as pump-probe experiments [31, 32, 33] allow insights into processes in the picosecond range, but are limited to certain model systems like myoglobin or PYP.

The major technological development enabling experimentalists to study protein dynamics starting from the most fundamental scale in the femtosecond regime was the invention of femtosecond lasers (Ti:Sapph) in the 1980s. It led to the new fields of femtochemistry and femtobiology almost three decades ago [34, 35]. Several different variants of ultrafast spectroscopy covering the full range of the UV to the mid IR and terahertz have been realized [36, 37, 38, 39]. During the last 15 years
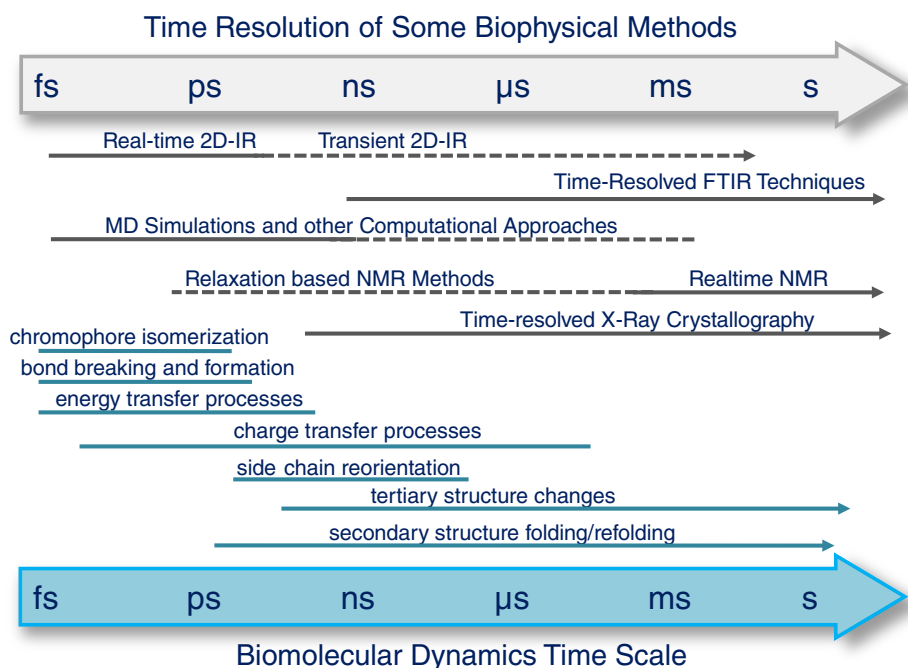
Figure 1: The timescale covering biomolecular dynamics spans more than ten orders of magnitude from the femtosecond regime (10^{-15} s to seconds and longer. Processes happening on the fastest, most fundamental timescale in (bio)chemistry include bond breaking and formation and chromophore isomerization as fastest steps within femtoseconds, followed by processes as proton transfer or side chain reorientation, which happen within picoseconds or longer. Secondary and tertiary structure changes happen on the nanosecond to millisecond scale or even longer. Complex biochemical processes such as signal transduction across the synapse, involving different partner proteins and ligands to fulfill a function span the entire timescale, starting out from the fast molecular motions within a protein to the formation of protein-ligand complexes leading to the start of a signal cascade below the millisecond time regime.

A huge body of biophysical methods exists to study these types of effects, with few able to address the ultrafast processes. Those include optical multidimensional spectroscopy, like 2D-IR spectroscopy. An alternative for to study a limited number of model systems with great temporal and spatial resolution is time-resolved X-ray diffraction. A well-established method to study protein dynamics is NMR spectroscopy, real-time approaches resolve millisecond to microseconds, relaxation approaches reach the picosecond regime. All methods are supported well by computational approaches like molecular dynamics simulations.

the technological development moved on from transient one-dimensional spectroscopy to multidimensional spectroscopy with two or more frequency axes, in analogy to NMR spectroscopy [40, 41]. The first frequency range to demonstrate the possibility of multidimensional optical spectroscopy was the mid-IR [40, 42, 43, 44]. 2D-IR and 3D-IR as well as transient 2D-IR have been demonstrated and became established as broadly used techniques, also to address biophysical questions, nowadays [42, 45, 46, 47, 48, 49, 50, 51, 52]. Multidimensional variants of optical spectroscopy have been demonstrated and are increasingly used in the visible and ultraviolet range as well (known as 2D-ES, 2D electronic spectroscopy, [53, 54, 55, 56, 57]) in addition to mixed multidimensional spectroscopy [58, 59, 60].

Vibrational spectroscopy in general is a highly sensitive technique for measuring protein secondary structure changes and dynamics by monitoring the amide bands [42, 61, 62, 63]. The intrinsic real-time resolution limit of ultrafast vibrational spectroscopy is around 50 fs [44]. This
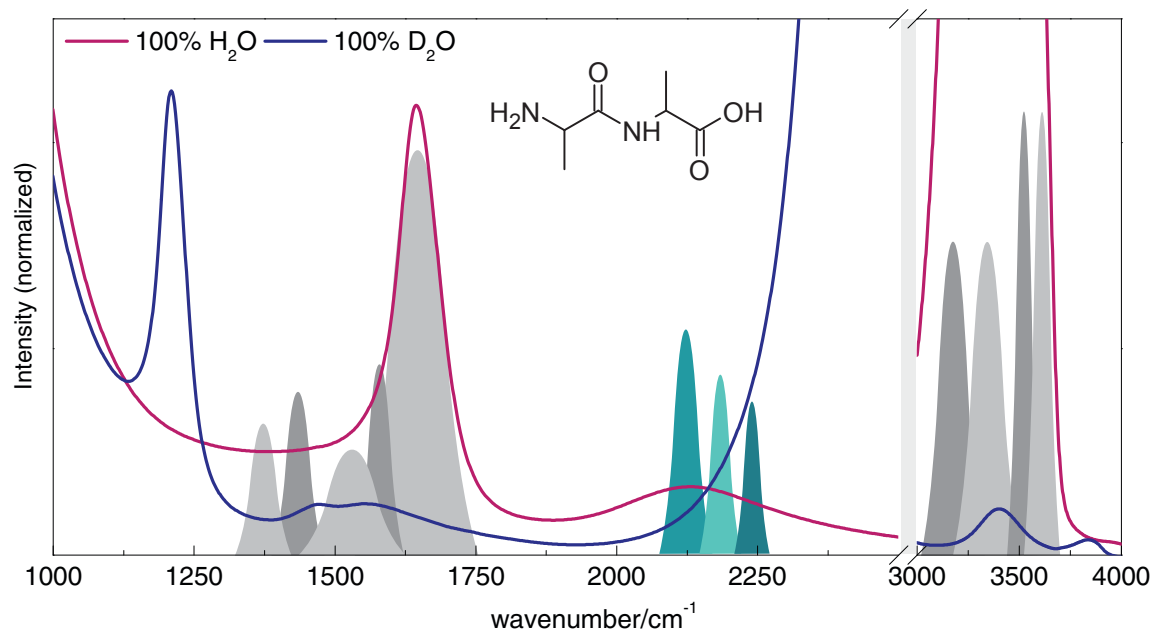
Figure 2: Why are novel vibrational probes necessary? FTIR absorption spectra of H_2O (red) and D_2O (blue) with typical protein vibrations indicated in gray and possible vibrations of *novel vibrational probes* indicated in blue-green. Shown are azides (approx. 2100 cm^{-1}), thiocyanates (approx. 2150–2170 cm^{-1}) and nitriles (around 2250 cm^{-1})

makes 2D-IR a highly important experimental technique for biophysics especially, as it is one of very few techniques matching the fast time range of molecular dynamics simulations nowadays routinely used to describe and predict protein dynamics [17, 18, 19, 20]. Fastest (structural) changes can be tracked by 2D-IR in the femtosecond and picosecond regime combined with the intrinsically high spatial resolution on the level of chemical groups inherent to vibrational spectroscopy.

However, in proteins the spatial resolution is limited. The high sensitivity of IR to observe vibrational modes turns into a restriction in resolution as spectra become highly congested and absorption bands are comprised of contributions by all similar IR-active modes in a protein molecule. Thus the ability to assign spectral features to localized modes is limited for proteins. Despite this problem of spectral congestion, equally present in time-resolved IR and multidimensional IR spectroscopy, many experiments have been conducted with high local resolution [39, 64, 65, 66, 67, 68, 69, 70, 71, 72]. In those experiments either a very specific marker vibrations in difference spectra are assigned or,question like proton transfer or hydrogen bonding are addressed. Some experiments make use of intrinsic native vibrations, from co-factors, chromophores or ligand such as CO in Myoglobin [47, 73, 74].

Many protein systems however lack intrinsic vibrational markers or the scientific question addresses e.g. backbone or conformational dynamics. A possible way to overcome the limitation in spatial resolution by spectral congestion is the manipulation of the system of interest and the site-specific introduction of specific vibrational probes. Those should absorb in the biological free window in the range between 1800–3000 cm^{-1} and can be utilized to monitor localized structural changes. The traditionally used approaches of isotope-labeling or chemical modification have limitations and require elaborate sample preparation protocols. Often the sample amount is limited and labeling is not very efficient, making these approaches ill-suited for 2D-IR spectroscopy of

proteins because that technique needs higher labeling yield and sample amounts.

Thus novel vibrational probes and new routes of sample preparation are highly desired. The new field of synthetic biology and protein engineering is emerging and provides new potential vibrational probes suitable for the study of proteins as well as new approaches for their site-specific incorporation [75, 76]. A particular promising way to challenge the problem of spectral congestion is the use of unnatural amino acids with chemical groups absorbing well separated from protein bands, such as azides or nitriles. Using a artificial genetic code expansion [77, 78, 79] or a supplementation based incorporation approach [80, 81] it is possible to express proteins labeled to a high percentage and ideally with sufficient sample yields. Chemical groups ideally suited to be tested as novel probes include azide, nitrile or thiocyanate; all of which have been used in IR spectroscopy previously and absorb between 2000 cm^{-1} and 2200 cm^{-1}. Those groups are additionally favorable because their absorption is relatively well separated from solvent vibrations. For a most versatile novel vibrational probe experiments both in H_2O and D_2O should be possible.

With a versatile vibrational probe, that ideally can be incorporated site-specifically in many proteins without too many restrictions, multidimensional ultrafast IR spectroscopy will be enabled to address a huge variety of long-standing biophysical questions, which up to now can not be investigated experimentally.

A site-specific probe that can be placed randomly and directly during protein expression will enable direct study of the local microenvironment in a protein (for example in [82, 83]). This will give important insights into the protein interior, helping to unravel e.g. enzymatic mechanisms [84] or mapping out binding interfaces in protein-ligand complexes. Combined with the intrinsically fast real-time resolution of 2D-IR spectroscopy fluctuations of the potential energy surface, which reflect fast conformational dynamics of a protein, can be monitored and will allow to study side chain dynamics with previously impossible accuracy. This application of probing the site-specific environment and local dynamics is shown in this thesis on the PDZ domain, which is also highly interesting in another respect: One of the most fascinating phenomena in protein biophysics is information transfer within and between protein domains, also known as allostery. It is intriguing that a protein-protein interaction domain, such as the PDZ domain, must transfer the information of its ligand binding status to attached domains. In a simplified model it might be expected that this information is transduced to neighboring protein domains by pure mechanical means through prominent secondary and tertiary structure changes. The PDZ domain however, is the best studied example of an allosteric protein which does not undergo structural changes upon ligand binding. Different simulations have found that in the PDZ domain a network of coupled amino acid residues is present, which is believed to function as a wire for information transfer [9, 10, 85]. Physically this phenomenon can be understood as vibrational energy transfer or heat transduction between two distant sites, a process being subject of intensive studies in ultrafast vibrational spectroscopy. The timescale of few picoseconds and the nature of the process as directional energy flow make it an biophysical question ideally suited to be addressed by 2D-IR spectroscopy, which will only be possible using site-specific vibrational modes.

The aim of this thesis is to test the feasibility of unnatural amino acids as such site-specific vibrational probes and demonstrate different applications in biophysics, including the experimental study of vibrational energy flow in proteins and the direct investigation of ultrafast structural dynamics.

Part I

Introduction and Theoretical Background

1 Principles of 2D-IR Spectroscopy

Two-dimensional Infrared Spectroscopy (2D-IR) is a third order nonlinear optical spectroscopy. With its intrisinc high time-resolution and a high sensitivity for structural changes, inherent to vibrational spectroscopy, it is ideally suited to investigate ultrafast dynamics in complex molecular enivronments such as liquids or biological complexes. The upgrade from first order spectroscopies to a multidimensional implementation similar to multidimenstional NMR spectroscopy with two or more frequency axes holds great promise for novel insights into equilibrium and non-equilibrium molecular dynamics starting in the subpicosecond time range. For a comprehensive understanding of 2D-IR and the observable ultrafast dynamics in a molecular system, quantum dynamics and theory of nonlinear spectroscopy are required, but basic concepts and information content of 2D-IR spectra can be understood in a less formal way.

The chapter is mainly based on the book *Concepts and Methods of 2D Infrared Spectroscopy* by Peter Hamm and Martin Zanni [44]. Good introductions into 2D-IR can be additionally found in the reviews [40, 50, 86] and in the book *Two-dimensional Optical Spectroscopy* by Minheang Cho [37]. A comprehensive textbook on the theory of nonlinear optical spectroscopy is the work of Shaul Mukamel [87].

1.1 Vibrational Spectroscopy

Vibrational spectroscopy is the study of the quantum system formed by all vibrations in a molecular environment. Therefore to understand the processes accessible by 2D-IR spectroscopy, which include vibrational anharmonicity and coupling, vibrational energy transfer and frequency fluctuations of oscillators, a brief recapitulation of the basics of vibrational spectroscopy is helpful.

Infrared spectroscopy studies vibrational modes in molecules by means of the absorption of infrared light resonant to a transition between energy levels, another type of vibrational spectroscopy is Raman spectroscopy which is based on inelastic scattering. Both are sensitive to molecular vibrations and thus can probe different properties such as molecular structure or dynamics.

Every molecule has $3N$ degrees of freedom, 3 degrees describing the translation in $\vec{x}, \vec{y}, \vec{z}$ direction and 3 degrees describing the rotation of the overall molecules in spaces around the $\vec{x}, \vec{y}, \vec{z}$ axis. For every nonlinear molecule with $N > 2$ atoms $3N - 6$ vibrational modes remain. For example a model protein with 100 amino acids of only Alanine contains 1003 atoms, resulting in 997 vibrational modes. [62]
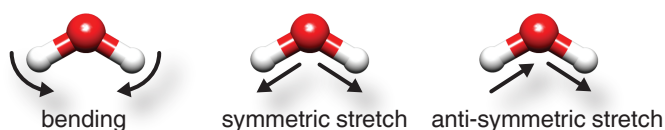

Figure 1.1: H_2O has three different vibrational normal modes, which are bending, symmetric stretch and anti-symmetric stretch vibrations.

bending   symmetric stretch   anti-symmetric stretch

Vibrational modes include symmetric and asymmetric stretch, bending, wagging and scissoring modes. The three different vibrational normal modes in H_2O are shown in Figure 1.1. Modes can be degenerate when energies are similar. For a mode to be *IR active* a change of the dipole during replacement of the atoms is required. The intensity of an IR absorption scales with the transition dipole moment. Vibrational modes which are not *IR active* are *Raman active*.

To calculate the energy of a vibrational mode, the most basic model is a harmonic oscillator assuming equidistant energy levels.

$$\nu = \frac{1}{2\pi}\sqrt{\frac{k}{\mu}} \tag{1.1}$$

with μ as the reduced mass of two point masses $\mu = \frac{m_1 \cdot m_2}{m_1 + m_2}$. The potential energy of a harmonic oscillator is given by

$$E_n = h\nu(n + \frac{1}{2}) \tag{1.2}$$

with ν as the transition frequency and $\Delta E = h\nu = hc\bar{\nu} = h\frac{c}{\lambda}$ as the energy difference for a transition. A more accurate description of the energy levels of a vibrational mode is derived by assuming an anharmonic oscillator described by a Morse potential:

$$V = D_e(1 - e^{a(r_e - r)})^2 \tag{1.3}$$

with D_e as the finite dissociation energy and a as the curvature of the potential. The energy levels of an anharmonic oscillator are given by:

$$E_n = h\nu\left(n + \frac{1}{2}\right) - x\left(n + \frac{1}{2}\right)^2 \tag{1.4}$$

with x as the anharmonicity constant of $x = \frac{h\nu}{4D_e}$. The Morse potential describes the decreasing energy gap between higher vibrational levels:

$$E_{n+1} - E_n = h\nu_0 - \frac{(n+1)(h\nu_0)^2}{2D_e} \tag{1.5}$$

with the transitions frequency between the respective energy levels calculated as

$$\nu = \frac{a}{2\pi}\sqrt{\frac{2D_e}{\mu}} \tag{1.6}$$

For the transition between energy levels in the anharmonic oscillator different selection rules apply, instead of $\Delta\nu = \pm 1$ as the only allowed transition, also transitions of $\Delta\nu = \pm 2, \pm 3, \pm n$ are allowed, leading to overtones in IR spectra. Another consequences of the anharmonic potential is, that coupling between modes is possible, which can be investigated in great detail by 2D-IR spectroscopy.

Vibrational Modes in Proteins. A protein's vibrational spectrum is composed of contributions from the peptide backbone as well as side chain signals. The main characteristic absorptions in an FTIR spectrum of a protein are depicted schematically in Figure 2 in the motivation. They relate to specific vibrations of the peptide units in the protein backbone and characteristic side chain vibrations. [61, 62, 63, 88, 89]

The N−H stretching vibrations generate the amide A and amide B bands at 3300 cm^{-1} and 3070 cm^{-1}. Those vibrations are sensitive to changes in the hydrogen bond network of the peptide

backbone. The Amide I band around 1650 cm^{-1} is due to modes consisting mainly of the C=O stretch vibrations of the peptide units in the backbone. This is a very important frequency range for the investigation of secondary structure dynamics. At 1550 cm^{-1} the Amide II band is found, which is comprised by modes based on the out-of-phase NH in plane bending and the CN stretching motion of the peptide bonds. The Amide III mode leads to a band between 1200 cm^{-1} and 1400 cm^{-1} and is comprised of the in-phase contributions of the NH in plane bending and the CN stretching vibration.

Other important vibrational modes found in proteins are those of amino acids side chains. For example the CO stretch vibrations of the carbonyls in Asp or Glu side chains are found above 1700 cm^{-1}. The ring mode vibrations of Tyr or Phe are very specific as well and can be found around 1500 cm^{-1}.

1.2 2D-IR Spectroscopy

Two-dimensional infrared spectroscopy is the multidimensional upgrade of regular IR spectroscopy, comparable to two-dimensional NMR in comparison to one-dimensional NMR. Already in the first publication to two-dimensional NMR the application of 2D spectroscopy in infrared spectroscopy was envisioned [41]. However it took about three decades before the first 2D-IR spectrum was reported by Hamm, Lim and Hochstrasser [42].

As outlined in the motivation, 2D-IR spectroscopy is of arising importance in physcial chemistry and used to investigate structural dynamics of a wide range of molecules. The observables in 2D-IR spectroscopy are the energies of the vibrational eigenstates of the molecules investigated as a function of time, couplings between those eigenstates (see Figure 1.6), the population of states as well as the amplitude and relative orientation of their transition dipole moments. These observables together with additional informations derived about correlations between states, leading to cross peaks and the dynamic change of peaks, provide valuable insights into a wide range of molecular systems.

Different types of scientific questions have been addressed in the recent years. Those include the dynamics of hydrogen bonding networks of molecules in solution or within water [90, 91, 92, 93] as well as structure elucidation of small (organic) molecules and peptides [94, 95, 96, 97, 98, 99] or exchange between different conformations [47, 100, 101, 102, 103] or energy transfer and relaxation processes [104, 105, 106, 107, 108, 109, 110, 111, 112].

2D-IR was mainly applied to small organic compound or organo-metall complexes with defined, well separated vibrations. Applications to protein dynamics and biophysical questions are emerging as well, however due to spectral congestion those studies are limited to e.g. secondary structure dynamics, ligand dynamics or are carried out on smaller modell systems which contain vibrational probes such as isotope labeled CO groups [49, 51, 96, 113, 114, 115, 116, 117]. Others include measurements of the ligand CO in Myoglobin and other heme-containing proteins [47, 118].

Appart from multidimensional spectroscopy in the infrared other optical spectroscopies with two frequency axes have been demonstrated and become of increasing importance. The most prominent is 2D-Vis, first performed by Brixner et al. [119], others are 2D-UV [53, 54, 55, 56, 57] or mixed techniques which allow for surface specific experiments [58], subensemble specific photochemistry [59] or detailed investigation of vibronic coupling [60]. Another extension of the 2D-IR approach is the introdcution of an additional trigger to study non-equilibrium dynamics, either by exciting a processes by a visibile light pulse as in transient 2D-IR pioneered by Jens Bredenbeck et al. [46, 86, 120, 121] or by a temperature jump as demonstrated by the Tokmakoff group to study

protein folding [122, 123, 124, 125].

1.2.1 Experimental Implementation of 2D-IR Spectroscopy

2D-IR spectra can be recorded in two fundamentally different approaches, either in the frequency domain as was the case for the first ever reported 2D-IR [42] or in the time domain with subsequent Fourier Transformation in analogy to moder NMR spectroscopy. This was first demonstrated by Zanni et al. [126]. Both approaches have been shown to yield largely the same information [127] and mainly differ in terms of time-resolution, spectral resolution along the pump axis, technical implementation as well as data processing (Fourier transformation 2D-IR data have to be phase corrected).

The simplest implementation of a 2D-IR setup is in the frequency domain and briefly sketched in Figure 1.2. Here the pump probe or hole burning approach, also known as double resonance 2D-IR is used, which is combining a broad band IR probe pulse which generates the signal along the ω_{probe}-axis, in the used convention on the x-axis, with a narrow band IR pump pulse that is sketched along the ω_{pump}-axis, which is the y-axis in the used convention[1] For 2D-IR in the time
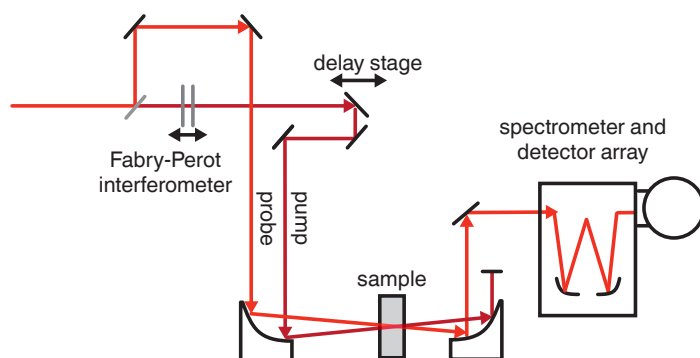
Figure 1.2: Schematic drawing of a 2D-IR setup in the frequency domain. A Fabry-Perot interferometer is used to narrow the pump pulse. Figure inspired by [44]

domain not only two pulses are required but instead of the pump pulse a pulse pair is used. Thus three independent pulses with two defined time-delays and a fourth pulse used as local oscillator overlapped with the signal during heterodyne detection are used. The time domain approach is also referred to as photon echo approach or Fourier transformation 2D-IR. To record 2D-IR spectra in the time domain, several different technical setup have been demonstrated [44].The most versatile is a heterodyned photon echo experiment with four independent laser beams inplemented in a box-CARS geometry. A good compromise between versatility and experimental complexity is offered by a collinear geometry for Fourier transform 2D-IR, realized by using a Mach-Zehner interferometer to generate a pulse pair in a pump probe geometry [128, 129] or for example using the recently demonstrated TWINS approach [130].

Using a mid-IR pulse shaper as developed by the Zanni group it is possible to record 2D-IR spectra both in the time domain as well as in the frequendy domain [131, 132, 133]. The pulse shaper can be used to generate either a pulse pair as mentioned above or to prepare a narrowband IR pulse just like it is used in the double resonance approach.

As all data presented in this thesis are recorded in the frequendy domain using the pump-probe geometry, only this approach is discussed in more detail. The schematic setup is shown in Figure 1.2. A broad band mid-IR pulse, generated by a tunable OPA [134] is split by a beam-splitter

---

[1]There is up to now no standard for drawing 2D-IR spectra and thus axis are interchanged.
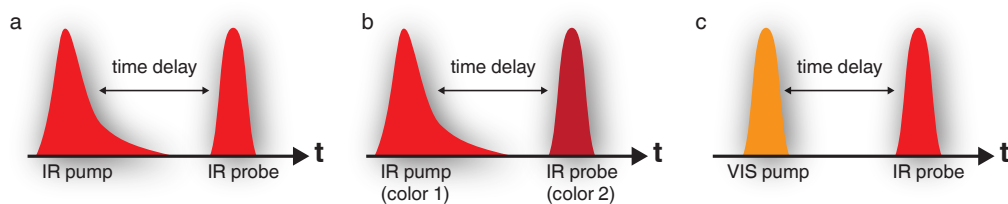
Figure 1.3: Different pulse sequences used in this thesis. In a) 2D-IR spectroscopy in pump-probe approach with narrow band pump pulse (from FP), b) 2C-2D-IR spectroscopy with pump and probe pulses of different IR colors, the pump pulse is narrowed in the frequency domain by the Fabry Perot etalon and thus elongated in the time domain to approx. 1 ps. c) VIS-IR (transient IR) using a visible excitation pump pulse followed by a IR probe pulse. Here the pump pulse is not narrowed and short in the timedomain.

into a pump and a probe beam. The pump beam has a higher energy and is narrowed in the frequency domain by using a Fabry-Perot interferometer. The Fabry Perot interferometer changes the pulse in the time domain as indicated in Figure 1.3 a and b, the pulse get a long tail in the time domain, which is causing the lower time resolution of frequency domain 2D-IR in comparison to time-domain or photon echo 2D-IR.

The pump pulse has a Lorentzian shaped bandwidth and can be described as follows:

$$E(\omega) = E_0(\omega) \frac{1-R}{1-Re^{i\frac{2d\omega}{c}}} \tag{1.7}$$

R is the reflection coefficient of the mirrors in the Fabry Perot interferometer, which is wavelength dependent, therefore specific mirrors for a certain frequency range have to be used to get optimal pulse shapes and energies for the pump pulse.

The signal is calculated as the difference between the pumped and the unpumped recorded intensities:

$$S(\omega_{\text{probe}}, \omega_{\text{pump}}, t) = log \frac{I_{\text{pump}_{\text{ON}}}}{I_{\text{pump}_{\text{OFF}}}} \tag{1.8}$$

The signal size scales with the squared extinction coefficent (ε) of the investigated vibrations and linear with the intensity of the pump pulse.

1.3 Features of a 2D-IR Spectrum

A 2D-IR spectrum (such as the schematic spectrum shown in Figure 1.6) contains different types of peaks, diagonal peaks for every absorption band in the spectral range probed and possible cross peaks between different oscillators, which can be generated by a wide range of mechanisms.

Figure 1.4: Principle of anharmonicity and signal generation for 2D-IR by combining ESA, GSB and SE contributions. The 2D-IR spectrum shows real data (discussed in chapter 4) of CNP in THF for a waiting time of 1.5 ps.

1.3.1 Diagonal Peaks

The diagonal peaks correspond to the absorption spectra of the respective molecule. Usually for every absorption band a diagonal peak can be observed. In Figure 1.4 a diagonal peak for the CN stretching vibration in cyanophenylalanine is shown with a schematic anharmonic oscillator to explain how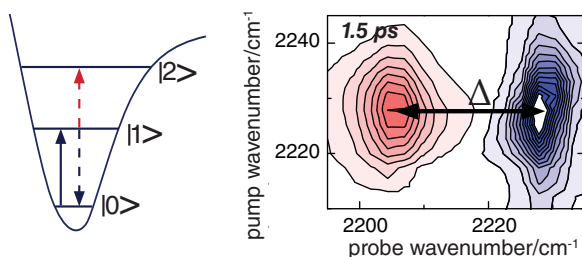 a 2D-IR signal is generated. As 2D-IR spectroscopy is a difference spectroscopy, the signals are calculated from the absorption change between the pumped and the unpumped spectrum. The pump pulse is resonant to the $|0\rangle$ to $|1\rangle$ transition and creates a population in the $|1\rangle$ state.

The probe pulse can interact in different ways with this population. As the probe pulse is broader in frequency then the pump pulse it can be absorbed both by the population in the $|0\rangle$ state as well as the population in the $|1\rangle$ state. The transition from $|1\rangle$ to $|2\rangle$ is referred to as excited state absorption (ESA). Due to the anharmonicity of the potential this transition is lower in energy than the energy gap between $|0\rangle$ to $|1\rangle$.

This is the reason, why 2D-IR spectra can be recorded (otherwise signals from the $|0\rangle$ to $|1\rangle$ transition and the $|1\rangle$ to $|2\rangle$ transition would cancel) and why the contributions to the 2D-IR signal from this transition are at lower wavenumbers. The probe pulse can also create again a transition from $|0\rangle$ to $|1\rangle$, which has a smaller intensity than than without absorption of the pump beam, why it is referred to as ground state bleach (GSB). Furthermore, stimulated emission (SE) from $|1\rangle$ can be induced by the probe pulse.

The main information is that frequency fluctuations as a function of time (i.e. spectral diffusion) can be measured. Thus, the homogeneous line width can be obtained and processes which lead to inhomogeneous broadening can be investigated. The contributions to the spectrum from GSB and SE are depicted as a blue (negative signal), the ESA signal is shown as red (positive) part in the spectra[2].

Spectral Diffusion. The dynamic lineshape of the peaks in a 2D-IR spectrum yields important information on the dynamics of the quantum states involved. In Figure 1.5 spectra of the azide stretch vibration in the model system azidohomoalanine are shown. The pronounced tilt of the diagonal peak for the short waiting time of 1 ps can be clearly observed as well as the vanishing of the tilt for the longer waiting time of 3.5 ps. The cause of the tilt is inhomogeneous broadening of the diagonal peak, that is the azide absorption band is broadened of contributions from several different subensembles, which e.g. experience an different microenvironment. Thus the tilted diagonal peak is in principle constituted of the underlaying diagonal peaks for all members of the subensemble. Upon a longer waiting time the tilt vanishes because of exchange between the states and thus equilibration. Thus 2D-IR spectroscopy can directly access fast equilibrium fluctuations.

The measure of this process is the frequency frequency correlation function (FFCF) given by $C(t) = \langle \delta\omega(t)\delta\omega(0)\rangle$ [50, 135, 136]. Using this function the frequency and amplitute of the fluctuations in a molecular system in equilibrium can be described. The FFCF is the results aimed for in spectral diffusion studies, which are of increasing importance especially in 2D-IR spectroscopy of proteins [50, 137, 138, 139, 140]. It can be extracted from 2D-IR spectra by a CLS (center line slope) analysis. The inverse of the tilt along the diagonal peak as function of waiting time is analyzed.

This approach has to be used with care as other competing processes can influence the lineshape and then the CLS approach is not meaningful anymore. In case of perfect inhomogeneous line broadening the CLS value would be 1 but in experiments smaller values are normally observed as

---

[2]As plotting of spectra is subject of convention different variations for color schemes and positive and negative signals exist in the literature.
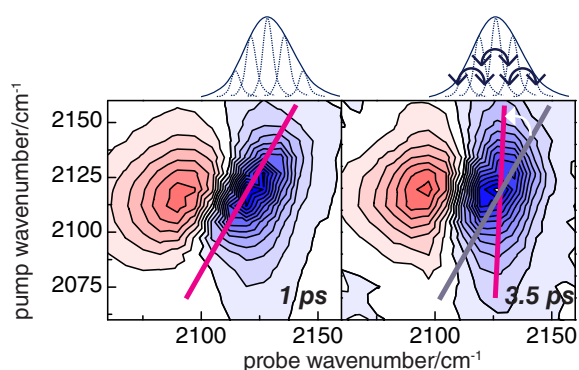
Figure 1.5: Principle of spectral diffusion. The shown spectra are real measured data of Aha in H_2O for the waiting times of 1 ps and 3.5 ps. They are discussed in detail in chapter 4.

perfect broadening only happens for the shortest waiting times. With time the CLS value drops to 0 when the peak appears upright.

1.3.2 Cross Peaks

The other type of peaks in 2D-IR spectra are cross peaks which can be created by various mechanisms and reflect interactions between the respective vibrational modes. Cause of cross peaks appearance include anharmonic coupling, population transfer between states or relaxation processes such as intramolecular vibrational energy redistribution (IVR).

Cross Peaks can be generated in any molecular system with several vibrations. In Figure 1.6 the level scheme of two coupled vibrational oscillators is depicted. The molecule can be described by a 2D potential:

$$V(r_1, r_2) = V_1(r_1) + V_2(r_2) + \beta_{1,2} r_1 r_2 \tag{1.9}$$

with $V_n(r_n)$ being the Morse potentials (Equation 1.3) describing a single oscillator and $\beta_{1,2}$ as the coupling between the two oscillators. The coupling between two oscillators might be described by transition dipole coupling

$$\beta_{ij} = \frac{1}{4\pi\epsilon_0} \left[\frac{\vec{\mu}_i \vec{\mu}_j}{r_{ij}^3} - 3 \frac{(\vec{r}_{ij} \cdot \vec{\mu}_i)(\vec{r}_{ij} \cdot \vec{\mu}_j)}{r_{ij}^5} \right] \tag{1.10}$$

The coupling introduces a difference in energy all states in the anharmonic level scheme in Figure 1.6, leading to cross peaks. This shall be illustrated for the upper left cross peak in Figure 1.6.

Due to anharmonic coupling the energy gap between the $|00\rangle$ state and the $|10\rangle$ state (transition 2) is different from the energy gap between $|01\rangle$ and $|11\rangle$ (transition 1), although in both transitions one quantum is put into the first oscillator. This reflects the influence of the second oscillator on the first oscillator (i.e. coupling). Upon pumping the second oscillator, thus a difference signal is recorded due to the frequency shift of the first oscillator (bleach of transition 2 and induced absorption of transition 1). In the absence of coupling the two would cancel exactly.

The strength of the coupling is responsible for the size of the shift for the energy levels and can be extracted from the 2D-IR spectra by the off-diagonal anharmonicity, which is the energy difference between the positive and negative parts of the cross peak. As anharmonic coupling is changing the potential of the investigated oscillators in a time-independent manner, cross peaks generated by this mechanism are observed instantanously in the 2D-IR spectrum. A good explanation of signal generation in 2D-IR spectra is given in [127].

If coupling is caused by transition dipole coupling, it can be described by Equation 1.10. The off-diagonal anharmonicity revealed by the cross peaks therefore contains information about the
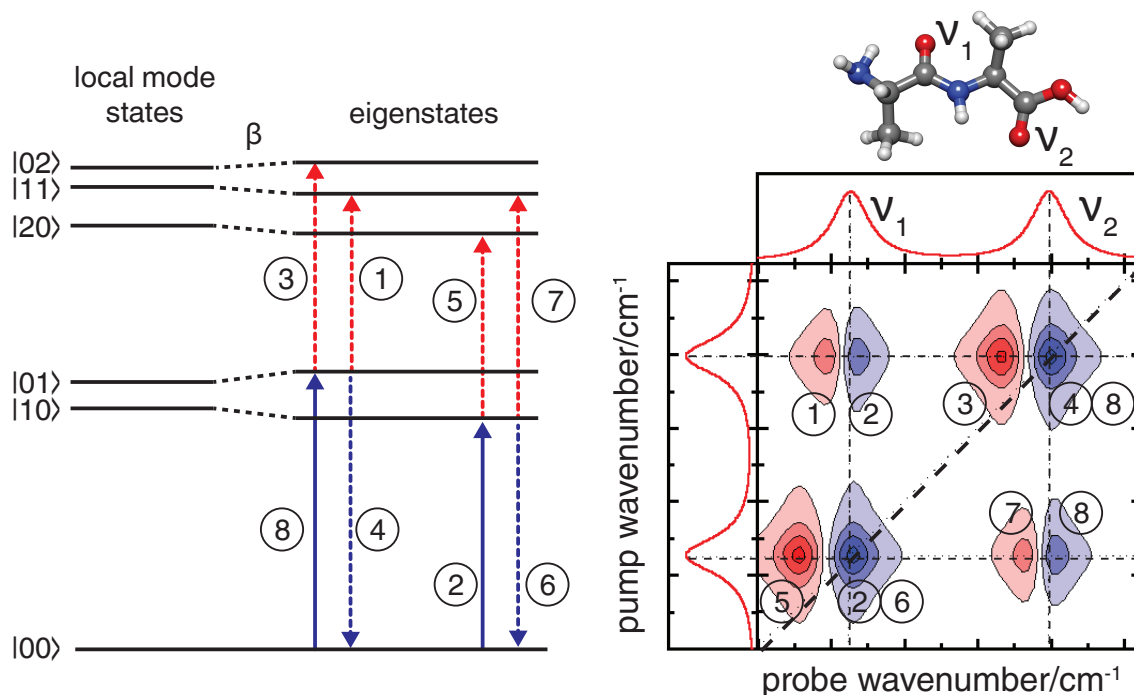
Figure 1.6: A model system which contains two coupled oscillators, such as the di-peptide shown here is well suited to explain the different signals in a 2D-IR spectrum. The level scheme of two coupled oscillators is shown on the left. β is the coupling between oscillators which induces a shift of energy levels. The dotted transistions are only possible to be probed after the pump pulse prepared the system. The probe pulse induces a transition from the ground state to the first excited state for the osciallator it is in resonance with (2, 8). The probe pulse can then induce either a transition related to excited state absorption (3,5) or a transition leading to stimulated emission back to the ground state (4, 6). In case of coupling addition transitions to the coupled eigenstate levels become visible (depicted as 1, 7).

relative orientation of transition dipoles. Still, information on relative orientation of oscillators is much more readily obtained from anisotropy measurements of the cross peaks then from evaluating anharmonicities [94, 95, 98, 99, 141].

Other mechanism can lead to the appearance of cross peaks between vibrational modes as well, which have different properties than cross peaks incuded by anharmonic coupling and might be time-dependent. Those include for example coherence transfer as investigated e.g. by Khalil et al. [142] or population transfer [127] caused by fluctuations of the couplings, mostly investigated in metal carbonyl complexes [143]. Another very important mechanism is exchange between different subensembles, just like chemical exchange in NMR spectroscopy. This could for example be the formation and breaking of hydrogen bonds as investiated e.g. by Fayer and Co-Workers [100] or the change between different ligand binding states in a protein as investigated by Bredenbeck et al. [47]. The type of experiment aimed to investigate exchange is named 2D-IR exchange spectroscopy or 2D-IR-EXSY.
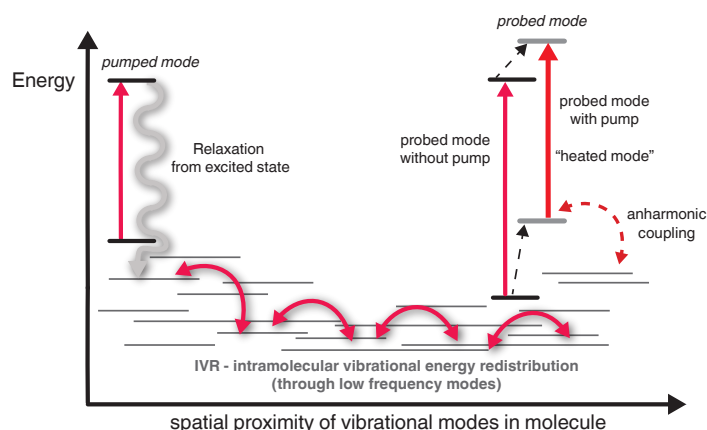
Figure 1.7: Schematic representation how intramolecular vibrational energy redistribution (IVR) or more general vibrational energy flow can lead to cross peaks in 2D-IR spectra. Energy from a pumped, highly localized, vibrational mode is dissipated into low frequency, delocalized modes. Those can be anharmonically coupled to other high frequency modes, generating a heated ground state, which results in a frequency shift leading to a cross peak in the 2D-IR spectrum. The figure is inspired by [104].

Intramolecular Vibrational Energy Redistribution (IVR) as Mechanism for Cross Peak Generation. IVR is another mechanism, which can lead to cross peak formation in 2D-IR spectra. In Figure 1.7 a schematic level scheme for a molecule is given to explain the appearance of cross peaks generated by IVR through the molecule. In case a transition is excited by the pump pulse the excess energy is distributed through low frequency, delocalized modes in the molecule by the IVR mechanism.

The physical process is in principle a relaxation from a vibrationally excited state, which can decay into at least two, but most likely many lower energy (low frequeny) vibrational modes under fulfillment of energy conservation,

$$\omega_a = \omega_b + \omega_c \tag{1.11}$$

Those low frequency modes are anharmonically coupled among each other as well as they are coupled to other high frequency, localized modes. Excitation of low frequency modes through IVR thus can lead to frequency changes of the high frequency localized modes, which become visible as a transient difference signal. This signal decays again when the complete energy is transfered to the solvent. As the distribution of the vibrational energy via the IVR mechanism is not happening instantanously but the energy needs to be transported through the molecule first, the cross peaks generated by IVR have a specific peak time, which is a measure for the spatial proximity of the involved high frequency modes.

Two speed regimes for IVR, ballistic and diffusive, have been discussed. In case of a ballistic energy transfer the mean distance is linear proportional to the transfer time $< x > \propto t$ [144, 145] whereas in the diffusive regime the distance is proportional to the square root of time $< x > \propto \sqrt{t}$ [110, 146, 147, 148]. The mechanisms of energy transport in different speed regimes as well as the underlaying principles as to when energy is transported by which mechansim are subject of extensive research in ultrafast spectroscopy [104, 109, 111, 145, 148, 149, 150, 151, 152]
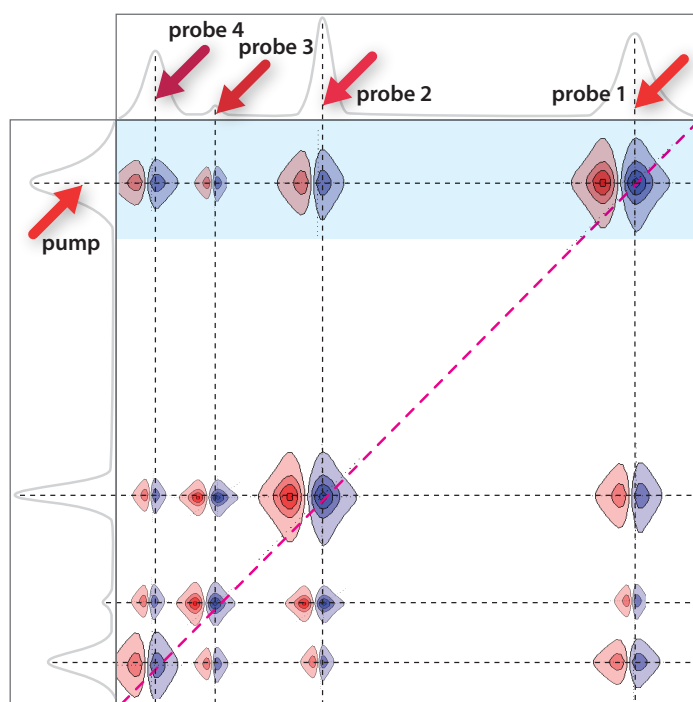
Figure 1.8: Schematic representation of 2C-2D-IR, an approach used in this thesis employing two independent tunable optical parametric amplifiers as infrared light sources. OPAs normally have a band width of 200-300 cm^{-1}, which is not sufficient to cover a whole absorptions spectrum (e.g. from 1500 cm^{-1} to 2200 cm^{-1}. To access cross peaks in this range one OPA is centered as pump on the vibration of interest, the other OPA is shifted between the different spectral windows as probe.

2C-2D-IR as Approach to Measure Cross Peaks. As cross peaks in 2D-IR spectra contain very valuable information about the molecular system under study it is of huge interest to record those with high resolution and between spectrally separated modes as well. This is a technical challenge as the mid-IR pulses used for pumping and probing the investigated transitions are generated by an OPA with subsequent DFG [134], which are tunable over a wide range but have a limited spectral width of 200 cm^{-1} to 300 cm^{-1}. This is sufficient to study cross peaks between similar vibrations such as the carbonyl modes of a metal carbonyl, but not enough to study the coupling or energy transfer between all important vibrational modes in a protein or when a vibrational probe, which absorbs in the free window between 1800 cm^{-1} and 3000 cm^{-1} is used. To allow for the measurement of cross peaks between such very separated vibrational modes a technique of two-colour 2D-IR (2C-2D-IR) or dual frequency 2D-IR is used [153, 154].

To record cross peaks between separated modes in the pump probe approach, two independent tunable OPAs are used. As depicted in Figure 1.8 it is possible to record a stripe of a full spectrum with all the cross peaks corresponding to one diagonal peak. In the time domain it would be necessary to record the full spectrum before Fourier transforming the data. The 2C-2D-IR spectra in this thesis are recorded by using one OPA for pumping a transition of interest (indicated by the pump in figure Figure 1.8) and then probing the different spectral windows where a cross peak is expected independently using a second OPA. The final 2C-2D-IR spectrum is then assembled by the individual spectra.

2 PDZ as Example for Vibrational Energy Flow and Dynamic Allostery in Proteins

The process of IVR or vibrational energy transfer (VET) introduced in Chapter 1 as potential mechanism of cross peak generation in 2D-IR spectra is not limited to small molecular systems.

In fact VET is a general principle of energy relaxation abundant in all molecular systems. The energy from an excited vibrational mode is dissipated over several relaxation pathways. Those include relaxation into low frequency modes of a molecule. How energy is dissipated and transported in such macro molecules as proteins with their thousands of degrees of freedom is a major topic of research in theoretical chemistry and biophysics [148, 155, 156].

The interest in vibrational energy flow is driven by its key role in the most recent understanding of long-range communication in proteins [3, 155, 157, 158]. In several different proteins energy transfer pathways have been predicted. They are are found to function as relaxation pathways of excess energy and might be involved in information transfer through a protein [148, 159, 160, 161]. This is newly proposed mechanism of the classical principle of allostery, one of the fundamental concepts in biochemistry [162, 163, 164, 165, 166]. The best theoretically studied example for anisotropic energy transfer along a conserved amino acid network is the PDZ domain [9, 10, 167, 168], which is introduced in this chapter.

2.1 Allostery

The process of information transfer within a protein or more general a biological macro molecule is referred to as allostery, one of the key principles in biochemistry. All processes where an effector at one binding site triggers a function or regulates the protein at a distant site are allosteric in nature. Thus allostery is a intrinsic property of most proteins and a highly studied field [162, 165, 169].

A Classical Understanding of Allostery. The understanding of how information is transferred through a protein started with a pure mechanical and structure-based understanding in the 60s [170, 171]. The classical text-book example for an allosterically regulated protein is hemoglobin. It illustrates the importance and function of allosteric regulation. In hemoglobin—which consists of four sub units, two α-chains and two β-chains—the binding affinity for the native ligand O_2 changes when one binding sites at the heme co-factors in only one of the four sub units is filled. This change from R to T state leads to an increase in oxygen binding affinity and a 1.7 fold higher transport efficiency for oxygen. [172].

The allosteric regulation in hemoglobin was first described with the MWC (Monod-Wyman-Changeux) model [158, 166, 170, 171] which describes a two-state system that is switched by an allosteric effector. As illustrated in Figure 2.1 an allosteric effector induces the change for all sub units. This can be described with a purely mechanistic and structure-based model in which the mechanical force of the conformational change in one sub unit affects the whole protein to change the conformation in every sub unit.
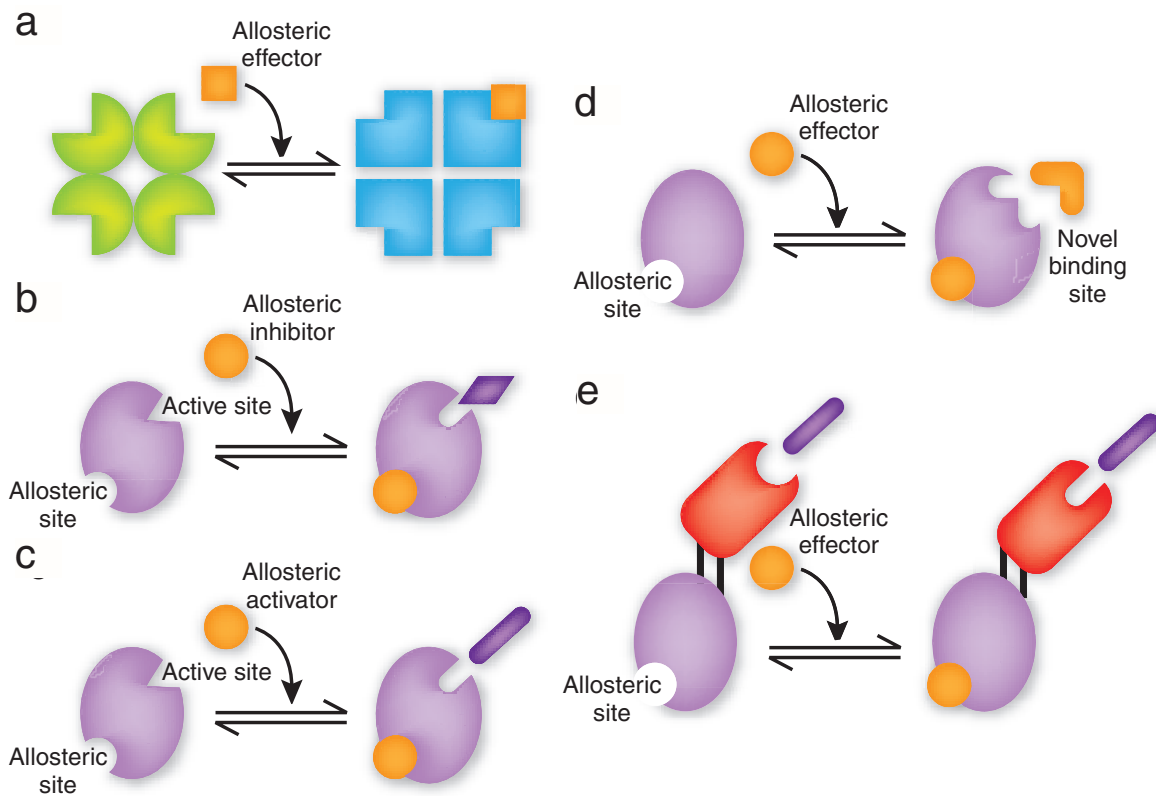
Figure 2.1: Schematic overview of different types of allostery. a) shows the classical MWC model (Monod-Wyman-Changeux), which is also valid for hemoglobin. b) shows how an allosteric inhibitor changes the conformation to reduce binding affinity whereas c) shows the opposite case with an allosteric effector, which enables binding. d) shows how the binding of an allosteric effector at a regulatory side can introduced a conformational change at a distant site which leads to the generation of a novel binding site. e) shows a fusion protein of an allosterically regulated domain and an enzyme, a construct known as allosteric switch as the activity of the enzyme is controlled indirectly by the attached allosteric domain. Reprinted with permission from Macmillan Publishers Ltd: Nature Chemical Biology [166], copyright 2008.

In the last decades the understanding of allosteric regulation expanded from the MWC model and its sequential counterpart known as KNF model on to an understanding of allostery as intrinsic property of dynamic proteins. Not only the direct regulation of enzymes or proteins like hemoglobin, that transport small molecules, is understood and described by allostery but also long-range communication in larger multi-domain proteins becomes a well studied field [165, 169, 173].

Especially in signal transduction it is important to understand how the binding of a small effector molecule starts a cascade of signaling events over hundreds of proteins. Signaling networks are highly studied and full description of cellular communication routes emerge. However the initial step of communication within a single protein domain is not yet understood in all cases. Using small protein-protein-interaction domains as model systems, different mechanism of intra- and inter-domain communication have been proposed [9, 10, 162, 174, 175, 176].
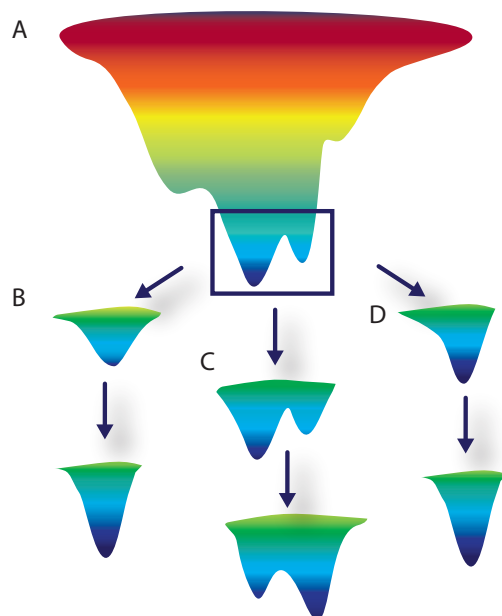
Figure 2.2: Allostery regulation can be understood on the free energy landscape of a protein (a). The protein fluctuates in its ground state and upon ligand binding (indicated by the lower arrows) its conformational distribution is narrowed (b). This is known as induced fit. The protein may also populate different conformation states equally but favor one state upon ligand binding. This is known as conformational selection (c). Combinations where the protein shifts state and is trapped in an energy minimum upon ligand binding are also possible (d).
Figure inspired by [173].

A Dynamic Picture of Allostery.   Along with the understanding of proteins as dynamic entities rather than three-dimensional rigid structures, the description of different conformational states using an energy funnel picture emerged [165, 173, 177]. The concept of energy landscapes is mainly known from protein folding where an unfolded protein samples its conformational space along a reaction coordinate in the energy funnel to a local minimum. This is an intriguing description of a dynamic protein with different functional conformations as well. In this model (sketched in Figure 2.2) a protein is correctly folded in the deepest wells of the funnel but can have different conformational states which are populated with a different probability, a thermodynamic description of the statistical sampling of the low states in a protein's energy landscape. The protein in equilibrium fluctuates and changes between these conformational states. Through an external trigger an excitation such as ligand binding or the hydrolysis of ATP the energy landscape changes. In one case the protein narrows its conformational distribution upon ligand binding, known as induced fit (Figure 2.2 b), in another case the equilibrium between two or more states is shifted towards one favored conformation, known as conformational selection (Figure 2.2 c) or a combination of shifting the energy state and a narrowed conformational distribution is possible (Figure 2.2 d).

The conformational space of a protein is a multidimensional and complex problem and difficult to describe theoretically. To avoid the use of the full energy landscape, treatment of protein dynamics in terms of normal modes has been introduced [148, 155, 156, 158, 178]. Using the normal mode picture another description of allostery can be derived, which can be understood as allostery without conformational change [166, 179]. Normal modes in a protein are either localized vibrational modes or delocalized vibrational modes which may encompass whole protein. If the protein conformation fluctuates and the energy at a given site change this can be understood as energy injection in a localized mode. Using the physical description of intramolecular vibrational energy redistribution or vibrational energy transfer [155, 156, 180] anisotropic energy flow between distant sites in a protein can be understood and related to allostery.

Energy flow in proteins or smaller model systems has been well studied by theoretical models [10, 85, 146, 148] as well as experimentally in model compounds and peptides with ultrafast vibrational

spectroscopy [109, 112, 145, 150, 152, 181, 182, 183, 184]. The experimental investigation of protein fluctuations and the role of protein dynamics in allostery was mainly limited to NMR studies with lesser time resolution [3, 23, 24, 164, 185, 186].

One of the best studied systems for different types of dynamic allostery is the family of PDZ domains. For these systems several simulations have predicted a coupled network of amino acid residues connected by a transfer pathway for anisotropic vibrational energy flow [9, 10, 167, 168]. Experimental insight is provided by NMR studies [187, 188] and the first studies of dynamics related to allostery using optical spectroscopy have been demonstrated lately [189]. PDZ domains and the different types of allostery postulated in these domains are discussed in the remainder of this chapter.
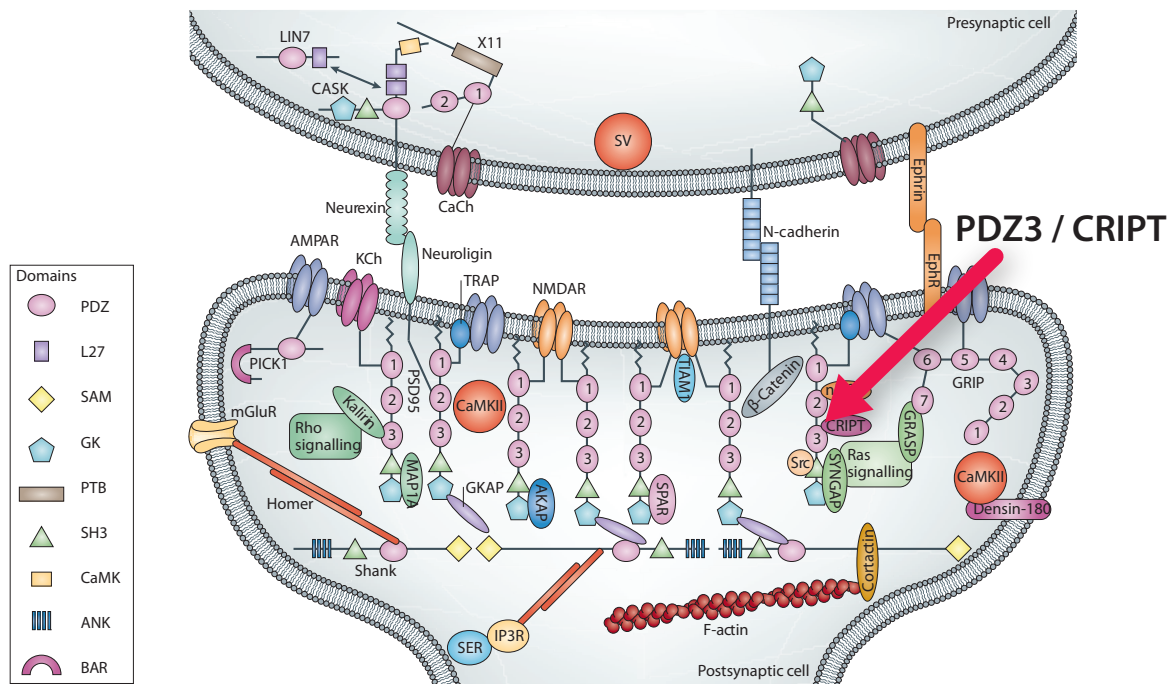
Figure 2.3: Post synaptic density: Organization of protein complexes with focus on PDZ containing scaffold proteins. The arrow indicates the interaction between PDZ3 of PSD-95 with its native ligand, the CRIPT protein. Reprinted with permission from Macmillan Publishers Ltd: Nature Reviews Neuroscience [8], copyright 2009.

2.2 PDZ Domains

The family of PDZ domains (post synaptic density protein-95/disks large/zonula occludens-1) is one of the most abundant and important families of small modular protein-protein interaction domains [187, 190]. Similar modular protein protein connecting domains include the families of PTB domains, SH2 and SH2 domains and WW. PDZ domains can be found in all kingdoms, from bacteria to higher animals. They are normally part of multi domain proteins complexes. Their applications include signaling, scaffolding and trafficking of major protein complexes such as the assembly of the synapse [7, 8, 191, 192, 193]. PDZ domains are classified on the conserved binding motif special for binding the C-terminus of their target protein [190, 194] and show high ligand specificity.

Almost all PDZ domain proteins are found in the cytosol. PDZ is of high importance and very specialized as a main organizing domain of protein complexes at the plasma membrane, including trans-membrane proteins, membrane associated proteins and periplasmic proteins. Functions mediated by protein complexes assembled by PDZ domains include signaling pathways and ion permeability [195]. It was found that even though the main function of PDZ domains is rearrangement of protein domains and scaffolding, e.g. "gluing proteins together" for them to function [196], they might as well be involved in regulation of their target proteins.

The PDZ domain family has be widely studied both theoretically and experimentally. The domain is a prototype for allosteric communication and long range interaction upon ligand binding [157, 186, 197, 198, 199, 200, 201]. The best studied examples include PDZ2 from hPTE1E and PDZ3 from PSD-95. For both domains similar findings have been made but overall it still remains subject of debate how long-range communication and energy transfer is happening in these domains [197].
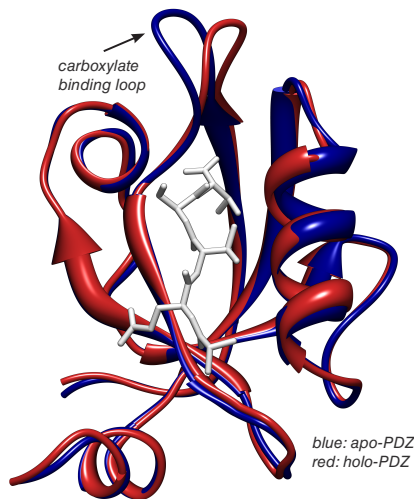
Figure 2.4: Comparison of the structures for apo- and holo-PDZ3 in complex with CRIPT as pentamer (KQTSV). Reproduced in UCSF Chimera [202] using pdb files 1BFE and 1BE9, representing the structure of PDZ 3 as derived from X-ray crystallography [203]. Depicted are only residues 301 to 403, the remaining residues in the pdb file are vector-derived and therefore not part of the canonical PDZ fold. It can be clearly seen that only subtle conformational changes are happening upon ligand binding, especially pronounced in loop 2, the carboxylate binding loop.

Structure of the 3rd PDZ Domain of PSD-95 The 3rd PDZ domain of PSD-95 was the first PDZ domain whose structure was solved using X-ray crystallography by Doyle et al. [203] for the residues 302 to 402. Structures for the apo-protein and holoprotein in complex with the CRIPT peptide as pentamer have been solved (pdb entries: 1BFE (apo), 1BE9 (holo)). The observed globular and compact fold is common to all different PDZ domains and contains six β-sheets plus two α-helices and is shown in Figure 2.4. PDZ3 is different as it has an additional α3-helix, which is unique to this domain and not present in other PDZ domains. The hydrophobic protein core is assembled by two antiparallel β-sheets, forming a β-sandwich. One β-sheet is comprised of β-strands βA, βF, βD and βE. The opposite β-sheet is assembled by βD, βC and βB. The peptide ligand is bound as antiparallel β-strand between βB and αB. These two structural elements form the binding pocket and are connected by the carboxylate binding loop, which displays the sequence Gly-Leu-Gly-Phe (GLGF). PDZ domains have been previously named and described after this conserved sequence (named GLGF repeats). In the carboxylate binding loop the C-terminus of the peptide ligand is bound with high specificity.
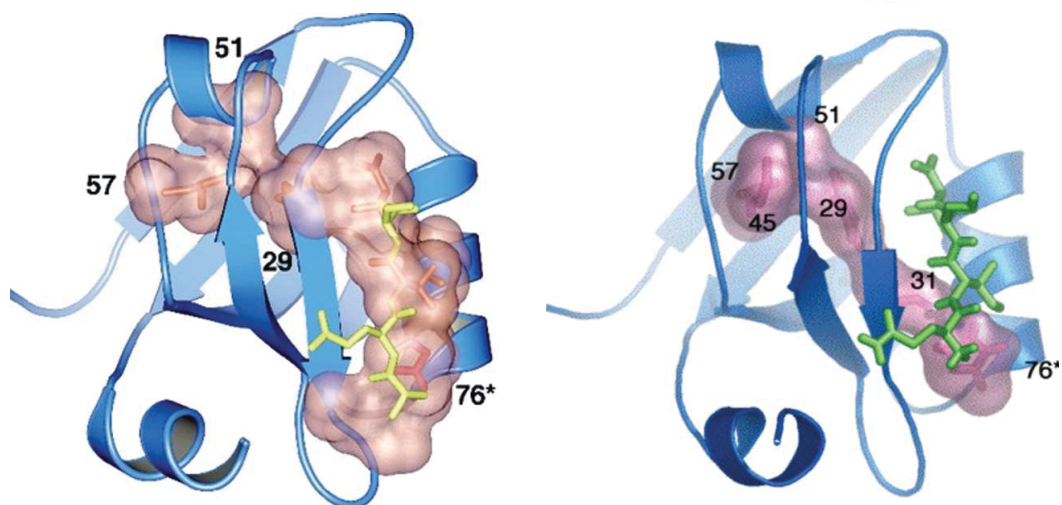
Figure 2.5: The family of PDZ domains was the first where an intramolecular *wire* for information transfer was discovered. Shown are the two mainly discussed amino acid networks in PDZ3, which are derived by independent theoretical approaches. The left shows the initially predicted pathway based on evolutionary conserved residues, which are thermodynamically coupled. This pathway was predicted by Lockless and Ranganathan [9]. The right shows the pathway predicted by Ota and Agard [10], which is derived from a classical simulation of heat transfer in the protein domain. The energy was injected at position His76 and a similar but distinctively different pathway has been found. Figure reprinted from Journal of Molecular Biology [10], Copyright (2005), with permission from Elsevier.

2.3 Energy Flow and Dynamic Allostery in PDZ3

The family of PDZ domains with its important member PDZ3 from PSD-95 is the best studied example for allosteric long-range communication within a single protein domain.

The first investigation of information transfer from the binding site to residues at a distant site in the protein was carried out by Lockless and Ranganathan in 1999 [9]. Using a statistical analysis of a set of more than 250 sequences of PDZ domains they found a conserved set of amino acid residues which are thermodynamically related and named this a energetically coupled pathway of connectivity. The pathway proposed by them starts in the binding groove at His372 and continues along αB, includes the ligand residues which are bound as antiparallel β-sheet and then continues to the distant surface. Based on theses studies, interest in a molecular understanding of information transfer in PDZ domains sparked and several simulations and experiments were performed.

The most intriguing investigation of this information transfer pathway in the picture of vibrational energy flow was carried out by Ota and Agard in 2005 [10] and is shown in Figure 2.6. They performed an anisotropic thermal diffusion (ATD) molecular dynamics simulation, which is a classical treatment of heat transfer through the protein. Instead of the expected finding of redistribution of the injected heat via isotropic diffusion they found a very similar pathway of connected amino acids (the sequence of PDZ3 with residues of the respective pathways indicated is shown in Figure 5.2 in Chapter 5).

This energy transfer pathway functions as a preferred wire for the anisotropic heat transfer through PDZ3 and connects as well the binding pocket starting at His372 with the distant protein surface. In contrast to the pathway predicted by Lockless and Ranganathan the pathway predicted by Ota and Agard is not through the αB helix, which form the binding pocket, but through the ligand

Figure 2.6: Ota and Agard [10] used an approach named anisotropic thermal diffusion and simulated heat transport in PDZ3. This type of simulation is a classical heat transfer simulation similar to related simulations in solids. The protein is treated alone without solvent molecules. They injected heat at position His372 and followed its propagation along a coupled network of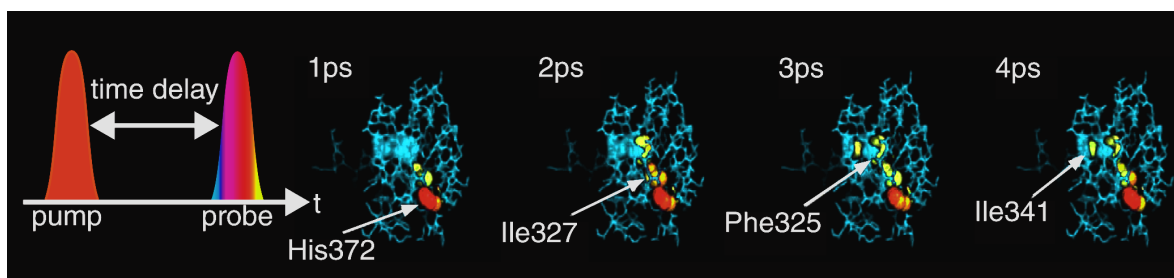 amino acid residues. A pronounced preference for the proposed network was found and no heat transfer to other residues in proximity. The goal of my experimental developments is to design an experiment similar to this simulation. Figure reprinted and modified from Journal of Molecular Biology [10], Copyright (2005), with permission from Elsevier.

to the other side of the binding pocket and then through the protein core. A comparison of both pathways is shown in Figure 2.5. The simulated heat transfer can be understood as vibrational energy flow and occurs (in the simulation) on a timescale of a few picoseconds, which makes it a very interesting subject to be studied by ultrafast vibrational spectroscopy. However the right tools for the site-specific tracking of vibrational energy flow needed yet to be developed [204] (see Chapter 8 and Chapter 9).

Another type of simulation, which is in fact very close to an ultrafast spectroscopic investigation of the proposed pathway, was performed by Sharp and Skinner [167]. They used a pump probe approach in a MD simulation to find a very similar pathway. The problem of intra domain long-range interaction was also tackled by Kong and Karplus, who tested another member of the family of PDZ domains to report as well on a related pathway [168]. Not only for the PDZ domain allosteric pathways have been predicted by theoretical simulations. Other examples include gene regulation factors [205] or Photoactive Yellow Protein [160, 206].

Experimental evidence for the existence of long-range couplings in the PDZ domain family is hard to achieve. Different methodological approaches, including NMR spectroscopy and double mutant cycles for kinetic measurements, have been performed. The experiments focused on the study of the ligand binding dynamics and tried to extrapolate a model for dynamic allostery. Reported experimental results partly show conflicting results, which might be due to different experimental approaches [157, 186, 188, 189, 197, 201, 207]. A different type of long range interaction or allostery than predicted previously has been found by NMR studies [188]. The PDZ3 domain posses a unique αC helix, which is not present in other PDZ domains. It was found, that even though αC does not seem to be involved in ligand binding as judged by the crystal structure, it changes the binding affinity of the PDZ domain for its peptide ligand, indicating an allosteric regulation by the presence of that helix.

The most recent theoretical understanding of PDZ function was presented by Steiner and Caflish in 2012 [208]. They investigated the PDZ3 domain, especially the structure data with and without ligand towards difference and comparison with MD simulations. They state that PDZ3 achieves its ligand binding specificity by conformational selection, as they found three different energy basins for the apo-protein without peptide ligand with only one of the basins being occupied in case of ligand binding. The simulated structure between the three conformations varied by the distance of βB and αB which form the binding pocket. The two structural elements perform a scissor like

motion and the conformation with the shortest distance is the ligand binding conformation. This property of conformation selection makes PDZ3 interesting for studies of ultrafast protein dynamics as well as this kind of conformational fluctuations on the free energy landscape of the protein are in general accessible by 2D-IR spectroscopy.

Part II

Novel Site-Specific Probes for (ultrafast) Infrared Spectroscopy

3 Site-Specific Incorporation of Unnatural Amino Acids

Site-specific reporter groups that are introduced into proteins as side chains of unnatural amino acids (UAAs) provide a new level of spatial resolution for IR spectroscopy because they can carry functional groups with vibrations outside of the congested spectral window of native side-chain vibrations.

Two main approaches of genetic engineering can be distinguished: supplementation based incorporation (SPI) and stop codon suppression (SCS) based methodologies.[1] SPI uses a structural analog for a canonical amino acid whose code is not degenerated (methionine or tryptophan) and uses the native translation apparatus whereas SCS uses an orthogonal tRNA/amino-acyl-tRNA-synthetase pair, which does not interfere with the native translational machinery. Excellent reviews describe the details of each method [78, 80, 81, 209, 210, 211, 212, 213, 214, 215, 216] and Figure 3.1 shows an overview of the two approaches in comparison with native protein biosynthesis. Complementary labeling strategies to attach vibrational probes to proteins and different functional groups which can be used in IR spectroscopy are discussed as well.

3.1 Unnatural Amino Acids as a Tool in Biophysics

During the last decade the field of synthetic biology has emerged. One core discipline is genetic and protein engineering. Proteins with specialized function can be designed and expressed. By using unnatural amino acids which are added to the amino acid alphabet, artificial chemical groups are introduced into protein side chains. [77, 80]. Different unnatural amino acids with infrared sensitive side chains have been demonstrated to be incorporated successfully [79, 217, 218]

This ability to design and produce recombinant proteins with specific function is very promising for the development of novel biophysical tools, not only for IR spectroscopy. Examples for applications of site-specific UAAs in other fields include click chemistry [219, 220, 221], fluorescence spectroscopy or FRET [209, 222, 223, 224] and the incorporation of site-specific spin labels for EPR spectroscopy [225, 226].

A main advantage of using genetic engineering methods over post-translational chemical modifications for sample preparation is that direct co-translational incorporation of a probe during protein biosynthesis yields a recombinantly expressed protein which already contains the label of interest. This makes possible a high labeling yield of the protein sample and there is no need for further purification steps to separate labeled and unlabeled species since the labeling work is done by the *E. coli*. In IR spectroscopy higher specific labeling yield leads to better signal-to-noise ratio and less background contributions from side products.

---

[1]The details of the underlying molecular biology and biochemistry are beyond the scope of this thesis, therefore only a brief summary of the strategies is delivered.
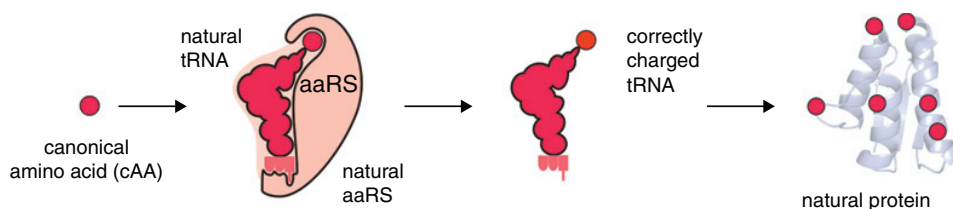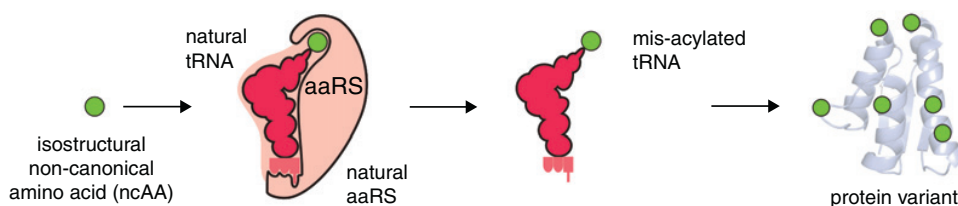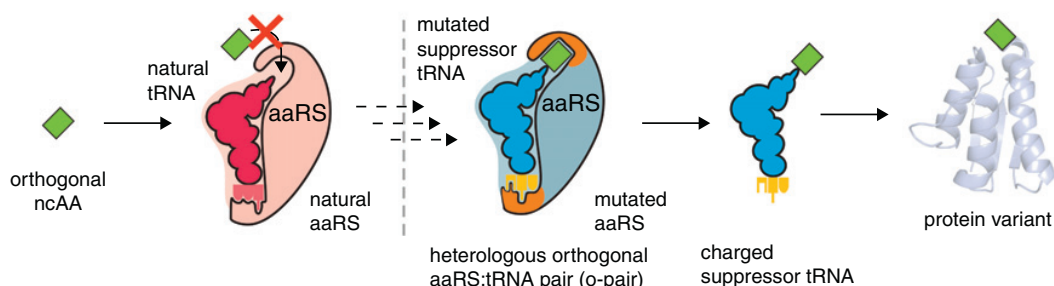
Figure 3.1: For native protein biosynthesis a codon-specific tRNA is charged with the corresponding canonical amino acid by a aminoacyl-tRNA synthetase (a). This results in a correctly charged tRNA, where anticodon and amino acid correspond to each other as written in the genetic code. During translation this charged tRNA is bound by the ribosome and the canonical amino acid is encoded in the expressed protein. To interfere with the native transcription and translation apparatus two general approaches are used. For the supplementation based incorporation method (SPI, shown in b) a proteinogenic amino acid is substituted with an isostructural non-canonical (or unnatural) amino acid, which can be bound by a native tRNA synthetase. This yields a mis-acylated tRNA with a native codon (for either Trp or Met, as those are the only canonical amino acids with a non-degenerated code) but an UAA attached. This tRNA is processed in regular manner during translation leading to a proteome wide substitution of the canonical amino acid to its structural homologue. The stop codon suppression approach (SCS, shown in c) summarizes all techniques which work with an artificial codon or a reassigned stop codon for that an orthogonal pair to tRNA and tRNA synthetase are transformed from another organism. The orthogonal tRNA is loaded by the synthetase, which most often has an engineered binding side for the UAA of interest, and then processes by the ribosome for the codon which is suppressed. This approach leads to incorporation of an UAA only at the position of interest.
Reprinted from [80], Copyright (2012) with permission from Elsevier.

3.2 Supplementation Based Incorporation of UAAs

In the supplementation based incorporation method (SPI) an amino acid is replaced by an isostructural analog during protein biosynthesis in an auxotrophic *E. coli* strain. As one of the proteinogenic amino acids is not synthesized by the auxotrophic *E. coli* it needs to be supplemented into the growth medium. The isostructural UAA is used instead and incorporated at every position in a protein with a codon for the respective proteinogenic amino acid. The SPI method leads thus to a proteome-wide substitution with the used UAA. [80, 212, 227]. For only two amino acids, methionine and tryptophan, an unambiguous genetic code and tRNA/tRNA synthetase pair exist natively. Those amino acids are the main targets for the SPI approach as reported in the literature [80, 212]

In a strain such as *E. coli* B834 for methionine, an isostructural amino acid can be incorporated at every position with a codon for methionine [218]. This type of approach is routinely used in protein expression for X-ray crystallography to introduce heavy atoms (via selenocysteine) for solving the phase problem [227].

Normally an auxotrophic *E. coli* needs to be grown with the missing amino acids supplemented in the growth medium. Several UAAs have been shown to be compatible with the native translation apparatus. To avoid cytotoxic effects of the supplemented UAA the *E. coli* culture is first grown with the proteinogenic amino acid as supplement and only during protein expression the isostructural UAA is supplemented in the growth medium. This approach ensures that bacteria grow normally and all regulatory pathways and the biosynthesis machinery are functioning normally and have methionine at crucial sites incorporated.

The SPI approach is easy to implement in a biochemical laboratory, because it requires only an auxotrophic bacterium, the expression plasmid for the protein of interest and the UAA to be used as supplement. To allow for site-specific and single-residue labeling, the over expressed gene needs to contain no native methionine codon. Because the methionine codon functions as start codon in translation, every protein-encoding gene starts with a methionine codon. The N-terminal methionine is often removed *in vivo*, but to provide a pure sample for 2D-IR spectroscopy, leftover methionine analog at the N-terminus should be removed by cleavage. The construct used for incorporation of Aha during this thesis used a TEV-cleavage side.

Examples for UAAs incorporated using the SPI Approach. Figure 3.2 presents an overview of UAAs which are structural homologues to methionine or tryptophan. Among those that can be incorporated into proteins several are interesting for biophysical applications [223, 228].

The methionine analog Azidohomoalanine (Aha, no. 14), which is used for click chemistry [218, 220, 229], is highly interesting for application in IR and 2D-IR, because it carries an azide group which absorbs at 2100 cm^{-1}. It is one of the best studied UAAs to be incorporated by the SPI approach. Its chemical synthesis is described in [230, 231, 232] and a modified *E. coli*, which can both synthesize Aha and incorporate it into a recombinantly expressed protein has been engineered recently [221]. Aha is one of the novel vibrational probes tested for their application potential in 2D-IR in Chapter 4.

The tryptophan analog Azulenylalanine-alanine (AzuA, no. 35 in Figure 3.2) has applications in studies of vibrational energy flow [112] or FRET [233]. It so far has not been incorporated via SPI directly but there was preliminary success using the SCS method [234]. AzuA is discussed in Chapter 8 and Chapter 9 of this thesis.
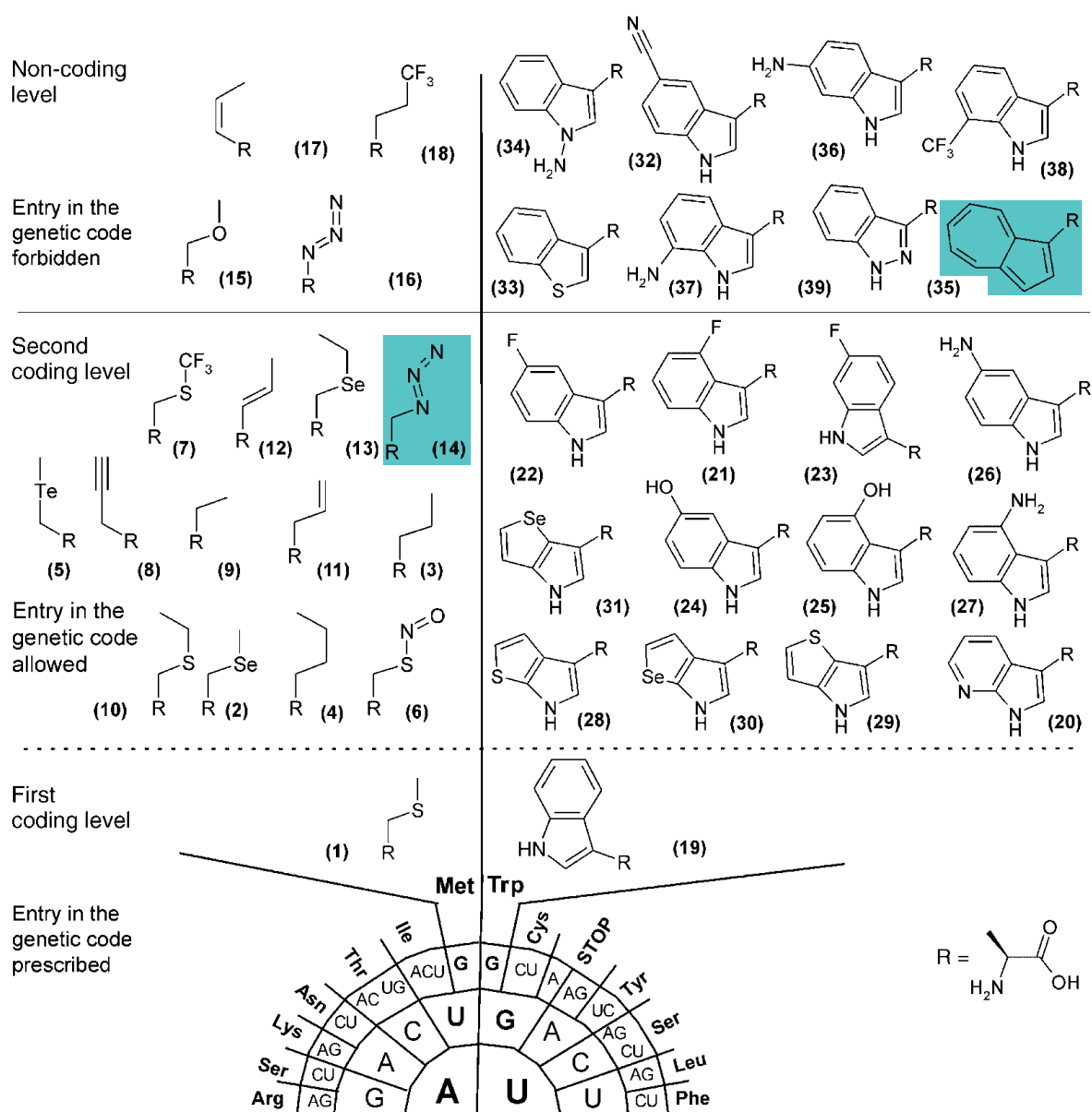
Figure 3.2: Examples of UAAs, which can be incorporated via a supplementation based incorporation approach as surrogates of the canonical amino acids Tryptophan and Methionine. Incorporation into proteins is possible up to the second coding level. For the SPI approach the endogenous translation apparatus is used in an auxotrophic strain. The genetic code for the two amino acids Methionine and Tryptophan is not degenerated (there is only one codon for each of them) as shown in the section of the codon table in the bottom of the figure. The most interesting UAA for IR spectroscopy that can be incorporated this way is Azidohomoalanine. Azulenylalanine, which is used in this thesis as well (see Chapter 8 and Chapter 9) can not be directly incorporated as tryptophan analog.
Reproduced with permission from [212], Copyright 2004 WILEY-VCH Verlag GmbH & Co. KGaA, Weinheim.
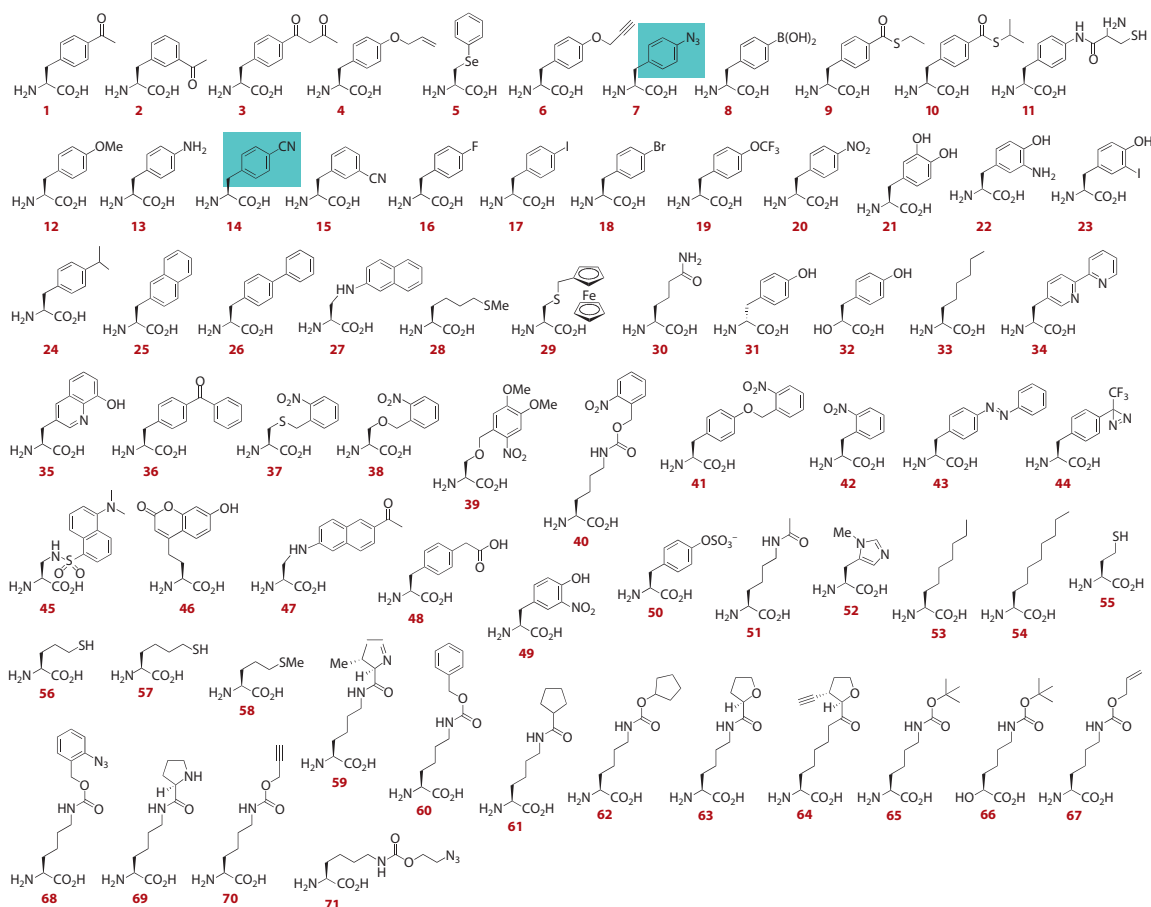
Figure 3.3: Examples of UAAs, which can be incorporated via genetic code expansion using an orthogonal tRNA/aminoacyl-tRNA synthetase pair, e.g. based on the TyrRS from *Methanocaldococcus jannaschii*. Some of those UAAs are interesting for use as vibrational probes in FTIR and 2D-IR spectroscopy. No. 14, Cyanophenylalanine (CNP) has been reported especially for this applications [79] and no. 7, Azidophenylalanine (N3P) are highly interesting for applications in proteins.
Reproduced from [209].

3.3 Stop Codon Suppression based Incorporation of UAAs

The other general approach to incorporate UAAs is the *stop codon suppression* (SCS) also called *suppression based incorporation*. This technique directly interferes with the endogenous biosynthesis machinery at the transcription level as it extends the available genetic code with an additional codon for the UAA that is to be incorporated. The most common implementation is the reassignment of a stop codon to a engineered orthogonal tRNA/tRNA-synthetase pair from another organism. The tRNA carries an anticodon that matches the stop codon to be suppressed and is loaded by the tRNA-synthetase, which is specifically adapted to the UAA of interest (see Figure 3.1 (c)).

An early demonstration of this approach *in vivo* was done by [235], encoding for a fluorinated phenylalanine in *E. coli* by transformation of a yeast suppressor tRNA$^{(Phe)}$ *amber*/phenylalanyl-tRNA synthetase pair. This yielded proteins with up to 75 % successful incorporation of the target UAA. The remainder was expressed with structurally related canonical amino acids.

The principle of using a native stop codon (in this case the *amber* codon UAG) and reprogramming

the intracellular translation machinery to read through this codon instead of terminating the protein biosynthesis was improved dramatically since then [209, 210, 213, 236, 237]. It generally works because in *E. coli* the *amber* codon is not used to the same extent as the other two stop codons. A major step towards better incorporation yields is the use of specifically engineered derivatives of orthogonal tRNA/tRNA synthetase pairs, with tRNA$^{(Tyr)}$/Tyr RS from *Methanococcus jannaschii* [78, 210] being the most prominent example.

Other than the native *amber* codon, quadruplet codons are another approach of extending the genetic code. The first demonstration was the use of AGGA as codon in combination with the tRNA$^{(Lys)}$/Lys RS pair from *Pyrococcus horikoshii* [214, 238, 239]. The discovery of the native pathway for the incorporation of pyrrolysine as 22nd proteinogenic amino acid in *Methanosarcina barkeri* by *amber* codon suppression [240] made the corresponding tRNA/tRNA synthetase pair (which is orthogonal to *E. coli*) another much used tool for the genetically encoded incorporation of UAAs with aliphatic side chains [216, 239, 241, 242].

To have acceptable expression yield and accuracy when incorporating a specific UAA into a protein, the tRNA synthetase needs to be optimized. This is achieved by evolving the binding side through repeated mutagenesis of residues in the substrate binding pocket. Positive and negative selection circles are then required until a mutant of the specialized tRNA synthetase with appropriate properties is found. The orthogonal tRNA and optimized tRNA synthetase are transformed in an *E. coli* expression strain and tested for compatibility with its transcription and translation machinery. The additional UAA has to supplemented in the growth medium. Recent approaches from molecular biology include engineering a bacterium with the ability to not only incorporate and cope with the additional UAA but also with its new biosynthesis pathway [243]. The SCS approach has not only been demonstrated in *E. coli* but was also successfully shown to work in higher organisms such as *Saccharomyces cerevisiae* [213, 241] or even mammalian cells [244].

Examples for UAAs incorporated using the SCS Approach. Figure 3.3 summarizes the set of UAAs for which incorporation with a SCS approach has been demonstrated [209].

More than 70 different chemical compounds were incorporated as UAAs, some of them of interest to IR spectroscopy. Cyanophenylalanine (CNP, no. 14 in Figure 3.3) was the first UAA introduced specifically as IR reporter group [79], but results from Chapter 4 show CNP is of limited use. Until now only a few applications for CNP in proteins for IR spectroscopy have been demonstrated [79, 245, 246, 247, 248].

Another interesting UAA is Azidophenylalanine (N3P, no. 7 in Figure 3.3). The incorporation was first demonstrated by [217] and some applications in IR spectroscopy of proteins have been demonstrated since then [82, 83, 136, 249].

Both CNP and N3P are tested in this thesis for their usage as vibrational probes in 2D-IR spectroscopy of proteins.

3.4 Potential Functional Groups as Probes for IR Spectroscopy

Many candidates for novel probes for IR spectroscopy of proteins exist beyond the UAAs discussed. Several different functional groups have been tested and there is a huge body of related work in the recent literature [75, 76]. In Table 3.1 an overview of potentially useful functional groups with their spectral absorption windows are listed. Most of them have been reported and tested for FTIR or 2D-IR spectroscopy in model compounds but not in proteins. Not all of them can be incorporated as side chain of UAAs, but several other approaches for their introduction into proteins are known and

group	structure	$\bar{\nu}$ (range)	Intensity
Azide	$R-N_3$	$2050\ cm^{-1}$–$2120\ cm^{-1}$	strong
Alkine	$R-C{\equiv}C-H$	$2120\ cm^{-1}$	weak
Nitrile	$R-C{\equiv}N$	$2250\ cm^{-1}$	medium
Carbon-Deuterium	$R-C-D$	$2100\ cm^{-1}$	weak
Isocyanate	$R-N{=}C{=}O$	$2230\ cm^{-1}$–$2280\ cm^{-1}$	strong
Cyanate	$R-O-C{\equiv}N$	$2130\ cm^{-1}$–$2260\ cm^{-1}$	medium
Thiocyanate	$R-S-C{\equiv}N$	$2130\ cm^{-1}$–$2170\ cm^{-1}$	medium
Isothiocyanate	$R-N{=}C{=}S$	$2030\ cm^{-1}$–$2200\ cm^{-1}$	strong
Thiol	$R-S-H$	$2580\ cm^{-1}$	weak
Metal-Carbonyl	$R-Re-(C{\equiv}O)_3$	$2000\ cm^{-1}$–$2100\ cm^{-1}$	very strong
	$R-Ru-(C{\equiv}O)_2(OH)_3$		

Table 3.1: Functional groups with vibrational absorption bands in the biomolecular free window between $1800\ cm^{-1}$ and $3000\ cm^{-1}$.

used. Some of them yield site-specific probes as well. Those include mainly chemical modifications of the purified proteins.

Isotopes of Carbonyls. One of the most common approaches in traditional FTIR spectroscopy is the introduction of isotope labels for a specific amino acid species during protein expression by using an isotope labeled precursor or amino acid in the growth medium. This is generally a good approach to help with assignment of vibrational modes, e.g. in case of a C=O group the difference between the natural isotope $^{12}C^{16}O$ and heavy isotopes like $^{13}C^{16}O$ or $^{12}C^{18}O$ leads to a wavenumber shift of about 2.2 % to 2.5 % to lower wavenumbers (for the Amide I region this means a shift from $1650\ cm^{-1}$ for natural isotopes to $1613\ cm^{-1}$ for $^{13}C^{16}O$ [62, 63]). This spectral shift can be used to analyze the change in vibration of a single labeled, site-specific oscillator separated from the main vibration. The main drawback of this approach is that all amino acids of the same type are labeled unless the sample is prepared by full synthesis. A huge body of work analyzing peptide and protein folding and protein function that uses isotope labeling exists. (e.g. [62, 63, 69, 114, 250])

Carbon-Deuterium Groups. Other novel probes are C−D modes [108, 251, 252, 253, 254], which can only be incorporated site-specifically by full synthesis of the protein samples. C−D modes absorb at $2100\ cm^{-1}$, thus the absorption bands are well separated from other protein bands. Their spectral characteristics have been investigated in detail in single amino acids and in proteins [108, 251, 252, 253, 254]. They are exceptionally noninvasive to the protein structure [255]. Their major drawbacks are that the achievable size of the protein system is limited because full chemical synthesis is needed and that the ε for the C−D stretch vibration is relatively small so that high sample concentrations are required.

Metal Carbonyls. This is yet another type of site-specific label which fulfills the requirement of high oscillator strength exceptionally well, but which is not derived from a native precursor class of molecules was the first to be studied in great detail by 2D-IR [46, 86, 120, 142, 256]. Both the Zanni and the Kubarych group gained insights into protein solvation and dynamics using a metal carbonyl attached e.g. to a histidine side chain. [137, 138, 257]. This is despite the fact that metal carbonyls

can be very invasive to the native protein structure.

Thiocyanate.   SCN has an absorption band well within the free spectral window, at 2150 cm^{-1} allowing for applications both in H_2O and D_2O. Thiocyanates can be created from cysteines in a two-step chemical reaction [258, 259, 260]. The advantage of this approach is that conventional sample preparation protocols can be used, and high protein expression levels are expected. However, the post-translational chemical modification has certain drawbacks in contrast to the newer approaches of using UAAs. When site-specific resolution is desired, only one cysteine can be present in the protein of interest. Additionally, a SCN group is not very stable (hydrolysis within a few days was reported in [258]). Furthermore chemical reactions never yield 100 % labeling. Depending on the sample conditions, much lower labeling yields have to be anticipated and by-products are difficult or impossible to separate. SCN is an important site-specific vibrational probe, because of its high electric field sensitivity. It can be used for direct measurements of the electrical field in proteins via Stark spectroscopy [84, 261, 262, 263, 264].

The approach of SCN labeling was tested in our group and is reported in the Bachelor thesis of Daniela Kern-Michler [265], which was supervised by the author but is not covered here. In addition to the development of a labeling protocol and detailed characterization of the SCN label by steady-state FTIR spectroscopy, we performed ultra-fast experiments (transient IR and 2D-IR measurements) on Methyl-Thiocyanate and SCN-labeled Hemoglobin, the results of which are reported in [260].

Other Chemical Groups.   Beside the discussed candidates for novel vibrational probes other functional groups might be useful based on their absorption frequency and (expected) extinction coefficient. Those include (but are not limited to) Alkines, which can be incorporated into proteins using an approach similar to Aha and which are among the best studied UAAs due to their wide applicability in click chemistry [219, 220, 266, 267]. But in contrast to azides or nitriles the expected signal intensity is weak.

Cyanates (OCN) and Isocyanates (NCO)have been studied in model compounds using 2D-IR and might be useful for protein studies as well [76, 268]. The natively present Thiol group (SH) is only a weak vibrational oscillator but was previously used in a proof-of-principle experiment as local probe in protein in IR spectroscopy [269].

4 Experimental Characterization of Azide- and Nitrile-Containing Unnatural Amino Acids

As outlined in the motivation and Chapter 3, unnatural amino acids carrying an azide (N_3) or nitrile (CN) group in their side chains make promising candidates for novel vibrational probes to be used for 2D-IR spectroscopy of proteins. Before those can be applied to study protein dynamics, the UAAs need to be thoroughly characterized to identify a suitable and versatile probe. Different influences on the vibrational lifetime and line shape need to be studied on the UAA alone to gain meaningful insights into protein dynamics when it is applied as site-specific probe.

An ideal probe should fulfill a wide range of specifications beside its spectral features, including photo stability and usability in different biologically relevant solvents. This chapter summarizes experiments conducted in search for a novel probe and discusses results on the UAAs azidophenylalanine (N3P), azidohomoalanine (Aha/N3A)[1], cyanophenylalanine (CNP) and cyanoalanine (CNA).

4.1 Introduction

A huge body of work is currently dedicated to the testing of novel vibrational probes for 2D-IR spectroscopy, including unnatural amino acids (reviewed in [75, 76]). The group of Peter Schultz suggested to use cyanophenylalanine (CNP) as genetically encoded, site-specific probe for IR spectroscopy and demonstrated the successful incorporation into myoglobin. They reported FTIR absorption spectra with reasonable extinction coefficient [79] and were able to also show that their myoglobin mutant, with CNP replacing the distal histidine, was still functional as shown by UV/Vis and FTIR spectroscopy of the mutant with and without CO ligand. Unfortunately I was not able to reproduce their results on myoglobin (see my diploma thesis [270]) and that initiated the search for other probes for 2D-IR spectroscopy. Several other groups in the 2D-IR and FTIR community work as well on testing and characterizing novel vibrational probes (as summarized in Chapter 3).

In this thesis several candidates of novel probes with special focus on azide- and nitrile-containing amino acids are compared. All are either aliphatic or aromatic amino acids with terminal nitrile or azide groups, derivates of either phenylalanine or alanine. Their spectral characteristics are investigated and reported in this chapter. The best candidate for application in proteins is identified. The tested candidates can either be incorporated by amber codon suppression as demonstrated for CNP and N3P [79, 217] or using the supplementation based approach as shown for Aha/N3A [218]. To complete the set of structurally related amino acids cyanoalanine (CNA) was tested additionally as aliphatic nitrile.

Azide and nitrile groups are well-studied by IR spectroscopy [43, 271, 272]. The absorption frequency for the azide stretch vibration is expected around $2100 \, \text{cm}^{-1}$ and the absorption frequency for a nitrile around $2200 \, \text{cm}^{-1}$ [273]. Both are reported to show a pronounced solvatochroism, which

---

[1] note that in this chapter azidohomoalanine was used in its boc-protected form for most experiments and this therefore abbreviated N3A in contrast to later chapters; the abbreviation Aha refers to the unprotected free amino acid.

makes them especially favorable as reporters of the local protein interior [274, 275, 276, 277, 278, 279].

In case of nitriles this effect has been known for very long [280, 281, 282]. The Gai group was the first to realize and demonstrate the major potential of using a nitrile group as reporter of a biomolecular environment [271]. In a series of experiments they demonstrated the huge sensitivity of the nitrile stretch vibration to the polarity of its solvent surrounding (using THF and H_2O as pure solvents as well as mixtures). In a first application to study a biologically relevant effect, they investigated the binding of a peptide to its receptor and were able to show that the IR frequencies indeed showed a shift as expected for a change towards a less polar environment. This effect of sensitivity to the surrounding electrostatics has been studied since to a great extent and also been utilized in Stark spectroscopy of proteins [84, 283, 284, 285]. Also nitriles have been used in several recent 2D-IR studies. The high sensitivity of the absorption band to solvent changes or hydrogen bonding and unbonding allows experiments like EXSY-2D-IR [52, 286]. Not only as site-specific reporter group incorporated into the peptide or protein chain [52, 248] nitriles were used in 2D-IR experiments, but also medically relevant ligands with nitrile groups served as insightful reporters of ultrafast equilibrium dynamics [287, 288]. A good review on the application of the nitrile stretch vibration as IR reporter group to study biomolecules is given in [52, 281].

As the azide stretch vibration is known to have a higher extinction coefficient than a nitrile or a thiocyanate stretch vibration, azide are especially interesting for 2D-IR applications. The first testing of an azide-derivatized amino acid to be used in proteins was carried out by Minheang Cho's group [274]. They tested the alanine-derivate β-alanine for its usability as vibrational reporter in comparison to an aliphatic nitrile and thiocyanate and found its extinction coefficient to be more than a 10 times higher for the azide than for the nitrile. Their experiments indicate a clear and similar correlation between the absorption frequency and the polarity and/or hydrogen-bonding property of the solvent with the azide frequency showing a similar blue-shift upon switching from a nonpolar solvent to H_2O. Later theoretical and experimental descriptions showed, that azides have a more complicated solvatochroism than nitriles [276, 278, 279], however they serve as very sensitive reporters of hydrogen-bonding. Especially the aliphatic azide azidohomoalanine was studied in detail [275, 289], because of the previously described relatively simple approach for incorporation into a protein [218]. Other azides proposed for usage in proteins include azidoproline [290] and azidophenylalanine [82, 83]. Generally a good introduction and review of recent developments in using site-specific probes in FTIR and 2D-IR spectroscopy is given by [75, 76].
A versatile vibrational probe for usage in proteins should fulfill the following requirements:

A High Extinction Coefficient.   A huge ε will allow for high signal strength at reasonable sample concentrations still operable with protein samples. Vibrational modes, which were investigated in the first 2D-IR experiments, including carbonyl oscillators [42, 46, 47, 95, 291, 292], have extinction coefficients around $1000 \, M^{-1} \, cm^{-1}$ leading to good signal size and reasonable signal to noise ration (SNR) for samples with sub-millimolar concentration, as required in 2D-IR studies of protein dynamics. Examples include e.g. studies of peptide and protein folding [113, 117]. In FTIR absorption spectra the signal size of an absorption band scales linear, whereas in 2D-IR spectra the signal size is proportional to the squared extinction coefficient. Therefore a high oscillator strength, reflecting a strong transition dipole and high extinction coefficient is crucial for a novel vibrational probe to be applied in proteins. If ε is twice as large that allows samples to be four times less concentrated, making 2D-IR experiments of proteins more feasible.
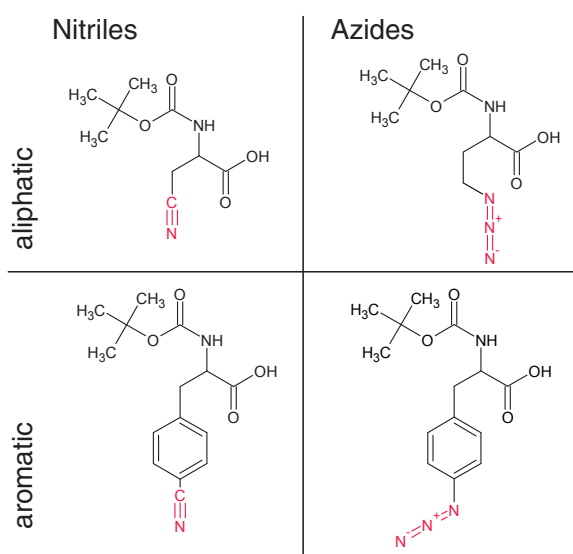
Figure 4.1: Structures of the four amino acid candidates tested in this thesis. The focus is on azides and nitriles, both aromatic and aliphatic. All structures are depicted in their boc-protected form, which has the advantage, that the system contains a peptide bond. The molecules are cyano-alanine (aliphatic nitrile), cyano-phenylalanine (aromatic nitrile), azidohomoalanine (aliphatic azide), and azidophenylalanine (aromatic azide).

Spectral Congestion. The absorption frequency of the functional group in the UAA should be separated from normal protein vibrations and ideally be in the biologically free window between $1800\,\mathrm{cm}^{-1}$ and $3000\,\mathrm{cm}^{-1}$. Oscillators natively present in proteins lead to spectrally crowed absorption spectra because of their overlap, especially in the amide regions (see Motivation). A new spectral label needs to be separated from those natively present absorptions to allow for studies with spatial resolution on side chain level. Several different functional groups are in principle suited to be used as vibrational probes are reported in Chapter 3.

Solvent Compatibility and Low Background. Application both in H_2O and D_2O. These are the major solvents for the investigation of proteins. H_2O is preferable because no re-buffering and difficult sample preparation is needed. However it is as well important to have a *Novel Probe*, which can be used in D_2O, because it might be interesting to do experiments, where one wants to measure signals of the backbone. Changes of the backbone are reflected by the amide I and amide II signals, comprised of contributions from the peptide bonds. Those bands are not accessible in H_2O because of the high solvent absorption. Regular FTIR spectroscopy of proteins therefore is normally performed in D_2O. Time-resolved 2D-IR measurements dedicated to study the coupling of a *Novel Probe* to vibrational modes of the protein backbone or monitor changes of the protein secondary structure on the vibration of the *Novel Probe* have to be carried out in D_2O.

Incorporation Protocol. The incorporation of a *Novel Probe* should be easy to achieve and not need difficult molecular biology or other expression systems than standard recombinant expression in *E. coli*. Possible incorporation strategies using latest developments from chemical biology are briefly described in Chapter 3. A relatively easy implementation of a labeling protocol is important, because proteins for 2D-IR must be produced in high yield with resulting protein mass of some mg to have sufficient protein amounts for 2D-IR measurements. Additionally a protein of interest needs to be very stable to reach protein concentrations in the mM range. Even more important is that the incorporation approach needs to yield high labeling percentages and ideally should allow to prepare protein samples with single incorporation sites.

Photostability. Not only equilibrium 2D-IR studies are aimed for with a labeled protein sample but as well transient IR and transient 2D-IR spectra might be interesting. Especially when the studied protein is a photo receptor. Then it is necessary that the novel probe is stable upon visible excitation. For example this would be the case for a study in myoglobin where the carbon monoxide ligand can be excited and removed from the binding side by 530 nm light (as used in the 2D-IR study by [47]) or in a photoreceptor like proteorhodopsin with the excitation wavelength of approx. 525 nm [68] or in the small photo receptor PYP with the low excitation wavelength of around 450 nm [293]. This is especially important to be tested on the azide containing UAAs as azides are used traditionally in photocrosslinking studies of proteins [294, 295]

Vibrational Life Time, Anharmonicity and Sensitivity to the Surrounding. The vibrational lifetime is a crucial information about a novel probe because it determines the time window that can be accessed using the new label. The anharmonicity is another important characteristic of a vibrational probe, as it determines the splitting between the negative and positive contributions to a 2D-IR spectrum by the excited state absorption (ESA) and the combination of stimulated emission (SE) and ground state bleach (GSB). Of major importance for applications in proteins is a pronounced sensitivity to the environment of the studied vibration. Given that azides and nitriles are very sensitive reporters of their local environment it is to be expected that their 2D-IR spectrum shows possibly strong spectral diffusion. This means for short waiting times the diagonal peak is elongated along the diagonal, which reflects the inhomogeneity of the local surrounding. With increasing waiting time the environment fluctuates and the inhomogeneity vanishes, leading to the 2D-IR diagonal peak becoming less elongated along the diagonal or even circular.

4.2 Experimental Design

The following experiments have been conducted with the four proposed candidates CNP, N3P, N3A and CNA. The experimental conditions are mentioned in the figure captions, details about the experimental setup for the ultrafast measurements can be found in Appendix A and details on the quantum chemical calculations in Appendix C.

Solubility Test. Every amino acid was tested towards its solubility in different solvents, those included H_2O (or NaOH to enable solubility), DMSO, THF, CCl_4, $CHCl_3$ and C_2H_3N. For this the boc-protected form of all the amino acids was used.

Extinction Coefficient and Solvatochroism. For the four amino acids candidates concentration-dependent FTIR absorption spectra in the solvent tetrahydrofuran, which is a good mimic for the protein interior [271], have been recorded. Of the three best candidates also FTIR absorption spectra in aqueous solution have been measured to monitor the influence of the solvent on the absorption frequency.

DFT Calculations. Of all amino acids DFT calculations to assign the recorded FTIR spectrum, have been carried out using different complex basis sets to allow for a detailed assignment (see Appendix C for computational details). It is not easy to do an unambiguous assignment of all characteristic modes, even with the help of DFT calculations. Especially difficult and partly misleading is the assignment for the aromatic amino acids CNP and N3P. More details on how to use

experimental results from ultrafast IR spectroscopy for unambiguous assignment can be found in Chapter 7.

Illumination test to monitor Photostability.   Of both azide-containing amino acids N3A and N3P, UV/Vis spectra were measured to monitor long-term stability upon visible radiation using a high-power LED. Its crucial to determine the photo stability, especially of the azide-derivates, because azide containing compounds are often used in photo-crosslinking, to ensure a broad applicability for the novel probe in different ultrafast experiments.

Vibrational Life Time and Anharmonicity.   Of the three amino acids with a high enough extinction coefficient for applications in proteins ultrafast broad band IR spectra have been recorded. The first measurement for the three remaining label candidates (N3A, CNP, N3P) was the determination of the vibrational life time and the anharmonicity in the example solvent THF.

Transient IR Spectra and 2C-2D-IR of Aha and N3P.   For the three remaining candidates transient IR data with pumping the absorption serving as a probe have been recorded for the full spectral window covered by the FTIR. Of the two azide-containing amino acids Aha and N3P full data sets of 2C-2D-IR spectra for different waiting times have been recorded. The 2C-2D-IR approach is an technique used in our group to measure cross peaks between separated absorption bands, utilizing two independent optical parametric amplifiers to allow for disentangled light sources for pump and probe beam. Using independent pump and probe light sources it is possible to access not only diagonal peaks in a 2D-IR spectrum but as well cross peaks, which are separated by some hundred wavenumbers. See Chapter 1 for details. This experiment is important to see the influence of couplings between the novel probe and e.g. CO oscillators of the peptide bond for planned studies of protein structural dynamics.

2D-IR to monitor Spectral Diffusion.   The diagonal peak of the azide or nitrile group in the 2D-IR spectrum was measured for different waiting times with high spectral resolution. These data allow for the determination of the spectral diffusion characteristics, which is a mandatory prerequisite for application of the respective UAA in proteins. Of the best candidate, Aha, the spectral diffusion in H_2O has been tested as well, because this is the solvent crucial for application of the proposed label in proteins.

4.3 Results and Discussion

In the following all experimental results are described and discussed with focus on identification of the most versatile novel vibrational probe to be applied for protein studies (those are described in the following chapters). The main result of the investigation is the finding, that Aha has the best combination of properties to be used in proteins, but the other candidates have application potential as well.

4.3.1 FTIR and UV/Vis Spectra, Extinction Coefficients, and DFT Calculations

In Figure 4.2 the FTIR spectra of the four investigated candidates are depicted. Two things can be recognized at first glance: The nitrile containing amino acids have a lower extinction coefficient than the azide-containing amino acids and the aromatic amino acids show a higher extinction
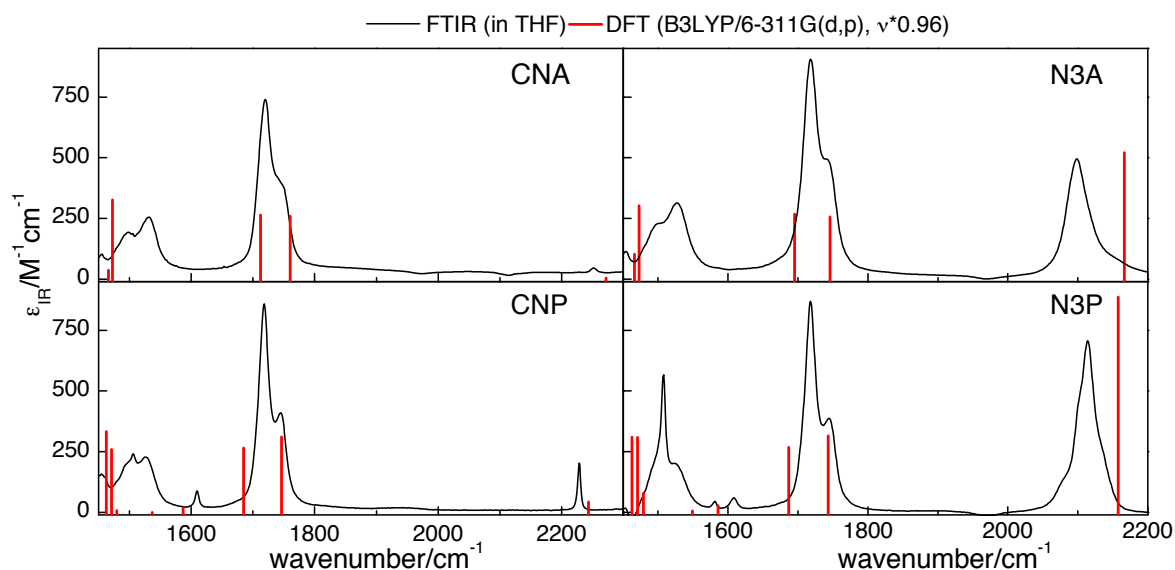
Figure 4.2: FTIR spectra with results from DFT calculations for all four investigated label candidates. All spectra are measured in THF and show the extincting coefficient. To calculate the extinction coefficient accurately experiments with different concentrations have been measured. Solutions of 100 mMstock per molecule were prepared and measured against THF (99.9%, Sigma-Aldrich, anhydrous, inhibitor-free) as background. Experiments were performed using a Bruker Tensor FTIR spectrometer, equipped with DTGS detector, in a sample cell as described in [296] with spacer thickness of 50 μm. DFT calculations have been performed using Gaussian09 [297], results are scaled by a factor of 0.96 [298], see Appendix C for more details.

coefficient than the aliphatic amino acids with the same attached group. Cyanoalanine has the lowest extinction coefficient of the investigated label candidates of approx. $18\,M^{-1}\,cm^{-1}$ and a very narrow line width. Overall the integral of the aliphatic nitrile stretching vibration is very small, indicating a small transition dipole moment, which excludes cyanoalanine as novel probe in proteins. The obtained center frequency for CNA in its boc-protected form at $2251\,cm^{-1}$ in THF matches the previously reported value of $2252\,cm^{-1}$ for the Fmoc-protected molecule [271]. A value for ε is not reported in the literature.

Azidohomoalanine as the aliphatic azide has an extinction coefficient of $506\,M^{-1}\,cm^{-1}$ in THF and a reasonably narrow line width. The extinction coefficient for the azide stretch in Aha is a bit lower than the observed one for the amide I vibration, which shows two distinct absorption bands for the two carbonyl oscillators present in the test molecule Fmoc-Aha. The obtained center frequency of $2099\,cm^{-1}$ for the azide stretch vibration in THF matches reported values, whereas the extinction coefficient was up to now reported differently, with values ranging from about $300\,M^{-1}\,cm^{-1}$ [139] in THF to $1570\,M^{-1}\,cm^{-1}$ in H_2O reported by [289], with which we disagree (see Chapter 5 for the values in H_2O as well as [299] for a detailed report on the experiments for determination of the extinction coefficient).

In CNP the line width is smaller than for Aha but the extinction coefficient is bigger than for cyanoalanine. The extinction coefficient is approx. $194\,M^{-1}\,cm^{-1}$ for the boc-protected derivate in THF. The extinction is much smaller than the amide I mode but more than 10 fold higher than for cyanoalanine. The value for ε is of the same magnitude than reported by [271] who found $220\,M^{-1}\,cm^{-1}$.

For N3P the biggest extinction coefficient is found of all investigated attached groups. The

aromatic azide stretch vibration has an extinction of $736 \, M^{-1} \, cm^{-1}$. The extinction coefficient for the azide moiety is approx. the same as for the amide I vibration. The line width is comparable to the aliphatic azide in Aha. For the ε of the azide stretch vibration of N3P not values have been reported in the literature so far. In comparison to CNP in N3P an additional absorption band in the ring mode region around $1600 \, cm^{-1}$ was found, which is confirmed by the DFT calculations and was contributed to a degeneration and splitting of the ring vibration.
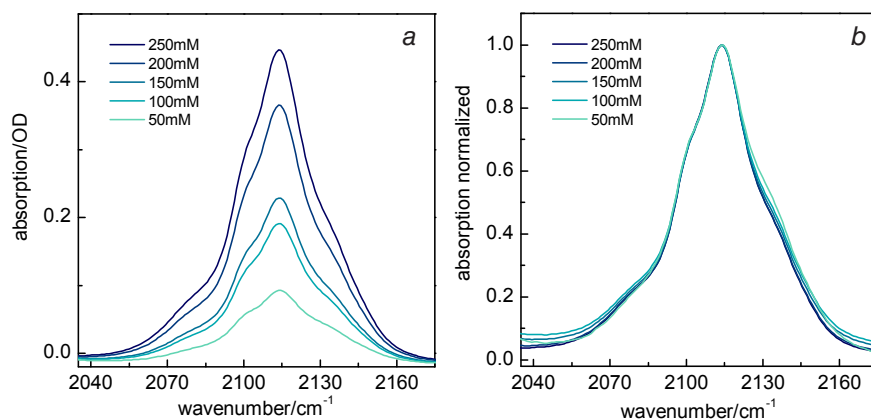
Figure 4.3: Concentration dependent FTIR absorption spectra of the azide stretch vibration in N3P in THF. Data were recorded on a Bruker Tensor FTIR using a DTGS detector and a cuvette with $50 \, \mu m$ path length

In N3P a disturbance of the line shape for the azide stretch vibration is observed. All other tested molecules posses a symmetric line shape with only one absorption band. In case of N3P about four sub bands can be observed in the azide stretch vibration (as can be seen in in more detail in Figure 4.3). The presence of sub bands in the azide absorption can be explained by a Fermi Resonance (possibly between the symmetric stretching of the azide at $1200–1300 \, cm^{-1}$ with aromatic C−H deformation at $800 \, cm^{-1}$) [300], because the splitting into sub bands vanishes upon isotope substitution [301]. In Figure 4.3 concentration-dependent FTIR spectra of N3P in THF are shown. The line shape indicating at least four sub bands is consistent for all concentrations, as can be very well seen in Figure 4.3 b for the normalized spectra. This excludes concentration effects as source for the complicated line shape of the azide stretch vibration in N3P.
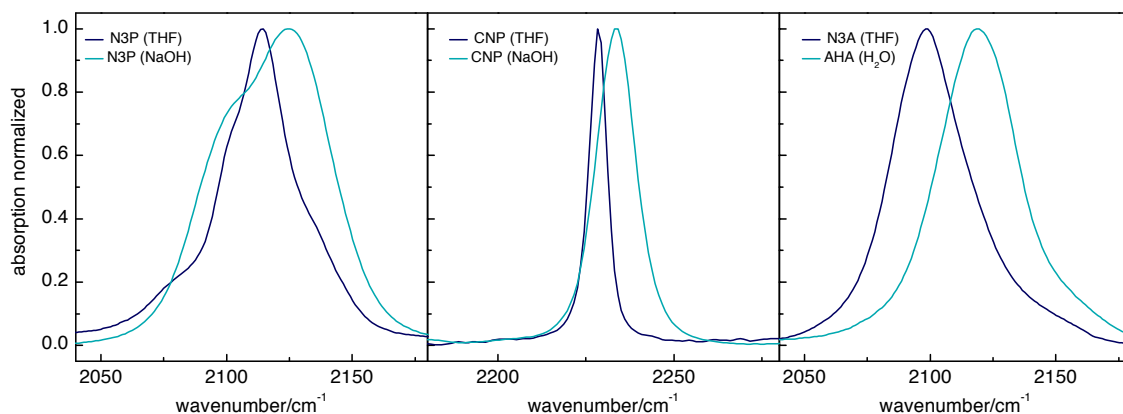
Figure 4.4: FTIR spectra for N3P, CNP and N3A in THF and aqueous solution in comparison. Spectra are measured under different experimental conditions and therefore only the normalized absorption bands are shown. As the boc-protected derivates of azido- and cyano-phenylalanine are difficult to solve in pH-neutral H_2O, those have been measured in NaOH (under basic conditions).

To investigate the previously reported sensitivity of the azide and nitrile groups to the surrounding solvent environment also FTIR absorption spectra in aqueous solution have been measured of N3P, CNP and N3A. Those are shown in Figure 4.4. For all three tested UAAs a blue-shift of the center frequency of either the nitrile or the azide stretch vibrations is observed, which is in agreement with reports from the literature [52, 254, 275, 279, 281, 286, 289]. For N3P and CNP a pronounced effect on the line width included by the more polar and hydrogen-bonding environment in H_2O can be clearly observed, which is not as distinct in N3A. But also for the aliphatic azide stretch vibration a broadening in H_2O occurs, which is analyzed and discussed in more detail in Chapter 5. For N3P the line shape of the azide stretch absorption is not as disturbed in H_2O as in THF, which might explain the misinterpretation that the sub bands are induced by the surrounding (solvent or protein) or why a Fermi Resonance for this molecule was ignored by part of the literature for experiments conducted in H_2O [249].
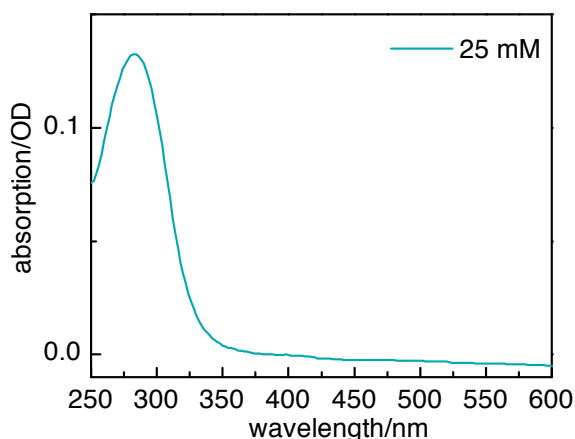
Figure 4.5: UV/Vis absorption spectrum of Aha in H_2O recorded using a Jasco V670 UV/Vis spectrometer. Samples with varying concentrations were placed in a cuvette with path length of 1 cm, which had an optical transparency starting at 250 nm

Amino acids containing azide groups in their side chain are commonly used in click-chemistry and photocrosslinking of proteins [220, 294, 302, 303, 304, 305]. Therefore the photo physical

amino acid	$\bar{\nu}$ (THF)	$\bar{\nu}$ (H_2O)	ϵ (THF)	τ GSB/SE (THF)	τ ESA (THF)
CNA	$2251\,cm^{-1}$	no data	$18\,M^{-1}\,cm^{-1}$	no data	no data
N3P	$2114\,cm^{-1}$	$2125\,cm^{-1}$	$736\,M^{-1}\,cm^{-1}$	0.542 ps/4.607 ps	1.1 ps/5.66 ps
Aha	$2099\,cm^{-1}$	$2119\,cm^{-1}$	$506\,M^{-1}\,cm^{-1}$	0.83 ps/4.89 ps	0.77 ps/4.87 ps
CNP	$2228\,cm^{-1}$	$2234\,cm^{-1}$	$194\,M^{-1}\,cm^{-1}$	1.07 ps/4.64 ps	1.19 ps/6.05 ps

Table 4.1: Overview on spectral characteristics for the four tested novel probes.

properties and photo reactivity in the UV/Vis spectral range of N3P and Aha have to be taken into account for different applications, especially in transient 2D-IR of photoactive proteins. The UV/Vis spectra of both samples (N3P and N3A) were recorded and for N3P a stability test was conducted. In Figure 4.5 the UV/Vis absorption of Aha for different concentrations in H_2O is shown. It can be clearly seen, that the absorption band is situated below 350 nm, results for N3P are similar and not shown. Thus the azide-containing amino acids are suitable for applications in the most common photoactive proteins or for photo activable reactions (e.g. measurements in PYP or BR as well as in Myoglobin, in all of those an excitation wavelength above 400 nm have been used) [4, 38, 47, 306, 307, 308, 309]. For N3P FTIR spectra in THF after different illumination times using either a 400 nm LED or a white-light LED have been recorded to record structural changes upon irradiation. Even after 5 h and 8 h irradiation no instability of the compound could be observed (data not shown).

4.3.2 Anharmonicity and Vibrational Lifetimes

Based on the extinction coefficient three of the four tested compounds fulfill the first requirement for applications in proteins and have a sufficient oscillator strength to allow experiments with concentrations in the low µM regime. Those are N3P, CNP and N3A. For those three UAAs broad band IR pump IR probe spectra have been recorded. Results are shown in Figure 4.6. Experiments with N3P have been conducted with the high-power OPA as IR light source for the pump light, where as experiments with CNP and Aha have been conducted using the regular OPA for both pump and probe pulse generation (see Appendix A for details on the experimental setup). Broad band IR experiments are conducted in the way that the pump pulse is not narrowed by a Fabry Perot (FP) etalon (as done for all 2D-IR experiments presented in this thesis) but the whole OPA spectrum and thus the full IR intensity is used for pump the vibrational mode of interest. This generates much higher signal intensities and allows for a higher time-resolution in the femtosecond range, because the pump pulse length is not stretch in the time domain by the FP (see Chapter 1 for an explanation of the different possible time-resolutions).

From the broad band spectra the anharmonicity of the azide- and nitrile absorption bands can be deduced. In Figure 4.6 a and b the data for N3P are shown. The excited state absorption (ESA) induced signal has its maximum at $2090\,cm^{-1}$. The bleach signal which is caused by contributions from stimulated emission (SE) from the first excited state as well as by ground state bleaching (GSB) has its maximum at $2119\,cm^{-1}$. This results in an anharmonicity of about $30\,cm^{-1}$. The bands are not completely separated but overlapping and cancel each other. This can be seen in the region around $2100\,cm^{-1}$, the ESA induced signal seems to be blue shifting for longer time delays, because of a positive signal contributed by the heated ground state. As the band consists of several sub states, a single anharmonicity cannot be given.

Figure 4.6 c shows the broad band IR data for CNP. Here the bands are well separated and between
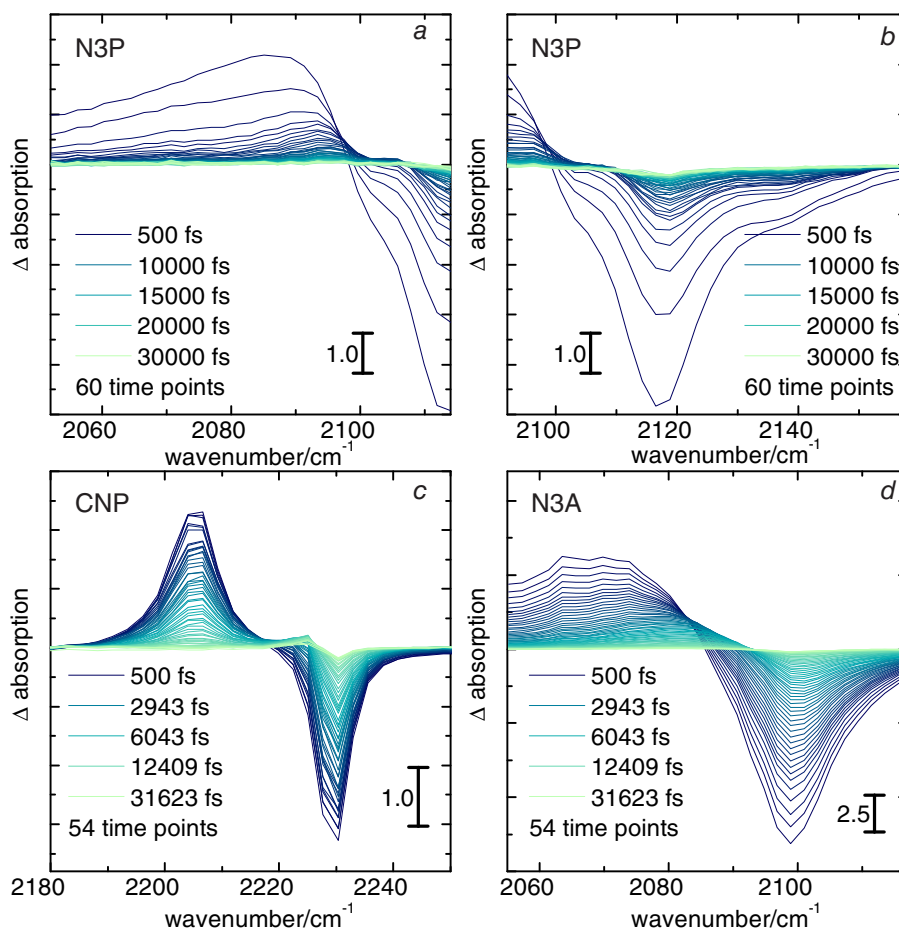
Figure 4.6: Time-resolved IR-pump - IR-probe absorption spectra of the three amino acid candidates tested for ultrafast measurements. Data were recorded with a broad band pump pulse matching the respective absorption maximum (bleach). The pulse length was in the order of 100 fs allowing for fast time-resolution. For N3P the pump light was generated using the high-power OPA (see Appendix A) with approx. 13 µJ intensity before the Fabry-Perot etalon. Data for CNP and N3A were recorded with pump light generated using the regular OPA with approx. 2.5 µJ before the Fabry-Perot etalon. Samples of N3P had a concentration of 250 mM and were measured in a flow cell with 25 µm spacer thickness, conditions for CNP and N3A were 25 mM and 250 µm spacer thickness. Because of these different experimental values no absolute numbers for signal sizes are given in the plots.

both additionally the positive signal contributed from the heated ground state, which occurs after longer waiting times at 2225 cm^{-1}, can be observed. The center wavenumber of the ESA induced positive signal is at 2205 cm^{-1}, the center wavenumber for the bleach signal is at 2230 cm^{-1}. This results in an anharmonicity of 25 cm^{-1}, which is smaller than the approximated anharmonicity for the azide vibration in N3P. The well separated bleach and ESA signals makes CNP a good candidate for usage in applications, where the change of anharmonicity is of interest. The good separation is a results of the very narrow line width of the nitrile stretch vibration in comparison to the azide absorption band.

The broad band IR spectra of N3A in THF are shown in Figure 4.6 d. Here the maximum of the bleach signal is at 2099 cm^{-1}, the ESA signal at 2074 cm^{-1}, which results in an anharmonicity of
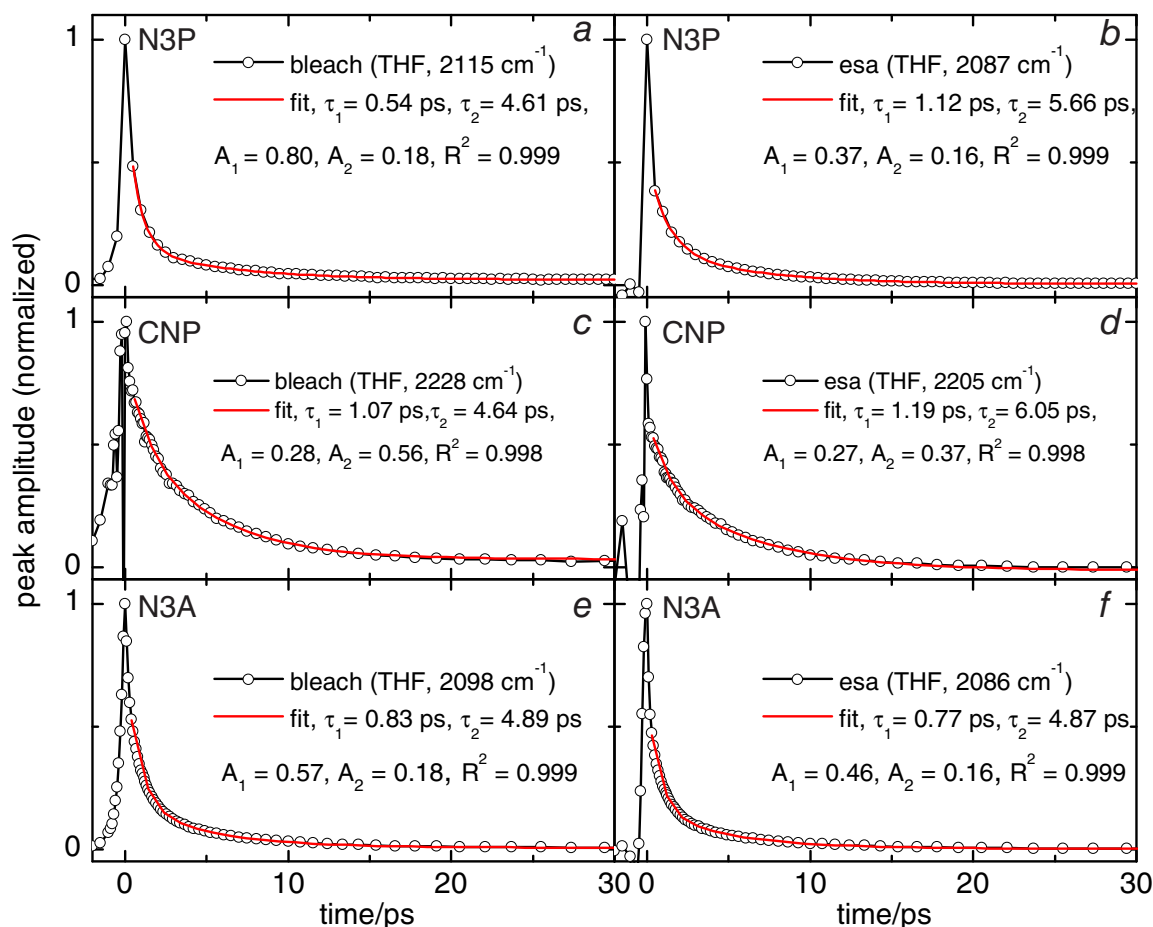
Figure 4.7: Vibrational lifetimes of the functional group (azide or nitrile) of the three amino acid candidates (N3P, CNP, N3A) from broad band IR pump IR probe experiments shown in Figure 4.6, see that caption for experimental details. Data correspond to the time-dependent intensity of either the bleach signal (contributions from ground state bleach (GSB) and stimulated emission (SE)) or the signal for the excited state absorption (ESA). To extract the vibrational lifetime of either the azide or nitrile stretch vibration the data have been fitted using a bi-exponential decay.

approx. 25 cm^{-1}. However as for N3P here the bands are clearly overlapping and for longer waiting time the hot ground state (which can be distinguished in the spectra for CNP) overlaps with the ESA signal including a shifting of the overall band.

From the time dependence of the signals obtained in the broad band IR experiments the vibrational life times of the azide and nitrile stretch vibrations in the tested UAAs can be deduced. The corresponding transients to the bleach and ESA signals of all three molecules are shown in Figure 4.7. Data are fitted by a bi-exponential function. The observed lifetimes can be found in Table 4.1. The results clearly show that CNP has the longest vibrational life time of the three compounds investigated with 6.05 ps as τ_2 for the ESA. The use of the ESA for the determination of the vibrational lifetime is more accurate then the use of the signal at the fundamental which is more strongly overlapping with the signature of the hot ground state.

The vibrational life time obtained for N3P is slightly shorter with 5.66 ps for τ_2 of the ESA signal

vibrational mode	peak time N3P	peak time CNP	peak time N3A
amide I	2.2 ps	5.1 ps	1.5 ps
carboxylate	3.5 ps	6.2 ps	2.3 ps
ring mode	1.3 ps/1.4 ps	3.6 ps	no data
amide II	3.9 ps	8.1 ps	2.7 ps
ring mode	1.2 ps	2.1 ps	no data

Table 4.2: Peak times of transients depicted in Figure 4.9 as observed by fitting a bi-exponential function (using Origin 8.5) to the transient data.

and Aha has the shortest lifetimes with 4.87 ps.

The vibrational lifetimes of CNP, N3P and N3A do not differ a lot. While CNP has a slightly longer lifetime, its extinction coefficient is lower, thus the time window for spectral diffusion measurements will be comparable and in the range of about 5-10 ps. A much longer vibrational life time of 106 ps was found for an aliphatic thiocyanate stretch vibration[2], in contrast the extinction coefficient of the SCN is much lower [260]. So for experiments aiming at the measurement of picosecond dynamics up to more than 10 ps thiocyanate might be the vibrational probe of choice.

4.3.3 Time-Resolved IR Spectra

The possibility to measure coupling to other vibrational modes or to observe differently induced cross peaks with other vibrational modes is of interest for the study of a molecular system, for example in experiments, where the azide or nitrile vibration is excited and coupling or energy transfer to the peptide backbone (e.g. the amide I mode) shall be studied.

To investigate this type of signals all model compounds were used in their boc-protected form in time-resolved IR experiments. In Figure 4.8 cuts through 2C-2D-IR spectra are shown. The narrow-band pump pulse was centered on the maximum bleach signal for either the azide or nitrile absorption, whereas the probe was adjusted to different spectral windows, covering the range between 1450 cm^{-1} and 1800 cm^{-1} as well as the region around the azide (2100 cm^{-1}) or nitrile (2200 cm^{-1}) vibration. In this range all other characteristic IR absorption bands such as the amide II, amide I and ring mode vibrations are present.

In Figure 4.8 the cross peaks between all vibrational modes present in the FTIR spectrum in Figure 4.2 and the azide and nitrile vibration are observed. In this spectra again the anharmonicity of the signals can be extracted as well as the cross peak anharmonicity. The cross peaks observed in this spectra are not induced by direct coupling or e.g. population transfer but by vibrational energy transfer between the azide or nitrile group to the other vibrational modes investigated. The distinction between processes leading to cross peak generation can be made by the time-dependence of the signals, if cross peaks would appear instantaneously the mechanism would clearly be direct coupling. In these experiments the cross peaks show a correlation between the spatial proximity and the peak time (the time for the signal to reach its maximum, listed in Table 4.2). This can be understood more precisely from the transients shown in Figure 4.9. Plotted is the time dependence of the signal intensity of all peaks shown in Figure 4.8. It can be seen for example, that the two carbonyl absorptions in the amide I region have different peak times Table 4.2, based on this it can be unraveled which signal corresponds to the peptide unit and which signal corresponds to

---

[2]Experiments carried out in the group, but which are not part of this thesis.
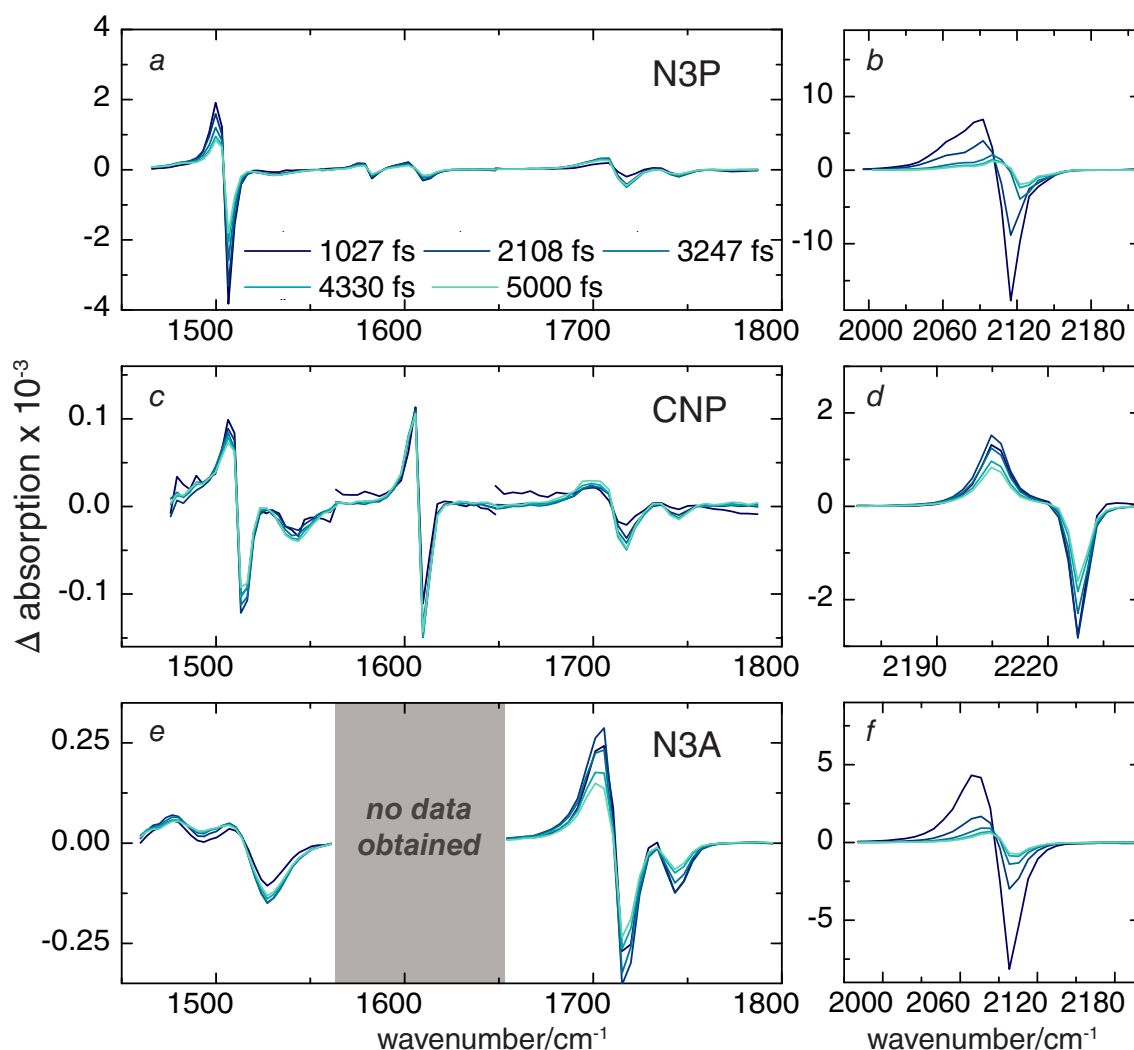
Figure 4.8: Transient IR spectra with pump pulse centered on the absorption maximum for either the azide or nitrile groups for the three amino acid candidates N3P, CNP and N3A. All data are measured in THF. Shown are data for parallel polarization of pump and probe pulse. The pump pulse had a width of approx. $17\,\text{cm}^{-1}$ in all experiments. All experiments were conducted using the high-power OPA as light source for the pump light (see Appendix A for details about the setup). Samples had a concentration of 50 mM, the spacer thickness was $125\,\mu\text{m}$. Note that signals for N3A in the amide II region are recorded with a concentration of 25 mM (and not scaled). Concentrations between experiments might vary, because of the high fugacity of the solvent THF.

the carboxylate. How those peak times can be used for assignment of the FTIR absorption spectrum is discussed in detail in Chapter 7.

For all three molecules the amide II signal from the peptide unit has the slowest peak time. All in all for N3A the fastest peak times for those signals are observed, which can be explained by the shorter distance between the azide group and the peptide unit. In CNP the longest peak times are observed. The main explanation for this is the longer vibrational life time of the nitrile mode. In CNP as well the smallest signals are observed due to the lower extinction coefficient. N3P has the
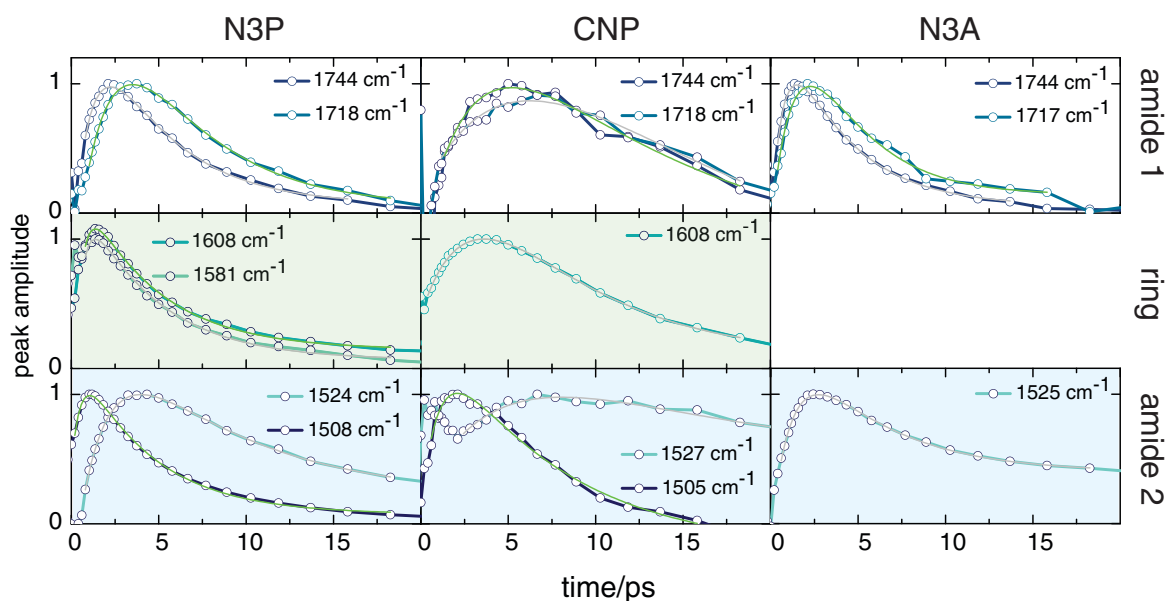
Figure 4.9: Transient data for all main modes of the three amino acid candidates. Plotted is the time dependent absorption change of the corresponding bleach signal for all peaks in the amide I region, ring mode region and amide II region (as shown in Figure 4.8). For N3P and N3A the bleach signal for a single pixel is shown, whereas for CNP the integrated bleach signal is plotted to achieve better signal-to-noise ratio. All samples were in the boc-protected form, experiments were done in THF with parallel polarization of pump and probe, for details about the experimental setup see Appendix A. Data are fitted by a bi-exponential function to better observe the time, when the maximum intensity is reached. Those peak times are reported in Table 4.2.

highest signal intensities, as was expected based on the high extinction coefficient and the observed peak times for all signals are slightly longer than for the same modes in N3A because of the larger distance between the azide mode and the peptide backbone due to its bigger side chain. They are shorter than in CNP, which might be caused by the Fermi Resonance speeding up VET.

Judging from the results of the broad band experiments and the transient IR data presented in this section azidohomoalanine seems to be a very good candidate for usage in proteins, because of its fair signal intensity, but its vibrational life time is very short and only allows for studies in a time window between about 1 ps to 5–10 ps. Azidophenylalanine has similar properties and higher signal intensities, which in principle makes it a better candidate for usage in proteins, which can not be highly concentrated. But the big disadvantage of using N3P in time-resolved and especially 2D-IR measurements can be seen in the data in Figure 4.8 as the azide line shape is highly disturbed and complicated by a Fermi Resonance. This could be cured by using isotopologues [301]. Cyanophenylalanine in comparison to the other two is the only nitrile-containing compound, which was tested in ultrafast measurements. Its nitrile stretch vibration has a similar life time. Already in the transient IR data it can be seen that the signals are much weaker than for the azide absorptions, thus it might be difficult to use CNP in proteins with small concentrations.

4.3.4 2C-2D-IR Spectra

Additionally to the time-resolved IR spectra a full set of 2C-2D-IR spectra [104, 153] has been recorded for the two azide containing UAAs N3P and N3A in the range from 1480 cm^{-1} to 1800 cm^{-1}, covering three different spectral windows for N3P (amide II, ring mode region, amide I) and two

Figure 4.10: 2C-2D-IR spectra of N3A in THF. Shown are all cross peaks observable between the azide vibration at 2099 cm^{-1} and the other characteristic vibrations in the region between 1450 cm^{-1} to 1800 cm^{-1}. Data were recorded in two different spectral windows for the cross peaks and in addition for the diagonal peak. All experiments have been carried out on the 150 line grating, samples had a concentration of 50 mM for the diagonal signals and the amide I region, the data in the amide II region have been recorded with 25 mM concentrated samples. All measurements have been done using a sample cell with 125 µm spacer. The pump pulse had a width of 16.5 cm^{-1} adjusted by the FP, the IR intensity before was 13.7 µJ. The signal intensity is given in the plot, contour levels are set so that cross peaks have the same intensity ($\pm$ 0.1 mOD).

different spectral windows for N3A (amide II, amide I) was measured. As explained in chapter 1 (see Figure 1.8 the approach of 2C-2D-IR in the frequency domain using two independent tunable OPAs as pump and probe allows to record cross peaks between vibrations, which are further separated than the regular width of an OPA spectrum. A similar technological approach in the time domain for accessing cross peaks in 2D-IR spectra which are too far separated for being covered with the same excitation light source was first reported by Hochstrasser and Rubtsov and became widely known as dual-frequency 2D-IR [104, 153].

In Figure 4.10 the 2C-2D-IR spectra of N3A in THF are shown for four different waiting times. It was possible to record all expected cross peak signals between the azide vibration and vibrational modes in the amide I and amide II region. From the full 2C-2D-IR data similar information as from the the 2C-2D-IR cuts in Figure 4.8 can be deduced with the additional possibility of a more details line shape analysis. Figure 4.11 shows a similar data set for N3P with the additional cross peaks
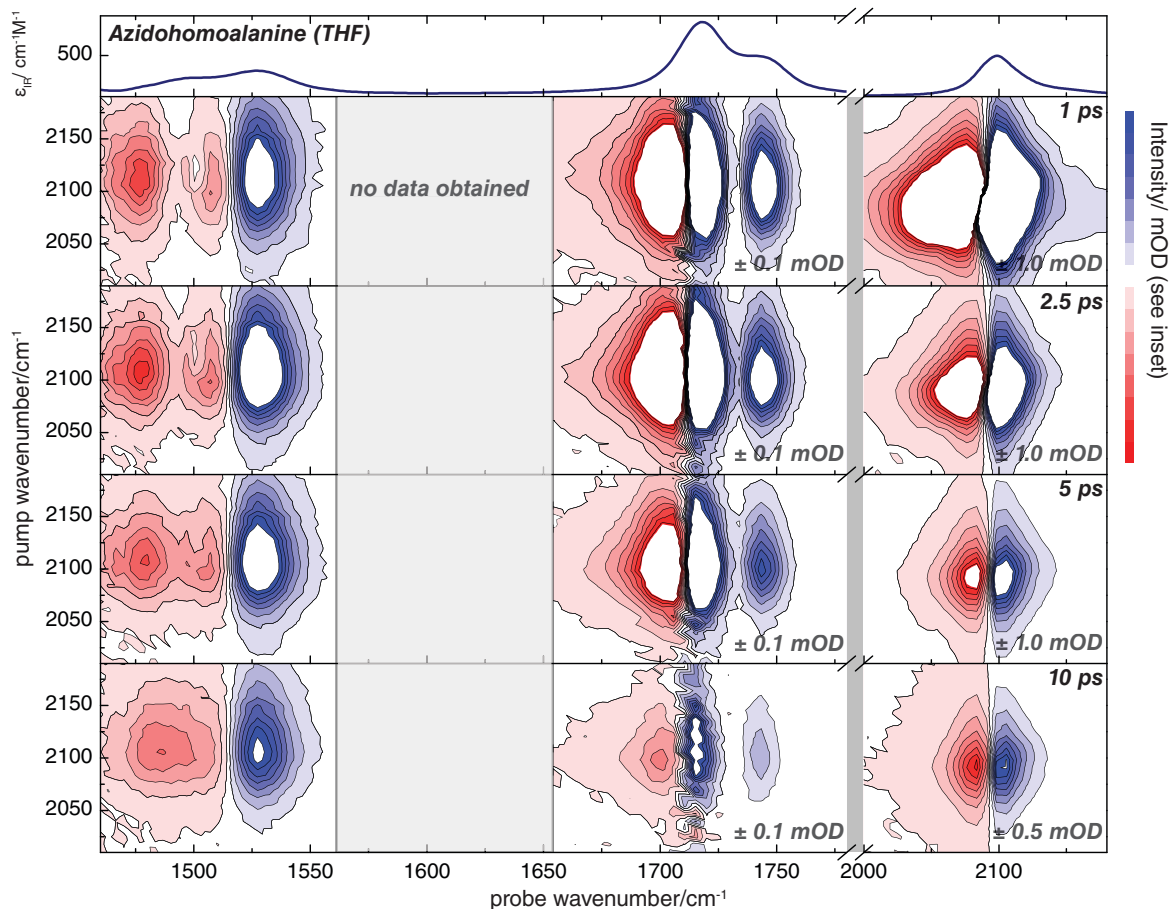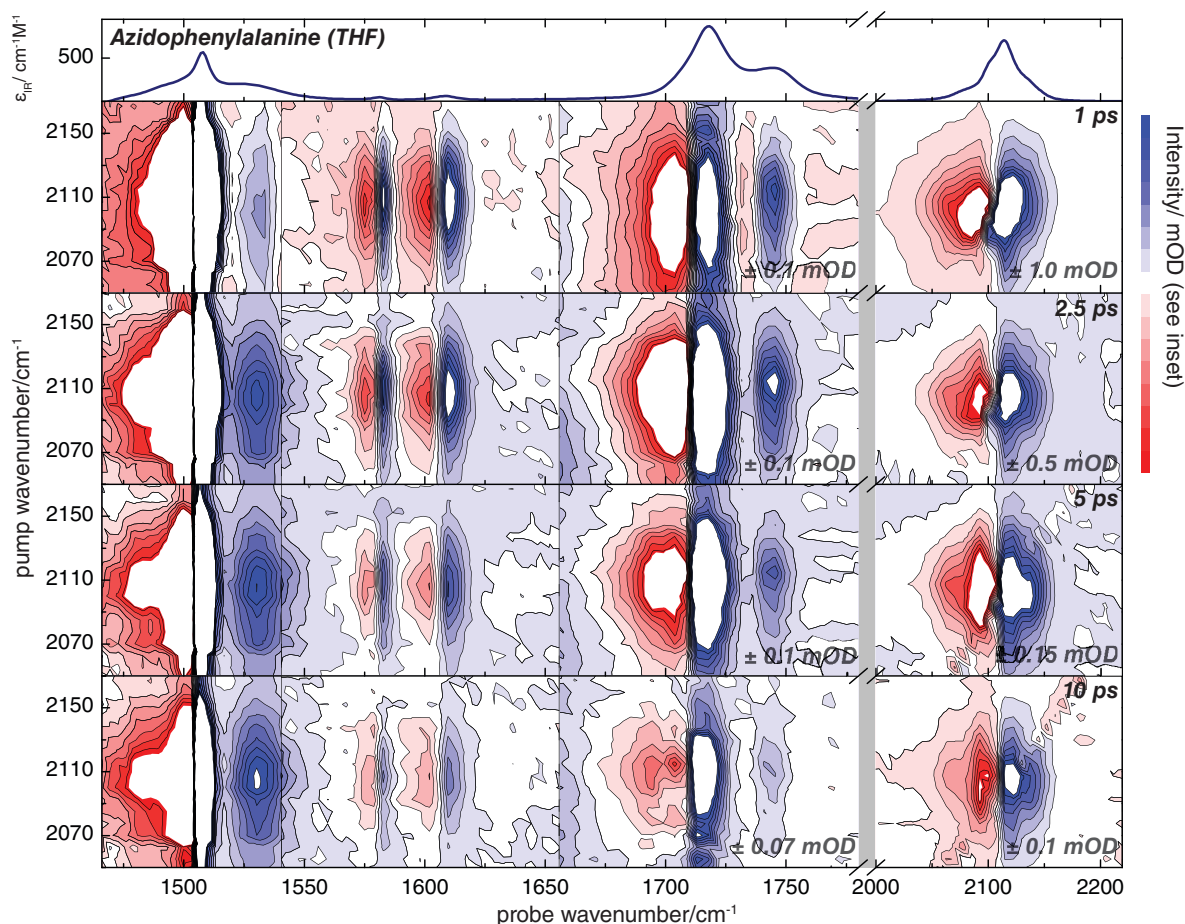
Figure 4.11: 2C-2D-IR spectra of N3P in THF. Shown are all cross peaks observable between the azide vibration and the other characteristic vibrations in the region between 1450 cm^{-1} to 1800 cm^{-1}. Data were recorded in three different spectral windows for the cross peaks (amide I, amide II and ring modes) and in addition for the diagonal peak. All experiments have been carried out on the 150 line grating, samples had a concentration of 50 mM, a flow cell with 125 μm spacer was used. The pump pulse had a width of 12 cm^{-1} adjusted by the FP, the IR intensity before was 13 μJ. The signal intensity is given in the plot, contour levels are set so that cross peaks have the same intensity (± 0.1 mOD for 1 to 5 ps, ±0.07 mOD for 10ps). Note that the 2C-2D-IR experiments in the ring mode region have been conducted with a new sample in comparison to the amide I region because of the high fugacity of THF as solvent and signal sizes therefore have to be compared carefully.

for the ring modes observed. Overall the signal sizes, even for the small cross peak signals in the ring mode region and for the amide II mode are well above the noise level and can be detected for times up to 10 ps with good signal to noise ratio. When comparing the two data sets it can be seen, that the diagonal peaks for N3P show already a slightly disturbed line shape induced by the Fermi Resonance [300, 301]. Recent experiments by the Nibbering group addressed a similar phenomenon (the Hydrogen-bond enhanced Fermi Resonance in Aniline) and studied the exact relaxation pathways by polarization dependent 2D-IR experiments [310]. A similar analysis could be carried out for N3P to characterize the Fermi Resonance between the azide and the ring modes more.

In N3P it is difficult to interpret data in the amide II region. Those signals are dominated by the

strong contribution from an additional ring mode (see chapter 7 for details), for the cross peak between the azide vibration and the amide II mode from the peptide unit the GSB/SE contribution can be measured whereas the ESA signal is canceled by the strong signal for the ring mode. The same is not true for N3A, here even two signals for the excited state absorption can be found in this spectral window, with one corresponding to the true amide II signal from the peptide bond and the other possibly originating from methylene group vibrations. [62]
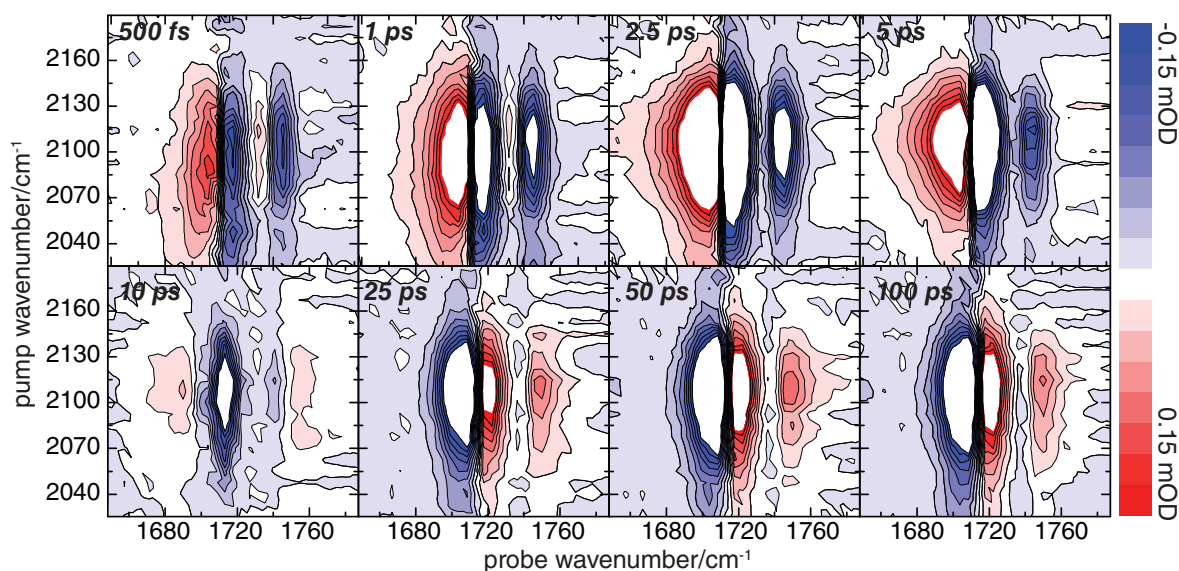
Figure 4.12: 2C-2D-IR spectra of N3P in THF, shown is the time dependent signal for the cross peak between azide region (pump) and carbonyls (probe) for high concentrations, between 10 and 25 ps the sign for GSB/SE and ESA switches, indicating an intermolecular effect of heat transfer between the N3P molecules via the solvent. Data are plotted with 16 contour levels, equally spaced between ±0.15 mOD as cut-off. These data were recorded with high concentration (250 mM) and thin spacer (25 μm).

In Figure 4.12 the cross peak signals in the carbonyl region of N3P are shown as observed under different experimental conditions. In contrast to the data shown in Figure 4.11, which are taken with samples of 50 mM concentration, these experiments were carried out with a concentration of 250 mM. Here intermolecular heat transfer via the surrounding solvent leads to the inversion of the signal at around 10 ps as due to the high concentration heating of the solution by the deposited pulse energy becomes large enough to significantly influence the spectra. This is a very important result, because it shows the limit for sample concentrations and clearly demonstrates, that intermolecular effects might have to be considered in the interpretation of data.

Overall the 2C-2D-IR spectra yield information on interaction between the vibrational modes. In the tested molecules the cross-peaks are all generated by vibrational energy transfer. Using two independent OPAs as light sources for pumping and probing to record 2D-IR data in the frequency domain is a very intuitive approach for expanding the observable spectral region and to access cross peaks far separated from the pump transition. The information gain in comparison to cuts through the 2C-2D-IR spectra as those shown in Figure 4.8 is limited in this specific case. As a proof-of-principle experiment, however it was successful and the VET induced cross-peaks between all vibration modes and the pump azide transition were possible to record.

4.3.5 Spectral Diffusion
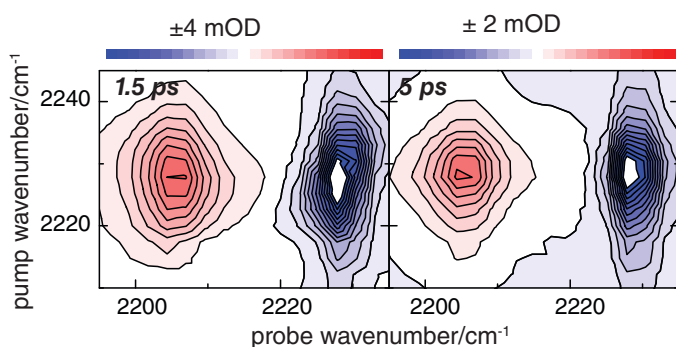
Figure 4.13: 2D-IR Spectra of CNP in THF. Shown is the diagonal peak for the nitrile stretch vibration at 1.5 ps delay and 5 ps delay between pump and probe pulse. Data were recorded using the 300 line grating. The sample concentration was 50 mM and the spacer thickness for the measurement cell was 125 μm. The pump pulse had a bandwidth of 12 cm^{-1} adjusted by the Fabry Perot etalon, the IR intensity was 13 μJ right in front of the FP.

Spectral diffusion, as described in Chapter 1, is an effect intensively studied by 2D-IR spectroscopy. The instantaneous inhomogeneous broadening of a IR absorption is equilibrated by exchange of the subspecies over a short time, leading the initially tilted 2D-IR peak to turn upright. For usage in proteins this is about the most important property of a novel vibrational probe, since in spectral diffusion measurements changes in the microenvironment or e.g. hydrogen bonding configuration might be accessible. For a meaningful analysis of protein dynamics monitored by the spectral diffusion of the novel vibrational probe a previous investigation of the dependence of the vibrational frequency on the surrounding of the respective vibration is mandatory. To explore the response of the respective vibration on dynamics of the surrounding (solvation dynamics in the present case), 2D-IR data of the nitrile or azide stretch vibration of the three compounds CNP, N3P and N3A in THF have been recorded with high resolution using the 300 line grating.

In Figure 4.13 the 2D-IR data for CNP are shown. The inhomogeneity of the nitrile vibration for 1.5 ps delay can be seen by the small tilt of the central slope. In the signal for 5 ps these inhomogeneities are already vanished. Due to the small extinction coefficient as well as the very narrow line width of the nitrile stretch vibration the spectral diffusion process is difficult to observe in these spectra in detail using the spectral resolution possible with the current setup. The narrow line width reflects the weak solvatochroism of the vibration and is a limitation for using CNP as good monitor for local dynamics in proteins. Even though the nitrile stretch vibrations posses the longest vibrational life time, which would allow to access protein dynamics in a longer time window than using an azide as probe, the lack of pronounced spectral diffusion makes CNP not the most favorable UAA to be used in proteins.

In Figure 4.14 the spectral diffusion process for the azide band in N3P is shown. The data are recorded in two overlapping spectral windows to access the full diagonal peak in high resolution and monitor the complicated lineshape. The main azide stretch vibration shows a distinct spectral diffusion. The signal for 1 ps waiting time has a pronounced tilt, which disappears for longer time and is not observable at 5 ps anymore. In principle the signal size and SNR make N3P a perfect UAA to be used in proteins. For a concentration of 25 mM a signal size of 13 mOD is observed, which means that experiments with protein samples of only 1 to 2 mM concentration would still be feasible. But just as for the IR absorption spectrum the 2D-IR spectrum is strongly perturbed by the Fermi Resonance. The spectra in Figure 4.11 contain cross peaks between the different states created by the Fermi Resonance. As the lineshape for the azide stretch vibration in N3P is this complicated even for the free UAA in a non-hydrogen bonding solvent, it is obvious, that it should not be applied to study conformational dynamics in proteins through spectral diffusion
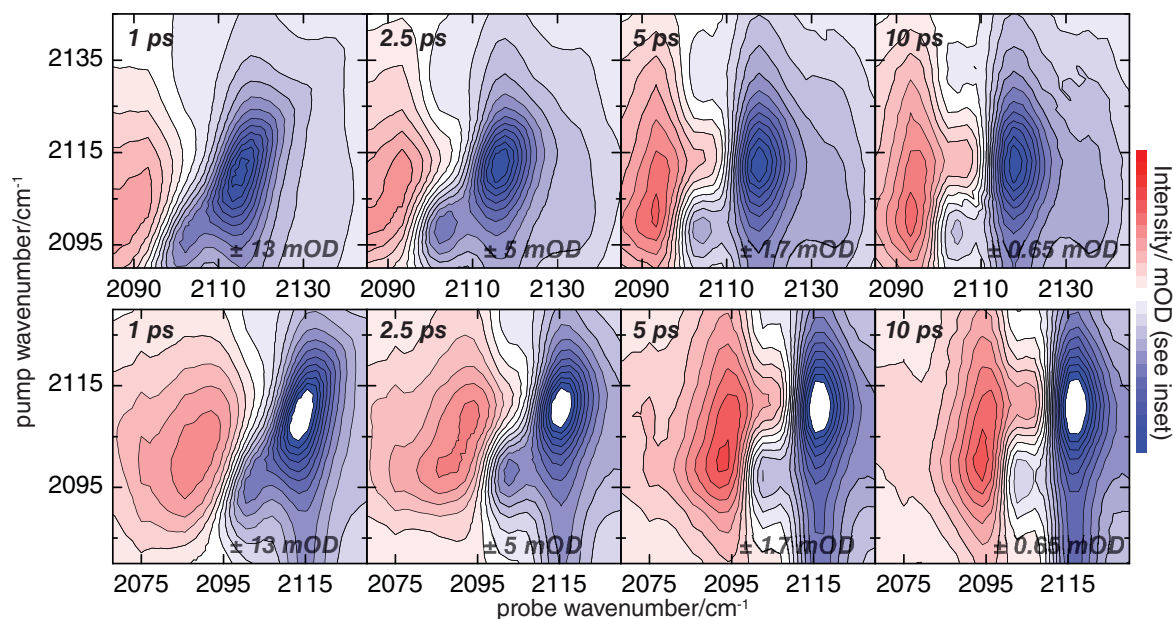
Figure 4.14: 2D-IR spectra of N3P showing its spectral diffusion properties in THF for different waiting times. Shown are two overlapping measurements windows. The measurement was carried out using the 300 line grating and the high power OPA as light source for the pump. The shown data are recorded with parallel polarization between pump and probe beam, the pump intensity was 12 μJ in front of the FP by which the pump band width was adjusted to 14 cm⁻¹. Samples had a concentration of 25 mM and were measured in a flowcell with spacer thickness of 250 μm.

measurements.

Figure 4.15 shows the 2D-IR spectra obtained for N3A in THF (upper panel) and for Aha (the free amino acid without boc-protection group) in H_2O (lower panel). In contrast to the spectra of N3P in Figure 4.11 here the lineshape is very clear (for both solvents) and also a pronounced spectral diffusion can be observed. Similar as found for the azide stretch in N3P the azide stretch in N3A/ Aha probes the inhomogeneities in its surrounding and thus the 2D-IR spectra for the shortest waiting time of 1 ps both show a clear tilting. Comparing the two spectra for 1 ps in more detail it can be seen, that the azide stretch in H_2O has to have more diverse microenvironment and experiences huger line broadening as indicated by the larger tilt of the signal in H_2O. This corresponds to previous findings that the azide absorption in Aha has a broader line width when exposed to a hydrogen bonding solvent. The observation of a difference in center wavenumber, inhomogeneous broadening and spectral diffusion kinetics for different solvents makes N3A/ Aha a very promising probe for applications in proteins. Also that it is possible to observe 2D-IR spectra with strong enough signals and decent SNR in H_2O is an important finding. As was reported by [139] and is discussed in greater detail in Chapter 6 the azide stretch vibration is directly situated in the region of the H_2O combination band. Thus a solvent background contributes to the signal for longer waiting times while additionally limiting the feasible spacer thickness. Data reported here are measured with 100 mM concentration, which is not feasible for protein samples, but the 2D-IR data for Aha in the lower panel in Figure 4.10 are only corrected by subtraction of a background for negative waiting time, thus it is not yet accounted for contributions from the H_2O background. A 10fold smaller signal than measured for 1 ps will still be detectable, bringing 2D-IR experiments in proteins into reach (see Chapter 6 for results). The data presented in Figure 4.15 can in principle
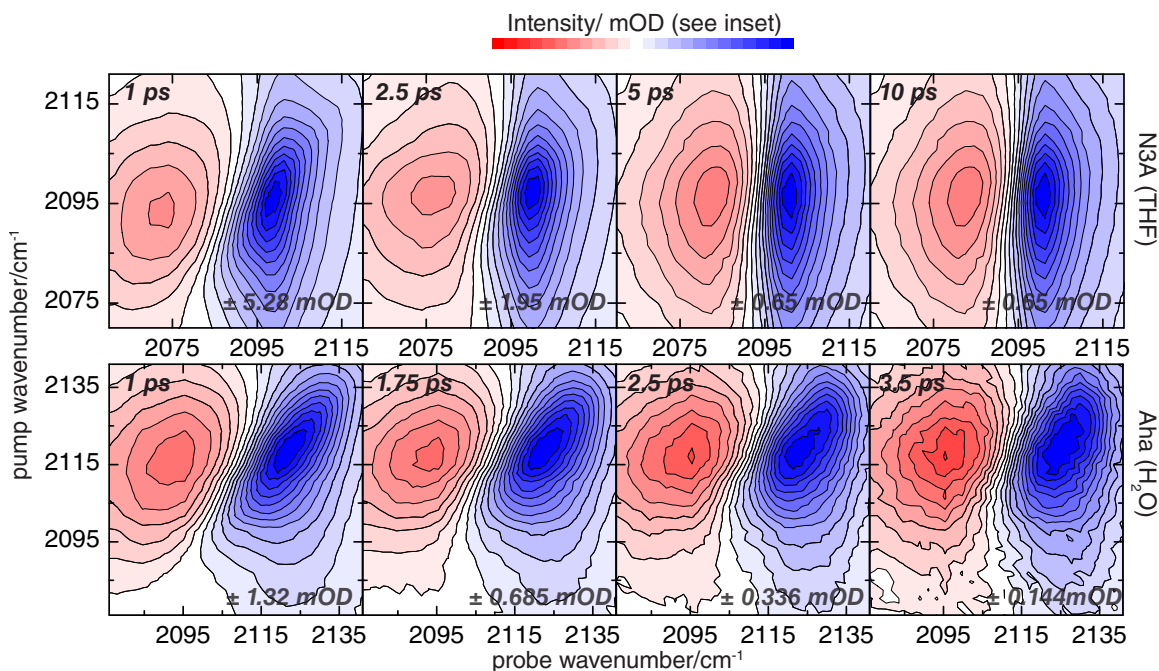
Figure 4.15: 2D-IR spectra of Aha showing its solvent dependent spectral diffusion properties for different waiting times. The upper panel shows the data for THF, the lower panel the spectra in H_2O. The measurements were carried out using the 300 line grating. The measurements in THF have been conducted using the high-power OPA as light source for the pump light. The sample had a concentration of 25 mM and was measured in a cell with 125 μm spacer thickness. The measurements in H_2O were carried out using the regular OPA as light source for both pump and probe pulse. Here the sample had a concentration of 100 mM and due to the high solvent absorption measurements have been carried out in a cell with 50 μm spacer thickness. For both experiments the width of the pump pulse was adjusted to 17 cm^{-1}. Note that for Aha in H_2O shorter and different waiting times than for Aha in THF are reported.

be analyzed further by a Center Line Slope Analysis (CLS) as performed by Bloem et al. [139] to extract the frequency-frequency correlation function (FFCF). The 2D-IR spectra themselves are highly resolved and thus allow to determine the solvent influence on the spectral diffusion dynamics directly.

4.4 Conclusion

Four different UAAs as candidates for usages as novel vibrational probes in proteins have been tested, specifically with respect to their usage in 2D-IR. Two nitrile containing amino acids and two azide containing amino acids were investigated. Experiments included a detailed analysis of all relevant properties for applications in proteins with special emphasis on usability in 2D-IR experiments. For a novel vibrational probe to be used in 2D-IR spectroscopy it is of crucial importance to posses a decent oscillator strength. This is the first key requirement as in contrast to FTIR spectroscopy in 2D-IR the signal size scales with the squared extinction coefficient and thus ε is particularly important for how low the sample concentration can be chosen. The aliphatic nitrile of the UAA cyanoalanine was found to be not passing this prerequisite as its ε was measured to be only 18 M^{-1} cm^{-1}, about a factor 40 times lower than found for the UAA with the best extinction

coefficient, azidophenylalanine. The difference in signal size for a similar concentration sample between using these two as probes thus would be a factor 1600, not taking into account other influences on the signal intensity such as line width or vibrational life time. All other three tested candidates posses an extinction coefficient which makes applications in proteins feasible. Those UAAs are N3P, CNP and Aha. All of them have different properties making them suitable for different applications.

Azidophenylalanine. The aromatic azide tested was azidophenylalanine. From the first experimental test of whether the UAA under consideration for applications in 2D-IR spectroscopy of proteins this one was the most promising as it exhibits an ε of $736 \, \text{M}^{-1} \, \text{cm}^{-1}$. But already in the FTIR spectra of the azide stretch vibration in THF a disturbance of the lineshape which can not be accounted for by inhomogeneous line broadening is found. Comparison with the literature reveals that aromatic azides posses a Fermi Resonance [300, 301], which makes N3P very unfavorable for applications in 2D-IR spectral diffusion measurements. For 2D-IR spectroscopy this property is even worse than for FTIR spectroscopy as it completely changes the expected characteristics and introduces a complicated lineshape with unpredictable spectral diffusion behavior, influenced also by energy transfer between the contributing states.. As analysis of the spectral diffusion dynamics of a novel probe (ideally with a center line slope plot) in different positions in a protein of interest will be one of the major applications, N3P is not suited to be used for this. As a novel probe to be used in IR spectroscopy of proteins N3P is only feasible in cases where an aromatic side chain needs to be replaced and protein concentrations are very low. However meaningful applications of N3P in vibrational spectroscopy will probably remain limited to similar experiments as reported by Ye et al., where spectral shifts as a consequence of a conformational change are investigated. [82, 83].

Cyanophenylalanine. The aromatic nitrile tested was cyanophenylalanine, which originally was the first UAA to be proposed for applications in IR spectroscopy [79]. It has a much lower ε than the azide compounds tested with $194 \, \text{M}^{-1} \, \text{cm}^{-1}$. Still it posses few unique features, which make it an important UAA for applications to study protein dynamics.

First of all the solvatochroism of the nitrile stretch vibration is discussed to be more more easily modeled in terms of local electrostatics, as compared to the azide stretch vibration, which is more affected by hydrogen-bonding [263, 279]. A linear correlation between the local electrostatics and the nitrile stretch vibration is reported in the absence of hydrogen-bonds, which can be accounted for in an analysis [140]. Nitriles have been proven as versatile probes in 2D-IR of proteins, with the most prominent example being the study of the inhibitor rilpivirine bound to HIV-1 reverse transcriptase [287, 288], where nitrile groups were present in the bound ligand. The usage of CNP as site-specific probe incorporated into a protein at position of interest will take this type of experiments to the next level. In this respect CNP has another advantage over the best candidate identified, Aha, which is its more versatile incorporation technique. As CNP is incorporated via artificial genetic code expansion, there is ultimately no limitation to which proteins can be tested (in contrast Aha is most suitable in Methionine free proteins). For ultrafast investigations of protein dynamics CNP has another beneficial property, which is its relatively long vibrational lifetime of 6.05 ps. This allow a longer time window to be accessed and resolved than with an azide probe. Additionally CNP has interesting photophysics as it is also employed as a fluorescent probe with a reported decay of up to 8 ns [311] allowing for combined experiments of IR and fluorescence spectroscopy [246].

Azidohomoalanine. The last UAA tested towards its application for 2D-IR of proteins is azido-homoalanine. It has been tested vigorously lately in IR spectroscopy [255, 279, 289, 312] and also been applied in a first 2D-IR experiment [139]. The great interest sparked because of its wide applications in click-chemistry and the relatively easy incorporation approach as methionine analog [218]. The results presented in this chapter also suggest Aha as the most versatile probe of the tested candidates. This is for several reasons, but mostly because of a combination of beneficial properties. First of all Aha, as it contains an azide group, has a relatively huge ε of $506\,\mathrm{M}^{-1}\,\mathrm{cm}^{-1}$, allowing for experiments with samples in the low mM range. As discussed the azide center frequency is more sensitive to hydrogen bonds than to local electrostatics, as demonstrated in Chapter 5 this property can be of use. The most important characteristic for using Aha in 2D-IR is its unperturbed lineshape and its pronounced solvatochroism leading to easily observed spectral diffusion, both in H_2O and THF, which enables studies of protein dynamics in the time window between 1 ps to 5-10 ps.

The results in this chapter suggest UAAs might be versatile probes for 2D-IR spectroscopy with azidohomoalanine as the best candidate to be used in applications. The remainder of this thesis focuses on different example applications of Aha as site-specific probe for conformational dynamics as well as energy flow in proteins.

Part III

Application 1: Probing of Protein Microenvironment and Conformational Dynamics

5 Site-Specific Probing of Local Environment and Long Range Interactions in PDZ3

To test the application potential of the previously identified novel vibrational probe Azidohomoalanine (Aha) in FTIR spectroscopy of proteins the PDZ3 domain was studied. This chapter describes in brief experiments aiming at demonstrating the value of an azide group as a site-specific probe. To show that despite its complicated solvatochromism the azide in Aha is a sensitive reporter of the hydrophobicity of its surrounding microenvironment, six mutation sites in PDZ3 were chosen. The absorption frequency was found to be correlated to the hydrophobicity as deduced from the known crystal structure. The second aim was to tackle the question of allostery and long range communication as introduced in Chapter 2.

The six mutants also were picked to be either part of the predicted pathway [10] or situated off-pathway. Ligand binding observed by FTIR spectroscopy revealed that indeed a localized vibrational probe can monitor small conformational changes not visible in the crystal structure which match the predictions of a coupled network.

Three mutants which are part of the predicted allosteric communication route [10], see Figure 2.6, are found to show subtle but distinct conformational changes upon ligand binding, whereas mutants used for control do not show changes. The results successfully demonstrate the potential of IR spectroscopy in combination with the Aha label for structurally resolved investigations in proteins and biophysical studies of protein function and give new insights for the understanding of ligand induced long-range communication in PDZ3.

The chapter is partly based on the manuscript *FTIR spectroscopy of Azidohomoalanine-labeled PDZ3 from PSD-95: Site-specific probing of local environment and ligand-induced long range interaction.* A lot of the experiments have been carried out by Katharina Eberl during her Bachelor Thesis [299] and after as student assistant supervised by the author.

5.1 Motivation

The characterization of structural changes and local effects in proteins is the key to functional understanding of any biological process. In this chapter the previously identified novel vibrational probe Azidohomoalanine (Aha) is tested in a first application as reporter of the local microenvironment in PDZ3. It is demonstrated what type of long-standing biophysical questions can be addressed and possibly answered using FTIR spectroscopy with high resolution on side chain level. The protein investigated is the 3rd PDZ domain of PSD-95 (as introduced in Chapter 2), a protein-protein interaction domain involved e.g. in diverse signal transduction processes, protein sorting and transport. Several different mechanisms for information transfer upon ligand binding from the binding cavity to opposite sides of the PDZ domain are predicted by theoretical and experimental approaches. Those include ligand induced conformational changes, allosteric long-range communication and conformational selection.

Here it is aimed to demonstrate how the approach [82, 289] (see also the Motivation of this thesis) of combining IR spectroscopy with site-specific vibrational probes in the side chain of UAAs to

(a) structure of CRIPT

(b) mutation sites in PDZ3
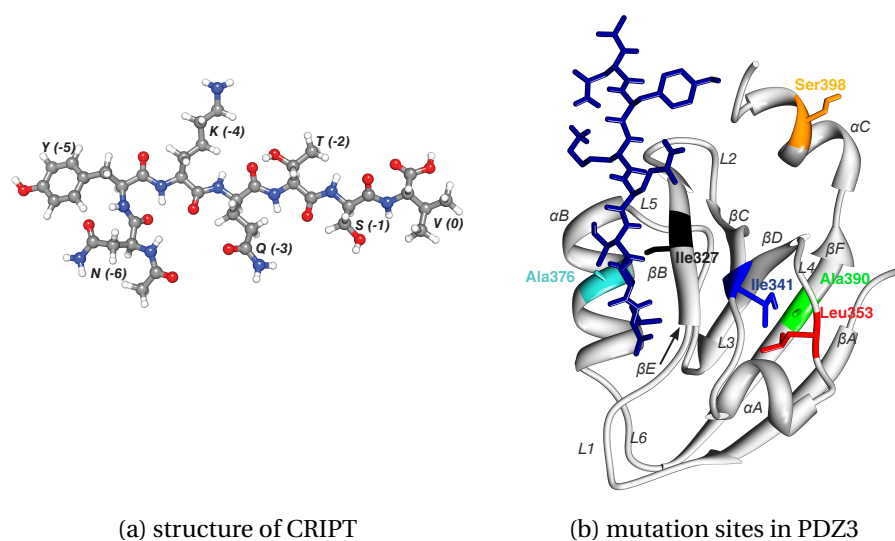
Figure 5.1: Shown are the structure of the CRIPT peptide as heptamer (ac-NYKQTSV), the peptide used as *native* ligand throughout the experiments in this thesis and the structure of PDZ3 based on the pdb entry 1be9 with mutation sites indicated.

access local information, can aid experimental data to these long-standing and controversially discussed questions in PDZ3.

In recent publications the potential of this approach for further understanding of protein function was demonstrated on GPCR function [82, 83] and recently used for quantitative measurements of electrostatics in a catalytic center [264]. As described in Chapter 4 the UAA Azidohomoalanine (Aha), which contains an aliphatic azide group seems to be an ideal candidate for applications in proteins. Aha can be incorporated into all proteins which can be expressed in *E. coli* as methionine analogue [218] and is incorporated co-translationally, allowing for high labeling yield (see Chapter 3 for more details).

By using the azide moiety of Aha as reporter group it might be possible to probe small changes in the protein microenvironment. As discussed by Minheang Cho's group [75, 274, 278, 313], the azide group is a good reporter for changes in the solvation shell, rearrangements in hydrogen bonding networks or folding events. In contrast to other vibrational marker groups, such as Thiocyanate and nitrile [258, 263], the azide center frequency is not linearly correlated to the electric field. But one huge advantage of the azide group in Aha is its higher absorption coefficient (as reported in Chapter 4 and the usability both in H_2O and D_2O [274]. In this chapter a first possible application of Aha as site-specific probe is demonstrated for the study of a protein microenvironment.

5.2 Experimental Design

Six incorporation sites in PDZ3 were chosen to fulfill a range of requirements. The mutants, shown in Figure 5.1 were picked because of their role in the predicted transfer pathway, as based on the simulation by Ota and Agard [10] and not on the calculations from Ranganathan and Lockless [9]. Three incorporation sites for Aha are part of the predicted pathway with Ile327 being directly in the binding pocket, Ile341 part of the protein core and Leu353 on the distant protein side. The other three incorporation positions are matching the first three by their distance from the initial

```
1be9:     GSPE 301FLGEE DIPRE PRRIV IHRGS TGLGF NIIGG EDGEG IFISF
PDZ-aha:      302GGEE DIPRE PRRIV IHRGS TGLGF NIIGG EDGEG IFISF
Lockless:     6LGEE DIPRE PRRIV IHRGS TGLGF NIIGG EDGEG IFISF
Ota/Agard:    6LGEE DIPRE PRRIV IHRGS TGLGF NIIGG EDGEG IFISF

1be9:      341ILAGG PADLS GELRK GDQIL SVNGV DLRNA SHEQA
PDZ-aha:   341ILAGG PADLS GELRK GDQIL SVNGV DLRNA SHEQA
Lockless:  45ILAGG PADLS GELRK GDQIL SVNGV DLRNA SHEQA
Ota/Agard: 45ILAGG PADLS GELRK GDQIL SVNGV DLRNA SHEQA

1be9:      376AIALK NAGQT VTIIA QYKPE EYSRF EANSR VNSSG RIVTN
PDZ-aha:   376AIALK NAGQT VTIIA QYKPE EYSRF EA
Lockless:  80AIALK NAGQT VTIIA QYKPE EYSRF EA
Ota/Agard: 80AIALK NAGQT VTIIA QYKPE EYSRF EA
```

Figure 5.2: Sequences of PDZ3, derived from pdb entry 1be9 [203], the used mutants (PDZ-aha) in this thesis and the sequences with positions for the conserved energy transfer pathways indicated as reported by either Ranganathan and Lockless [9] or Ota and Agard [10].

starting point of the proposed energy transfer at His372 (for further details see Chapter 9) to be used in the later planned ultrafast experiments for direct tracking of energy flow. Those three positions are additionally matching other requirements. Ala376 is located at the opposite site of the binding pocket (than Ile327), Ser398 is located in the α_3-helix, which is discussed to be involved in a different type of allostery [188, 207] and Ala390 is as well part of the protein core (as is Ile341) but not predicted to be involved in allosteric communication. In Figure 5.2 the sequence of the first published crystal structure [203] from pdb entry 1be9 is compared to the positions involved in allostery as predicted by either Ota and Agard [10] or Ranganathan and Lockless [9] and the mutants tested in this thesis. As can be seen many more positions of interest are present.

By comparing the spectroscopically observed hydrophobicity to the local environment in the X-ray structure of the holoprotein (pdb: 1be9, [203]) the capability of Aha as sensor for local hydrophobicity was tested. To show the application potential of Aha for monitoring protein function and demonstrate the advantage of sensitive reporter groups for subtle, local conformational changes, ligand binding studies with FTIR of PDZ3 with its native ligand, the CRIPT peptide were performed.

5.3 Results and Discussion
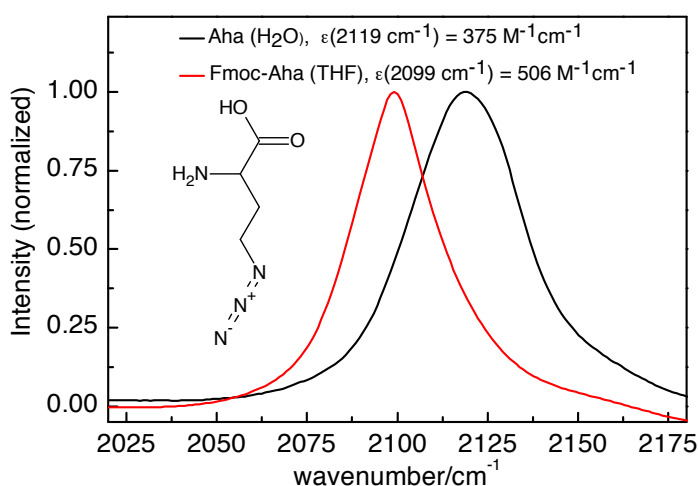
Figure 5.3: Normalized FTIR absorption spectra of Aha in H_2O and Fmoc-Aha in THF. Concentration dependent measurements with concentrations ranging from 5–25 mM were performed in H_2O (with 100 μm spacer) and tetrahydrofuran (with 50 μm spacer). All measurements were averaged for 128 scans and performed using a Bruker Tensor FTIR spectrometer equipped with liquid nitrogen-cooled MCT detector. An additional long pass filter with a cut-off at 4 μm was used. The mirror speed was set to 20 kHz. Settings were chosen to use the optimal range of the detector.

The presented results aim to demonstrate that the azide moiety of Aha (structure shown in Figure 5.3) is well suited to monitor local microenvironments in proteins. Based on this, it is aimed to establish that biophysical processes like ligand binding can be studied using Aha as site-specific

label in IR spectroscopy. The final problem addressed is whether the novel resolution on side chain level helps to gain new insights into unanswered questions like the nature of the long-range interaction for allosteric communication in PDZ3.

5.3.1 FTIR Spectroscopy of free Azidohomoalanine

In Figure 5.3 the vibrational absorption spectra of free Aha in H_2O (black line) and Fmoc-Aha in THF (red line) are shown. Concentration dependent FTIR measurements between 5 and 25 mM yield the extinction coefficients of the azide stretch vibration in both solvents. For H_2O we found $\epsilon = 375 \, M^{-1} \, cm^{-1}$ at a center wavenumber of $2119 \, cm^{-1}$ the corresponding values in THF are $\epsilon = 526 \, M^{-1} \, cm^{-1}$ at a center wavenumber of $2099 \, cm^{-1}$. THF was used to mimic the nonpolar protein core [274]. Because free Aha is insoluble in THF the Fmoc protected derivative was used. In contrast to Chapter 4, were for reasons of comparison the boc-protected form of Aha was used, here the Fmoc-protected derivative was used as the sample was available as a solid whereas the boc-protected sample is a very viscous fluid, not accurately to weight.

The results show how the azide center frequency is sensitive to the hydrophobicity of the environment. The results correspond well with the frequency shifts reported by Cho et al. ([274]) and Raleigh and Co-Workers [275, 289]. However, significantly smaller values for ε than reported in [76] ($1570 \, M^{-1} \, cm^{-1}$) are obtained, which match results presented in [274] and [139]. As discussed previously [76, 276, 314] the azide vibration is a suitable reporter group of local changes in the hydrophobicity. A first use in a model protein was reported by [289]. In contrast to other reporter groups, like thiocyanate [264] or nitrile [263], where the vibrational absorption frequency is linearly correlated to the electric field, azide can not be used for quantitative measurements of the field as discussed by [275] because of its ability to form hydrogen bonds and thus some concurring effects shift the center frequency.

However, with the following results it is demonstrated that azide is a good reporter group for the qualitative study of local environment. Not only the shift of the center wavenumber from $2119 \, cm^{-1}$ between H_2O as polar solvent with a dielectric constant of 78.5 down to $2099 \, cm^{-1}$ in the nonpolar solvent THF with a dielectric constant of 7.4 [315] (protein interior 2–10) can be used to gain insight into changes of the microenvironment. The line shape and line width add additional information. For the free Aha a change in line width when shifting from the polar, hydrogen-bonding solvent H_2O with a broad line width of $37 \, cm^{-1}$ to the nonpolar, non hydrogen bonding solvent THF with an observed line width of $28 \, cm^{-1}$ is found. This lets expect a line broadening for solvent exposed azides with an overall integrated signal size being comparable between non-exposed and exposed azides.

5.3.2 FTIR Spectroscopy of Aha-labeled PDZ3 and Analysis of Microenvironment

At all positions shown in Figure 5.1, Aha was introduced and for those six different mutants (residues 302–402, numbering according to [203]) FTIR spectra of the azide absorption were recorded. The FTIR absorption bands are shown in Figure 5.4, with the maxima for Aha in H_2O and THF indicated by arrows. All mutants show their azide absorption within the expected range from $2099 \, cm^{-1}$ to $2119 \, cm^{-1}$.

In comparison to this, Figure 5.5 shows the protein microenvironment for each of these mutants (based on available X-ray structures [203]). The surrounding residues are colored based on their polarity. This analysis links the observed variations of center wavenumbers and line shapes to the
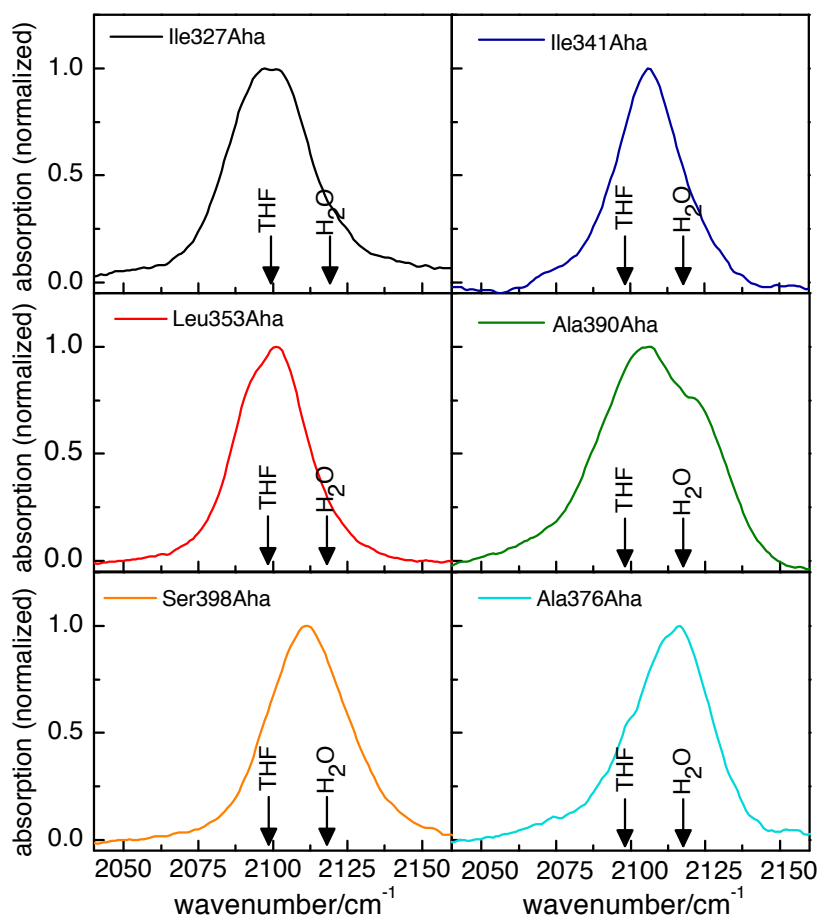
Figure 5.4: Absorption spectra for all six mutants of PDZ3 with Aha introduced at different positions. The signals are normalized for better comparison. Data was acquired in aqueous phosphate buffer, pH 6.8, with a spacer thickness of $100\,\mu$m and concentrations varying between 3–4 mM. Obtained signal sizes varied between 5–10 mOD depending on sample concentration.

individual hydrophobic environments of the mutants. The structural insights gained by this analysis strongly support the usage of Aha as direct reporter of local microenvironment in proteins.

Ile327Aha The residue 327 is positioned in the ligand binding pocket in β-strand B with the azide group oriented towards the protein interior and buried deeply between hydrophobic amino acid side chains (Figure 5.5 a and b). The azide vibration of Ile327Aha is centered at 2099 cm^{-1} indicating a high hydrophobicity as expected from the structure. The center frequency for this mutant is the lowest observed for all studied mutants with the same center wavenumber as Aha in THF. But in contrast this mutant has a broader line shape of 32 cm^{-1} with two submaxima, separated by approx. 2 cm^{-1}, which could be reproduced in several independent measurements. A possible reason for the splitting of the band might be, that the side chain can adopt slightly different orientations within the protein core, where it will experience different levels of hydrophobicity, as indicated in Figure 5.5 b.

Leu353Aha Leu353Aha is located in loop 4 between α-helix A and β-strand D, oriented towards the hydrophobic core of the protein domain, which is assembled by six β-strands, including β-strands A, D and F. The center frequency is 2101 cm^{-1} with a side maximum at approx. 2095 cm^{-1} (Figure 5.4). The line width of 28 cm^{-1} FWHM is smaller than for Ile327Aha. The results indicate a highly hydrophobic surrounding in combination with less local inhomogeneity than for

mutant	N$_3$ absorption [cm^{-1}]	FWHM [cm^{-1}]	structural element
Aha (H$_2$O)	2119 cm^{-1}	37 cm^{-1}	-
Aha (THF)	2099 cm^{-1}	28 cm^{-1}	-
Ile327Aha	2097 cm^{-1}/ 2101 cm^{-1}	32 cm^{-1}	beta
Ala376Aha	2111 cm^{-1}/ 2116 cm^{-1}	32 cm^{-1}	alpha
Ser398Aha	2111 cm^{-1}	33 cm^{-1}	alpha
Ile341Aha	2106 cm^{-1}	29 cm^{-1}	beta
Leu353Aha	2094 cm^{-1}/ 2101 cm^{-1}	28 cm^{-1}	loop
Ala390Aha	2106 cm^{-1}/ 2122 cm^{-1}	45 cm^{-1}	beta

Table 5.1: Center wavenumber of the azide stretch vibration for the six mutants investigated. Values for free Aha in THF and H$_2$O as given for comparison

Ile327. It seems two main orientations are favored. As shown in Figure 5.5 c and d the azide group is buried by nonpolar side chains, while polar residues are only present near its peptide bond

Ile341Aha   The amino acid residue Ile341 is located at the end of β-strand C and is part of the hydrophobic core of PDZ3 as well. In contrast to Leu353Aha, where the azide group is deeply buried in the hydrophobic core and thus only in proximity to hydrophobic side chains of the β-sheets, in this mutant the azide group is oriented more towards the surface of the protein (see Figure 2.4). βC is not part of the main antiparallel β-sheet forming the core of the PDZ motif, but is the outer strand of the opposite β-sheet formed by βB, βC and the peptide ligand. Here Ile341 is located close to loop 3, in a presumably more flexible region of the protein. The absorption spectrum for mutant Ile341Aha shows one maximum at 2106 cm^{-1} with almost symmetrical line shape and a line width of 29 cm^{-1} similar to Leu353Aha (Figure 5.4, Table 5.1). This finding indicates a homogeneous microenvironment in close proximity of the azide group. As visualized in Figure 5.5 e and f, the azide moiety is embedded between nonpolar residues.

Ala390Aha   The residue Ala390 is located in βF with its side chain oriented towards the protein interior. The corresponding FTIR absorption spectrum shows a main absorption band at 2016 cm^{-1} and an additional pronounced shoulder at 2122 cm^{-1} (Figure 5.4). The band has a broad line shape with a FWHM of 45 cm^{-1} indicating a complex microenvironment or hydrogen bonding as well as high flexibility. The shoulder implies the presence of a different sub ensemble with possibly a different orientation of the side chain, than for the main conformation. This can be explained when revisiting the surroundings of side chain 390. In Figure 5.5 g and h the azide at position 390 is shown from opposite sides. It can be clearly seen how one half of the surrounding residues has polar side chains (indicated in light to dark blue) whereas the other side is composed of highly hydrophobic residues. A slightly different orientation towards both sides of this cavity explains why we observe two highly separated sub ensembles in the FTIR spectrum.

Ser398Aha   The azide side chain in the mutant Ser398Aha is introduced in the C-terminal α-helix C, which is unique to PDZ3 and lacking in all other PDZ domains [188] (Figure 2.4). The corresponding FTIR absorption spectrum has a maximum at 2111 cm^{-1} and a line width of 33 cm^{-1} (Figure 5.4). Similar as for Ile341Aha the line shape is relatively symmetric, indicating a homogeneous environment. As shown in Figure 5.5 i and j, the azide is in proximity to polar and charged side chains, illustrated by the light and dark blue color, but mostly solvent exposed. The combination of these
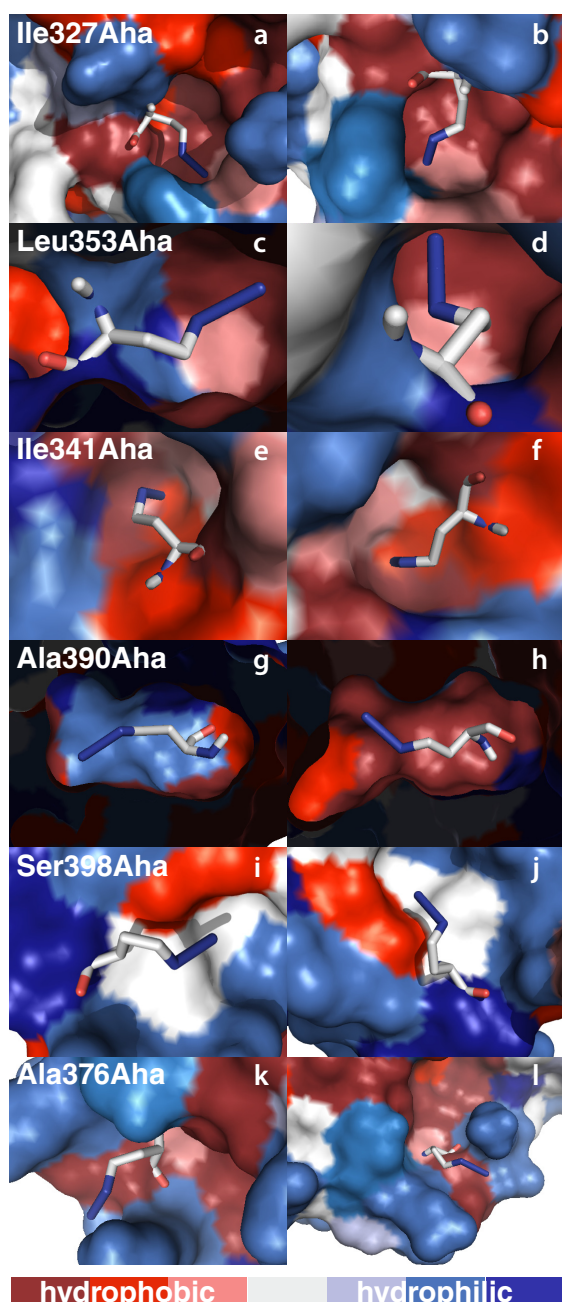
Figure 5.5: Microenvironment of Aha in the six described PDZ mutants. The orientations are derived based on a combined approach of alignment to known structure (from pdb entry 1be9, [203]) together with molecular docking (using AutoDock 4.2 [316]) using Aha as flexible residue [317]. Details are described in Appendix C. All amino acids are colored based on their hydrophobicity according to the free energy of the amino acid side chain for the transition from cyclohexane to H_2O in the gas phase (values obtained from [318]). Shown is the surface of the whole protein with the surface volume of Aha subtracted. The Aha residue is shown as sticks. The figures were prepared using PyMol [319].

effects explains why the measured azide absorption frequency is close to the center wavenumber in water for this mutant.

Ala376Aha In Ala376Aha the azide is located in α-helix B, which forms part of the binding pocket, as shown in Figure 5.1. This mutant has the highest azide absorption wavenumber with its center at 2116 cm^{-1} and a line width of 32 cm^{-1} (Figure 5.4). The asymmetric line shape indicates an inhomogeneous microenvironment. The azide group is mostly water exposed and not surrounded by protein side chains, illustrated in Figure 5.5 by free space. Due to this, the center wavenumber is

approximately the same as for free Aha in H_2O, the small shift towards lower wavenumbers might be explained by the difference of surface water to bulk water, since the water molecules in the ligand binding pocket, where the azide is located in this mutant, possess a different and higher ordered structure than water molecules surrounding free Aha. Also, following the results by [278] and [279] the azide moiety is a sensitive sensor for hydration because of its frequency blue shifting upon hydrogen bonding. As the azide group in Ala376Aha does not have a complete solvation shell as Aha in free solution but part of its surrounding is the protein the difference between the center frequency found for Ala376Aha to free Aha can easily be explained.

Figure 5.6: Aha in two different secondary structure elements, an α-helix and a β-strand.

Possible Influences of Higher Ordered Structure on Azide Frequency. The comparison of the center wavenumbers reported in Table 5.1 with the related secondary structures hints towards a direct correlation of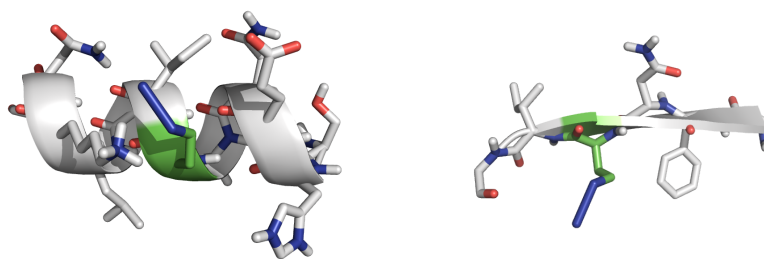 azide absorption to the containing structural element. For the β-strand mutants Ile327Aha, Ile341Aha and Ala390Aha the maxima are at 2099 cm^{-1} and 2106 cm^{-1}. For Leu353Aha, which is located in a loop, the azide vibration is observed at 2100 cm^{-1}, indicating that this region is hydrophobic. For Ser398Aha and Ala376Aha higher values with 2111 cm^{-1} and 2117 cm^{-1} are found, both residues are located in α-helices. As discussed by [275] and [276] several effects need to be considered for interpretation of the frequency shift of the azide. Especially the distribution of partial charges and presence of unbound electron pairs in two of the three nitrogen atoms generates several interactions sites for the building of hydrogen bonds that differently influence the frequency shift, with experimental data indicating that Hydrogen-bonding leads to a blue-shift and line-broadening (this work and [279]). This experimental observations of frequency shifts thus might not only monitor the direct microenvironment around the azide moiety, but an effect of the secondary structure and possible interactions with the peptide backbone could be considered. α-helices posses an overall dipole moment that might lead to an effect explaining the observed correlation and in [313] an blue-shifting of the azide absorption upon interaction with carbonyl groups from the peptide backbone is discussed. These two effects could explain the findings here. In an α-helix the peptide bond is hidden in the helix core and not accessible for hydrogen bonds to the azide whereas in an β-strand electrostatic interactions and hydrogen bonds are present to stabilized a β-sheet as can be seen in Figure 5.6. But the finding of red-shifted azide absorptions in β-strands and blue-shifted azide absorptions for Aha in α-helices are inverse to the effect of electrostatic interaction with the peptide backbone as proposed originally by Oh et al. [313]. The results can be better explained in comparison with the findings by Wolfshorndl et al. [279], who reported that azides are especially sensitive to hydration and the highest blue shift of the azide frequency was found in water, even in comparison to solvents with additional H-bond donors. A

similar result, supported by quantum chemical calculations was reported by Choi et al. [278]. As the azide in the two tested α-helices (mutants Ala376Aha and Ser398Aha) is more water-exposed than the azide in the three mutants positioned in a β-strand, which is part of the hydrophobic core, this explanation is very likely. Thus these results on *random* positions and the previous explanation of wavenumber shifts as result of the hydrophobicity of the microenvironment strongly suggest that single effects like blue-shifting of the center wavenumber upon hydrogen bonding or red shifting through interaction with H_2O [278] are not mainly accountable for the experimentally observed absorption spectrum. However to validate and understand the competing effects of electrostatic interactions and hydrogen-bonding to the solvent H_2O molecules on the azide center wavenumber or line shape, further experiments in different proteins and different microenvironments as well as support from theory will be needed.

5.3.3 Study of Ligand Binding (CRIPT) to PDZ3
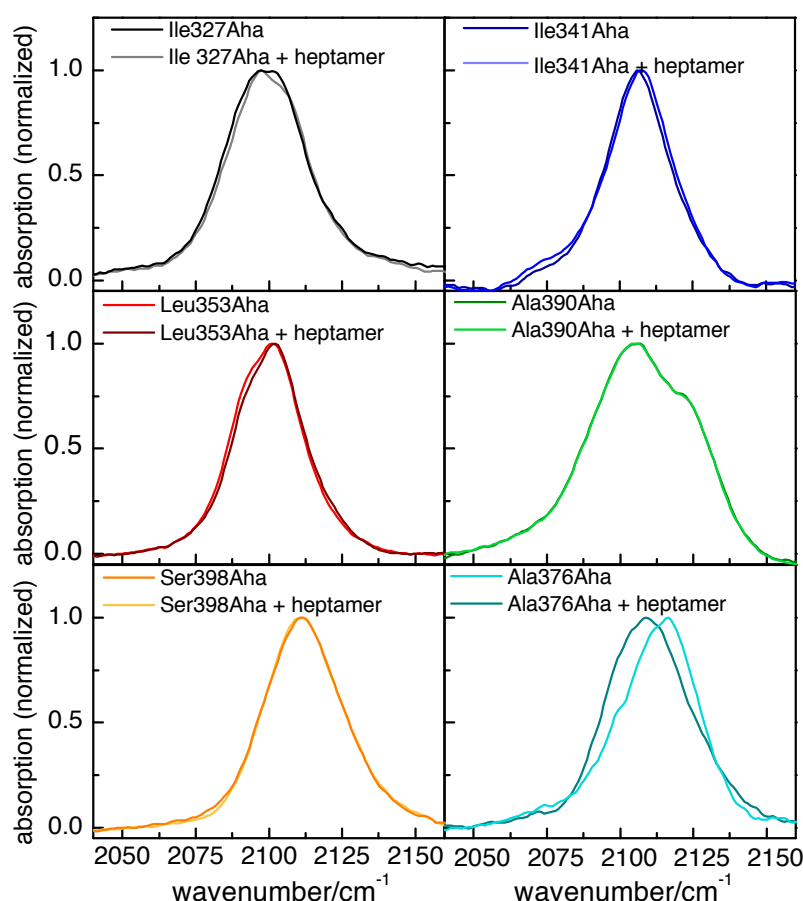
Figure 5.7: Absorption spectra for all six mutants of PDZ3 with Aha introduced at different positions in complex with the CRIPT peptide as ligand. The signals are normalized for better comparison. Data was acquired in aqueous phosphate buffer, pH 6.8, with a spacer thickness of $100\,\mu\text{m}$ and concentrations varying between 3-4 mM. Measurements with the native CRIPT peptide acNYKQTSV as ligand were performed with 1.5–2 fold excess of ligand to obtain maximum binding and repeated to ensure they are reproductive. Additional information on experimental conditions and data processing can be found in Appendix B.

The binding of a conserved C-terminal motif with a special sequence of hydrophobic and charged residues is characteristic for all PDZ domains. For PDZ3 from PSD-95 this is Thr/Ser-X-Val. A well studied interaction partner is the CRIPT protein, whose c-terminal sequence ac-NYKQTSV is used as a peptide ligand in these studies. Based on previous structural data, especially the X-ray analysis of the ligand binding [203], but also NMR-studies on allosteric effects of the small c-terminal alpha-
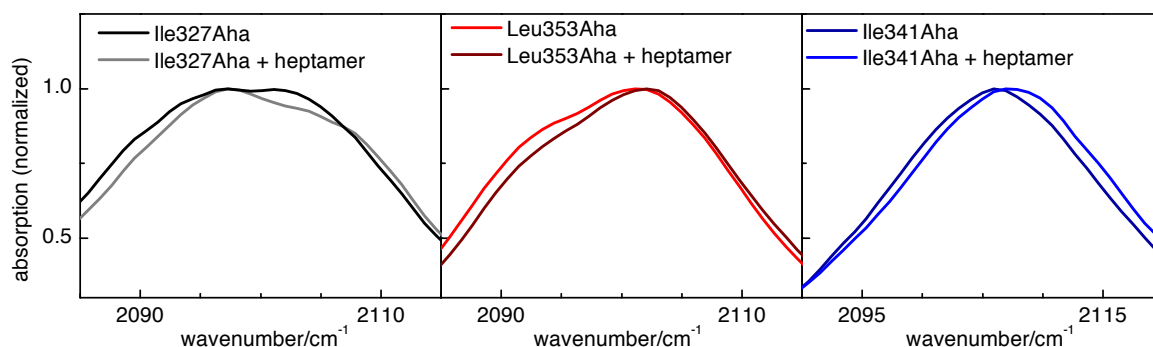
Figure 5.8: Magnified FTIR absorption spectrum of the three PDZ mutants (Ile327Aha, Ile341Aha, Leu353Aha) which show a spectral shift upon ligand binding, indicating a small conformational change.

	K_d [µM]
WT	2.87 ± 0.2
Ile327Aha	24.7 ± 0.4
Ala376Aha	22.6 ± 0.5
Ser398Aha	1.89 ± 0.2
Ile341Aha	2.52 ± 0.2
Leu353Aha	2.49 ± 0.05
Ala390Aha	2.97 ± 0.07

Table 5.2: Binding constants for PDZ3 mutants with CRIPT peptide acNYKQTSV as obtained by Isothermal Titration Calorimetry. The experimental details are given in Appendix B

helix unique to PDZ3 [188], the mutants were tested for the capability of Aha as a potential probe for ligand binding. Furthermore, it was assessed whether IR spectroscopy, using azide as a local reporter group, can add insights to the long standing debate on allosteric communication mechanisms upon ligand binding in PDZ3. From the X-ray structures, only subtle changes in the secondary structure are predicted (in loop 2, [203]) and thus the local environment of the azide moiety of Aha at the discussed positions should not change significantly. An exception is expected for mutant Ala376Aha in the binding pocket as its hydration status changes upon ligand binding. The ligand binding to all mutants shown in Figure 2.4 was tested by isothermal titration calorimetry (results in Table 5.2, details on the experiment in Appendix B) and FTIR absorption spectroscopy (Figure 5.7).

The binding constants for the Aha labeled PDZ mutants to the ligand acNYKQTSV are in good agreement with results for wild type PDZ (Table 5.2) and literature values [188, 320]. Mutations in the binding pocket (Ile327, Aha376) lower the binding affinity for the native peptide ligand, but the binding constants are still in the lower µM range, so the mutants seem to be mainly undisturbed. Combined with observations from CD spectroscopy (see Appendix B), that the secondary structure of all mutants is preserved, we conclude, that the introduction of Aha does not alter the functionality of the PDZ3 domain.

The FTIR spectra of all mutants with and without peptide ligand are shown in Figure 5.7. For mutants Ile327Aha, Ile341Aha and Leu353Aha small changes in the spectra are observed (a magnification of the respective parts of the spectra is shown in Figure 5.8), especially in the line shape, upon ligand binding, which were reproducible in several independent experiments. In Ile327Aha the azide group itself is not directly involved in ligand binding, but the residue is coordinated over hydrogen bonds between protein backbone and the ligand as shown in Figure 5.9 b. So it is not expected that ligand binding directly alters the absorption for the azide. The reason for the

observed shift thus might be a small local rearrangement induced by the hydrogen bonding of the related peptide bonds, leading to the tightening of a previous possible position proximal to the very hydrophobic residues in the surrounding. This is possible explanation why an increase for a already present sub band indicating a higher population of this sub ensemble for the mutant Ile327Aha is found. The same can not be true for the observed shifts in Ile341Aha and Leu353Aha. Those residues are not directly involved in ligand binding but located in β-strands which form the hydrophobic core of the PDZ3 domain. Both residues are discussed to be involved in the predicted allosteric network (in the pathway as proposed by [10]). The observed spectral shifts indicate a subtle conformational change leading to rearrangements of the direct microenvironment of the two residues. In contrast mutants Ala390Aha and Ser398Aha do not show any changes upon ligand binding. Ala390Aha is as well located in the protein core, but here the azide group does not sense a change of the microenvironment. In the mutant Ser398Aha the Aha residue is located in the C-terminal α-helix unique in PDZ3. This α-helix was found to highly influence the binding affinity for the CRIPT peptide [188] with several direct interaction sites with the ligand detected in NMR studies carried out by [207]. No influence of ligand binding to the azide center wavenumber or the spectral line shape can be found in Ser398Aha. As the side chain is oriented away from the ligand this finding is not to surprising. A better test to map whether an extended binding interface as proposed by [207] involving the α-helix C is present in PDZ3 would be performed by replacing either Tyr397 or Phe400 with a UAA as local probe. The biggest change is observed for the mutant Ala376Aha. Here the center wavenumber of the azide absorption changes from 2117 cm^{-1} to 2108 cm^{-1}. This huge frequency shift of 9 cm^{-1} might be explained by the exclusion of surrounding water molecules from the binding pocket. The azide is located in the α-helix B, which forms the other outer half of the binding pocket. But in contrast to Ile327, Ala376 is not directly involved in ligand binding (as seen in Figure 5.9 a), but sticks out from α-helix B towards the solvent as is reflected by the high wavenumber observed for the ligand free Ala376Aha at 2117 cm^{-1}.
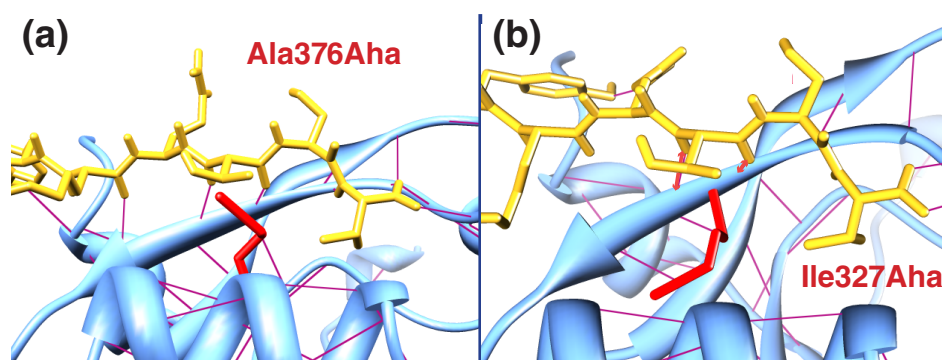
Figure 5.9: The mutants Ala376Aha (a) and Ile327Aha (b) in complex with the native CRIPT ligand (as peptide acNYKQTSV). Structures are taken from pdb entry 1be9 [203] with the orientation of Aha modeled based on results from flexible docking. The orientation of the peptide ligand is obtained from docking as well. Hydrogen bonds of the complex are indicated in red with prominent interaction of the backbone of Aha indicated by arrows. In the mutant Ala376Aha the azide group is located in α-helix 2, which forms half of the binding pocket. But the residue 376 is not involved in ligand binding. In contrast in mutant Ile327Aha the azide group is located in β-sheet 2, that forms the second half of the binding pocket. As is indicated by red arrows the residue 327 is involved in ligand binding by hydrogen bonds formed between the protein backbone and the peptide.

5.3.4 Allostery and Long-Range Communication in PDZ3

PDZ3 is not only an example for a protein-protein interaction domain, but an intensively studied prototype system for allostery. As first introduced by [9] and further developed by [10] different computational approaches show a coupled network of amino acid residues, that might transmit information upon ligand binding [187]. Several experimental attempts [188, 197] tried to prove the existence of the predicted energetically coupled network but up to today the theoretical predictions can not be validated.

The presented FTIR results using Aha as a local probe in PDZ3 add some information. Three of the investigated mutants, Ile327, Leu353 and Ile341 were chosen because they are part of the predicted sparse network. The three other mutants are not part of the predicted pathway with Ala376 located in the binding pocket, Ser398 in the α-helix that increases the binding affinity for the CRIPT peptide and Ala390 positioned far apart from any interaction site.

In Figure 5.7 the absorption spectra of the free PDZ and their change upon ligand binding are plotted. As discussed above for residues Ile327 and Leu353 a subtle change of the line shape goes along with the decrease of one sub band in favor of the increase of a main maximum (at 2097 cm^{-1} for Ile327 and at 2102 cm^{-1} for Leu353). For Ile341 a small shift of the center wavenumber is observed. At these residues which are part of the predicted energetically coupled network [10], a small change of the microenvironment seems to happen upon ligand binding. In case of Ile327 this can be explained by direct interaction with the peptide ligand. The azide group itself is not directly involved in ligand binding, but the residue is connected to the ligand via backbone H-bonds. The reason for the observed shift thus might be a small local rearrangement induced by the hydrogen bonding of the mentioned peptide bonds, which changes the relative populations of the two sub ensembles, producing the double peak in the ligand free spectrum. This is not possible for Leu353 or Ile341, where the change of the azide absorption clearly indicates a subtle conformational change, thus supporting the idea of the presence of an long-range effect of ligand binding on local structure in PDZ3. Overall the observed frequency shifts indicate a subtle conformational change and not a huge conformational rearrangement, which fits well with the reported findings from X-ray structures.

However, instead of explaining these findings only by the presence of an allosteric network, conformational selection as predicted by [208] from MD simulations might be an alternative mechanism leading to the observed change in line shape. This mechanism postulates that the protein domain indeed undergoes conformational fluctuations and one conformation is favoured for ligand binding, which is in contrast to the earlier predicted binding mechanism of induced fit based on the very similar X-ray structures[203]. The spectral change from showing sub ensembles to one favored conformation in Ile327 and Leu353 can be interpreted as adopting one favored conformation for ligand binding. The mutant Ala376, not directly involved in ligand binding but located in α2, that forms part of the binding pocket, is discussed by [208] to experience some small structural rearrangement upon ligand binding through a predicted scissor-like closing of the binding pocket in the protein-ligand complex. The FTIR data show a huge change for the absorption frequency of Ala376 upon ligand binding, but due to the sensitivity of Aha to surrounding water and the exclusion of water from the binding pocket, these findings do not safely support the theoretical prediction. Further experiments using the demonstrated combination of FTIR and the Aha label, dedicated to investigate the scissor motion, are needed.

A different allosteric effect, special for PDZ3, was introduced by [188]. They investigated the effect of α3, unique to this PDZ domain and found a huge effect on ligand binding affinity. The FTIR data do not provide new insights into the effect of α3 on ligand binding, because Ser398 is

oriented away from the predicted interaction surface between α3 and the CRIPT peptide. The highest binding affinity for this mutant was found in the ITC measurements (reported in Table 5.2) with a significantly lower binding constant as for the wild type, emphasizing the importance of α3 for high ligand affinity.

The presented results add experimental evidence to the hypothesis of long-range communication in PDZ3 upon ligand binding. They clearly show allosteric conformational changes at distinct residues not connected to the binding pocket (Ile341, Leu353) in good agreement with previous predictions [10].

5.4 Conclusion and Outlook

This study aimed to demonstrate a first application of UAAs as site-specific probes in IR spectroscopy and to show that Aha is a sensitive reporter group for the study of protein microenvironments. It was tested whether the enhanced local resolution enables IR spectroscopy to unravel unanswered biophysical questions. PDZ3 from PSD-95 was used as test protein for studying ligand binding functionality and its allosteric mechanism. Previous results suggested, that IR spectra of Aha in proteins might be hard to interpret due to several competing effects. The complex solvatochromism of Aha, as discussed by [275, 276, 279], might hinder the direct interpretation of IR absorption spectra. It was stated, that analysis of the different contributions to spectral shifts from hydrogen bonding or changes in hydrophobicity would be needed. Here it is demonstrated how versatile Aha as spectral probe is for the study of biophysical problems, even though its center wavenumber is only qualitatively correlated to the hydrophobicity of the surrounding and probably can not be used for quantitative measurements. The observation of free Aha in an polar or nonpolar solvent directly shows the sensitivity of azide to polarity and the results for six different incorporations sites in PDZ3 show how sensitive Aha is to monitor different protein environments. The direct comparison of the experimentally obtained data for hydrophobicity with known X-ray structures demonstrates that Aha is well suited for this application. All obtained center wavenumbers predict the hydrophobicity of the microenvironment correctly. This demonstrates how, despite several different physical effects influencing it, the azide absorption is still usable for the investigation of the local protein microenvironment.

When used as reporter group for protein function, like ligand binding in the example of PDZ3, Aha is excellently suited as well. Two of the investigated mutants are located in the binding pocket and for both not only a change of center wavenumber was found but also molecular explanations derived from the binding mechanism. In mutant Ile327 only the peptide backbone is involved in ligand binding, leading to a small change for the azide absorption due to changes of hydrogen bonding to the backbone, whereas in mutant Ala376 we were able to observe how water is excluded from the binding pocket.

Azidohomoalanine is a suitable tool for testing subtle conformational changes, which indicate long-range communication, as shown for Leu353 and Ile341. The data presented here, demonstrate how the combination of IR spectroscopy and a new site-specific spectroscopy probe can be used to study difficult biophysical phenomena, such as allostery. The results supporting the presence of a coupled network of amino acid residues, are a first evidence how the use of site-specific spectral probes will change the scope and add novel applications to IR spectroscopy. Further experiments are necessary to prove or disprove the predicted allosteric mechanism in PDZ3 and study long-range effects in more detail. The novel approach of combining FTIR spectroscopy with UAAs as site-specific probes to enhance spatial resolution is not a stand-alone technique but the

gained results should be confirmed and discussed in context with other biophysical experiments. To achieve deeper understanding of the complex allosteric mechanism in PDZ3 and the several dynamic processes happening, additionally NMR experiments in collaboration with the group of Harald Schwalbe are underway.

6 Monitoring of Ultrafast Equilibrium Dynamics in PDZ3

One of the many applications of 2D-IR spectroscopy on a site-specific probe in a protein is the investigation of ultrafast equilbrium dynamics. The spectral diffusion dynamics of the azide moiety in Aha are modulated by fluctuations of the environment and thus is in principle possible to probe conformational dynamics of a protein in an experiment. To explore the technical feasiblity and the possible information gain of this appraoch again the PDZ domain was used as first target. Of the six introduced and discussed mutants from Chapter 5, Ala390Aha and Ile327Aha were chosen for demonstration of 2D-IR experiments

This chapter is organized as follows: The first section covers motivatin and experimental design, the second shows results on free Aha in water, the third section reports 2D-IR results on PDZ Ile327Aha, the fourth section contains results on the mutant Ala390Aha and the fifth section covers results on the mutant PDZ Ile327Aha with and without ligand.

6.1 Motivation

As outlined in Chapter 2 allostery and conformational dynamics of a protein can be understood in an energy landscape picture [173]. Those only slightly differing conformations which constitute the native state of a protein interchange between each other on picosecond time scale. For the understanding of processes such as the predicted conformational selection in ligand binding in PDZ3 [208] experimental insights into the equilbrium fluctuations of the protein structure are of huge importance.

In this chapter the first 2D-IR spectra of an Aha labeled protein are reported. The aims of this study were first of all to determine the time window accessible by 2D-IR spectroscopy when using Aha as label. The vibrational life time of the azide stretch vibration was determined before in THF, but other parameters affect the actual measurement window as well, foremost of all the possible sample concentration and the competing solvent background from a heated H_2O combination band.

The second aim was to show that it is indeed possible to record a 2D-IR spectrum of an Aha labeled protein. Before any biologically relevant informations can be extracted from a 2D-IR spectrum of a UAA in a protein a proof-of-principle experiment was necessary. The spectra can then be discussed in terms of the third aim of these experiments, which is to demonstrate how Aha can be used for monitoring fluctuations on the free energy landscape in the time frame of several picoseconds.

Not only conformational dynamics of the protein lead to inhomogenous broadening of the azide vibration but solvent dynamics are well known to influence 2D-IR spectra and thus it was planned to test whether solvent reaarengements can be observed as well. Also it would be interesting to see whether exchange between conformational sub ensembles on picosecond timescale can be observed using the azide moiety as reporter group.

To test the ability of the proposed approach for investigating conformational selection it was tested if the ligand binding is influencing the protein flexibility and therefore spectral diffusion.

6.2 Experimental Design

All experiments were carried out using the setup as described in Appendix A. The first set of experiments focused on Aha in H_2O to identify the needed concentration and spacer thickness for obtaining a 2D-IR signal with the setup in a configuration using only OPA I for IR light generation. Acceptable experimental conditions to measure signals with good SNR and quality were determined. A crucial aspect for SNR is the background absorption of the solvent. In the region around 2100 cm^{-1} the combination band in H_2O can be found [321], which strongly absorbs the IR pump and probe light. Therefore samples can not be measured using a spacer thickness of higher than 50 µm, otherwise almost no light reaches the detector because of the high optical density of the sample.

The data presented in this chapter were obtained as 2D-IR spectra in the pump-probe approach with pump and probe light both generated using OPA I. The energy of OPA I was around 3 µJ for the chosen wavelength of 4750 nm, measured at the entrance of the 2D-IR setup. For the measurements the pump pulse had a band width between 12 and 15 cm^{-1}. All data were recorded using the 150 line grating. The polarization of the pump and probe beam relative to each other was set to parallel.

All experiments of protein samples were performed with sample concentrations around 15 to 18 mM. Samples were prepared from frozen aliquots of purified protein (see Appendix B) and controlled by MALDI for high labeling yield.The protein concentration was determined by a Lowry assay. The samples were concentrated using Vivaspin 500 centrifugal concentrators with a MWCO value of 5000 and possibly aggregated protein was removed in a final centrifugation step. Samples were not pumped through the measurement cell [296] as in contrast to experiments presented in chapter 9.

The mutants chosen for 2D-IR measurements are Ile327Aha and Ala390Aha. Both of them are interesting to demonstrate different aspects of using UAAs as labels in 2D-IR of proteins. Ile327Aha is located in the binding pocket and involved in ligand binding but as well part of the predicted energy transfer pathway [10]. In the FTIR data it was found, that Ile327Aha posses two absorption maxima which show a subtle change upon ligand binding. Thus this mutant is an ideal candidate to test the influence of ligand binding on the azide absorption as well as potentially help to gain understanding into the conformational dynamics of the protein in its bound and unbound state. Ala390Aha is located in the hydrophobic core of the protein and had two very distinct absorption bands in the FTIR spectrum, which do not show any change upon ligand binding. This mutant is interesting for comparison as it would be expected to show a different spectral diffusion dynamics.

6.3 Results and Discussion

6.3.1 2D-IR on Aha in H_2O

This section focuses on free Aha in water using experimental conditions, which allow comparison to protein measurements. Figure 6.1 shows 2D-IR spectra of free Aha in H_2O measured with the 150 line grating. Spectra with higher resolution measured using the 300 line grating are discussed in chapter 4.

The spectra shown in Figure 6.1 were recorded for the waiting times -20 ps, 1 ps, 1.25 ps, 1.75 ps, 2.5 ps, 3.5 ps, 5 ps and 10 ps. The signal intensity observed in these spectra of a sample with a concentration of 100 mM is ±1.25 mOD for a waiting time of 1 ps and decreases to 0.065 mOD for a waiting time of 5 ps, reflecting the time window accessible by the vibrational life time of the azide group (for further discussion see chapter 4). Those data shown in Figure 6.1 are corrected by subtraction of the heated background at 10 ps to account for solvent contributions. The influence
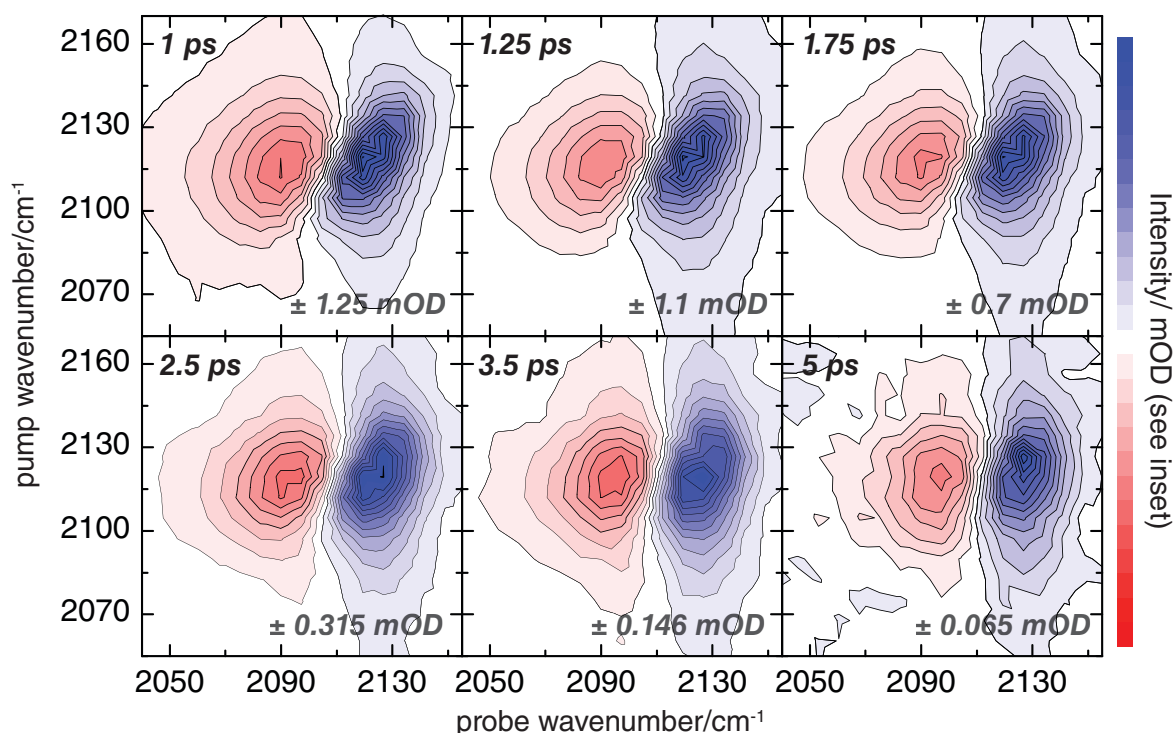
Figure 6.1: 2D-IR spectra of the label Aha in H_2O. Shown is the diagonal peak for the azide stretch vibration, which has its absorption maximum at 2119 cm^{-1} (see figure 5.3). The spectra are corrected for background contributions from the heated H_2O band by subtraction of the 10 ps signal. Data were recorded using the 150 line grating with a sample of 100 mM Aha in H_2O with 50 µm spacer thickness. The pump pulse was narrowed using the Fabry-Perot and had a band width of 15 cm^{-1}, the IR intensity generated from OPA I was about 2.8 to 3 µJ at the entrance of the 2D-IR setup. The contour levels in the plot are chosen to show the maximum signal.

and disturbance of spectra by H_2O in the region around 2100 cm^{-1} was already shortly mentioned in chapter 5.

The azide absorption at 2119 cm^{-1} is almost ideally centered on top of the combination band in H_2O at about 2125 cm^{-1} comprised of contributions from the bending vibration as well as librations [321]. The H_2O band is visible in the 2D-IR spectra after vibrational relaxation and cooling of the molecule as can be seen in the spectra in Figure 6.2 already at 2.5 ps. The combination band has a broad line width and therefore it is possible to account for the heated background by simple subtraction of a signal at longer waiting times (e.g. 10 ps) where the 2D-IR spectrum is dominated by the solvent background (seen in Figure 6.2 for 10 ps). The simple subtraction does not take the time dependence of the water background into account. For protein samples this was accounted for by subtraction of a long term background scaled by a time dependent factor for the respective times (this was done for data shown in Figure 6.6 and Figure 6.8 [1]).

In Figure 6.3 cuts through the 2D-IR spectrum shown in Figure 6.1 for the pump centered at 2112 cm^{-1} are shown, which show that the line shape of the azide band in H_2O is unperturbed (as in contrast to the azide stretch mode in N3P as discussed in Chapter 4) and similar to the line shape observed for the azide stretch vibration in THF (see Figure 4.6).

The effect of vibrational cooling and relaxation of the azide stretch vibration can be seen in the

---

[1]A script for the time-dependent fitting of the H_2O band was written by my colleague Luuk J.G.W. van Wilderen.
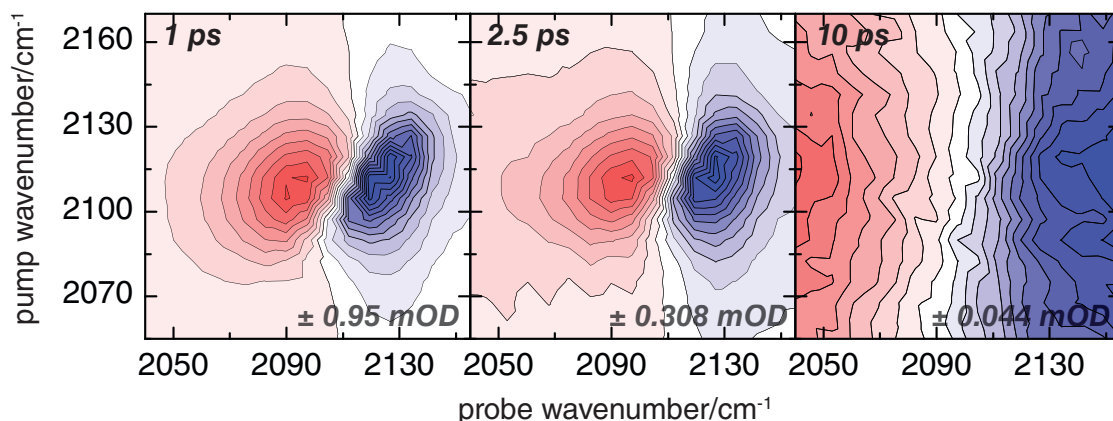
Figure 6.2: 2D-IR spectra of the label Aha in H_2O. The data are from a different measurement as those in figure 6.1, with similar sample conditions (100 mM, H_2O, 50 μm spacer). The data are corrected by subtraction of the negative background signal at -20 ps instead of subtraction of the heat background at 10 ps.

transients shown in Figure 6.4. Here the transient signal for the bleach of the azide absorption is shown both in THF and H_2O (THF data from experiments reported in chapter 4). It can be seen, that the decay of the signal is faster in THF. The transient for the azide stretch vibration in H_2O can be fitted with a bi-exponential function with $\tau= 0.52$ and 0.53 where as the τ in THF is 0.71 and 0.72. It seems that in the hydrophobic and non-hydrogen bonding solvent the azide vibration relaxes faster or vibrational cooling by heat transfer to the solvent is faster than in the polar and hydrogen-bonding solvent H_2O.

In the 2D-IR spectra in Figure 6.1 also the spectral diffusion dynamics, which are accessible with the resolution provided by the 150 line grating, can be observed. As was already discussed in chapter 4 the spectral diffusion properties of a novel vibrational probe are the key to the study of local dynamic changes in a protein on the picosecond timescale. Judging by the data in Figure 6.1 the application of Aha in H_2O to measure site-specific structural dynamics in proteins appears feasible for a time-window up to 5 to 10 ps. For a detailed analysis, measurements with the 300 line grating would be more appropriate.

Figure 6.3: Time-dependent cuts through the 2D-IR spectrum of Aha in H_2O recorded on the 150 line grating with waiting times comparable to protein measurements.
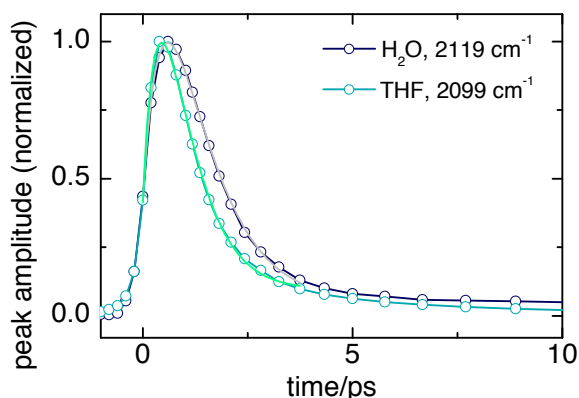
Figure 6.4: Transients for the bleach signal of Aha both in H_2O and THF, recorded with the narrow band pump pulse centered on the main azide absorption. The data are corrected fo a heated background from H_2O and fitted with a bi-exponential function.
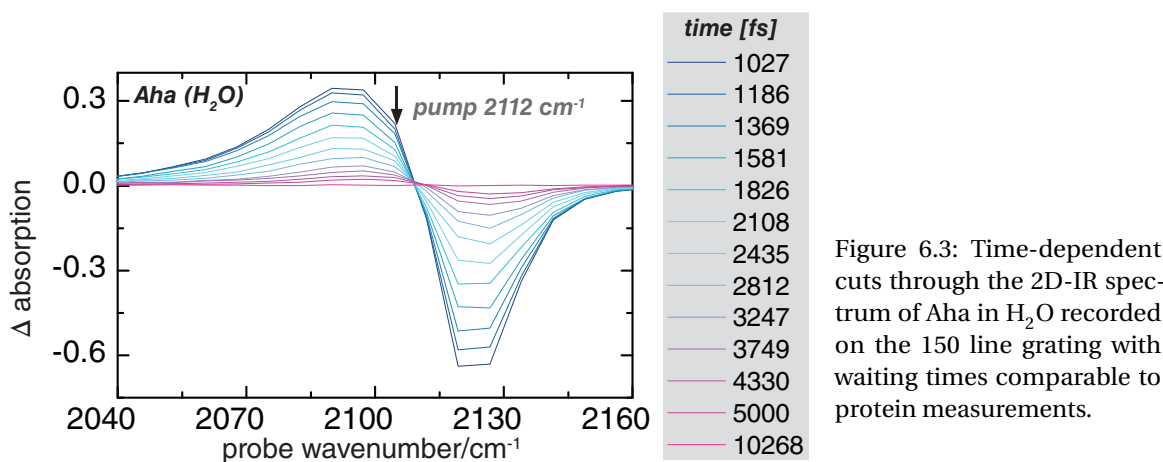
6.3.2 2D-IR on Ile327Aha

The first experiments to demonstrate that it is indeed possible to measure 2D-IR spectra of an Aha-labeled protein have been carried out on the PDZ mutant Ile327Aha.

This mutant site is located in the binding pocket of PDZ as shown in Figure 5.9 b.Aha is involved in ligand binding via its peptide backbone with the azide group pointing towards the protein interior. The site is believed to be a key position for the allosteric communication in PDZ3 [9, 10]. For this mutant it was shown in Chapter 5 that the azide group is positioned in a hydrophobic pocket which forms part of the binding groove and that indeed ligand binding to this mutant can be monitored on the center wavenumber, indicating a change in the local microenvironment.

Figure 6.5: 2D-IR spectra of the PDZ mutant Ile327Aha in H_2O. Data are corrected by subtraction of the heat background at 10 ps to remove solvent contribution to the signal. Note the leaking pump pulse leading to artifacts along the diagonal, most notable for the 2.5 ps signal. The sample conditions were approx. 15 mM protein in phosphate buffer and 50 µm spacer. The width of the pump pulse was adjusted to 16 cm^{-1}, data were recorded using the 150 line grating.

The FTIR spectrum of this mutant, which was discussed in more detail in chapter 5 shows two sub bands and one of the goals of this first 2D-IR study was to find out if it is possible to reproduced this observation in a 2D-IR spectrum. In Figure 6.5 the very first 2D-IR spectra of an Aha labeled protein sample are shown. The current literature only discusses Aha in a peptide ligand (and not incorporated in a protein) for 2D-IR [139]. The sample concentration was approximately 15 mM before a final centrifugation to remove particles. For the 1 ps signal an intensity of 0.126 mOD was observed. The tilt of the peak is very pronounced. Since the data are recorded with the 150

line grating the resolution is not as high as possible. Based on the 1 ps signal it can not be safely stated, that two submaxima are observed as in the FTIR spectrum. Between the time delay of 1 ps and the time delay of 2.5 ps almost no spectral diffusion can be observed. At 1.75 ps the impression to observed two submaxima in the bleach signal might be gained, which would need further confirmation with data of higher signal intensity. The spectral diffusion behavior of the azide side chain in Ile327Aha indicates that no conformational changes are happening in the time frame between 1 ps and 2.5 ps. Also no rearrangements of the side chain itself or changes of the micro environment are happening on the time scale accessible, which means that the position of the side chain is very rigid and its surrounding is inhomogeneous on this timescale.
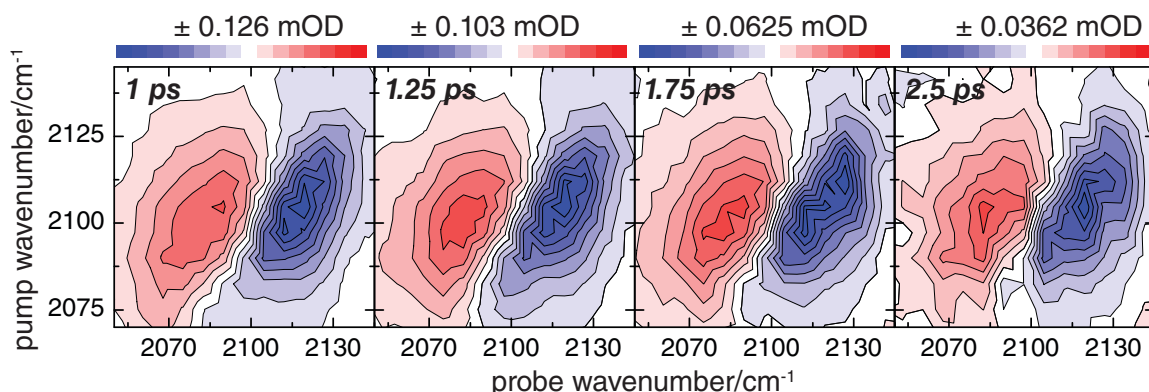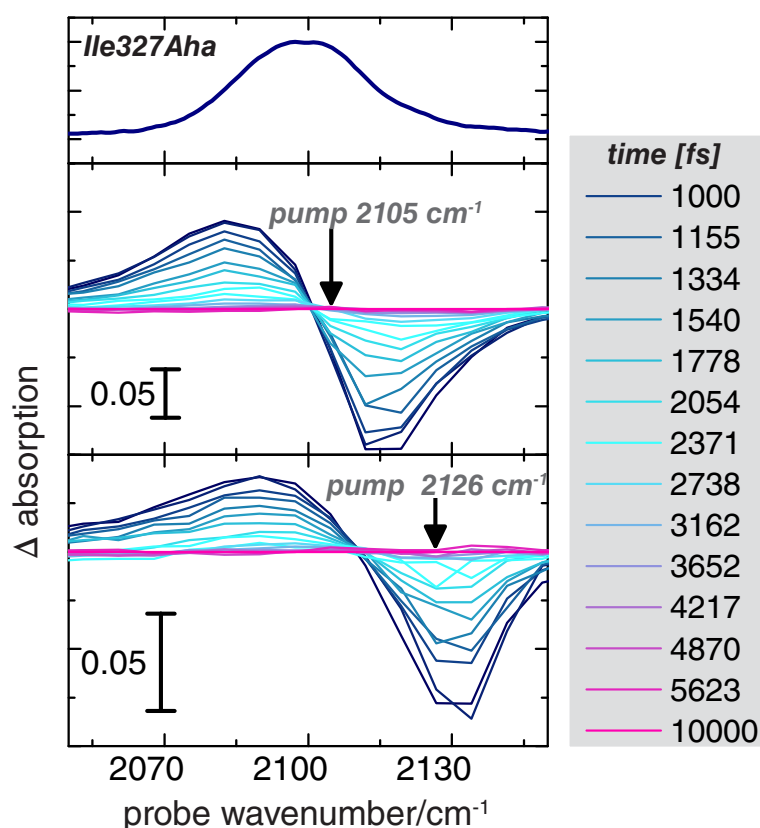

Figure 6.6: Time-dependent cuts through the 2D-IR spectra of the PDZ mutant Ile327Aha in H_2O. Data are corrected by subtraction of the heat background at 10 ps to remove solvent contribution to the signal. The sample conditions were the same as for data reported in Figure 6.6, data were recorded using the 150 line grating.

To reach a higher signal intensity either the sample concentration needs to be higher, which is not possible for a protein sample. Or the pump power needs to be enhanced. This is in principle possible with the setup used, however the high-power OPA used for experiments reported in chapter 4 was not in operation for the experiments presented in this chapter. This is why also no data of a protein sample recorded with the 300 line grating and thus higher spectral resolution are presented. Using the OPA I as pump and probe light source for measuring a protein sample in H_2O with a thickness of 50 μm on the 300 line grating is not possible, because almost no light can be detected.

In Figure 6.6 cuts through the 2D-IR spectra for two different pump positions are shown. In comparison with the FTIR spectrum it can be seen, that the center of the azide bleach signal seems to have shifted towards higher wavenumbers by 10 cm^{-1}. This finding indicates, that the azide group in this sample is exposed in a less hydrophobic environment or is exposed to more hydrogen
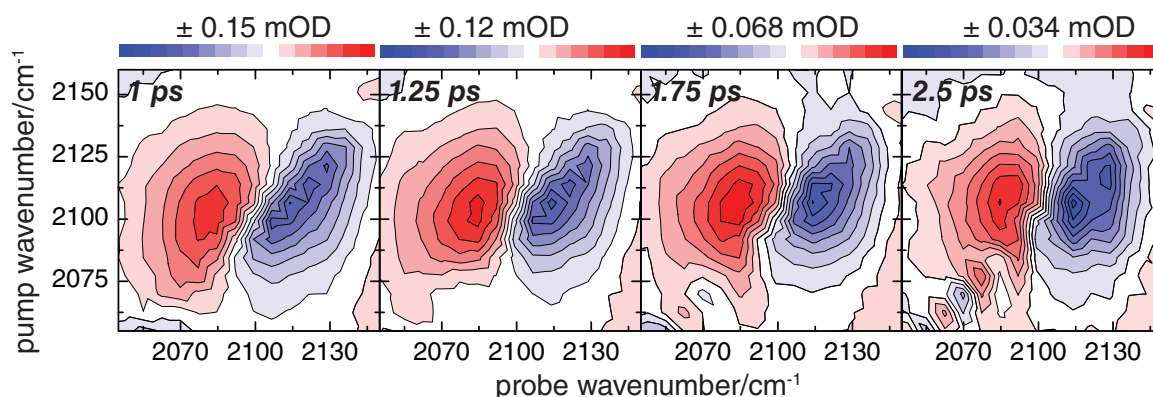
Figure 6.7: 2D-IR spectra of the PDZ mutant Ala390Aha in H_2O. Data are corrected by subtraction of the heat background at 10 ps to remove solvent contribution to the signal. Note the leaking pump pulse leading to artifacts along the diagonal, most notable for the 2.5 ps signal. The sample conditions were approx. 15-18 mM protein in phosphate buffer and 50 µm spacer. The width of the pump pulse was adjusted to 16 cm^{-1}, data were recorded using the 150 line grating.

bonds [279] as in less concentrated samples of the correctly folded protein. An explanation might be partly unfolding of the protein sample or instability. From the data presented here it can be safely stated, that is possible to record 2D-IR spectra of an Aha-labeled protein, that the signal intensity is high enough to allow for acceptable signal-to-noise-ratio and that it is possible to analyze spectral diffusion behavior qualitatively, but that sample preparation has to be improved towards better protein stability. Additionally signals should be recorded with higher spectral resolution and higher excitation power.

6.3.3 2D-IR on Ala390Aha

The second mutant, which was chosen for exploring Aha as label in 2D-IR spectra of proteins is **Ala390Aha**. For this mutant two distinct sub band in the FTIR absorption spectrum have been found as was discussed in chapter four and shown in Figure 5.7. In the FTIR spectra the sub bands are found at 2106 cm^{-1} and 2122 cm^{-1}. This mutant is a good candidate to test whether it is possible to resolve these two submaxima and measure exchange between the two sub populations (in an EXSY experiment like in [86, 118]).

The data are shown in Figure 6.7, the sample conditions were as described previously. The sample concentration was 15 mM and a spacer thickness of 50 µm was used. The data are recorded for the same time points as the data reported for the PDZ mutant Ile327Aha. It has to be noted that for the spectra in Figure 6.7 there are artifacts along the diagonal contributed from the leaking pump pulse, which are not easy to remove from the spectra, because the data were corrected by subtraction of a positive background at 10 ps. The signal size of the azide absorption in the mutant Ala390Aha in Figure 6.7 is comparable to the signal size of the azide in mutant Ile327Aha shown in Figure 6.5.

For the sample at 1 ps waiting time the signal intensity is ±0.15 mOD, which decreases down to ±0.034 mOD for 2.5 ps. The peak shows a very pronounced tilt along the diagonal axis at 1 ps. Spectral diffusion can be observed in the data set presented in Figure 6.7 in contrast to the data for Ile327Aha in Figure 6.11. For the longest waiting time of 2.5 ps the tilt decreased so that the peak appears alomost upright and inhomogenous broadening is vanished.

The resolution of the 150 line grating is not sufficient to completely resolve if there are two
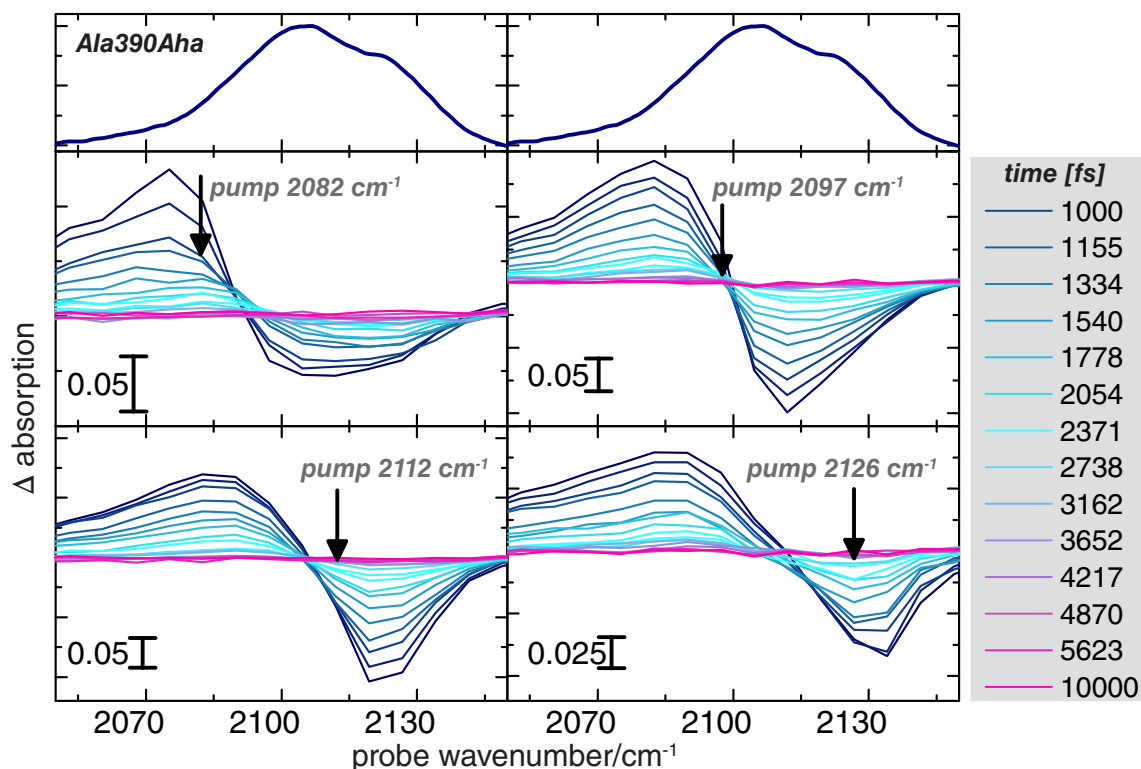
Figure 6.8: Time-dependent cuts for the PDZ mutant Ala390Aha in H_2O for different pump wavenumbers. Data are corrected by subtraction of the heat background at 10 ps to remove solvent contribution to the signal. The black arrow indicates the pump position. The upper panel shows the corresponding FTIR spectrum for this mutant. The sample conditions were approx. 15-18 mM protein in phosphate buffer and 50 µm spacer. The width of the pump pulse was adjusted to 16 cm^{-1}, data were recorded using the 150 line grating.

submaxima present in the 2D-IR data. In the spectrum for 2.5 ps two submaxima seem to be observed, one with a center at 2110 cm^{-1} and the second with a center at 2125 cm^{-1} for the bleach signal. However this observation has to be discussed with care because of the leaking pump light. That spectral diffusion is happening already on a 2.5 ps timescale indicates first of all, that the surrounding of the azide group changes on the timescale of 2.5 ps. As was discussed in chapter 5 and shown in Figure 5.5 g and h Ala390 is located in the protein interior. The azide group is surrounded half by polar amino acid side chains and half by nonpolar side chains. This is reflected by the spectrum in Figure 6.7 because strong spectral diffusion can be observed, which is only the case for an initially inhomogeneous surrounding, which equilibrates on the time scale of the spectral diffusion process. The spectral diffusion process is not finished at 2.5 ps, but the data indicate that the sub ensembles are interchanging. Generally speaking the protein conformation fluctuates on its free energy landscape and even within the short time window of 2.5 ps side chain dynamics are occurring. The resolution and signal intensity as well as the accessible time-window in this experiment are not sufficient to measure actual exchange between the two sub ensembles.

A further insight into the structural dynamics might be gained in a P2D-IR experiment [99].

The data in Figure 6.7 can be analyzed in more detail by the cuts through the 2D-IR spectrum along a defined pump positions which are shown in Figure 6.8. Those were measured in an independent experiment and averaged for a higher number of scans to allow for better signal-to-noise ratio.

Figure 6.9: Transients for the bleach signal of Ala390Aha in H_2O, recorded with the narrow band pump pulse centered on the main absorption for two different pump wavenumbers matching the sub bands in the absorption spectrum.

Comparison of those cuts with the FTIR spectrum of the PDZ mutant Ala390Aha shows that the maximum of the bleach signal cor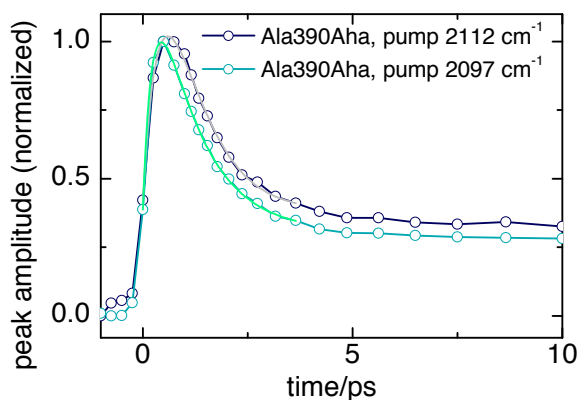responds to the maximum of the FTIR spectrum (in contrast to the data discussed in the previous section). This indicates that the protein sample is folded correctly and the time-dependent spectra can be analyzed qualitatively and might yield important information on the biomolecular dynamics.

Figure 6.9 shows the transients for two of the bleach signals in Figure 6.8 with the pump centered at 2112 cm^{-1} or 2097 cm^{-1} respectively. Those transients are not directly at the position of the maxima reported in the FTIR spectrum but are the best of the recorded data in terms of non spectral overlapp between the two bands and signal size. The bleach signal in Figure 6.8 for the pump at 2097 cm^{-1} possibly reflects the sub ensemble which has its absorption maximum in the FTIR spectrum at 2106 cm^{-1} whereas the bleach signal for the pump at 2112 cm^{-1} corresponds more to the sub ensemble with the absorption maximum at 2122 cm^{-1} in the FTIR. The transient signals in Figure 6.9 indicated a slightly different vibrational lifetime for the two sub ensembles (note that those data are not corrected with a weighted background as in contrast to the cuts shown in Figure 6.8).

When comparing the data with the results for the free Aha in either H_2O or THF a similar effect is seen. The peak time for the azide in H_2O was shortly after the peak time in THF (Figure 6.4), indicating that the polar solvent extends the lifetime. This corresponds to the effect seen in Figure 6.9 for the azide group in Ala390Aha, with the bleach signal for higher wavenumbers (which means a more polar environment - see chapter 5) showing a slightly later peak time than the bleach signal for lower wavenumbers. Thus it can be state, that indeed two different conformations of the PDZ mutant Ala390Aha are observed in the 2D-IR spectrum and that it is possible to access and distinguish different sub ensembles of the protein on its free energy landscape.

Comparison of Spectral Diffusion in Ala390Aha and Ile327Aha   In Figure 6.10 an overlay of the 2D-IR spectra of the mutants Ile327Aha and Ala390Aha as contour lines is shown. The upper panel shows the directly measured data as they were shown in Figure 6.5 and Figure 6.7, the lower panel shows a smoothed version of the contour levels using the built-in algorithm of Origin 8.5 (parameter given in caption). Almost no differences in the tilt of the bleach signals at 1 ps can be be observed. Both mutants seemingly have a similar broadening the azide band by different sub ensembles. However already and 1.25 ps and more pronounced at 1.75 ps as well as 2.5 ps a difference in the spectral diffusion dynamics can be observed. As discussed above the azide group in Ile327Aha does not reflect any changes of the microenvironment because no spectral diffusion and thus no exchange between sub ensembles can be observed. In contrast in the mutant Ala390Aha
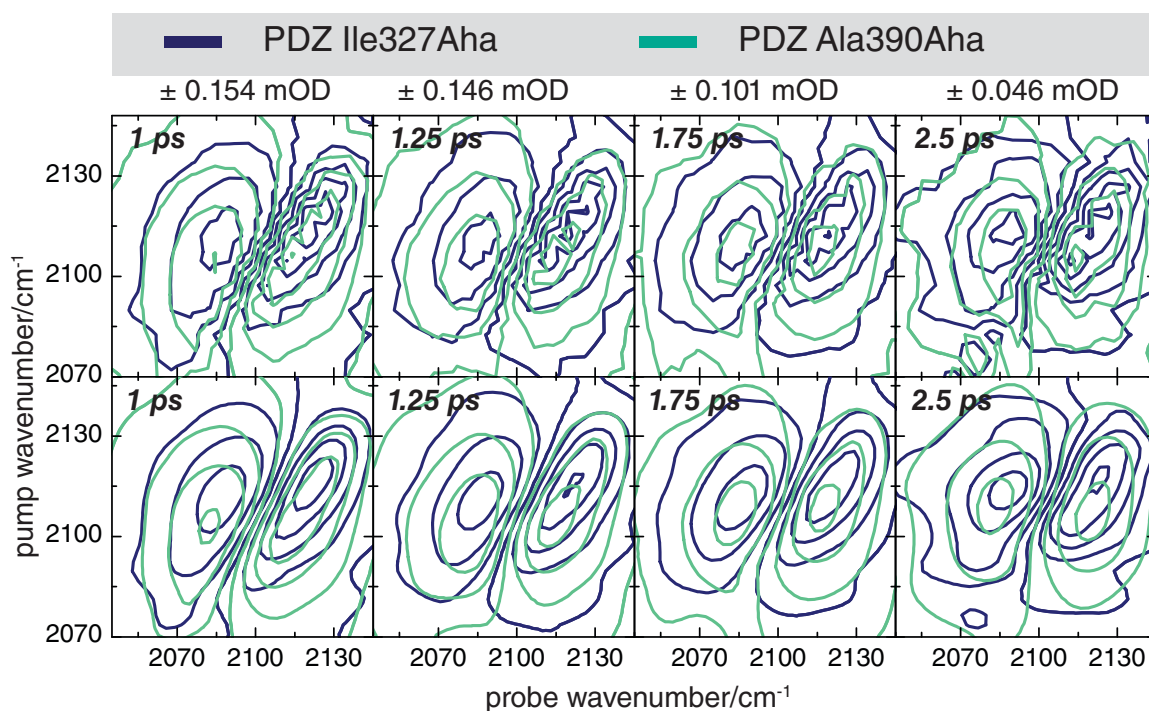
Figure 6.10: 2D-IR spectra of the PDZ mutants Ile327Aha and Ala390Aha in H_2O shown as contour lines. The upper panel shows the directly measured data, the lower panel shows smoothed contour lines using the built-in algorithm from OriginPro 8.5 with extrapolation to 100 points and the smoothing parameter 0.005 . Data are corrected by subtraction of the heat background at 10 ps to remove solvent contribution to the signal. The sample conditions were approx. 15 mM protein in phosphate buffer and 50 μm spacer. The width of the pump pulse was adjusted to 12.5 cm^{-1}, data were recorded using the 150 line grating.

the spectral diffusion process is similar as for Aha in H_2O (shown in Figure 6.1) indicating flexibility of this side chain and conformational fluctuations in the surrounding within 2.5 ps.

6.3.4 Ligand Binding observed with 2D-IR in Ile327Aha

The last experimental set presented in this chapter investigates whether ligand binding influences spectral diffusion characteristics observed in a 2D-IR spectrum of the PDZ mutant Ile327Aha. As described previously this position is located in the binding pocket and proposed to be part of the coupled network of amino acids [10]. A subtle change of the FTIR absorption spectrum can be found in the presence of the native ligand the CRIPT peptide (see Figure 5.7), which interacts with the incorporated Aha via the peptide backbone.

In Figure 6.11 the 2D-IR spectra of the mutant Ile327Aha without and with the heptameric CRIPT peptide are shown. The data were recorded with the same sample, first spectra without the ligand were recorded and then peptide was added to the same sample. The data for the ligand-free sample are very similar to the spectra shown in Figure 6.5, with a bit higher signal size with 0.161 mOD. This is because the sample concentration was slightly higher with 15 to 18 mM before the final centrifugation to remove scattering particles.

The center wavenumber of the bleach signal is around 2115 cm^{-1}, which indicates again that the protein might be slightly unfolded or has experienced a destabilization leading to a more polar environment for the side chain at residue 327. However it was possible to conduct the experiment

Figure 6.11: 2D-IR spectra of the PDZ mutant Ile327 in H_2O without and with the heptamer acNYKQTSV as ligand. Data are corrected by subtraction of the heat background at 10 ps to remove solvent contribution to the signal. The sample conditions were approx. 15 mM protein in phosphate buffer and 1.5 fold ligand excess and 50 µm spacer. The width of the pump pulse was adjusted to 12.5 cm^{-1}, data were recorded using the 150 line grating.

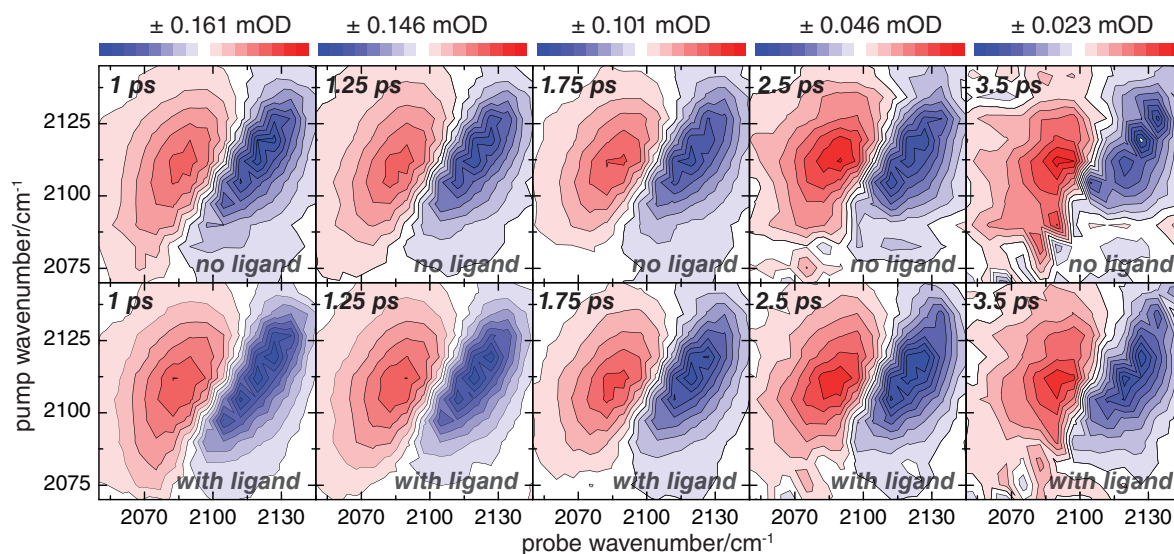in the presence of the ligand and to prepare a sample with 1.5 fold ligand excess which was still soluble and did not show effect of protein precipitations at this very high concentrations.

The spectra in Figure 6.11 suffer from a similar problem as the data shown for the mutant Ala390Aha in Figure 6.7. The pump pulse leakage which is not easy to remove from the spectra after correction by subtraction of a positive background signal to account for the heated solvent background lead to small artifact signals along the diagonal most notably for the longer waiting times at 2.5 ps and 3.5 ps. Comparing the data of the ligand free PDZ mutant with the data of the protein-ligand complex shows that up to 1.75 ps the data seem almost identical whereas at 2.5 ps to 3.5 ps subtle difference can be observed. Comparing the data for 3.5 ps shows that in the spectrum without ligand the bleach maximum is centered at 2115 cm^{-1} (on the pump axis) whereas the bleach signal for the sample of the protein-ligand complex is centered more at 2108 cm^{-1}.

This can be observed in more detail in Figure 6.12 when overlaying the spectra in a similar way as it was done for comparing the two different mutants in the section above. The upper panel show the raw data as presented in Figure 6.11 and the lower panel shows the data with the smoothing algorithm of OriginPro 8.5 applied. It can be clearly seen, that up to 1.75 ps the ligand binding almost has no influence, the contour levels of the two spectra lay on top of each other. This indicates that ligand binding to PDZ does not influence the microenvironment of the azide group in equilibrium on this very short timescale. For the signals at 2.5 ps and 3.5 ps in the smoothed data a slightly difference between the center maxima for the bleach and ESA signals can be observed. In case of the protein-ligand complex the center maximum is shifted a bit towards lower wavenumbers.

This very similar to the findings from static FTIR measurements reported in chapter 5. Here it was found that the absorption maximum is shifting by about 1-2 cm^{-1} upon ligand binding to lower wavenumbers. However these observations in the 2D-IR spectra have to be discussed with care, because of the overall shift of the bleach signals in comparison to the FTIR spectra. In Figure 6.14 this can be seen more clearly. Here cuts through the 2D-IR spectra in Figure 6.11 are shown (data
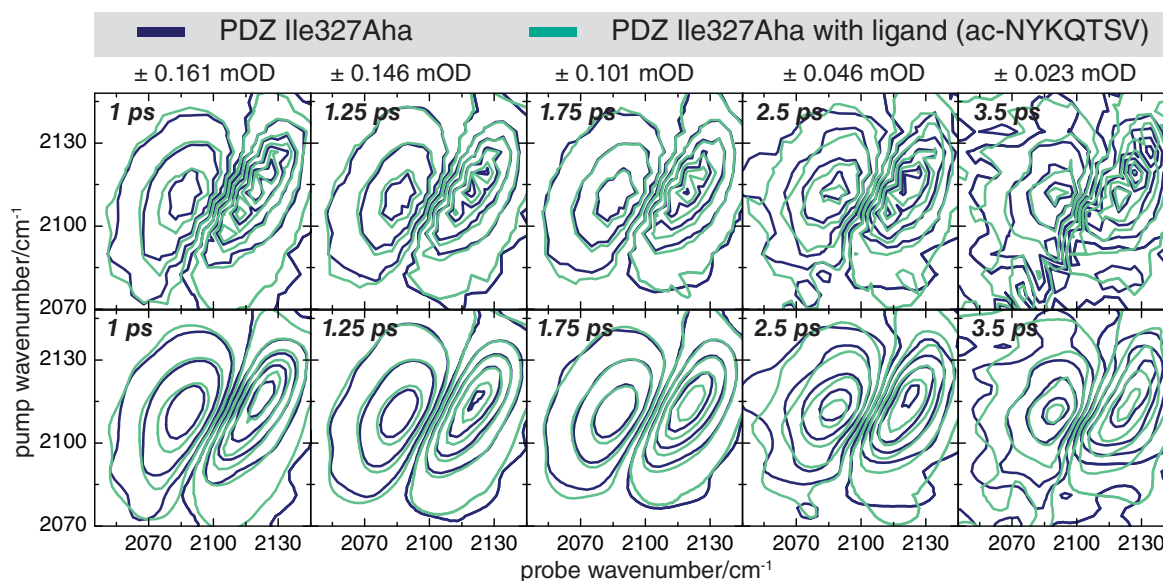
Figure 6.12: 2D-IR spectra of the PDZ mutant Ile327 in H_2O without and with the heptamer acNYKQTSV as ligand shown as contour lines. The upper panel shows the measured data, the lower panel shows smoothed contour lines using the built-in algorithm from OriginPro 8.5 with extrapolation to 100 points and the smoothing parameter 0.005. Data are corrected by subtraction of the heat background at 10 ps to remove solvent contribution to the signal. The sample conditions were approx. 15 mM protein in phosphate buffer and 1.5 fold ligand excess and 50 µm spacer. The width of the pump pulse was adjusted to 12.5 cm^{-1}, data were recorded using the 150 line grating.

were recorded in an independent experiment and averaged for a higher number of scans than the full 2D-IR spectra). The left column of Figure 6.14 shows the data for the free PDZ mutant Ile327Aha and the right column shows the data for the protein-ligand-complex. The top panel shows the FTIR absorption spectrum. In dark blue the FTIR absorption spectra, which were reported in chapter 5 are reproduced. Those were measured with a sample concentration of 3 to 4 mM, the spectra in light gray are FTIR absorption spectra of the samples, which were measured in the 2D-IR setup. Those FTIR spectra were recorded after the 2D-IR measurements were carried out.
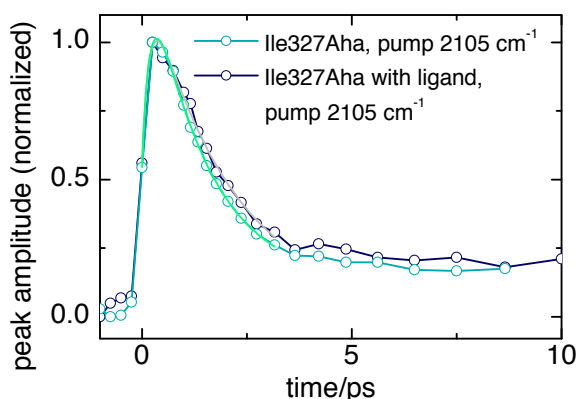
Figure 6.13: Transients for the bleach signal of Ile327Aha with and without ligand, recorded with the narrow band pump pulse centered on the main absorption. Note that these data are not corrected for the heated solvent background.
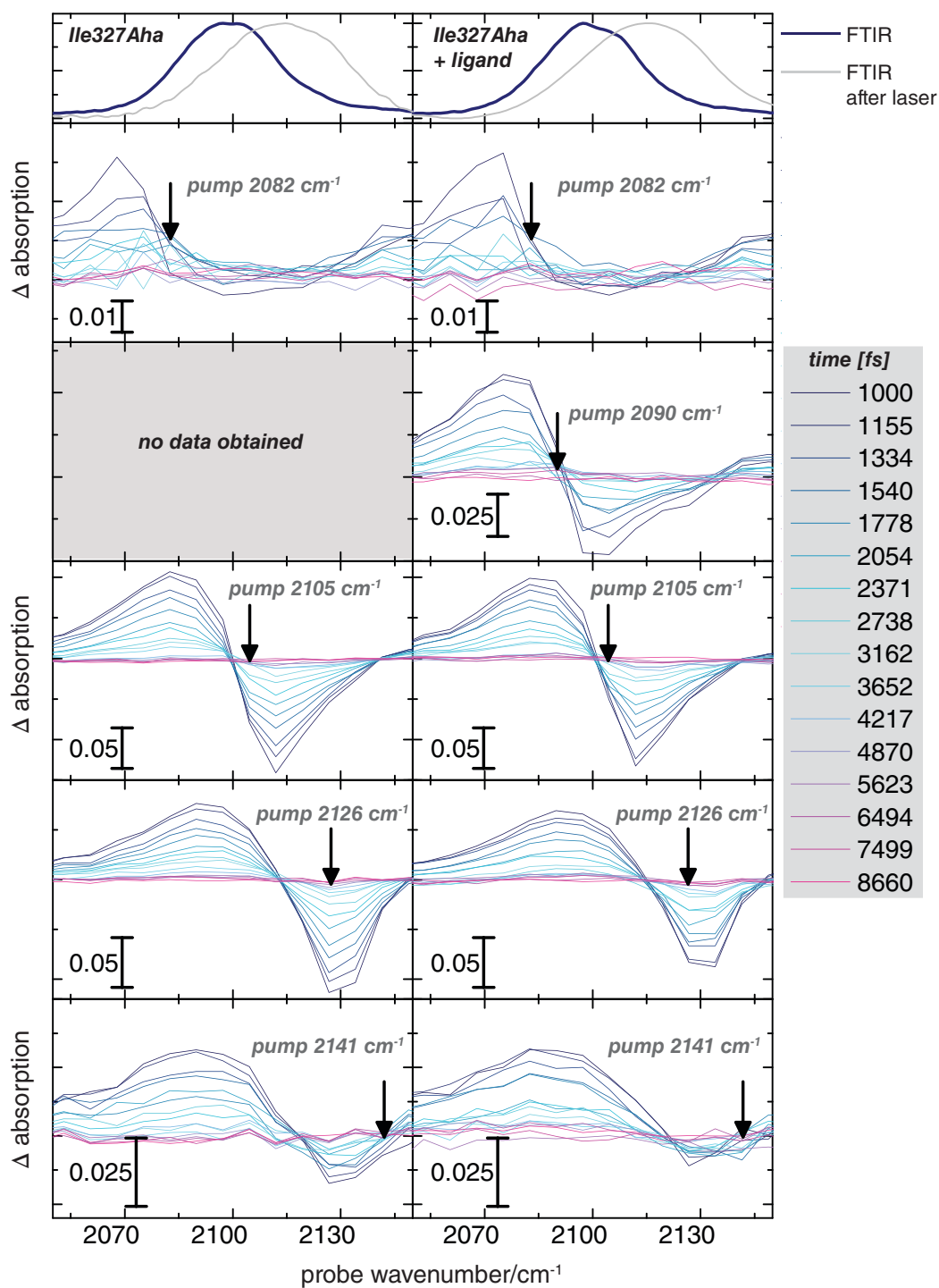
Figure 6.14: Cuts for the PDZ mutant Ile327Aha in H$_2$O for different pump wavenumbers and with heptamer as ligand (left column). Data are corrected by subtraction of the heat background at 10 ps to remove solvent contribution to the signal. The black arrow indicates the pump position. The upper panel shows the corresponding FTIR spectrum for this mutant. The sample conditions were approx. 15-18 mM protein in phosphate buffer and 50 μm spacer. The width of the pump pulse was adjusted to 16 cm^{-1}, data were recorded using the 150 line grating.

In the cuts shown in Figure 6.14 it can be seen that center wavenumbers of the bleach signals correspond more to the FTIR absorption spectra of the samples after the 2D-IR measurements (gray) and do not reflect the line shape and center maxima as would be anticipated from the FTIR absorption spectra in blue. This is probably due to the high concentration and the insufficient buffer capacity of the phosphate buffer used for preparing the samples. Thus the samples might be partly unfolded and it is not certain that the ligand is still bound in the same configuration.

Therefore experiments need to be improved further first by increasing the buffer concentration or switching to a buffer with higher buffer capacity and second the experiments could be conducted (after rebuilding the setup again, which was not possible during this thesis) with the OPA II used as high-power light source for generating the mid-IR light used for the pump pulse. The OPA II has about 3 to 4 times higher output power than the OPA I, which was used in for the experiments in this chapter. The higher output power would allow for measurements to be carried out with sample concentrations of around 4 to 5 mM, which is a similar concentration as used for the experiments reported in chapter 5.

Due to the effect that the sample seems to be not folded correctly, no qualitative analysis of the protein dynamics is undertaken. In Figure 6.13 the transient signals for the spectra at the pump position 2105 cm^{-1} are shown. A comparison indicates that ligand binding is not influencing the vibrational lifetime of the azide group in PDZ. As the spectra in Figure 6.11 are clearly affected by pump pulse leakage all discussions of what is causing changes in the line shape or life time are only qualitativly and data should be processes further for a detailed analysis.

6.4 Conclusion and Outlook

The objective of the presented experiments was to demonstrate how Aha as example for a versatile UAA can serve as novel vibrational probe in 2D-IR of proteins and what kind of information are accessible. The data show that it is possible to record spectra of an Aha-labeled protein with acceptable SNR to extract information about underlaying conformational dynamics in the studied PDZ domain. The data are intended as proof-of-principle and already show that using Aha as site-specific probe different questions such as conformational selection in PDZ or flexibility of the protein core can be addressed.

Line Shape Analysis.   The data shown in Figure 6.11 of the azide moiety in the PDZ mutant Ile327Aha in the case without and with the native ligand can in principle be analyzed further. The typical analysis for spectral diffusion data is a *Center Line Slope (CLS)* analysis [139, 249]. A related analysis describing the different influences of inhomogeneous and dynamic broadening is the calculation of the eccentricity of diagonal peaks (as shown for Horseradish peroxidase in [118]). However because the samples of the mutant Ile327Aha seem to unfold or at least destabilize under the current experimental conditions and because of the leaking pump pulse, which could possibly be reomved with a higher level of data correction, a more quantitave analysis is not performed.

The partly unfolding can be seen in Figure 6.14, in the top panel the FTIR absorption spectra are depicted. The blue spectra show the case for 3-5 mM high concentrations, the light gray spectra show the data of the samples after laser measurements. A possible explanation for the shift and broadening of the azide absorption about 10 cm^{-1} to higher wavenumbers is a less hydrophobic environment as well as inhomogeneous broadening due to diverse sample environment. The samples probably destabilized due to insufficient buffer capacities of the used phosphate buffer for

the high protein concentrations of approx. 15 to 18 mM, which were needed to demonstrate the principle feasibility of those type of experiments.

Better quality data are expected for a repeated experiment using the high-power OPA II as pump light source. Using three to four times higher excitation power and at the same time less concentrated samples of around 4 mM should yield similar signal sizes with a much smaller likelihood of protein unfolding. With this smaller concentration additionally effects on the ligand binding contributed by inter-molecular interactions and too high viscosity will be minimized. In general those experiments will benefit enormously if strategies for better signal sensitivity could be implemented.

Comparison with published 2D-IR Spectra of Novel Vibrational Probes in Proteins. The above reported data demonstrate how Aha can be utilized as vibrational probe and gave first insight into local dynamics in the PDZ domain (for the mutant Ala390Aha) on a few picosecond timescale. It is a intriguing demonstration of the capabilites of 2D-IR spectroscopy and shows how the proposed combination of ultrafast 2D-IR with site-specific probes can be used to study fast conformation dynamics in proteins.

The results can be compared to those obtained by Bloem et al. [139], who used Aha as label incorporated in the peptide ligand. They found similar results for the usability of Aha as label in protein as demonstrated here in this thesis.

Other examples of 2D-IR spectra of proteins containing unnatural amino acids as novel probes include the data presented by Thielges et al. [136, 249] on Myoglobin with N3P as label. It has to be stated that Aha has to be favored over N3P because of the much simpler line shape. Thielges et al. discuss spectral diffusion of the N_3 absorption band as result of changes in the free energy landscape. As demonstrated in this thesis in chapter 4, N3P has a complicated line shape and already in the 2D-IR spectra of free N3P sub bands distorting the effects of inhomogeneous broadening are present. The Fermi Resonance of the N_3 band with the ring modes leads to four submaxima for the free amino acid which should not be neglected when analyzing 2D-IR data of the N_3 band in a protein. Furthermore the distortion of the line shape through the Fermi Resonance forbids the use of a CLS analysis, which was done in the paper by Thielges et al. Another example of 2D-IR data of a protein with label is shown by Chung et al. [322], who incorporated CNP into villin headpiece. In comparison to CNPAha is smaller and therefore more versatile to replace a wide range of native protein side chains and it has a larger ε what allows for better SNR.

A completely different type of label was tested by Woys et al. [257] as well as by King et al. [137], this type of vibrational probe is unique because a metal-carbonyl is used. The label has the advantage of longer lifetime and a large transition dipole. However, it is mainly useful for attachment to the protein surface, because it is too large to be included at arbitrary positions of the protein and disturbance of the protein fold is to be expected.

Part IV

Application 2: Real-Time Investigation of Vibrational Energy Flow

7 Assigning Infrared Spectra Based on Vibrational Energy Transfer
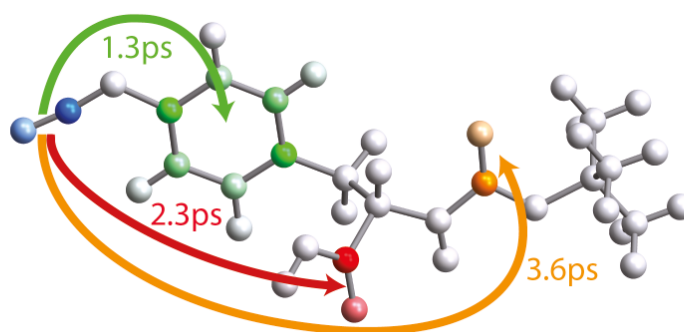
Figure 7.1: VET induced peak times in azidophenylalanine (N3P) reflect spatial proximity of functional groups and thus can be used for unambiguous assignment of the absorption spectrum. The figure is reproduced with permission from [111].

Signals derived in ultrafast 2D-IR measurements contain important information about the studied system, not only in their line shapes (as discussed for spectral diffusion in Chapter 6) or in case of cross peaks between functional groups (as demonstrated in 2C-2D-IR measurements in Chapter 4) but important information can be gained from the time dependence of the cross peaks (as introduced in chapter 2).

In this chapter the time dependence is used to assign vibrational modes to functional groups of the molecule based on the assumption that *vibrational energy transfer* (VET) is the underlying mechanism for cross-peak generation with a clear distance dependency.

The unnatural amino acid N3P, which was studied with 2C-2D-IR in chapter 4 is used as a model. Its FTIR spectrum contains a few well separated absorption bands. But still it is difficult to assign those peaks unambiguously by educated guessing. Results from DFT calculations were compared with 2C-2D-IR transfer times to obtain the assignment. It is demonstrated how the everyday task in analytical chemistry of assigning vibrational absorption bands to chemical groups is assisted or even made possible by using information derived from ultrafast vibrational energy transfer.

This chapter is based on the publication *Ultrafast hopping from band to band: Assigning infrared spectra based on vibrational energy transfer*, and is reproduced here with permission from WILEY-VCH Verlag GmbH & Co. KGaA, Weinheim: Angewandte Chemie Int. Ed. [111], copyright 2013.

7.1 Motivation

Infrared spectroscopy is widely used in fundamental and applied chemical research. Applications cover tasks in analytical chemistry, such as process monitoring or product identification [323, 324] as well as cutting edge studies elucidating reaction mechanisms [325, 326, 327, 328] or resolving ultrafast biomolecular dynamics and functions [66, 67, 329]. Typically, analysis of an IR spectrum starts with assignment, i.e., with establishing a connection between the bands observed in the spectrum and the moieties of the molecule that are involved in the corresponding vibrations.

For small molecules, vibrations often can be assigned based on experience, aided by databases that list functional groups and the typical wavenumber range of their absorption bands. However, the database approach quickly becomes infeasible if several groups are present that cause vibrations in the same wavenumber range or if a certain group is present several times in a molecule. A way to obtain assignment information in such cases is isotope labeling, which might involve complex synthesis.
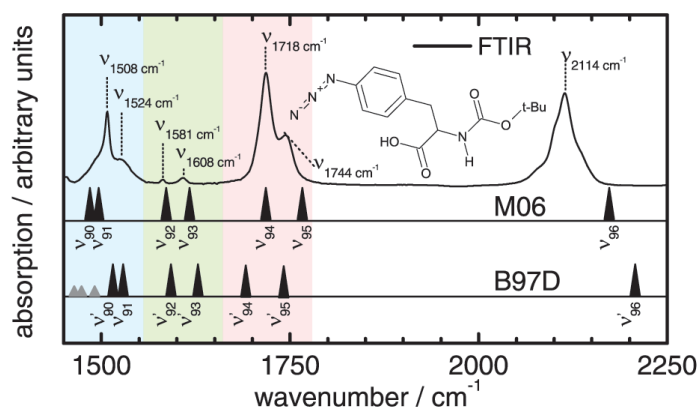
Figure 7.2: Structure and IR absorption spectrum of N3P. The band positions obtained from DFT computations using the M06 functional and the B97D functional are indicated with black triangles (scaling factors of 0.962 and 1.015 are used for M06 and B97D, respectively). Small gray triangles indicate methyl group absorptions of the t-butyl moiety. Their absorption is less than 5 % of the neighboring vibration ν_{90} The background colors blue, green and red mark the different spectral regions discussed in the text. This figure is reproduced with permission from [111].

The standard tools for assignment are quantum chemical computations. However, even for seemingly simple cases such as the FTIR absorption spectrum of N3P (shown in Figure 7.2), contradicting results can be obtained from different computational methods, as illustrated by the results presented here. Furthermore, there are cases where the computation of vibrational modes can be intrinsically difficult, such as excited states or reaction mixtures containing unknown species. A broadly applicable experimental approach to aid assignment is therefore highly desirable.

In this chapter it is demonstrated how time-dependent infrared pump-probe spectroscopy allows one to solve assignment problems. For this purpose, a vibration of the molecule is selectively excited using an infrared excitation pulse with narrow bandwidth and the response of the other vibrations is investigated by a delayed probe pulse, which is in principle only a *cut* through a 2C-2D-IR spectrum (as introduced in chapter 1 and 4).

When the initially excited vibration relaxes low-frequency modes become excited and intramolecular vibrational energy transfer (VET) across the molecule occurs between low frequency modes

[104, 148]. Through-bond transfer rates of 2.6–5.5 Å/ps have been reported for different molecules [77, 104, 144, 330]. The high-frequency vibrations investigated here are anharmonically coupled to the low-frequency modes and respond to VET by red shifting [331]. Because transfer times correlate with through-bond distances [77, 104, 144, 145, 330], the order in which the bands in the spectrum respond to the initial excitation reflects the distance between the vibrating groups in the molecule. This is critically important information for band assignment.

As an example for the broadly applicable method of VET based assignment the results gained in Chapter 4 on the novel probe azidophenylalanine (N3P), which is used as a protein label for IR spectroscopy [76, 82] are discussed here. The boc-protected form (structure shown in Figure 7.2) was studied, thereby adding a peptide bond to the model system.

7.2 Results and Discussion

7.2.1 Classical Assignment using Databases

In Figure 7.2 the FTIR absorption spectrum is shown. Referring to a database of group frequencies [273], as is typically done for IR band assignment, several bands in the wavenumber range 1400–2200 cm^{-1} are expected. Asymmetric azide stretching is usually found in 2080–2170 cm^{-1} and therefore the band at 2114 cm^{-1} is assigned to the azide moiety. The structure of the band is attributed to a Fermi Resonance [301] as already discussed in Chapter 4. Carbonyl stretching of the carboxylate moiety is expected between 1705 cm^{-1} and 1730 cm^{-1}; carbonyl stretching of the carbamate moiety (amide I) is expected between 1705 cm^{-1} and 1722 cm^{-1} [273].

Two bands (at 1744 cm^{-1} and 1718 cm^{-1}) can be observed in the corresponding spectral range, but it is not possible to definitively assign which one belongs to the carboxylate and which one belongs to the carbamate. An amide II vibration of the carbamate moiety is expected as well [273]. This should occur between 1510 cm^{-1} and 1550 cm^{-1}, and we observe bands at 1508 cm^{-1} and 1524 cm^{-1}. Furthermore, several ring vibrations are expected in the range from 1450 cm^{-1} to 1665 cm^{-1}. Ring vibrations are therefore the likely cause for the small absorption signals at 1581 cm^{-1} and 1608 cm^{-1}. However, a ring vibration could also be responsible for one of the bands in the amide II range.

Thus the database approach to assign an FTIR absorption spectrum is not sufficient to assign even such seemingly easy spectra as measured for N3P.

7.2.2 Assignment using DFT Calculations

To clarify the assignment of the carbonyl bands and the assignment in the amide II range, the normal modes of N3P were computed using density functional theory (DFT)[1]. The vibrational wavenumbers computed using the M06 and the B97D functionals[2] [332, 333] are displayed below the experimental data in Figure 7.2.

Figure 7.3 shows the localization of the respective normal modes. The localization of modes ν_{96} to ν_{92} is almost identical in both calculations, with the highest wavenumber mode being the azide stretching vibration. Both methods suggest that the carbonyl stretching of the carboxylate ν_{95} is at a higher wavenumber than the carbonyl stretching (amide I) of the carbamate ν_{94}. The two modes with next lower wavenumbers in both computations are localized on the phenyl ring, with

---

[1]DFT calculations were carried out by Jens Bredenbeck and the author. All calculations have been performed using the cluster at Center for Scientific Computing, Frankfurt.

[2]M06/6–31+G(d,p)/PCM/UFF and B97D/6–31+G(d,p)/PCM/Bondi; see Appendix C for computational details.
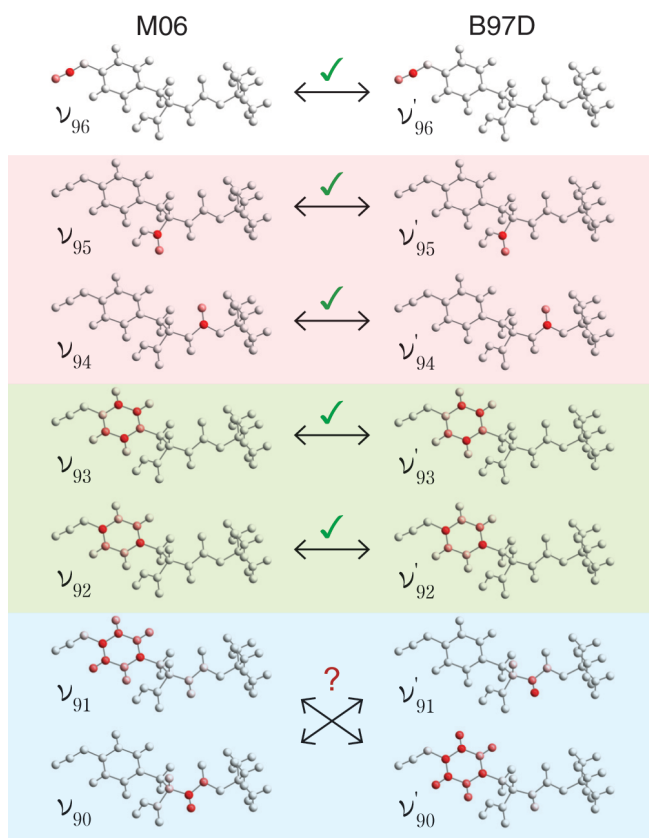
Figure 7.3: Localization of vibrational normal modes computed using DFT with the M06 and the B97D functionals. The red color coding of the molecular structures represents the vibrational energy per atom. The color scale is normalized to the maximum vibrational energy localized at a single atom for each mode. Both computations agree on the assignment of the azide asymmetric stretch, which is the mode excited in the pump-probe measurements, the two carbonyl modes and two of the ring modes. However, the order of the amide II mode of the carbamate and the third ring mode is interchanged. Red, green and blue background colors correspond to the spectral regions marked in Figure 7.2. This figure is reproduced with permission from [111].

the higher one involving predominantly the four H-substituted C atoms ν_{93} and the lower one involving mainly the other two C atoms ν_{92}.

In the amide II wavenumber range, the computations predict two modes: an additional ring mode and an amide II vibration of the carbamate. While the two computations are in agreement about the localization of the two vibrations, there is disagreement about the order of the modes. The computation using the M06 functional predicts the ring mode at higher wavenumber, whereas the computation using the B97D functional predicts a higher wavenumber for the amide II mode.
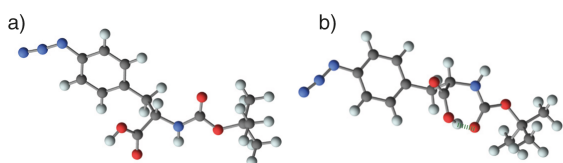
Figure 7.4: a) Open conformation of N3P. b) The hydrogen bonded conformation of N3P can be ruled out as the hydrogen-bonded carbonyl would show an absorption band downshifted by about 20-30 cm^{-1}, which was not observed. This figure is reproduced with permission from [111].

Conformations Intramolecular hydrogen bonds could lead to additional transfer pathways, which would have to be taken into account when analyzing the experiment. In N3P, a hydrogen bond between the azide group as hydrogen bond acceptor and the N−H or the O−H group as potential donors would likely influence energy transfer. However, due to the large distance and stiffness introduced by the phenyl ring between the azide and the potential hydrogen bond donors the existence of such an intramolecular hydrogen bond as indicated in Figure 7.4 can be excluded safely. No rotamer can be formed that brings the N−H or O−H group close enough to the azide group. A

minor effect on the observed transfer times could occur if there was a hydrogen bond between the O−H of the carboxyl moiety and the C=O of the carbamate moiety.

Participation of C=O in such a hydrogen bond would lead to the appearance of a C=O band downshifted by about 20–30 cm^{-1} compared to the free C=O. The observed C=O band of the carbamate (1718 cm^{-1}), however, is at the very high end of the expected range (1705–1722 cm^{-1}) [273]. Presence of a hydrogen bonded population would cause an additional band at about 1690 cm^{-1}, which is not observed in the absorption spectrum shown in Figure 7.2.

7.2.3 Unambiguous Assignment using Transfer Times
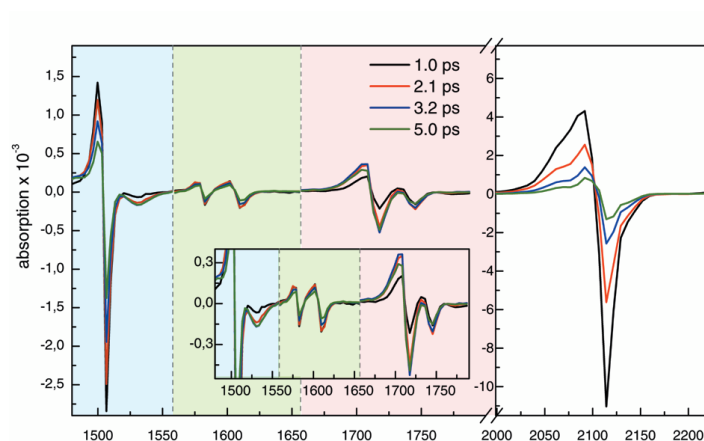
Figure 7.5: IR pump-probe spectra of N3P in THF for different delay times. The pump pulse was centered on the azide absorption. Different spectral regions were probed with an independently tunable OPA. The borders between regions probed in individual experiments are indicated by dashed gray lines. Red, green and blue background colors correspond to the spectral regions marked in Figure 7.2. The figure is reproduced with permission from [111].

To resolve the uncertainty resulting from the calculations, unambiguous assignment of the vibrational modes can be obtained from measurements which monitor VET using ultrafast IR pump-probe spectroscopy. The results of these experiments (described in detail in Chapter 4 and Appendix A) are shown in Figure 7.5.

Both vibrations, which absorb in the amide II range and can not be unambiguously assigned using DFT calculations, are located at different through-bond distances from the azide and VET originating from the excited azide group will lead to a much faster response of the ring vibration compared to the amide II vibration; this allows clear assignment of the bands in the absorption spectrum to the vibrational modes.

Figure 7.6 shows the change of the absorption of the bands (transient IR spectra shown in Figure 7.5) as a function of time after direct excitation of ν_{96} at 2114 cm^{-1} (the azide stretch vibration). t_{max} indicates the time of maximum signal obtained by bi-exponential interpolation of the data in the vicinity of the maximum [330].

The upper panel shows the responses of the two bands at 1744 cm^{-1} and 1718 cm^{-1}, which are attributed by classical assignment to carbonyl vibrations. Both DFT computations attribute the higher wavenumber band to the carboxylate moiety (ν_{95} and ν'_{95} in Figure 7.3, spatially closer to the azide) and the lower wavenumber band to the carbamate moiety (ν_{94} and ν'_{94} in Figure 7.3), which is spatially further away from the azide. The experiment strongly supports this assignment, as the higher wavenumber band responds earlier in time ($t_{max}^{1744} = 2.3$ ps) than the lower wavenumber band ($t_{max}^{1718} = 3.6$ ps). The middle panel shows the time dependence of the absorption bands that are attributed to the ring modes. The response is much faster than that of the carbonyl modes with $t_{max}^{1608} = 1.4$ ps and $t_{max}^{1581} = 1.3$ ps and reflects the proximity of the azide group and the phenyl ring. In these cases the two DFT computations agree well with each other as well as with the information
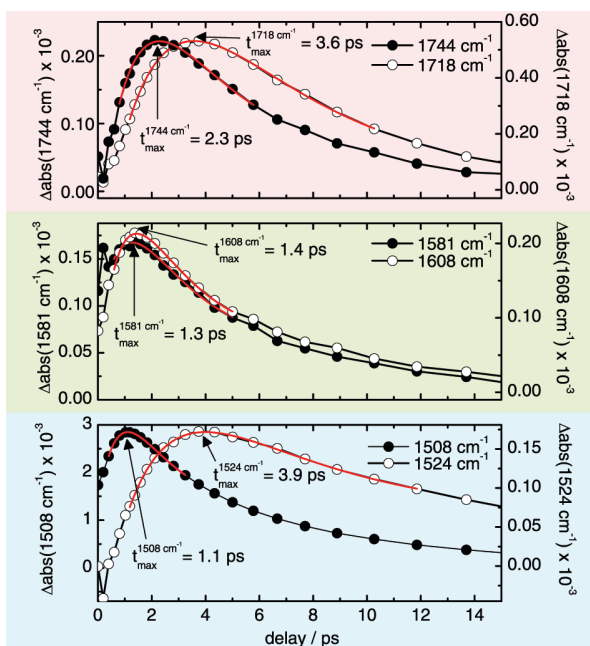
Figure 7.6: Absorption change of the bands as a function of time after excitation of ν_{96} (azide vibration at 2114 cm^{-1}). The red lines are bi-exponential interpolations in the vicinity of the maximum that are used to obtain t_{max}, the time of maximum signal. The black lines connect the measured data points and serve as a guide to the eye. Signals in the middle panel are vertically offset for better visibility (note the different origin of the y axes). The scales of each panel are chosen such that the two curves have the same positive amplitude. Red, green, and blue background colors correspond to the color coding in Figure 7.2. The figure is reproduced with permission from [111].

from time-resolved spectroscopy. To further distinguish modes such as ν_{92} and ν_{93}, which are delocalized over a similar set of atoms and therefore yield similar t_{max}, the angles between transition dipoles of excited and probed modes could be obtained from polarization resolved measurements and compared to computed angles. The assignment of the bands at 1524 cm^{-1} and 1508 cm^{-1} remains unclear from the computations because the results are contradictory. The computed band intensities (see Table 7.1) are not conclusive for assignment. Both computations predict a higher intensity for the amide II band, but a different order of bands. The energy transfer times, however, decide in favor of the assignment suggested by the B97D computation: the lower wavenumber mode responds very quickly with $t_{max}^{1508} = 1.1$ ps, which is in agreement with its assignment as a ring mode (ν'_{90} in Figure 7.3). The t_{max} observed for this mode corresponds with the times observed for the two other ring modes. In contrast, the higher wavenumber mode is slower, with $t_{max}^{1524} = 3.9$ ps. This time is comparable to the value of $t_{max}^{1718} = 3.6$ ps obtained for the carbonyl group of the carbamate. The assignment of the band at 1524 cm^{-1} as an amide II vibration of the carbamate suggested by the B97D computation (ν'_{91} in Figure 7.3) is therefore strongly supported; the contradicting assignment as a ring mode proposed by the M06 computation must be discarded. However, one should not deduce a superiority of the B97D functional over the M06 functional in computing

| computed IR intensities (km/mol) | | |
vibration	B97D	M06
ν_{90}/ν'_{90}	273.6	834.2
ν_{91}/ν'_{91}	365.9	62.3
ν_{92}/ν'_{92}	10.7	7.0
ν_{93}/ν'_{93}	27.5	37.4
ν_{94}/ν'_{94}	726.9	633.8
ν_{95}/ν'_{95}	415.5	420.3
ν_{96}/ν'_{96}	1720.4	1584.3

Table 7.1: Computed IR intensities using expensive DFT calculation approaches for the vibrational modes of N3P. See appendix C for details.

vibrational frequencies from this single result. With increasing density of vibrational bands in larger molecules, harmonic DFT computations that are frequently employed to aid assignment cannot be expected to predict exactly the right order of bands [334, 335, 336]. High level ab initio methods with anharmonic corrections, which have the desired accuracy to address the assignment problem, are not applicable in the majority of cases due to the prohibitive computational effort required [336, 337]. Therefore, an experimental approach to assignment, such as the one presented here, is of great importance.

7.3 Conclusion

This results demonstrate how VET-induced signals obtained from ultrafast IR-pump-IR-probe experiments or 2C-2D-IR experiments can aid the exact assignment of absorption bands. The fact that the time dependence of VET-induced absorption changes reflects the spatial proximity of the two modes which correspond to the excited and the responding absorption bands was used. In the present case of a molecule with little branching and no intramolecular hydrogen bond (see Figure 7.4) it has been sufficient for assignment to measure a data set with VET starting from one mode at the end of the molecule. For molecules with a more complex structure, two or more measurements with VET starting from modes located at different points in the molecule can be used to obtain additional assignment information. Also weaker bands than azide can be used to inject vibrational energy, as the low noise allows for the detection of smaller signals. Additionally, small signals can be increased by increasing infrared pump intensity, concentration or sample thickness. VET based assignment will be particularly useful when assignment using databases or quantum chemical computations is difficult, e.g., in molecules where vibrational frequencies of different functional groups are similar or for species that are difficult to compute, such as reactive intermediates and excited states. In mixtures the technique can reveal which absorption bands belong to the same species. Disentangling IR spectra of reaction mixtures which might contain unknown species is therefore another promising application when investigating reaction mechanisms.

8 A Donor-Acceptor Pair for the Real-Time Study of Vibrational Energy Flow in Proteins
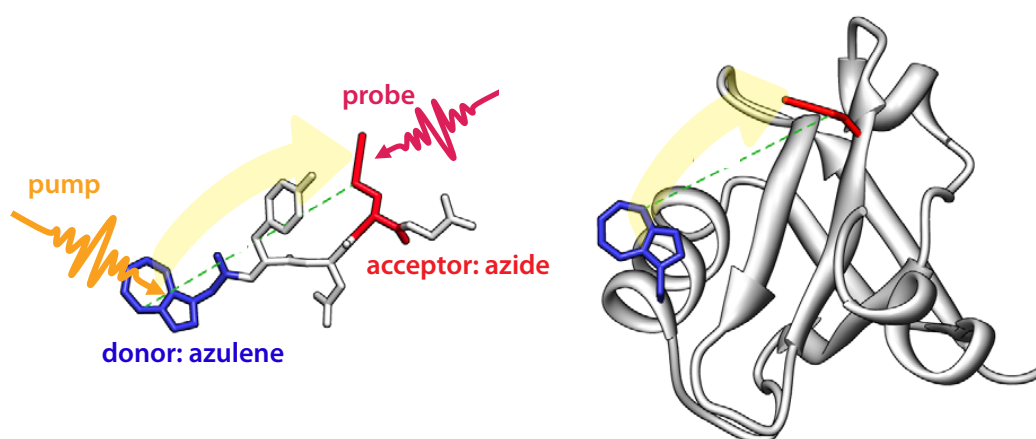
Figure 8.1: To follow directional energy flow (vibrational energy transfer - VET) in proteins suitable chromophores for the injection and tracking of energy are required. Azulene and azidohomoalanine comprise a promising donor-acceptor VET pair. The figure is reproduced from [112] with permission from the PCCP Owner Societies.

Novel probes are not only suitable for the sensing of changes in the microenvironment in a protein (as shown in chapter 5 and chapter 6) but due to the fact, that they can be positioned site-specifically a different type of application seems possible. Vibrational energy transfer (VET) is believed to play an important role in protein function. For PDZ an energy transfer pathway is proposed between the binding site and the distant protein surface, however, experimental evidence for such pathways is lacking. As described in the previous chapter and chapter 1, ultrafast pump-probe spectroscopy has been used to investigate VET in great detail in small molecules. This chapter describes the design of a novel approach to directly track energy flow in a protein by using a VET pair of an donor and acceptor molecule in remote analogy to FRET [1]. It consists of two artificial amino acids, β-(1-azulenyl)-alanine as heat source and the previously discussed novel probe azidohomoalanine as acceptor. Both can be co-translationally positioned site-specifically using independent approaches from chemical biology and are spectrally separated from protein bands. The VET pair is tested in a model peptide towards its applicability to proteins and first measurements in aqueous solution, the necessary prerequisite for application to proteins are presented [112, 338].

The chapter is partly based on the publication *A donor-acceptor pair for the real-time study of vibrational energy flow in proteins* and those parts are reproduced from reference [112] with permission from the PCCP Owner Societies.

---

[1]Fluorescence Resonance Energy Transfer or Foerster Resonance Energy Transfer
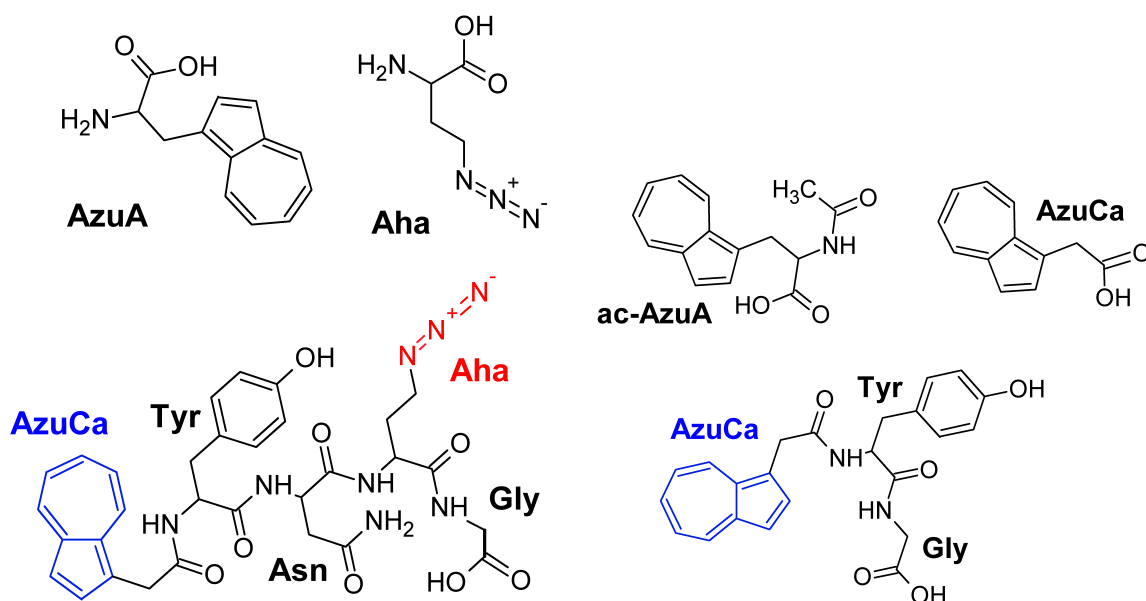
Figure 8.2: Structures of monomeric azulene compounds β-azulenyl-alanine (AzuA), β-(1-azulenyl)-N-acetyl-alanine(ac-AzuA) and azulene-1-yl-acetic-acid (AzuCa), the acceptor molecule Aha and the model peptide AzuP with the sequence ac-Azu-Tyr-Asn-Aha-Gly as well as the small peptide used for assignment with the sequence ac-AzuYG (AzuP'). AzuCa was a gift from Dirk Schwarzer, MPI Göttingen, ac-AzuA and AzuA were a gift from the group of Nediljko Budisa, TU Berlin (synthesis was performed by Michael Hösl and Patrick Durkin). Azu-Tyr-Asn-Aha-Gly (AzuP) and Azu-Tyr-Gly (AzuP') were synthesized using standard protocols for solid-phase-peptide synthesis by Marie Anders-Maurer (AK Schwalbe). Reproduced from [112] with permission from the PCCP Owner Societies.

8.1 Motivation

How vibrational energy is transported in a protein and how this transport might be related to biological function is a question of increasing interest [85, 147, 148, 152, 155, 156, 204, 206, 339, 340, 341, 342]. The role of vibrational energy transfer (VET) is very evident when it comes to efficient cooling of reaction sites or chromophores in proteins [85, 180, 343]. A more subtle role of VET is suggested by a number of theoretical studies, which have linked VET to intramolecular information transfer, i.e. allostery. In simulations, highly anisotropic, directional energy transfer has been observed, that connects distant sites in proteins and appears to be correlated with allosteric communication [10, 85, 167, 205, 206, 341, 344, 345]. However, experimental tools to study the anisotropic nature of VET in proteins and to map out long range energy transfer pathways with sufficient time and spatial resolution are lacking [148, 204]. In small molecules and short peptides, ultrafast pump-probe spectroscopy has been a powerful tool to study VET in great detail [77, 106, 108, 111, 148, 152, 183, 342]. In these experiments, a certain functional group is excited by either a UV/Vis pulse or an IR pulse and the subsequent transfer of vibrational energy along the molecule leads to a response of local vibrations that can be tracked by IR or Raman spectroscopy. In order to extend the approach of ultrafast pump-probe spectroscopy to proteins, important additional requirements have to be fulfilled. Due to the spectral congestion in these large systems, the use of specific spectrally isolated labels is crucial to warrant localized injection of energy and localized probing of the transfer, i.e. a protein compatible VET donor-acceptor pair has to be designed.

Figure 8.3: Level scheme for Azulene, indicating why it is a suitable molecule to be used as heat donor. It is a famous example of exemption to Kasha's rule, which states that photo emission with high yield only occurs from the lowest excited state. Azulene however, among other examples, shows photo emission upon ultraviolet excitation from its S_2 state instead of its S_1 state. Excitation to the S_1 state occurs upon absorption at ≈ 600 nm and is followed by fast relaxation through internal conversion on a timescale o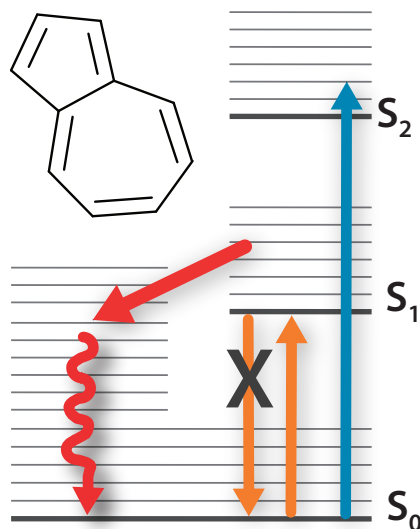ff ≈ 1ps [150, 350]. This means energy is not released as a emitted photon, as would occur in other molecules and no fluorescence takes place. Instead the molecule relaxes to the ground state and thereby the energy is transferred to higher excited vibrational states of the electronic ground state. This is possible because of a conical intersection between S_1 and S_0 state [350, 351].

8.1.1 Prerequisites for Donor and Acceptor

To map out energy flow between two distinct arbitrary sites in a protein, infrared and visible chromophores, that can be incorporated site-specifically, without disrupting the protein function or changing the overall structure, are needed. A large transition dipole of labels is mandatory to keep protein concentrations in reasonable limits while maintaining sufficient signal sizes. Previous pump-probe experiments on proteins only used native IR or UV/Vis chromophores and therefore where largely insensitive to the directionality of VET [181, 346, 347]. Resonance Raman probing allowed to monitor VET between the optically excited heme of cytochrome c and a nearby tryptophan [184, 348] as well as allosteric communication between the hemes of the α and β sub units in hemoglobin [349]. However, the vast majority of proteins do not contain a suitable combination of chromophores at all.

A promising way for the exact positioning of chromophores is offered by tools developed in chemical biology[80, 212, 234], including the use of artificial amino acids as novel vibrational probes as introduced in chapter 3. The extension of the amino acid alphabet by the incorporation of artificial amino acids through artificial genetic code expansion [78, 210] or the use of structural homologues as amino acid surrogates [218] already during the expression of the target protein enables the use of chromophores located in the amino acid side chain and allows for homogeneous labelling with a high labeling yield.

Here a donor-acceptor pair for tracking VET is presented. It comprises of an azulene chromophore as a "donor" which can be excited at 600 nm and injects vibrational energy into the peptide or protein under investigation and the azide chromophore of the favorite novel probe Aha serves as an "acceptor", which can be monitored at 2100 cm^{-1} to track VET in the system. It is shown that these labels combine a set of very favorable properties for the study of VET in biological macro-molecules. Co-translational incorporation of each of the labels into proteins has been demonstrated in the form of β-(1- azulenyl)-L-alanine and L-azidohomoalanine, respectively [218, 234, 352]. An important point is that the demonstrated methods of incorporation into proteins are orthogonal and applicable to the same protein sample, thus allowing for simultaneous labeling (see chapter 3 and 9 for more details).
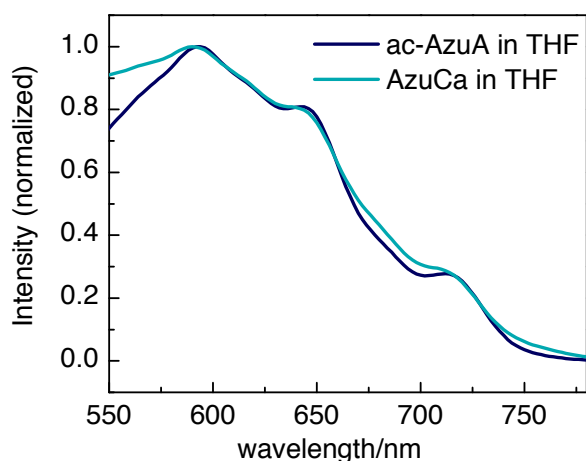
Figure 8.4: UV/Vis absorption spectrum of the two monomeric azulene compounds ac-AzuA and AzuCa, both in THF. Shown is the region between 550 nm and 780 nm were the S_0 to S_1 absorption is expected. The maximum absorption can be clearly seen at around 600 nm. Spectra were recorded on a Jasco V-660 spectrometer against THF as background in a 1 mm thick cuvette, concentrations were chosen to allow for an OD below 1.0. Reproduced (modified) from reference [112] with permission from the PCCP Owner Societies.

VET Donor. A favorable vibrational energy "donor" for studying VET should convert most of the energy of an absorbed photon into vibrational energy, and it should do this as fast as possible to provide a sharp onset for a time resolved measurement of VET. At the same time, the donor should not produce any side effects for its surrounding caused, for example, by isomerization or permanent change of dipole moment. Furthermore Vis chromophores are preferable compared to IR chromophores due to the approximately 10 times larger photon energy that is dissipated.

Azulene is an excellent candidate in these respects, as it undergoes ultrafast (sub-picosecond) internal conversion [350, 353, 354]from S_1 to S_0 (violation of Kasha's rule) [350, 351, 355] after 600 nm excitation, thereby converting basically the complete photon energy of 2.1 eV into vibrational energy without undergoing persisting structural changes [145] as visualized in Figure 8.3.

Due to these favorable properties, azulene has been previously used for studies of VET in hydrocarbon chains [145, 146, 150]. The advantage of depositing more energy when using Vis instead of IR excitation and to have a larger number of modes that can potentially couple and inject energy into the system under investigation comes at the expense of a somewhat larger chromophore. Recently azulene was as well proposed as label in FRET studies [233]. Previous studies of VET in model peptides used azobenzene as energy donor [152, 331], with the important disadvantage that the system is perturbed by chromophore isomerization [356].

As azulene-based VET donors for application in peptides and proteins, we investigated β-(1-azulenyl)-N-acetyl-alanine (ac-AzuA) and azulene-1-yl-acetic-acid (AzuCa), which both have their S_0 to S_1 absorption band at about 600 nm (see Figure 8.4). Results of transient IR measurements on those two chromophores in THF can be found in Figure 8.8.

Internal conversion after excitation at 600 nm is found to occur on similarly fast timescales as for free azulene [354] as reflected by the rapid onset of VET . Both chromophores are found to have excellent photo-stability, allowing for many days of sample usage under present measurement conditions.

VET Acceptor. An ideal "acceptor" chromophore for the direct tracking of VET needs to have its IR absorption band well separated from the protein vibrations (as introduced in the motivation of this thesis). Ideally the chromophore can be used both in H_2O and D_2O, which means it has to absorb between 1800 cm^{-1} and 2150 cm^{-1}. It needs to have decent oscillator strength and a narrow line width, which translates into a large difference signal from anharmonic frequency shifts induced by VET [331].
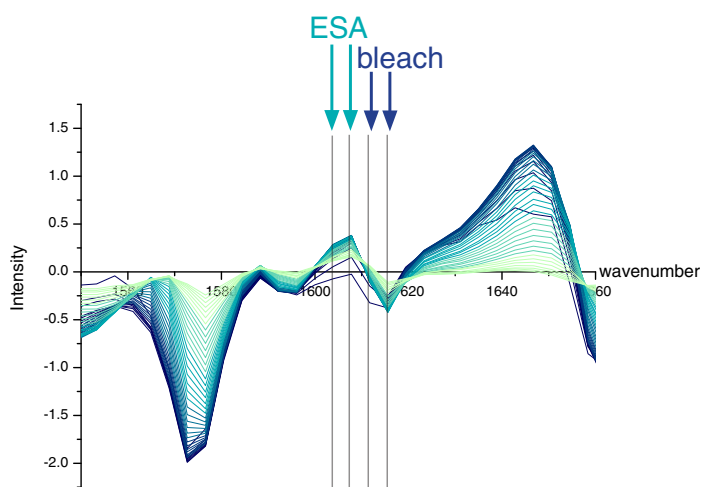
Figure 8.5: Example for data analysis. Shown are transient IR data for AzuP in the amide I region. Transients are either plotted as change of bleach intensity on one pixel, integrated bleach intensity (sum over more pixel) or in case of very small signals the amplitude, calculated from bleach signal and excited state absorption is shown in Figure 8.13 as demonstrated here for the mode at 1615 cm^{-1}. Reproduced from reference [112] with permission from the PCCP Owner Societies.

Azidohomoalanine was identified as preferable novel vibrational probe and and as a suitable candidate fulfilling those requirements already in chapter 4 and its usability in proteins was demonstrated in chapter 5 and 6. In this chapter another application of aha is shown as a part of the proposed donor-acceptor pair for the direct measurement of VET in proteins.

8.2 Experimental Design

To investigate the performance of the proposed azulene-azide donor-acceptor pair, a model peptide AzuP (AzuCa-Tyr-Asn-Aha-Gly) shown in Figure 8.2, which contains azulene incorporated as azulene-1-yl-acetic-acid (AzuCa) at the N- terminal position and azidohomoalanine close to the C-terminus was designed. In addition amino acids which display characteristic protein marker modes, such as tyrosine, asparagine and glycine providing the C-terminal carboxyl were added, in order to have additional spectroscopic indicators of VET. Of the peptide AzuP Vis-pump-IR-probe spectra covering the range from 1200 cm^{-1} to 2120 cm^{-1} were recorded. Experimental details on those ultrafast measurements can be found in Appendix A as well as the figure captions for the respective results. The transient IR spectra for AzuP in d_6-DMSO are shown in Figure 8.6 b. To aid the assignment of the observed bands, additionally the time resolved spectra of the azulene monomer AzuCa in the same solvent (d_6-DMSO) and of a shorter peptide AzuP' (Azu-Tyr-Gly) were measured under comparable conditions. The transient IR data for AzuCa are shown in Figure 8.6d, those of AzuP' are shown in Figure 8.7.

Data Analysis. Data were recorded as transient pump-probe spectra at a fixed pump wavelength of 600 nm with an excitation energy of approximately 5 μJ and magic angle polarization between visible pump and infrared probe. Resulting example spectra are plotted in Figure 8.5. For the shown transients, which were used to analyze peak times and help with band assignment, typically the bleach signal at one pixel was plotted. For small signals or broad signals, data are integrated by adding up several pixels. For some very weak signals the amplitude of the signal is shown, calculated from the intensity of the exited state absorption minus the intensities for the bleach signal. The modes, which are shown in Figure 8.9, are described in table Table 8.1.

transient	calculated from
2098 cm^{-1}	bleach single pixel at 2098 cm^{-1}
1728 cm^{-1}	amplitude, (ESA[1710 cm^{-1} + 1714 cm^{-1}]) - (bleach[1723 cm^{-1} + 1728 cm^{-1}])
1678 cm^{-1}	bleach, single pixel at 1678 cm^{-1}
1670 cm^{-1}	integrated bleach signal, sum of signal at 1668 cm^{-1} + 1672 cm^{-1}
1615 cm^{-1}	amplitude, (ESA[1604 cm^{-1} + 1608 cm^{-1}]) - (bleach[1612 cm^{-1} + 1616 cm^{-1}])
1516 cm^{-1}	bleach, single pixel at 1516 cm^{-1}
1398 cm^{-1}	bleach, single pixel at 1398 cm^{-1}

Table 8.1: Overview how transients in Figure 8.9 are calculated by either integrating the bleach signal for different pixels or calculating the amplitude between ESA signal and bleach signal.
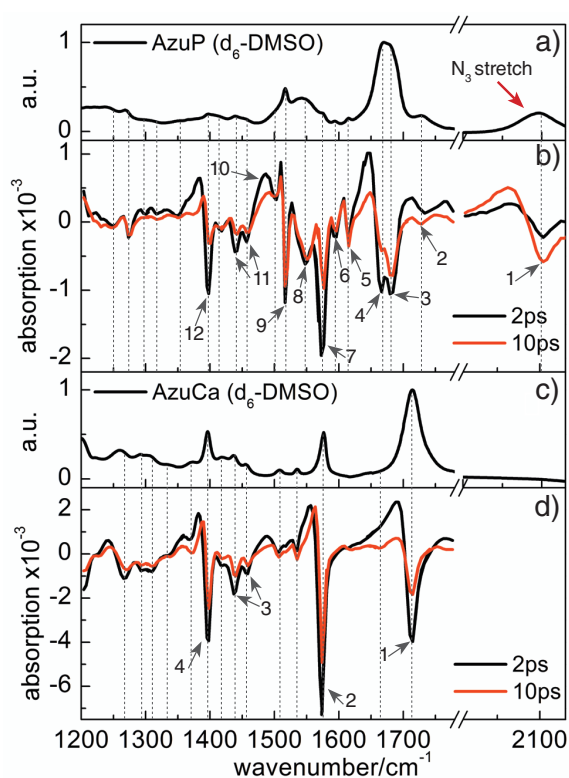
Figure 8.6: (a) FTIR and (b) transient IR spectra of the model peptide AzuP with 600 nm excitation wavelength. (c) FTIR and (d) transient IR spectra of the incorporated donor AzuCa. Numbered signals are discussed in the text. FTIR spectra were recorded on a Bruker Vector 22 DTGS detector. Concentration-dependent measurements of all azulene monomers with concentrations ranging from 25 to 250 mM in a CaF$_2$ cell [296] with an optical path length of 100 μm were performed. The model peptide AzuP was solved in d$_6$-DMSO (99.9 %, deutero, Germany) in concentrations from 10 to 50 mM for FTIR measurements performed as described above. No sign of concentration dependence has been found in these measurements.

Transient IR spectra were recorded as described in Appendix A. Samples were prepared with approx. 8-10 mM concentration for the peptide AzuP and 30 mM for AzuCa in d$_6$-DMSO, data were recorded with approximately 5 μJ excitation energy in a flow-cell with 250 μm spacer. The azide and glycine spectral window were collected with a 100 μm spacer due to larger solvent absorption, the corresponding signals where multiplied by 2.5 to compensate for the lower thickness. Reproduced from reference [112] with permission from the PCCP Owner Societies.

8.3 Results and Discussion

8.3.1 Transient IR Experiments on the Model Peptide AzuP

Energy transfer in AzuP starts at the azulene chromophore and is tracked along the peptide structure in the following. The bands 7, 11 and 12 in Figure 8.6 b are assigned to the azulene moiety, based on comparison with bands 2,3 and 4 of the azulene monomer AzuCa in Figure 8.6 d. Their response is instantaneous on the time scale of our instrument, as exemplified by the transient of band 7 (1398 cm^{-1} transient, Figure 8.13 a). The carbonyl group of AzuCa appears at 1714 cm^{-1} (band 1, Figure 8.6 d). In the peptide AzuP the vibration is shifted because of amide formation to 1670 cm^{-1}

(band 4, Figure 8.6 b). Due to its proximity to the azulene chromophore, it is the next vibration to respond to VET (t_{max} = 2.1 ps, 1670 cm^{-1} transient, Figure 8.13 b) after the chromophore itself. The next residue in the peptide sequence is tyrosine. Its ring modes [88, 89] contribute bands 5 and 9 in Figure 8.6 b. This assignment of the tyrosine is confirmed by comparison with the spectrum of AzuP' in Figure 8.7 and is in agreement with literature values [89]. The tyrosine vibrations show a t_{max} of 4.7 ps (1615 cm^{-1} transient, Figure 8.13 b) and 4.2 ps (1516 cm^{-1} transient, Figure 8.13 c), respectively. The next amino acid is asparagine. Here, an amide I like mode in the side chain at about 1680 cm^{-1} is expected [88, 89]. It overlaps with the other modes in the carbonyl range, which belong to the backbone and together generate a stronger signal (band 3, 1678 cm^{-1} in Figure 8.6 b), also due to their closer proximity to the chromophore. Additionally an NH wagging mode of the asparagines side chain is expected (1612 cm^{-1} in H$_2$O). A shift to lower wavenumbers in DMSO can be expected and tentatively band 6 is assigned to this mode. The band is absent in AzuP', which lacks asparagine (see data in Figure 8.7). As the band is small and overlaps with other bands no transient is shown in Figure 8.13. Next in sequence is the proposed "acceptor" chromophore azidohomoalanine. Its anti-symmetric azide stretching mode absorbs at 2100 cm^{-1}, perfectly separated from the other bands of the peptide. It responds with t_{max} = 7.0 ps (2098 cm^{-1} transient, Figure 8.13 a).

The peptide is completed at the C-terminus by glycine, which contributes band 2 in the transient IR spectrum of AzuP (carbonyl stretching of the carboxylic acid moiety), that peaks at t_{max} = 5.9 ps (1728 cm^{-1} transient, Figure 8.9 c). For the characteristic localized vibrational modes of the peptide a pronounced correlation between the through-bond distance of the vibrating moiety from the azulene chromophore and the time until the VET induced signal of this moiety becomes maximal is found [106, 111].

The data clearly illustrate how Vis-pump-IR-probe spectroscopy monitors directional energy flow through a molecule. It also impressively illustrates, that band overlap leading to spectral congestion especially in the amide I and amide II region is a severe problem already in very small peptides. In order to carry out systematic studies of directional VET in proteins, the use of an acceptor that can be monitored separately from the other protein vibrations is crucial.

The VET induced signal of the azide stretching band of the proposed acceptor azidohomoalanine is the dominating contribution at long delay times (Figure 8.6 b). Even upon VET originating at the azulene donor in a through-bond distance of approximately 2 nm, it reaches a signal size
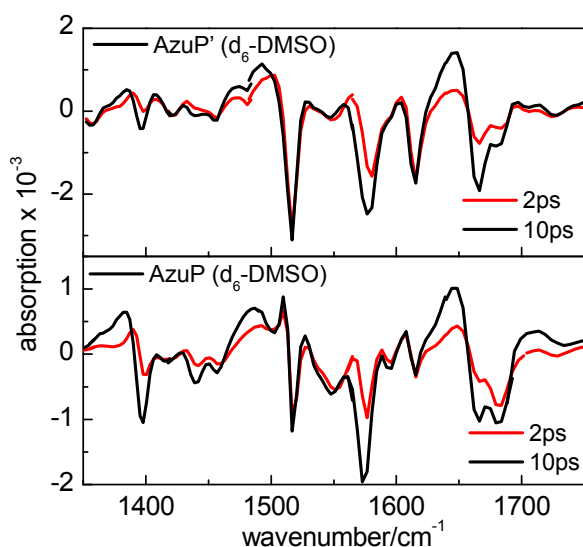
Figure 8.7: Transient IR spectra for the small assignment peptide AzuP' and the model peptide AzuP, both measured under similar conditions in d$_6$-DMSO, data in the lower panel are the same as in Figure 8.6. The assignment peptide does not contain an azide acceptor chromophore, therefore data are only shown for the region 1350 cm^{-1} to 1750 cm^{-1}. Reproduced from reference [112] with permission from the PCCP Owner Societies.
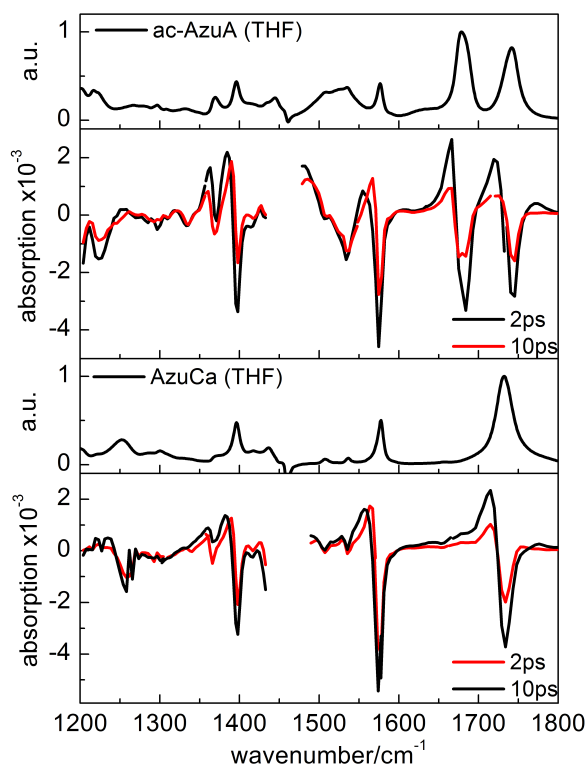
Figure 8.8: FTIR absorption spectra and transient IR spectra for the model compounds ac-AzuA (a (FTIR), b (transient IR)) and AzuCa (c (FTIR), d (transient IR)) measured in THF. Experiments were performed similar to those described above with a sample concentration of 25 mM for AzuCa and ac-AzuA. The spacer thickness used in the CaF_2-flowcell was 250 µm and an excitation intensity of 5 µJ. Reproduced from reference [112] with permission from the PCCP Owner Societies.

comparable to the total carbonyl signal of the peptide.

The experimentally observed t_{max} of 7.0 ps over a distance of three peptide bonds and the side chain bonds corresponds to previously reported transfer rates of 2.6 to 5.5 Å/ps [77, 104, 357]. The presented measurements have been carried out at 10 mM peptide concentration with a spacer thickness of 250 µm and an excitation energy of 5 µJ for the 600 nm pump. The concentration is in a range that is compatible also with many soluble proteins. The signal quality generated at this concentration (2098 cm^{-1} transient, Figure 8.9 a) impressively demonstrates that the proposed donor-acceptor pair is indeed suitable to monitor energy flow on a length scale of biological relevance, since the length of the investigated peptide corresponds to the radius of small proteins.

8.3.2 Relaxation in Model Systems of Different Size

The proposed VET pair of azulene as heat donor and Aha as heat acceptor is not only suitable for its designed purpose, the direct tracking of vibrational energy flow in a protein, as for example the PDZ domain. Moreover this novel donor-acceptor pair is an extremely useful experimental tool to study the characteristics and physical principles of vibrational energy flow.

One example of possible applications is the detailed investigation of the transfer mechanism in molecules of different chain lengths to find out how heat is transported, similar to experiments by the Rubtsov group on PEG chains [144, 357].

A first results of this kind can be found in the data presented here. In Figure 8.10 the transient signals of the characteristic ring modes of the azulene chromophore at 1398 cm^{-1} and 1575 cm^{-1} are plotted for the molecules AzuCa and AzuP, both in the same solvent (d$_6$-DMSO) so that a solvent effect can be excluded. The signals from AzuP are shown in light blue, the signals from AzuCa in dark blue. Signals are fitted by an bi-exponential function to visualized the peak time and decay
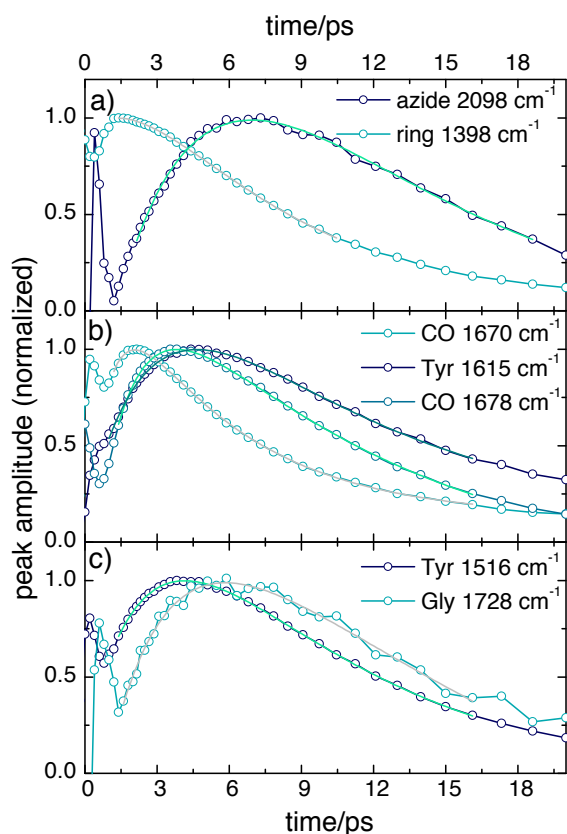
Figure 8.9: Transients for the model peptide Azu-Tyr-Asn-Aha-Gly, measured in d_6DMSO. Shown is the time dependent signal intensity of the signals shown in Figure 8.6. Data are fitted with a bi-exponential function to allow for better recognition of the peak maximum. The upper panel shows the results for the azide signal contributed from Aha and the characteristic ring mode of azulene, the middle panel shows peak intensities for signals in the amide I region, the lower panel shows the transient signals for the characteristic tyrosine ring mode and the carbonyl of the C-Terminus. Reproduced (modified) from reference [112] with permission from the PCCP Owner Societies.

better.

It can be directly seen, that relaxation of vibrational energy is faster in the larger molecule AzuP, which contains four additional amino acids and has a peptide chain length of more than 2 nm. In AzuCa for comparison the relaxation is much slower. However the peak times seem to be similar for the modes with approximately 1.4 ps (not completely resolved) in AzuCa for the ring mode at 1398 cm^{-1} and 1.3 to 1.4 ps (as well within the resolution limit) for the same ring mode in AzuP. For the other ring mode at 1575 cm^{-1} the peak time is found to be approximately 1.7 ps in AzuCa and 1.8 ps in AzuP, which is almost the same within the precision of the experiment.

This finding can be explained by the different number of vibrational modes in molecules with different size. As AzuCa has less modes in which the excess energy can be dissipated those modes will overall accept more energy and thus show a longer vibrational life time whereas in AzuP the energy can be dissipated into many more vibrational modes and thus the ring mode shows a shorter life time. Thus the propose donor acceptor pair is a suitable tool to investigate relaxation pathways within a molecule. These results are in agreement with previous studies reported by the Rubtsov group [144, 357] and by Schwarzer et al. [145, 150], who did already extensive studies of how VET efficiency and speed is affected in different molecular systems. The nature of the intramolecular vibrational energy transfer needs to be investigated in further detail, especially with respect to applications in proteins, e.g. with peptides of different chain length. This kind of experiment would allow to find out, if the VET process induced by exciting a delocalized mode as in the azulene chromophore has similar properties than VET, which is induced by excitation of a localized chromophore (e.g. as in the experiments presented in chapter 8 and [108, 111, 144, 338, 357].
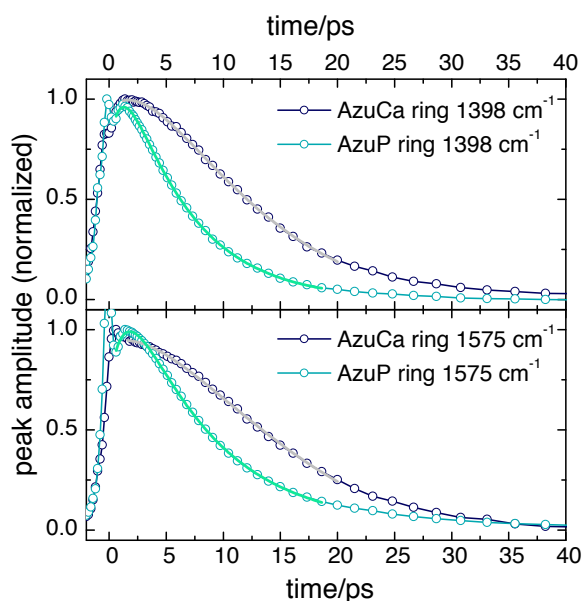
Figure 8.10: Transients of ring modes in AzuP and AzuCa, measured in d_6-DMSO, shown is the time dependence of the signal intensity for signals no. 7 and 12 from Figure 8.6 b and no. 2 and 4 from Figure 8.6 d.

8.3.3 Usability in Aqueous Solution

One major prerequisite for the application of the proposed VET pair in proteins is its functionality in aqueous solution. The solvent is known to influence heat transfer rates [358] and if relaxation of the heat from the excited azulene mode to the surrounding water would be faster or much more dominating than the VET process leading to signal generation in experiments, application in proteins will fail. Also that the energy which is relaxed via VET into the low frequency modes might be rather dissipated to the surrounding solvent molecules depending on the presence of hydrogen bonds is affecting the signal size for the VET induced signal of the azide stretch vibration.

To investigate the usability in aqueous solution compared to organic solvent, which can not be explained by theory directly, e.g. because computations including explicit solvent are costly and difficult, the transient IR signal in a di-peptide with the sequence AzuA-Aha was studied in d_6-DMSO and H_2O.

In Figure 8.11 the UV/Vis spectrum of the azulene compound AzuA (β-azulenyl-alanine) is shown. The absorption maximum for the S_0 to S_1 transition is found around 600 nm in H_2O, similar as for
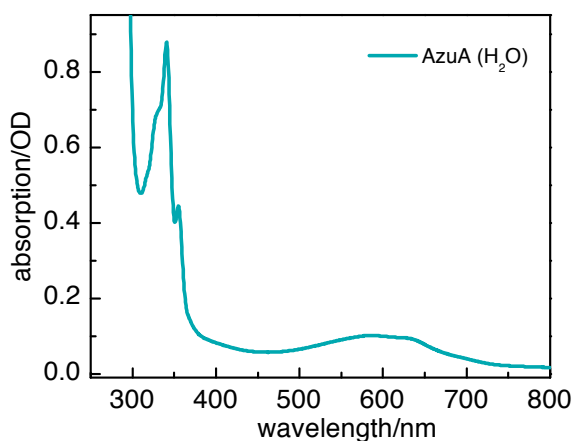
Figure 8.11: UV/Vis absorption spectrum of the free amino acid Azulenylalanine (AzuA) in H_2O, measured against H_2O as background. The concentration was approximately 2.3 mM. Data were recorded on a Jasco V-660 spectrometer. A cuvette with 0.1 cm path length was used.
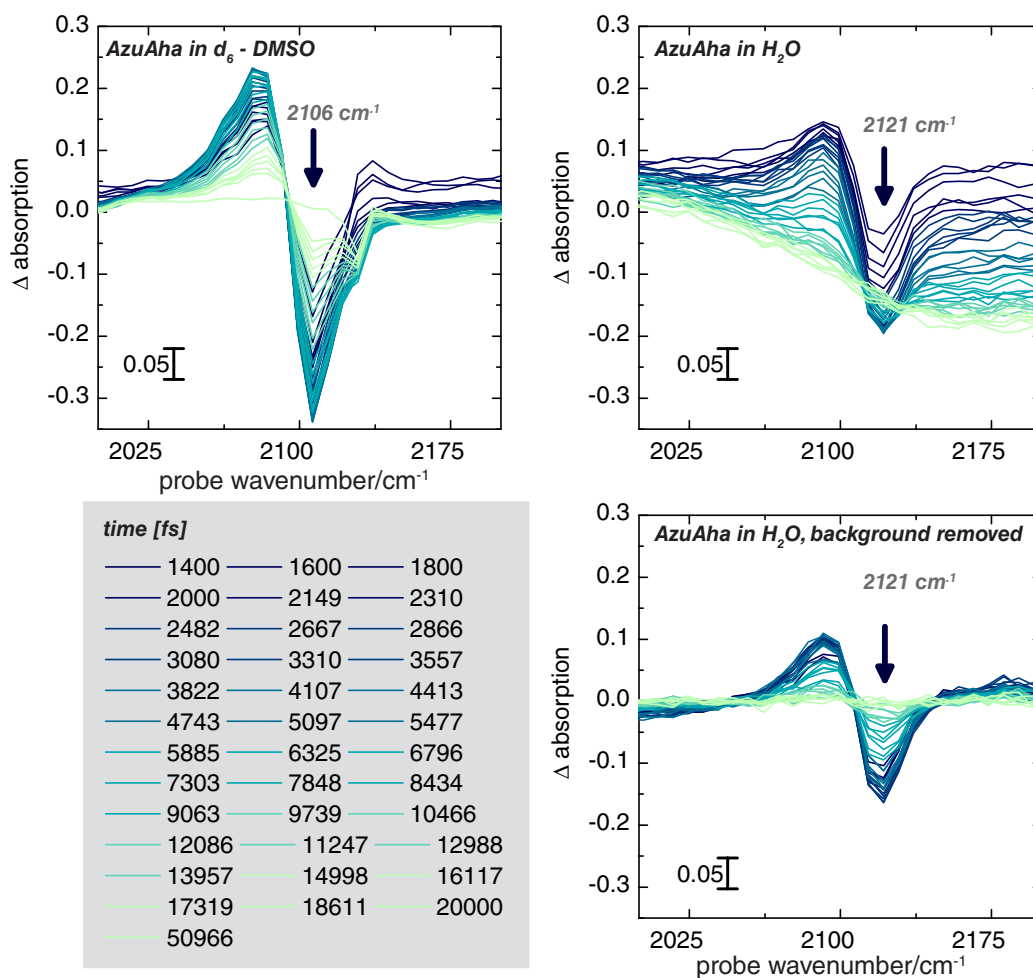
Figure 8.12: Transient IR spectra of the dipeptide AzuAha in d_6-DMSO and H_2O. The upper right panel shows the originally collected data for AzuAha in H_2O, only corrected by subtraction of a negative time signal as background. The lower right panel shows the data with a correction for the heat background contributed by the combination band of H_2O. Sample conditions for both experiments have been identical, the concentration was 25 mM, a spacer of 100 µm was used, excitation power at 600 nm was 5 µJ, spectra have been collected with 500 shots on the 150 line grating. The visible focus had a size of 120 µm and was stretch in time to approx. 400 fs by guiding the light through glass rods. The relative polarization of pump and probe beam was set to the magic angle.

the previously described azulene compounds AzuCa and ac-AzuA in THF (see Figure 8.4). Transient IR experiments were performed similar to the other experiments described in this chapter.

In Figure 8.13 the transient IR spectra of AzuAha in d_6-DMSO and H_2O are shown. The upper panel shows the azide signal without background correction for the solvent but only subtraction of a background for negative waiting times. The azide signal in H_2O is difficult to discriminate from the solvent contribution of the heated H_2O band (the same problem, which was discussed in more detail already in chapter 6) and is smaller than the signal in DMSO, the sample conditions were similar. The data for AzuAha in DMSO show a signal with a maximum amplitude of about 0.6 moD, whereas the amplitude of the signal in H_2O is only around 0.35 mOD. The lower panel

shows the azide signal without the heated solvent background. The background was removed by fitting a polynomial function of fifth order to the signal for longest waiting times and subtract it scaled to the intensity at the highest wavenumbers from all other spectra. The pure azide signal has an intensity of about 0.3 mOD for a concentration of 25 mM in a flow cell with 100 µm spacer thickness. This signal size would allow for measurements of a protein sample, proving further more the applicability of the proposed VET pair.
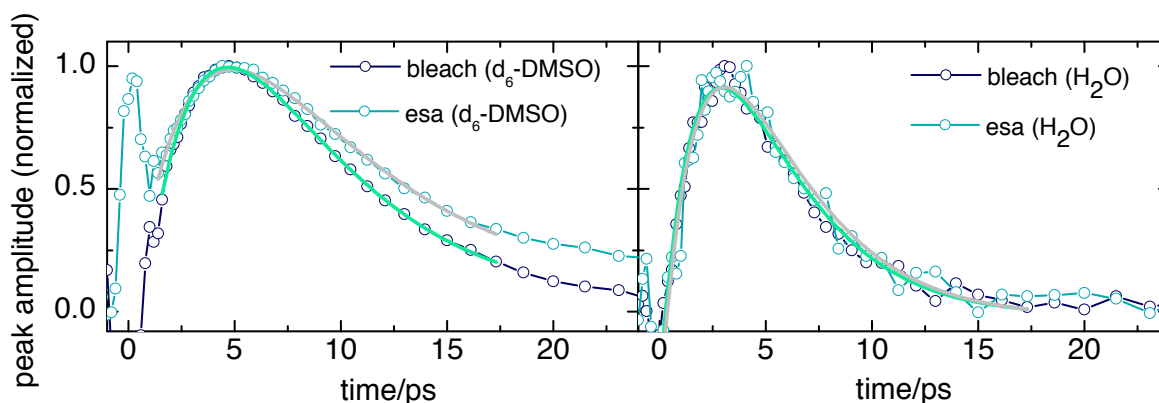
Figure 8.13: Transients of the azide stretch vibration of the di-peptide AzuAha in H_2O and d_6-DMSO.

Figure 8.13 shows the time dependence of the azide signal in DMSO in comparison to H_2O. It can be seen that the peak time for the azide vibration is faster than in DMSO with 4.94 ps for the bleach in DMSO and 4.62 ps for the ESA in DMSO. The signals in H_2O have peak times of 2.97 ps for the bleach and 3.14 ps for the ESA. This demonstrates how vibrational cooling affects the relaxation rates and the signal intensity, since the whole molecule is cooling faster in H_2O, not allowing for a similar amount of vibrational energy to reach the azide.

8.4 Conclusion and Outlook

In the light of the presented results the application of the proposed genetically encoded azulene-azide donor-acceptor pair for the study of anisotropic energy flow in proteins appears very promising. Both, donor and acceptor absorb at optimal spectral positions with respect to native protein transitions and aqueous solution. Also energy transfer to the solvent could be investigated by monitoring specific vibrations of the solvent. The VET donor mechanism works without troublesome perturbation of the protein structure and undesired effects on the spectrum by permanent dipole moment changes.

The proposed VET pair has shown excellent performance in a model peptide in terms of a sharp onset of VET and generation of a large transfer signal over a biologically relevant distance. Additionally the performance of the VET pair was successfully demonstrated in aqueous solution, which is a major limitation for applications in proteins. Vibrational cooling in H_2O was found to shrink the observable signal size, but big enough signals were observed to allow for testing the application in proteins.

Site selective incorporation of the labels either through synthetic approaches or during protein expression will allow to investigate VET in proteins in great detail. Anisotropy of VET in different types of secondary structure elements can be addressed, e.g. comparing transfer along the backbone and across hydrogen bonds in β-sheets. VET across different types of tertiary contacts can be

investigated, which do not play a role in the quasi one-dimensional case of small peptides but are hypothesized to be of importance in a protein setting.

Additionally the VET pair might be of interest to study the physical principles of VET in more detail, as the nature of heat transfer is still not understood completely.

The long standing theoretical predictions of distinct highly directional energy transfer pathways in proteins and their role in allosteric signalling can be subjected to rigorous experimental testing. First experiments towards this goal are presented in the following and final chapter of this thesis.

9 Towards Real-Time Investigation of Energy Flow in PDZ

This chapter describes the first steps towards real-time mapping of energy flow in the 3rd PDZ domain of PSD-95. A major goal of this thesis was to demonstrate whether the direct measurement of energy flow in PDZ is possible. It was intended to design an experiment mimicking the Anisotropic Thermal Diffusion Simulations from Ota and Agard [10].

As outlined in Chapter 2 and Chapter 8, energy flow in proteins is of major interest for the understanding of intra domain communication in proteins and signal propagation as well as for allosteric long-range effects. A huge body of theoretical work predicts the existence of energy transfer pathways in the PDZ domain as well as in other protein domains [9, 10, 148, 159, 160, 161, 167, 168, 359]. However experimental tools to access and directly observe this effect in real-time and proof the existence of energy transfer pathways are lacking [204].

As demonstrated in Chapter 8 the usage of a donor acceptor pair to monitor VET pathways is a possible approach to experimentally access those. Based on the positive results on the model peptide, it was planned to employ the proposed donor acceptor pair of azulenyl-alanine and Aha in the PDZ domain [338].

This chapter organized in the following sections. **First** the sample design is outlined, **second** the biophysical characterization of the investigated protein-ligand complex with the incorporated donor-acceptor pair is described, **third** first transient IR data of the model complex are reported and experimental challenges discussed. The chapter ends with possible experimental improvements and a outlook towards further research.

9.1 Sample Design

The general idea is to directly mimic the simulation by Ota and Agard [10] in an experiment. In Chapter 2 the idea of a conserved network of residues involved in long-range communication was introduced. One attempt, by which those networks were predicted was the simulation shown in figure 2.6. In this *anisotropic thermal diffusion* simulation heat (vibrational energy) was injected site-specifically into the system at position His372. The propagation of energy was followed by monitoring the change in rmsd of all residues in the PDZ domain which is equivalent to monitoring a temperature change. A preferred energy transfer pathway from His372 to Ile341 via Ile327 within 4 ps was found. In contrast the injection of heat at other positions yielded isotropic heat propagation throughout the protein.

The donor-acceptor pair described and tested in chapter 8 was designed to address this phenomenon in an experiment. Ideally heat would be injected at position His372 and the propagation of heat would be monitored at positions along the proposed pathway and away from the proposed pathway with a *thermometer* suitable for usage in proteins. This experimental idea is illustrated in figure 9.1. The resulting energy flow would be measured by monitoring the arrival time of heat at positions along the proposed energy transfer pathway. To proof if the heat transfer is indeed
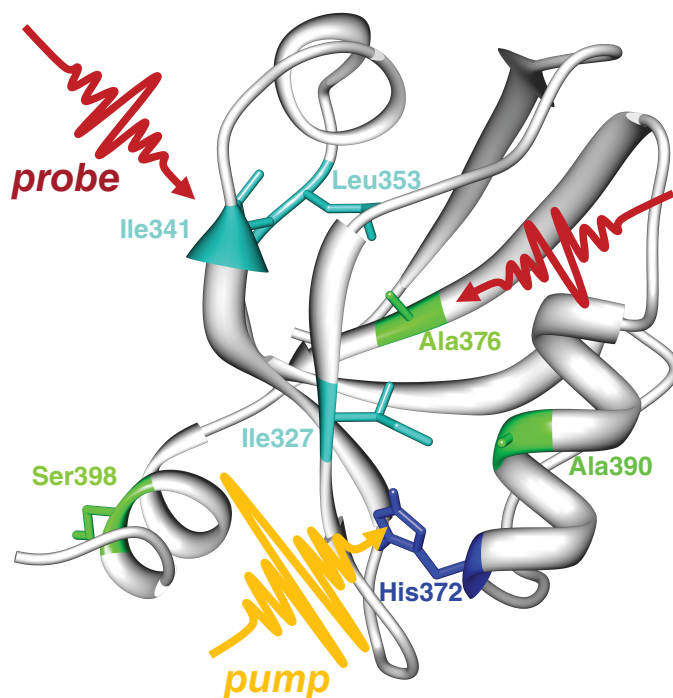
Figure 9.1: The ideal experiment to mimic Ota and Agards simulation and find out whether anisotropic heat transfer in PDZ exists: Heat injection via a pump pulse at position His372 (blue), reporting of heat arrival at three positions on the proposed pathway (light blue: Ile327, Ile341, Leu353) and three positions off the proposed pathway (green: Ala376, Ala390, Ser398) with similar distance from His372.

anisotropic and the proposed coupled network of (conserved) residues ([9]) serves as preferred *"wire"* for site-to-site communication it is necessary to observe if and when energy arrives at off-pathway positions. Therefore pairs of residues with similar distance from the injection point should be monitored (in figure 9.1 residues on-pathway are colored turquoises, off-pathway residues are colored green). The result would be pairs of energy transfer times within the picosecond range where ideally the set of on-pathway residues are reached by the energy within few picoseconds and the off-pathway residues might yield not signal at all.

9.1.1 Incorporation of Multiple Novel Probes

In the previous chapter the almost ideal compounds azulenyl-alanine as heat source and Aha as local thermometer were introduced. To implement the above outlined experimental idea, it would be necessary to incorporate both artificial amino acids site-specifically into the PDZ domain with the restrictions to keep the protein domain functional and generate high protein yield.

In the field of genetic engineering approaches for the simultaneous incorporation of two different non canonical amino acids are developed. The first demonstration of the simultaneous site-specific incorporation of two different artificial amino acids via the usage of an modified ribosome, which can process quadruplet codons, was demonstrated by Neumann et al in 2010 [214, 239, 360]. The usage of two independent orthogonal tRNA pairs was demonstrated as well [361]. A different approach using an poly-auxotrophic *E. coli* to introduce even three different artificial amino acids using the supplementation incorporation method was demonstrated by the Budisa group in 2010 as

Mutant pairs and distance to His372	
Ile327Aha and Ala376Aha	0.8 nm
Ile341 and Ser398Aha	1.7 nm
Leu353 and Ala390Aha	1.8 nm

Table 9.1: Mutant pairs of Aha labelled PDZ to mimic anisotropic thermal diffusion in an experiment. Distances are measured between C_β of His372 and C_β of the respective side chains.

well [81], approaches for the multiple encoding of artificial amino acids are reviewed in [211, 214].

All approaches have in common, that the double labelling with two different artificial labels is in principle possible, but expression yields are not in the range similar to regular recombinant protein expressions as desired of samples suitable for 2D-IR or transient IR. Using stop codon suppression approaches, as demonstrated by [239, 361], the protein yield will drop substantially, because the incorporation approach competes with the termination machinery of protein synthesis [237] and even though orthogonal tRNA/tRNA synthetase pairs (mainly from *Methanococcus jannaschii*) are used, those might be "leaky" for different amino acids than the desired artificial label. Thus the labelling efficiency for double labelling would be lower than desired for the difficult transient IR experiments planned.

The introduced donor acceptor pair of azulenyl-alanine and Aha [112] is in principle suitable for simultaneous incorporation into a protein. Azidohomoalanine is introduced in a supplementation based incorporation method as methionine analogue, thus the expression of an Aha-labelled protein requires a methionine auxotrophic *E. coli*. Azulenyl-alanine in contrast was proposed as candidate to be used as tryptophan analog in a similar approach in tryptophan auxotrophic *E. coli* [212]. However this approach is not sufficient for the incorporation of azulenyl-alanine [234] and a novel tRNA synthetase specific for azulene is required. This challenge is addressed in an ongoing cooperation with the group of Nediljko Budisa from TU Berlin.The design and optimization of an expression system in *E. coli* suitable to express an azulene-labelled PDZ with Aha incorporated additionally is out of the scope of this thesis and requires severe work from molecular biologists. To address the question of interest about energy transfer in the PDZ domain a protein-ligand complex was designed instead, which contains the donor in the peptide ligand.

9.1.2 Protein-Ligand Complex

To gain a suitable experimental system of PDZ with the introduced VET pair the above mentioned limitations had do be overcome. A different approach to introduce both artificial amino acids into the functional PDZ is to study the energy transfer in the presence of the peptide ligand and introduce the heat source azulenyl-alanine in the peptide ligand. This is actually matching both the simulations by Ota and Agard [10] as well as the study by Ranganathan and Lockless [9] who as well used the protein ligand complex for their studies, as simulations have been performed using the pdb file 1be9. Additionally meaningful results would be expected since the energy transfer pathway is believed to be important for allosteric long-range communication, a process happening in the presence of the native ligand.

To design a stable and measurable protein-ligand complex with the VET pair introduced several restrictions had to be addressed.

The binding constant of the designed complex needs to be similar to the binding constant of the wild type in complex with its native CRIPT ligand to allow for experimental results about the

peptides with azulene	origin	status
Azu-QTSV	derived from CRIPT	tested experimentally
Azu-KQTSV	derived from CRIPT	tested experimentally
KKET-Azu-V	derived from Saro et al. [320])	potential candidate

Table 9.2: Promising and tested peptide sequences for a ligand of PDZ3 with azulene incorporated as VET donor.

protein-ligand complex, as the majority of the peptide needs be in bound complex [1]. The heat source needs to be in the proximity of the originally proposed starting point for the energy transfer pathway, close to His372. The protein-ligand complex needs to be sufficiently stable to allow for high protein concentrations during the experiment.

Positions for Thermometer. Since Ota and Agard [10] proposed an anisotropic heat transfer starting at His372 and IVR shows a strong distance dependency, pairs of incorporation sites with similar distance from His372 have been identified. The mutation sides in PDZ introduced in chapter 2 and discussed in chapters 5 and 6 were originally chosen for this final experiment. Three of the six incorporation sides are positioned of the energy transfer pathway suggested by Ota and Agard [10]: Ile327, Ile341 and Leu353. The other three mutants Ala376, Ala390 and Ser398 are matching those three to generate three pairs of residues with one on pathway and one off pathway and the same distance from the proposed starting point of the energy transfer at His372.

Peptide Design. The peptide tested for docking were based on the sequence of the native peptide ligand CRIPT. The main focus was on short peptides with the conserved sequence NYKQTSV and azulene as N-terminal residue attached. The most promising peptides resulting from this approach in terms of distance to His372 in combination with predicted binding affinity are AzuKQTSV and AzuQTSV. A longer binding motif increases the binding affinity but in contrast moves the azulene group to far out of the binding pocket. A different approach for peptide design was to modify the sequence of another binding partner. Saro et al. [320] undertook a huge study of binding partners for PDZ3 and reported not only on CRIPT and CRIPT derived peptides but as well on the sequence KKETEV as good binding partner for PDZ3 (with a k_D of 18µM). The sequence was modified and for the variant KKETWV a binding constant of 2.8 µM was reported, indicating that a tryptophan at position -1 (see Figure 5.1) increases the binding affinity to PDZ3. Some docking attempts to the wild type with a peptide of the sequence KKETAzuV were carried out, but not for all mutants. This position for the introduction of the azulene donor is promising and needs further attention.

Docking Results. The whole set of possible combinations between incorporations sites for Aha and the different possible azulene-containing ligands was investigated using molecular docking (see Bachelor Thesis by Martin Essig [362]). Table 9.3 reviews the main results obtained for the binding of three ligands (AzuKQTSV, AzuQTSV and the native CRIPT) to the wild type PDZ3 domain as well as the six mutants.

---

[1]The Bachelor thesis in Biophysics of *Martin Essig* entitled "Ligandenoptimierung *in silico* mittels molekularem Docking" was dedicated to tackle the peptide design by testing several possible peptide candidates using molecular docking. The thesis topic was proposed by the author and works were supervised by her. The results of this thesis are partly reproduced in this chapter

Mut	AzuKQTSV		AzuQTSV		AcNYKQTSV	
	$\triangle G_{bind}$	K_d	$\triangle G_{bind}$	K_d	$\triangle G_{bind}$	K_d
WT	-8.91	0.292	-8.33	0.779	-7.04	6.86
Ile327Aha (r)	-8.06	1.24	-7.64	2.5	-5.86	50.49
Ile327Aha (f)	-7.48	3.27	-7.74	2.12	-5.56	84.0
Ile341Aha (r)	-8.00	1.37	-4.28	723.36	-6.58	14.93
Ile341Aha (f)	-8.63	0.476	-2.99	6480	-6.32	23.49
Leu353Aha (r)	-9.76	0.070	-8.71	0.413	-7.07	6.57
Leu353Aha (f)	-7.34	4.16	-3.13	5005	-6.90	8.77
Ala376Aha (r)	-9.00	0.253	-8.24	0.908	-7.16	5.69
Ala376Aha (f)	-6.75	11.33	-4.11	968.43	-6.35	22.22
Ala390Aha (r)	-9.01	0.246	-8.68	0.436	-6.80	10.29
Ala390Aha (f)	-8.88	0.312	-8.09	1.17	-6.64	13.47
Ser398Aha (r)	-9.51	0.107	-8.50	0.587	-6.81	10.18
Ser398Aha (f)	-9.31	0.150	-7.57	2.84	-7.12	6.01

Table 9.3: Computed binding constants as derived from molecular docking (details in Appendix C). All K_d given in μM, all $\triangle G_{bind}$ in kcal/mol. r and f denote rigid and flexible Aha, respectively.

Simulations were carried out both with the Aha side chain as rigid or flexible residue. For computational details see Appendix C. The computations predict if a stable complex with tight binding to the PDZ domain is formed. This can be evaluated when comparing the results for the wild type peptide with experimental values: The value for K_d obtained for the wild type in complex with the CRIPT peptide acNYKQTSV is 6.86 μM. The experimentally obtained value (see table 5.2) is 2.87 μM, leading to an difference between predicted binding affinity from molecular docking and measured binding constants of approximately factor two to three.

For the mutants in complex with the native peptide mainly similar results as for the wild type were obtained. The binding constants were predicted about a factor three lower than experimentally observed, the docking algorithm correctly predicted that the mutant Ile327Aha has the lowest binding affinity. Introducing additional flexibility to the azidohomoalanine side chain leads to even lower binding affinity. Still the approach seems to be suitable to predict whether a peptide ligand binds with a K_d in the micro molar range.

Two short peptides containing azulenyl-alanine as N-terminal group were docked into the binding pocket for all six mutants. Overall the results predict good binding of the ligand AzuKQTSV to all mutants with even higher binding affinity than for the native peptide. For the ligand AzuQTSV results between flexible and non-flexible Aha side chain vary dramatically, e.g. for the mutant Leu353Aha the binding constant is predicted to be in the nano molar range when Aha is kept rigid, but drops to the milli molar range with a flexible Aha. The results in combination with the approximate distances given in table 9.1 suggest, that AzuKQTSV is the ligand, which has the preferable binding properties.

9.2 Identification and Characterization of Stable Complexes

Based on the molecular docking results and considerations of the distance between azulene and Aha in different possible complexes, the mutant Ile327Aha (which is located directly in the binding
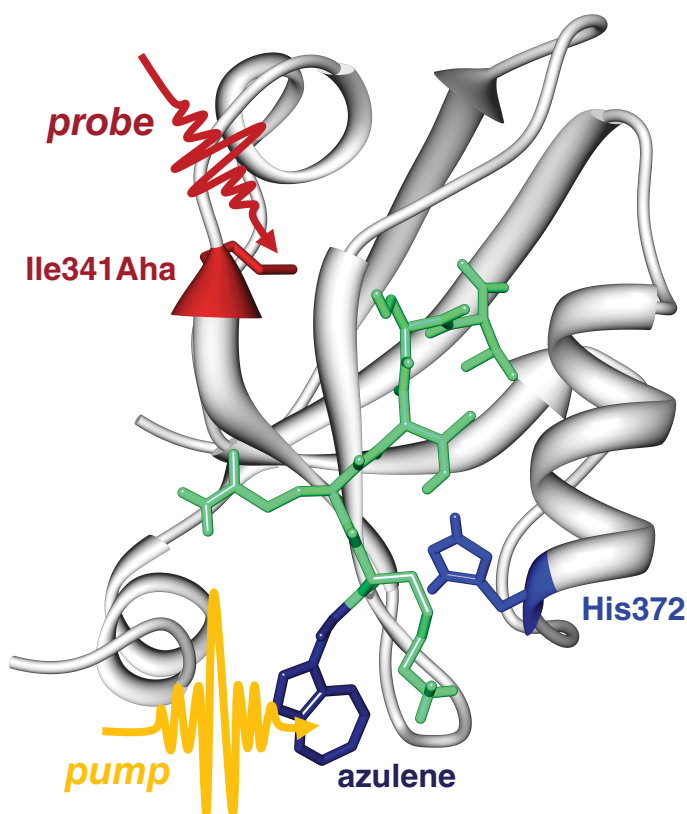
Figure 9.2: Structure of Ile341Aha in complex with AzuKQTSV as derived from Molecular Docking using the pdb file 1BE9 as starting structure.

pocket) in complex with either AzuQTSV (shorter distance) or AzuKQTSV (overall better binding predicted) seemed favorable for first experimental attempts.

Both peptides were synthesized and their binding affinity to Ile327Aha was investigated using ITC measurements, resulting in the necessity to test other mutants for usage in the first experiments.

Sample preparation of the PDZ domain with azulene containing ligands was complicated additionally, because the ligands are nonpolar and only slightly soluble in aqueous buffer directly. The ligand needs to be solved in DMSO first (for experiments d_6-DMSO was used to avoid high absorption at the same wavenumber as the azide absorption) and can then be diluted using buffer. DMSO is discussed to reduce protein stability and induce degradation of proteins, when added even in low percentage [363, 364, 365]. Therefore the stability of the wild type PDZ domain in complex with the native CRIPT peptide was tested in the presence of 2 % DMSO, the lowest possible concentration usable for solving the azulene-containing ligands.

ITC Results.   In figure 9.3 the ITC results for the PDZ wild type in complex with CRIPT in buffer (left) and in buffer with 2% (v/v) DMSO are shown [2]. Both show a good binding affinity for the ligand, without DMSO the binding constant is 2.87 µM, in the presence of DMSO the binding affinity decreases to 3.20 µM but is still in a similar range, indicating only a small effect of DMSO to the binding.

---

[2]Experiments are carried out as described in Appendix B
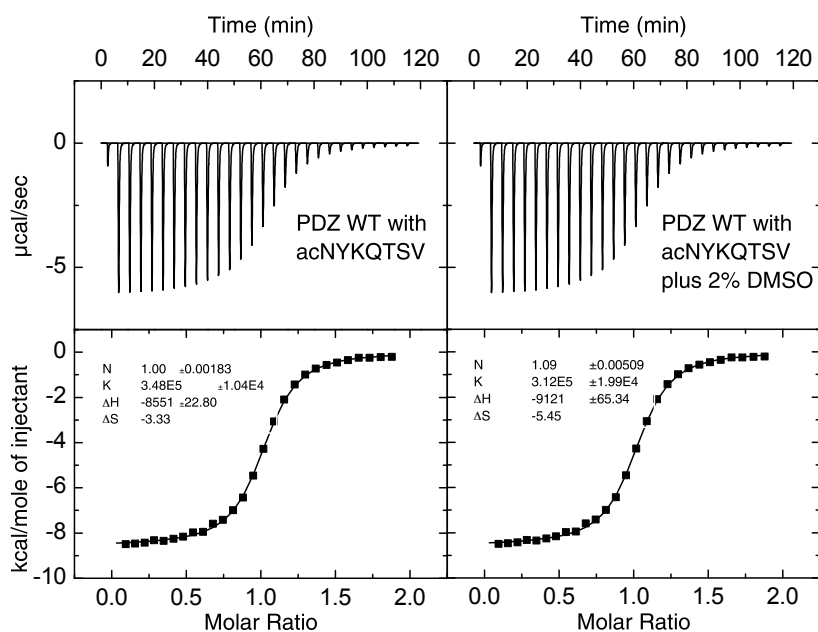
Figure 9.3: Isothermal titration calorimetry is used to determine the binding constants of the CRIPT peptide to the PDZ wild type. The left data show results for the wild type with CRIPT, the right data are recorded in the presences of 2% DMSO. The binding constant k_d for the native complex is 2.87 µM, with DMSO added, the binding affinity decreases to 3.20 µM.

The complex of PDZ Ile327Aha with AzuQTSV does not show any binding affinity in the ITC (data not shown). Based on the molecular docking results in table 9.3 the ligand AzuKQTSV should posses a K_d in the µM range but as shown in figure 9.4 the complex does not show tight binding in the ITC experiment. From the experiment a binding constant of 120 µM is determined. This binding affinity means that, if protein and peptide are in 1:1 stoichiometry in the sample solution, about 70% of the peptide are in complex with the protein, which leads to 30% free peptide and 30% free protein. This ratio is not ideal for time-resolved IR measurements and the experimental optimization of those. Assuming an experiment with protein concentration of 10 mM and 70% ligand binding under similar conditions as used in chapter 8 for the di-peptide AzuAha (see figure 8.12 a signal size of only 0.04 mOD can be expected for ideal conditions. Additionally a signal originating from heat transfer through the solvent might be measured. An alternative to measuring Ile327Aha in complex with AzuKQTSV is the next favorable on-pathway mutant Ile341Aha in complex with AzuKQTSV. For this complex a binding constant of 13 µM is determined experimentally, resulting in 90 % bound ligand in a 1:1 mixture of protein and peptide. This is favorable in comparison to a maximum binding of 70% for the complex of AzuKQTSV bound to Ile327Aha. To prove the technical feasibility of the predicted time-resolved experiments the complex of Ile341Aha with AzuKQTSV as depicted in figure 9.2 was used.

FTIR spectrum of Ile341Aha in Complex with AzuKQTSV. A FTIR absorption spectrum of Ile341Aha in complex with AzuKQTSV is shown in figure 9.5. For comparison the data for the mutant Ile341Aha both with and without the native peptide ligand are shown. The data of the complex with the azulene-containing ligand are recorded in phosphate buffer with d_6-DMSO added, the other data are the same as in Figure 5.7. The center wavenumber of the azide absorption is shifted by approximately two wavenumbers between the complex of Ile341Aha with acNYKQTSV and the complex of Ile341Aha and AzuKQTSV (in the presence of d_6-DMSO). The center wavenumber of the mutant Ile341Aha in complex with the ligand AzuKQTSV is at 2109 cm^{-1}. The line shape appears broadened and is disturbed at higher wavenumbers. This can be explained by the presence of
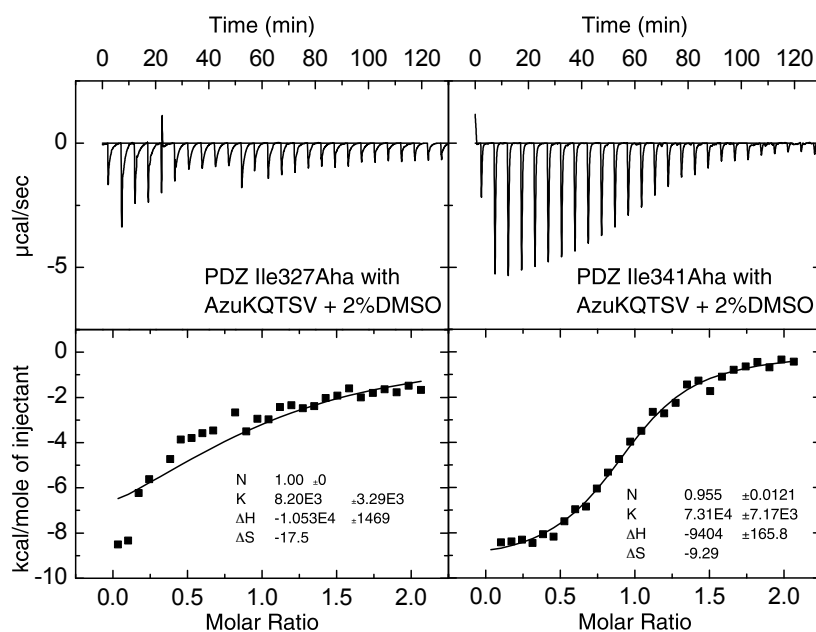
Figure 9.4: Isothermal titration calorimetry is used to determine the binding constants of the azulene-containing peptide AzuKQTSV to the PDZ mutants Ile327Aha and Ile341Aha, which are located on-pathway. The left data show results for Ile327Aha, the right data for Ile341Aha. The binding constant k_d for Ile327Aha with AzuKQTSV is 120 μM (in the presence of 2% DMSO), for Ile341Aha under similar conditions a k_d of 13 μM is determined.

d_6-DMSO in the sample and the difficulties to adjust the d_6-DMSO concentrations in the reference sample to the same value. d_6-DMSO has a small absorption peak at 2133 cm^{-1} ([366]), which is why the spectrum is disturbed. The putative broadening of the azide stretch vibration can be explained by two effects. One might be a slight denaturation of the sample in the presence of d_6-DMSO, especially since this data were recorded with a sample which was used in the laser measurement and stored cool for a short time before the absorption spectrum was recorded. The other explanation is that the broadening is partly an artifact because of difficulties with the baseline correction due to the d_6-DMSO absorption (which can be seen at the edges of the spectrum, where the baseline is not similar to the other data). Overall it has to be stated, that the absorption spectrum of the mutant Ile341Aha in complex with AzuKQTSV is similar to the absorption spectrum of this PDZ mutant in complex with its native ligand and that no full unfolding or degradation can be observed on the FTIR spectrum. If this would be the case the center wavenumber would be expected at around 2119 cm^{-1}, the wavenumber corresponding to water-exposed azide groups.

9.3 Transient IR Spectroscopy

Of the described complex Ile341Aha with the ligand AzuKQTSV transient IR spectra under different conditions have been recorded. The experimental conditions were optimized to allow for artifact-free signal determination.

For those experiments a high intensity of pump light with 600 nm was needed to allow for signals to be possibly obtained. As described in the previous section using a excitation power of 5 μJ with samples of approx. 10 mM concentration in a 100 μm thick flow cell a signal size of about 0.05 mOD is expected, if heat transfer occurs through-bond (as for experiments in chapter 7 and 8). In case of the energy transfer pathway predicted for PDZ the heat transfer or intramolecular vibrational energy transfer would not be conducted only over covalent bonds, but as well through non-covalent contacts. The transfer efficiency for this type of heat transfer is not known experimentally and thus a much smaller signal must be anticipated. Therefore experiments with higher concentrations
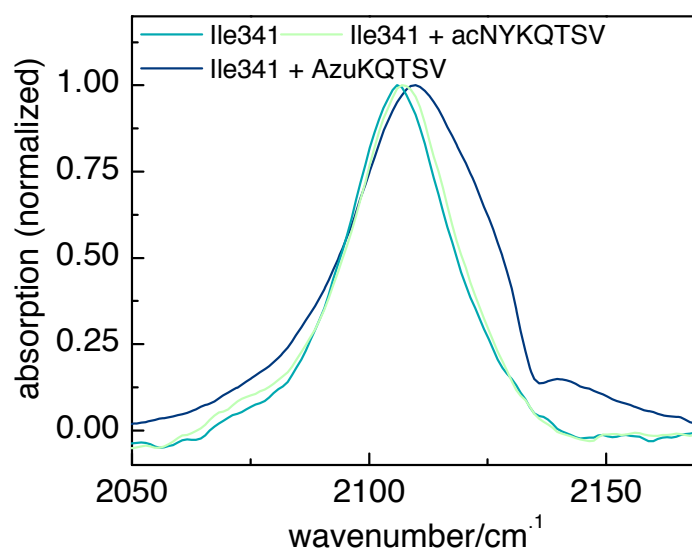
Figure 9.5: FTIR spectrum of the PDZ mutant Ile341Aha in complex with AzuKQTSV and 2 % DMSO. Data are recorded as described in Appendix B.

and/or higher excitation energy to allow for maximum signals are necessary.

9.3.1 Experimental Challenges

Samples had to be pump through a flow cell [296] to avoid re-excitation of the same complexes which contain chromophores not relaxed yet. The 600 nm pump light lead to huge artefacts recorded on the spectrometer. This happened only for the probe wavenumber of 4800 nm(2080 cm^{-1}) in combination with the protein sample. Due to the relatively huge absorption of the IR light in the solvent (phosphate buffer, H$_2$O) no filters were used in the IR probe light pathway between the sample position and the spectrometer. Unexpectedly scatters of the 600 nm pump light were recorded on the MCT detector array as huge artefact signals, because the 8th order of the 600 nm light in the spectrometer was diffracted along the same optical path at the first order signal for the 4800 nm to which the spectrometer was optimized. By placing a different filter, which does not decrease IR intensity but removes visible light in front of the spectrometer this problem was solved.

A different technical problem was denaturation and deposition of aggregated sample on the calcium fluoride windows upon heating of the sample through visible excitation leading to strong scattering effects. Using an excitation energy of 3 µJ it was possible to conduct the experiments without an increasing and strong background signal. But with higher pump light intensities as required for the experiment a huge artifact resulting from scattering of the pump light and deposition of denatured sample on the calcium fluoride windows was observed. In the last attempts to conduct these experiments this problem was solved by using a motorized computer-controlled micrometer screw (Newport Conex LTA-HS actuator with integrated controller) for constant moving of the sample cell in the pump focus. Thus spots of deposited sample by heating through the 600 nm pump light were avoided and it was possible to increase the excitation power to even 10 µJ allowing for possibly higher signal intensities.
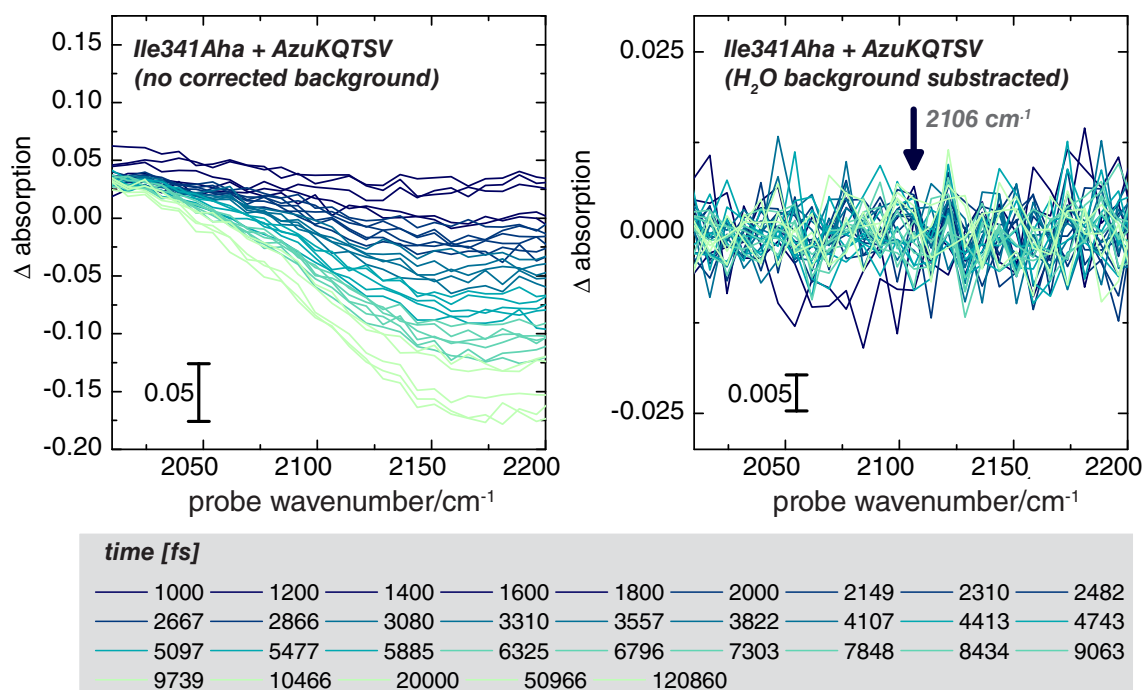
Figure 9.6: Transient IR spectra of PDZ Ile341Aha with the ligand AzuKQTSV. The left data are uncorrected, the right data are corrected by subtraction of the fit of a polynomial function of fifth order to the solvent heat background. The protein concentration was approx. 15 mM before a final centrifugation, peptide was added in the ratio 1:1. The OPA II was set to 600 nm and the pump power was adjusted to 10 µJ. The sample was pumped through the flowcell with a spacer thickness of 100 µm, data are recorded using the 150 line grating. The arrow indicates the wavenumber at which a signal of the azide is expected.

9.3.2 Results on Ile341Aha in Complex with AzuKQTSV

Oft the complex Ile341Aha with the ligand AzuKQTSV transient IR data have been recorded under optimized experimental conditions. All previously described improvements to avoid to the experimental difficulties and artefacts have been carried out. In figure 9.6 transient IR data of this complex in 1:1 stoichiometry between PDZ domain and azulene-containing peptide ligand are reported. Both were concentrated around 15 mM after a final centrifugation to remove aggregates, which might lead to scattering and high background noise. The data were recorded with an excitation energy of 10 µJ of the 600 nm light measured at the sample position. The center wavenumber for probing the IR signal was set to 4725 nm (2116 cm). The spectral window covers the range from 2000 to 2200 cm^{-1}, data were recorded on the 150 line grating. In the left panel in figure 9.6 data are shown without any correction for the long-time heat background, the right panel shows data after subtraction of a weighted background function. [3] A possible signal induced by vibrational energy transfer between the energy donating azulene chromophore and the energy accepting or monitoring azide moiety is expected at around 2100 to 2110 cm^{-1}. In the right panel of figure 9.6 no signal can be observed. As discussed previously the maximum possible signal intensity can be deduced from the results presented in chapter 8 on the di-peptide AzuAha. With the used

---

[3]A polynomial function of 5th order was fitted to the background at 120860 fs. It was subtracted from all other spectra scaled accordingly to set values on pixel 1 and 31 to zero.

parameters of approx. 15 mM protein/peptide concentration, a binding affinity which leads to about 90% bound ligand and an excitation energy of 10 μJ a maximum signal of about ± 0.16mOD is expected . The signal should arise at times of few picoseconds as based on the ATD simulations from [10]. This is about the same size as the background signal observed at 120 ps resulting from heating of the underlying combination band in H_2O . Thus a signal of this size should be possible to observe, however no signal is observed, even when the data are corrected for contributions from heated background. Technically the experiment worked well. This can be confirmed by the signal size of the water background at long waiting times. In the experiments on the di-peptide (see chapter 8, figure 8.12) in H_2O the background signal was about 0.2 mOD big for the sample with an concentration of the azulene chromophore of 25 mM and an excitation energy of 5 μJ at 600 nm. Assuming a linear correlation between signal size, concentration and excitation energy for the experimental conditions used here a background signal of about 0.24 mOD (0.2 mOD * 2 (for higher excitation)*0.6 (for lower concentration)) would be expected, the observed signal is about 0.2 mOD. This indicates, that the heat transfer from the azulene chromophore to the surrounding solvent is of similar size and efficiency. By this it can be stated, that the experimental conditions are similar to the experiments shown in chapter 8. Especially important is, that by this its proven, that the spatial overlap between pump and probe beam on the sample is ideal. For regular transient IR and 2D-IR experiments the overlap is adjusted by maximizing the signal size before a measurement (as done for experiments with the di-peptide) which was not possible for the experiments described in this chapter.

It has to be noted that signals around the size of approx. 0.01 mOD could have been observed in the experiments, this is the noise level as can be seen in figure 9.6 in the right panel. Every signal above this noise could have been extracted from the data using either the simple approach described above (subtraction of heat background) or in a more sophisticated way using global analysis. The data were analyzed by global analysis using a sequential model approach using a Matlab toolbox [367]. [4] However in the global analysis no component beside the expected solvent signals was found which might be assigned as azide signal. The only signals extricable are for very fast relaxation processes and the solvent heating.The results of the global analysis are not shown because no additional information could be extracted.

9.4 Discussion and Outlook

Currently from the sample side there is no way to improve the described experiment. Possible explanations why no signal was observed are not connected to experimental issues like weak or not ligand binding, artefacts from pump light, scattering, low concentrations, insufficient excitation energy or general failure of the experiment.

One remaining question is if the ligand is oriented in the binding pocket as suggested from the docking results. If the azulene is not in close proximity to the binding pocket or the ligand is bound in a different configuration, this could explain why no heat transfer was observed. To solve this question a collaboration with the group of Prof. Harald Schwalbe is underway to investigate the ligand orientation using NMR spectroscopy.

Another more fundamental explanation for the absence of a signal is, that vibrational energy transfer over non-covalent contacts, such as between the peptide ligand and the PDZ domain and through the protein, is to weak to be observed. From theory it is predicted, that energy transfer pathways in protein exists and the assumption that those can be monitored by local temperature

---

[4]The analysis was performed by my colleague Luuk J.G.W. van Wilderen.

changes or energy transfer between vibrational modes [85, 147, 148, 152, 155, 156, 204, 206, 339, 340, 341, 342] is made. But if and how vibrational energy is transported over H-bonds or van-der-Waals-contacts is not understood. Even the transport mechanism for vibrational energy transfer along covalent molecular chains [144, 149, 357, 368, 369, 370] is not exactly understood yet. The reason for the difference in heat transport between the demonstrated experiment and theoretical predictions as by Ota and Agard [10] might well be, that those simulations do not take into account the surrounding solvent as energy acceptor. Additionally the heat transfer efficiency over non-covalent contacts might be much weaker than for transfer through covalent bonds. Furthermore the ATD simulation showed the anisotropic heat transfer through the PDZ3 domain along the predicted amino acid network but was carried out without accounting for an influence of ligand binding.

The described experiment was designed to directly address the question if an energy transfer pathway in the PDZ domain exists. To better understand the physical mechanism of vibrational energy transfer in molecules over non-covalent bonds, a simplified model system needs to be investigated. For this we choose a polypeptide comprised of three β-strands which form an antiparallel β-sheet and incorporated azulene and Aha at different positions to compare energy transfer (speed, efficiency and more) over covalent vs. non-covalent bonds in a similar type of experiment as described above. [5] This is an important prerequisite for the accurate interpretation of the results presented in this chapter. If the energy transfer efficiency through non-covalent contact would be a factor 100 or 1000 smaller than for energy transfer through covalent bonds, this would easily explain why we did not observe any signal in the presented data.

The presented results are thus an important step towards the experimental real-time investigation of vibrational energy flow in proteins and continuative studies will add to a deeper physical understanding of long-range communication and allostery.

---

[5]This is research in progress in collaboration with the group of Prof. Nediljko Budisa and experiments are carried out mainly by Martin Essig for his master thesis [371].

Conclusion and Future Directions

The aim of this thesis was to demonstrate how UAAs carrying azide or nitrile groups in their side chain can be employed as novel vibrational probes for ultrafast 2D-IR spectroscopy of proteins, thereby creating a unique approach of combining labeling strategies from chemical biology with ultrafast laser experiments to study protein dynamics. The expectation was that site-specific probes enable types of experiments otherwise not possible, leading to new insights into protein function. The presented results demonstrate the enormous application potential of novel vibrational probes in ultrafast 2D-IR spectroscopy to the study of protein biophysics.

Novel vibrational probes sparked great interested in the whole FTIR and 2D-IR community. Thus a huge body of work has been published during the last years on characterizing and testing diverse probes for usage in proteins and nucleotides (reviewed e.g. in [75, 76, 314]). Research focused on $C-D$ vibrations [108, 251, 252, 253, 254], nitriles [263, 271, 281, 322, 372], azides [82, 139, 274, 276, 279, 289, 290, 373, 374, 375], thiocyanate [258, 260, 376] or metal-carbonyls [137, 138, 257].

In this thesis several UAAs, all with azide or nitrile groups as the vibrational reporter, have been evaluated towards their application potential as novel vibrational probes. The vibrational probes studied are all incorporated using methods from chemical biology and thus can be placed site-specifically while at the same time allowing for a pure sample with high labeling yield. The most favorable candidate was then used in studies of conformational dynamics and energy flow in the PDZ3 domain.

The results for the free amino acids (presented in Chapter 4) lead to the conclusion that the unnatural amino acid azidohomoalanine (Aha) is the most favorable of the tested candidates. This is due to a combination of several different characteristics and the aim for a most versatile probe. Aha has a high oscillator strength, a clear line shape which is crucial for spectral diffusion analysis and a vibrational life-time that allows measurement of few picosecond dynamics. Aha can be used both in H_2O and D_2O because its absorption band positioned in a way that background correction is straight forward. The incorporation of Aha as a methionine analog makes the sample preparation simple.

However the application of Aha as a local probe also has limitations. Foremost the lifetime of the azide vibration is not long enough to observe dynamics after about 10 ps, since the signal is decayed. Additionally the incorporation via the SPI approach results in all methionine codons being translated into Aha. This means only proteins without any natively present methionine are ideal candidates for 2D-IR studies using Aha as label or a methionine-free mutant needs to be designed. Other UAAs, like CNA or N3P from this thesis, are in principle much more versatile with respect to wide applications in all types of proteins, because they are incorporated via genetic code expansion and thus using a specific non-canonical codon. However as discussed in great detail in Chapter 4, those probes have other limitations either in terms of signal strength or line shape properties.

Allostery in PDZ

The experimental investigation of six mutants of the PDZ3 domain by FTIR spectroscopy (see Chapter 5) already gave strong hints towards the existence of the proposed coupled network of amino acid residues. The results presented are the first experimentally derived results, which support the transfer pathway suggested by Ota and Agard [10] and detect small conformational changes which have not been reported by NMR or X-Ray crystallography studies before. The subsequent 2D-IR investigation of conformational dynamics (see Chapter 6) in two of the six mutants showed how novel vibrational probes can be used to access picosecond dynamics. It was monitored that the binding groove is very rigid and not changing its conformation upon ligand binding, whereas the other mutant shows conformational fluctuations within few picoseconds. However the experiments to probe the existence of an energy transfer pathway in PDZ3 directly with real-time resolution as laid out in Chapter 9 have so far not been successful. Thus there remain many additional experiments to eventually prove the concept of long-range communication and dynamic allostery in PDZ3.

Other Incorporation Sites for Probes in PDZ3. The presently studied mutants were chosen not only because of their position on or off the pathway but as well to demonstrate the power of site-specific probes for the study of local environment and ligand binding. Given the results, that the three mutants, which are part of the proposed network show subtle conformational changes reflected by the shift of the azide absorption band upon ligand binding, more experiments to map out the proposed allosteric communication seem promising.

The current incorporation positions were chosen based on the results from the ATD simulation by Ota and Agard [10], which predicted different residues than the analysis based on thermodynamic coupling of residues presented by Ranganathan and Lockless [9]. The two predictions only agree about the start at His372 and the end of the transfer pathway on the opposite protein surface at Leu353 and Ala347 but show different residues as involved in the pathway in between (see Figure 2.5 and Figure 5.2). Most notably Ota and Agard [10] predict a more direct pathway from the binding groove through the β-sheets of the protein interior and not as Ranganathan and Lockless [9] first along the α_1-helix which forms part of the binding groove. In principle all residues listed in Figure 5.2 not yet tested as incorporation sites for Aha should be tested. The residue Phe325 is predicted by both theoretical approaches as important side chain for the transfer pathway. However this amino acid side chain will be difficult to replace by Aha without influencing the structural and functional integrity of the PDZ3 domain. To study whether at this position a small conformational change upon ligand binding, similar as observed for Leu353 and Ile341, occurs another UAA with aromatic side chain is needed. This could be N3P, which should preserve the protein structure and function, however the Fermi Resonance (see Chapter 4) will obstruct detailed line shape analysis and might hinder the monitoring of the small conformational change expected. The other residues to be replaced by Aha are either glycine side chains (G322, G329, G330, predicted by [9]) or other aliphatic amino acids (Ala347, Val362, Val386) with the exception of Lys380, which should be as well replaceable by Aha. Testing all those incorporation sites for conformational changes upon ligand binding in similar experiments as discussed in Chapter 5 will help to discriminate whether the predictions by Ranganathan and Lockless [9] or Ota and Agard [10] are more accurate to describe allostery in PDZ3. These experiments will add more details to the currently controversy [9, 197] discussed issue of long-range allosteric communication. In addition to these incorporation positions at least three to five other positions should be tested for strengthening the claim that Aha is indeed a useful monitor for subtle local changes.

Beside the conserved energy transfer pathway [9, 10] an additional allosteric effect involving α_3 had been reported specifically for PDZ3 by NMR spectroscopy [188]. Thus far only one of the six incorporation sites (Ser398) is located in this small α-helix which is unique for PDZ3 from PSD-95. The literature [187, 188, 199, 207] discusses a larger binding interface than only the groove between β_2 and α_1 as derived from the original crystal structure (see Figure 2.4, [203]), however the data do not report the specific interaction sites but rather discuss the lack of bonds despite the proven allosteric effect [188], whereas later NMR experiments show interactions outside the binding groove [207]. During the molecular docking experiments for designing an optimized peptide ligand (see Chapter 9 and [362]) we as well found preliminary evidence for non-covalent contacts between the N-terminal residue (-6 position, Figure 5.1a) of the heptameric CRIPT peptide and residues Tyr397 and Phe400 in α_3. Those are promising positions for either the incorporation of Aha to monitor the long-range interaction or maybe the incorporation of N3P as this UAA is structurally more related to the two aromatic residues which would be replaced. Even though N3P has the disturbed line shape by a Fermi Resonance this residue should be usable for the purpose of mapping the influence of non-covalent interactions on the local microenvironment. [82, 83] Additionally mapping the interaction surface using a larger peptide ligand (as done by [207]) would yield more detailed insights into the binding mechanism and specificity of PDZ3.

Direct Tracking of Vibrational Energy Flow in PDZ3. Current experiments to directly monitor vibrational energy flow in the PDZ3 domain in complex with an optimized peptide ligand containing azulene as VET donor have thus far not been successful to probe the predicted energy transfer pathway. Further experiments using e.g. a different peptide ligand, which puts the azulene in closer proximity to the starting point of the energy transfer pathway at His372 need to be conducted. The ideal experiment however to study also the biological relevance of the predicted VET pathway is on a double mutant of PDZ3 with azulene and Aha both incorporated into the protein. To conduct this experiment progress for the incorporation of AzuA with high expression yield using the SPS approach is needed. On this type of sample it would be possible to study the influence of the ligands presence or absence on the energy transfer. However an important prerequisite for this experiment is a deeper understanding of the transfer mechanism, e.g. supported by simulations matching the experimental conditions used in the reported experiments. As currently no signal from the azide moiety was observed but a strong heat signal of the H_2O combination band could be detected, the experiment worked out experimentally. Reasons for the lack of signal are discussed in Chapter 9, before the same experiments are repeated, more insight into the energy transfer efficiency through non-covalent bonds (see below) is needed and ways to enhance signal sensitivity need to be explored. Another possible approach would be following the energy flow using different probes and e.g. different positions. For example ruthenium carbonyl as probe (as proposed by King et al. [137] is attached to a protein on a histidine side chain. Incorporation of azulene as donor on the distant protein surface and monitoring energy transfer in the reverse direction using this much stronger but less native reporter group might allow to "see through" the non-covalent contacts.

Simultaneous Incorporation of two Probes and extended Application of 2C-2D-IR. To study conformational dynamics in greater detail than possible using one localized reporter group it might be useful to introduce two independent reporter groups into one protein. The simultaneous incorporation of two UAAs is currently a field of major research in protein engineering as discussed previously (see Chapter 3 and Chapter 9).Thus to demonstrate the benefit of two local probes in a protein, such as PDZ, it will be initially more feasible to combine two labeling approaches, like the

genetic encoding for Aha with the chemical conversion of a cysteine residue into a thiocyanate [258, 260, 265]. With two groups site-specifically place in a protein of interest 2C-2D-IR experiments will be possible to study cross peaks between the two unnatural oscillators. Those can yield information about relative orientation of side chains to each other and their time-dependent fluctuations. Using a polarization dependent measurement scheme also angles and the relative structure could be probed similar as demonstrated for a small organic system in [99]. A first question, which can be addressed by this kind of experiment is the study of the relative movement of the structural elements comprising the peptide binding groove in PDZ3. As Steiner and Caflisch showed in a MD simulation [208] in PDZ3 conformational selection might be a possible mechanism for peptide binding. The predicted scissor motion between β_2 and α_1 is difficult to address experimentally and might be possible to observe using two site-specific probes.

Energy Flow in Proteins and further Application of VET Pair

To directly track directional energy flow between two distant sites in a protein a novel VET pair was introduced and tested in Chapter 8. This VET pair comprised of azulene as donor and Aha as acceptor [112] and was originally intended for experiments in PDZ3. It can be also used generally to study IVR/VET in greater detail as well as monitor VET pathways in more complex systems than demonstrated before [109, 152].

Studies of IVR/VET Mechanism. In Chapter 8 briefly the possibility to gain insight into the general mechanism of IVR or VET by using the proposed donor-acceptor pair is introduced. One effect that was already reported in Figure 8.13 is the difference in transfer kinetics. The results on the dipeptide comprised of AzuA and Aha suggested a huge difference e.g. due to solvent polarity, solvent dynamics or hydrogen bonding effects. Thus far only the influence of DMSO or H_2O on the transfer efficiency has been monitored but further experiments on this di-peptide in different solvents may lead to detailed insight into the influence of solvent effects (like collision dynamics) on VET. Another phenomenon already mentioned in Chapter 8, which can be studied in more detail is the mechanistic nature of the intramolecular IVR/VET process itself. This is already subject to detailed studies e.g. by the Rubtsov [144, 357] and Dlott [77, 368] groups. Studies using our VET pair might add to the known principles. Already from results reported in Figure 8.10 it can be seen that the size of the studied system influences the relaxation and transfer of heat from the azulene chromophore through the molecule as monitored by its vibrational ring modes. In the small system AzuCa only very few vibrational modes with less delocalization are present as the system has much less degrees of freedom. Thus the ring mode shows a longer lived signal, whereas in the model peptide AzuP many more degrees of freedom, thus also more and highly delocalized vibrational modes are present, leading to a shorter life time per signal for the single vibration. Whether this very simple analysis holds true in differently complex systems as well as for IVR both in a ballistic and a diffusive transport regime needs to be understood by a close link between experiment and theory. The VET donor-acceptor pair is in this respect an ideal tool to gain more mechanistic understanding of vibrational energy transfer processes.

VET through non-covalent bonds using the WW Domain as Model System. One probable reason why no signal of energy flow from the azulene to the azide moiety in the PDZ protein-ligand complex studied in Chapter 9 was observed is that the proposed pathway involves non-covalent bonds. In contrast the through-bond transfer is very efficient has in all studied systems in this thesis

(see Chapter 7 and Chapter 8) yielded strong enough signals to be detected with concentrations, that were matched in the final experiments on the protein-ligand complex. One might expected that energy flow through non-covalent contacts and hydrogen bonds is less efficient and other relaxation pathways for the energy might be preferred. In contrast for PDZ3 the simulations by Ota and Agard [10] instead propose a very specific anisotropic transfer pathway involving non-covalent contacts. To study the mechanism and efficiency of VET (or heat transfer) along non-covalent bonds in comparison with covalent bonds and additionally whether a similar distance dependency for transfer through non-covalent bonds than for transfer through covalent bonds might be found an pure β-sheet peptide would be ideal. One very well studied protein domain comprised of three anti-parallel β-strands is the WW domain [377, 378], which is small enough to be fully synthesized. In collaboration with the group of Nediljko Budisa it is aimed to use this domain as a model system and designed different mutant pairs for the incorporation of the VET pair, either in opposite β-strands, connected only by non-covalent bonds or in similar distance in the same strand, connected by covalent bonds. This is work in progress, discussed in greater detail in the Master thesis of Martin Essig [371], which was supervised by the author.

VET Pathways in other Proteins. The assumption that VET pathways with importance for intermolecular long-range communication and allostery exist, was not only made for the PDZ domain but generally made for several proteins [147, 148, 155, 156, 160, 161, 178, 341, 359]. Even the claim, that allosteric long-range pathways, which might involve VET are an intrinsic property of proteins was made. The presented VET pair is a generalized way to investigate transfer pathways in all kind of different proteins. Thus far only vibrational energy flow in heme proteins has been tested experimentally using Raman spectroscopy [348, 349]. This is possible due to the presence of a natively occurring chromophore (the heme group) to inject heat for the direct tracking of energy flow. In case of all other proteins for which VET pathways and anisotropic energy flow have been suggested (among those are fluorescent and photoactive proteins such as GFP or PYP [160, 161] but as well other protein domains such as SH3 [379]) only an approach as the usage of our VET pair will allow for experimental investigation [204]. In principle the technique can be extended for the study of energy flow in all these different proteins. But first efforts towards introduction of only Aha as local probe into the blue-light receptor PYP have been proven to be very difficult [380]. This shows that even though the VET pair was designed for a very general usage, its application currently is limited by the molecular biology and sample preparation.

Further Applications of Novel Vibrational Probes

The usage of novel vibrational probes for studies of site-specific dynamics different from the reported application to PDZ3 in Chapter 5 and Chapter 6 is promising. Some examples of other biophysical question to be studied have been reported in the literature, e.g. the study of GPCR conformational changes using N3P as local reporter group by Ye et al. [82, 83]. In general the combination of ultrafast 2D-IR spectroscopy or FTIR spectroscopy with site-specific reporter groups will enable completely novel experiments. Some of the biophysical question possible to be address are mentioned in the following paragraphs.

Monitoring of Structure, Function and Folding. Unnatural amino acids as site-specific probes can be used to study structural dynamics in ultimately all kind of proteins. Especially interesting are those, which have ultrafast dynamics not accessible for NMR or X-Ray crystallography or in

which changes are expected but to small to be observed with other techniques. Those could for example include intrinsically disordered proteins or photo receptors. Current work in our group based partly on results of this thesis is dedicated to the study of structural dynamics upon photo chemistry in PYP [380]. Expectation is, that using Aha as probe close to the binding site of the chromophore details about the modulation of the speed of the photo cycle by different mutations in the active side can be measured in transient 2D-IR experiments. One other possible application of local probes is the study of of protein folding and unfolding events with side-chain resolution in similar fashion as introduced by the Tokmakoff group [117, 125], which employ a different scheme of transient 2D-IR using a temperature jump as trigger to start a non-equilibrium process. Using UAAs in a similar experimental scheme might lead to more insights into the cooperative nature of protein folding, potentially with pharmaceutical or medical relevance, similar as in experiments reported in [288, 381].

Probing of Local Microenvironment, Hydrophobicity and Electrostatics. Site-specific vibrational probes are not only useful to study conformational changes, but as reported and deeply investigated by the Boxer group [84, 140, 258, 283, 285, 382, 383] oscillators such as nitrile groups or thiocyanates can be used to quantitatively measure the electrostatics in a protein at position of interest. Only oscillators whose absorption frequency is linear correlated with the electric field of the surrounding environment (e.g. by the solvent) can be used for Stark effect based experiments. This holds true for nitrile, thiocyanate or carbonyl groups, but not for azides [275, 276]. Combining the approach of Stark Spectroscopy with 2D-IR on a protein which has a suitable label incorporated like a cysteine converted to a thiocyanate [260, 265] or e.g. CNP [79, 140] should allow for the measurement of time-dependent changes in the local electrostatics in a protein. This is for example interesting in the investigation of catalytic processes in the active site of an enzyme. For the steady-state case investigated by FTIR comparable experiments have been reported on the ketosteroid-isomerase [264]. Using time-resolved IR or 2D-IR spectroscopy would enable the a detailed mechanistic understanding and insight into ultrafast dynamics of biochemical catalysis.

Overall in this thesis the foundations for using UAAs as site-specific probes in FTIR and ultrafast 2D-IR spectroscopy have been developed. As only briefly discussed in this conclusion a huge variety of experiments and applications to all different kinds of biophysical problems can be undertaken based on the presented work.

Part V

Appendix

A Ultrafast Experiments

In this chapter the experimental setup and its different possible configurations are described briefly. A more detailed description of the components in the setup as well as the underlaying theory of nonlinear optics is given in the authors diploma thesis, which covered the first OPA and NOPA in great detail and the 2D-IR setup in brief [270]. Another very detailed description of the used setup is given in the PhD thesis of Andreas Messmer [141].

A.1 Overview of the Experimental Setup

An amplified Ti:sapphire laser system (Spitfire Pro XP, Spectra-Physics), which generates pulses with a wavelength of 800 nm, 1 kHz repetition rate, 3 W output power and a pulse duration of 90 fs, was used to pump two home-built optical parametric amplifiers (OPAs). Both OPAs are constructed as reported previously [134, 141, 270].

Signal and idler of each OPA were mixed in an $AgGaS_2$ crystal to generate mid-IR pulses by difference frequency generation (DFG).[134] The main difference between both OPAs is that one is pumped with similar energies (approx. 380 µJ) as previously described whereas the second OPA is pumped with a higher initial energy (approx. 1.7 mJ) and contains a larger BBO crystal to generate higher IR power, the $AgGaS_2$ crystal is thinner to prevent spectral narrowing. To avoid optical damage this crystal is placed not in the focus but before the IR focus (BBO: 10 mm x 10 mm x 4 mm, $AgGaS_2$ 5 mm x 5 mm x 0.5 mm).
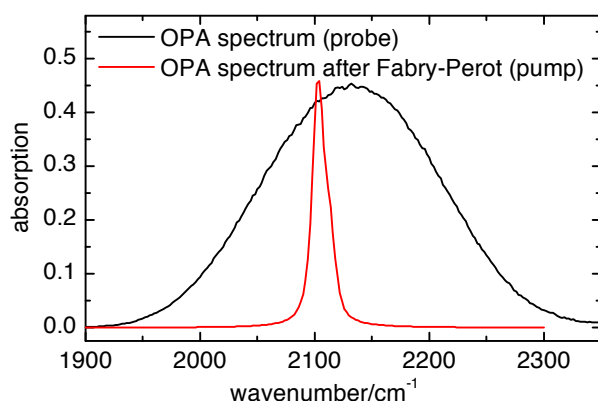
Figure A.1: A typical spectrum of the OPA I probe light and a corresponding pump pulse narrowed by the Fabry-Perot. The width of the OPA spectrum is 180 cm^{-1}, the width of the pump spectrum is 14 cm^{-1}.

Energies from OPA I varied between 1.5 to 3 µJ, energies from OPA II were up to 12 to 15 µJ depending on the center wavenumber. For later experiments OPA II was extended for generating 600 nm light to pump azulene (see below). The high-power configuration was only used for the 2C-2D-IR experiments reported in Chapter 4, all other 2D-IR spectra are measured using OPA I both for generating the pump and the probe.

Probe and reference pulses were obtained by splitting off a few percent of the mid-IR output of the first OPA by reflection from a BaF_2 wedge. Both probe and reference pulses were directed through the sample. The focused probe beam had a diameter of $\approx 80\,\mu m$ (FWHM) at the sample position. Narrow-band pump pulses (bandwidth given in the figure captions of the respective experimental results) were generated by sending the mid-IR output of the first or second OPA (depending on the experiment) through a computer-controlled Fabry-Perot interferometer [42] with using optimal mirrors for the FP for the respective wavelength range.

The beam was then focused into the sample with a focal diameter of $\approx 130\,\mu m$ (FWHM). The narrow band pump pulse was overlapped temporally and spatially with the broad-band probe pulse at the sample location. The reference pulse passed through the sample at a location spatially separated from the pump pulse. The time delay between the pump and probe pulses was altered using a computer-controlled delay stage (Physik-Instrumente, M-415.PD). Pump-probe spectra were recorded as function of the time delay using an imaging spectrometer (Horiba scientific, TRIAX 180) with a 32-pixel nitrogen-cooled HgCdTe detector array (Infrared Associates).

Visible Light Generation. The pump light for excitation of the S_0 to S_1 transition of azulene at 600 nm, as can be seen in Figure 8.4 was generated by frequency doubling of the signal light from the second amplification step in OPA II. The signal covers a range from 1200 to 1800 nm, tunable by adjustment of the time delays and the crystal orientation of the BBO in the general OPA part. The signal and idler are sent through a BBO crystal with phase matching conditions suitable to double s polarized light, what is only true for the signal and not the idler. The BBO was type I with a size of 6 mm x 6 mm x 0.5 mm with cut angles of $\Phi = 90\,° \Theta = 26.4\,°$. In this configuration pulses with approx. 590 to 620 nm could be generated. For shorter wavelength (approx. 590 to 600 nm) only intensities of a few μJ were achieved with 280 μJ power (signal and idler) from the 2nd stage of OPA 2.
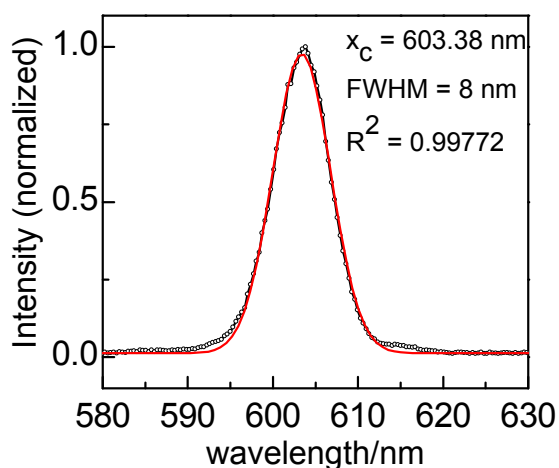
Figure A.2: A typical spectrum for the orange 600 nm light resulting from doubling the signal out of OPA 2. The center wavenumber of this spectrum is approx. 603 nm, the spectral width 8 nm. The intensity was measured with 18 μJ

The conversion processes was highly efficient for the wavelength range just above 600 nm, with typical intensities of 15 to 20 μJ purely for the doubled signal (measured after the light passed through a band pass filter for 600 nm $\pm$ 40 nm and guided along a mirror with low reflectivity for rests of signal and idler light).

Visible pump pulses were attenuated to energies of about 5 μJ at sample position, center wavelength $=$ 600 nm and a pulse length 400 fs as the pulses where stretched by guiding them through fused silica rods. The beam was focused into the sample with a focal diameter of $\approx 120\,\mu m$ (FWHM). The visible pump pulse was overlapped temporally and spatially with the broad-band probe pulse

at the sample location. The relative polarization of the pump and probe pulse was set to the magic angle.

A.2 Different Experiments performed in this Thesis

In this thesis different types of experiments have been performed. As experimental conditions are summarized in the figure captions of the respective results only a general overview is given here.

The types of experiments performed are the following:

Broadband IR Pump IR Probe Measurements.
Of the UAAs CNP, N3P and N3A broad band IR pump IR probe data were recorded using the OPA II (N3P) or OPA I (CNP, N3A) as pump with full spectral width and full power. The data were recorded with full achievable time resolution around 100 fs, which is determined by the cross-correlation between pump and probe pulse.

2D-IR and 2C-2D-IR spectra using two independent OPAs.
2C-2D-IR spectra were measured of the UAAs CNP, N3P and N3A in THF and Aha in H_2O with the pump pulse centered on the azide or nitrile absorption (N3P, N3A, Aha center wavenumber 2115 cm^{-1}, CNP center wavenumber 2225 cm^{-1}). The light for the pump pulse was generated using OPA II with energies in the range around 12 to 15 µJ before the Fabry-Perot. Different sets of semi-transparent mirrors have been used in the azide or nitrile region. Experiments were performed with parallel and perpendicular polarisation of pump and probe beam for the compounds CNP and N3P. For the compound N3A the relative polarisation was only parallel. All spectra shown in the thesis show data for parallel polarisation.

The center wavenumber of the OPA I, generating the probe pulses was adjusted to cover different spectral regions and to access spectrally separated vibrational modes (carbonyl modes (center wavenumber 1722 cm^{-1}), ring modes (center wavenumber 1602 cm^{-1}), and the amide II region (center wavenumber 1522 cm^{-1}). Samples were prepared with 50 mM concentration in THF and measured in a CaF_2 cell with an optical path length of 125 µm, all values are given in the figure caption of the respective results.

2D-IR spectra using OPA I.
Of Aha in H_2O and the PDZ mutants Ala390Aha and Ile327Aha (without ligand and in complex with acNYKQTSV) 2D-IR spectra in the azide region (center wavenumber = 2115 cm^{-1}) have been recorded. For all those experiments the OPA I has been used both for generating pump and probe light. In all those experiments the polarisation between the pump and probe pulse was set to parallel polarisation. All data have been recorded with the 150 line grating.

Transient IR Spectra with 600 nm Pump.
For the two test compounds AzuCa and AzuA time-resolved IR spectra with a fixed pump wavelength of 600 nm were recorded in THF, the spectral region between 1200 cm^{-1} to 1850 cm^{-1} was covered, only between 1438 - 1486 cm^{-1} no data were recorded due to high solvent absorption.

The model peptide Azu-Tyr-Asn-Aha-Gly (AzuP) was studied in d_6-DMSO due to solubility difficulties in THF. For comparison the monomeric test compound AzuCa was measured in d_6-DMSO

as well, since the peptide was synthesized using the carboxy derivate of the Azulenyl-Alanine. The center wavenumber of the probe pulses was adjusted to cover different spectral regions and to access spectrally separated vibrational modes between 1200 cm^{-1} and 2150 cm^{-1}.

The experiments of the dipeptide AzuAha were performed both in d$_6$-DMSO and H$_2$O. Here only data in the window with center wavenumber of 2150 cm^{-1} were recorded. Samples were prepared with approx. 10 mM concentration for the peptide, 25 mM for AzuCa and ac-AzuA in THF, 30 mM for AzuCa in d$_6$-DMSO and 25 mM for AzuAha both in d-$_6$-DMSO and H$_2$O. Data were recorded in a flow-cell with CaF$_2$ windows, a continuous sample flow and an optical path length of 250 µm for AzuCa and ac-AzuA in THF as well as for AzuP in d$_6$-DMSO. The azide and glycine spectral window in AzuP was collected with a 100 µm spacer due to larger solvent absorption, as where the measurements of AzuCa in d$_6$-DMSO.

The final experiments were of the PDZ mutant Ile341Aha in complex with the azulene-labelled peptide AzuKQTSV. The technical challenges of these experiments as well as all the conditions are described in full detail in Chapter 9.

B Protein Sample Preparation and Characterization

B.1 PDZ Expression and Purification Protocol

The third PDZ Domain from PSD-95 (sequence from *Rattus norvegicus*) was expressed in *E.coli* using the vector pGDR11. A construct encoding for residues 303-402 (numbering similar as in [203]) with an N-terminal His-Tag followed by a TEV-cleavage side before the amino acid sequence of interest was used (bought from *MrGene*)[1]. This construct encoding the PDZ mutant was designed to remove the start codon during purification to leave only one side with azidohomoalanine per mutant. Six different point mutations were introduced using the *Site-Directed Mutagenesis* kit by *GeneArt*. The mutants were designed to cover diverse positions in the structure, including the water exposed surface of the protein, the hydrophobic binding pocket as well as positions for Aha in α-helices and β-strands. Two positions were chosen in the binding pocket to investigate ligand binding effects.

The large-scale expression and purification was carried out by Sabrina Oesteritz. The protein was expressed in *E.coli* B834 (methionine-auxotrophic) using M9 minimal medium (1.4 l M9 salt (5x), 28 g glucose, 14 ml 1 M $MgSO_4$, 700 µl $CaCl_2$, 1.4 ml trace elements, 70 mg thiamine, 70 mg biotine, 700 mg ampicillin for 7 liters). Azidohomoalanine (Iris-Biotech) was supplemented at 50 mM final concentration in the main culture used during induction of expression with IPTG and time of over expression following a modified protocol from those described in [218] and [220]. The cell lysate was purified using a Ni-NTA affinity column. Then the purified protein was digested with TEV protease to cut off the N-terminal residues of the expressed construct, that contain the His-tag as well as the residue encoded for by the start codon. This normally is a methionine that as well is replaced by Aha. Thus the cleavage is necessary to prevent presence of two azide groups in the final protein. The digested solution was purified further by a reversed affinity column. Protein concentration for all samples was determined using a Lowry assay.

B.2 Protein Sample Characterization

All samples were controlled for purity and labeling yield by SDS-PAGE and MALDI. An example for the SDS-PAGE can be found in Figure B.1. To verify non-invasive mutations before using the respective sample in any experiments, the secondary structure of purified Aha- labeled PDZ3 (after the labeling efficiency was quantified by MALDI) was compared to the wild type structure using CD spectroscopy (see Figure B.3). Furthermore the mutants were tested for their functionality by ITC binding studies. The results are reported in Table 5.2; examples for the ITC results are shown in Figure B.3. The whole set of biophysical characterization data for the six mutants is described in the Bachelor Thesis of Katharina Eberl [299], which was supervised by the author.

---

[1] The cloning was done by Silvia Eger, Uni Konstanz.
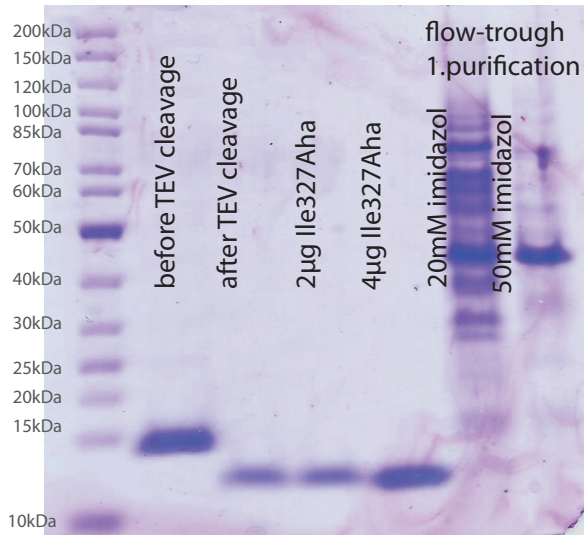
Figure B.1: Example of an SDS-PAGE showing the different purification stages of a PDZ expression. Shown are results for the mutant Ile327Aha. Column order is the following: (1) Marker, (2) PDZ3-Aha construct after first affinity chromatography, before TEV cleavage, (3) raw PDZ3-Aha construct after TEV cleavage over night (4) and (5) differently concentrated purified PDZ3 after reverse affinity column, (6) and (7) flow-through of first affinity column for different imidazol levels.
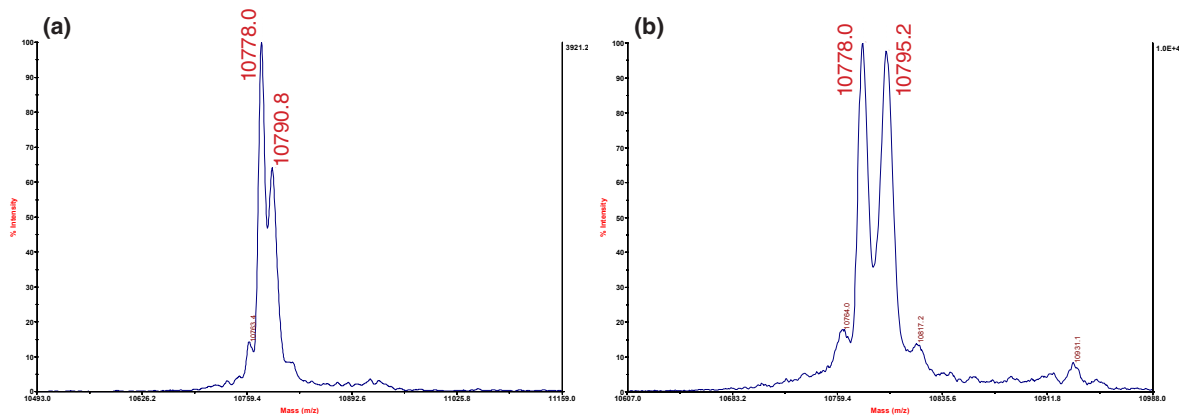
Figure B.2: MALDI for the mutant Ile327Aha with PDZ wild type as internal standard. The molecular weight for the WT is 10.777 kDa, for the 100 % labeled PDZ-Ile327Aha is should be 10.790 kDa, the methionine variant has a 5 Da higher weight. The left MALDI spectrum shows a expression where the incorporation failed and methionine got incorporated at the position of the AUG codon. The right MALDI spectrum shows an example for the achieved labeling quality with a high yield (about 100 %) of azidohomoalanine incorporated for the AUG codon.

PDZ mutant	with methionine MW [kDa]	with Aha MW [kDa]
Wild type	10.777	
Ile327	10.795	10.790
Ile341	10.795	10.790
Ser398	10.821	10.816
Ala376	10.837	10.832
Leu353	10.795	10.790
Ala390	10.837	10.832

Table B.1: Molecular weight for all mutants of PDZ3 with either methionine (no successful introduction) or Aha incorporated. Weights are calculated from the sequence using the ProtParam tool on ExPASy.

MALDI. All samples were controlled by MALDI after complete protein expression, purification and digestion by TEV protease to find out the labeling quality with Aha. The molecular weights for all mutants and the wild type PDZ sequence, both with methionine (in case there was no incorporation of Aha) and Aha are listed in Table B.1. To verify a molecular weight difference of 5 Da for approx. 11 kDa protein, all data are calibrated with the wild type protein as internal standard. We show here representative specta for Ile327Aha and Ala 376Aha, both show a clear labeling with Aha that can is estimated to be ca. 90 %. Molecular weights for mutants were calculated using the ProtParam tool on ExPASy server. Labeling efficiencies were estimated comparing the calculated mass difference for the wild-type and the measured mutant (see table) to the measured mass difference. With a small theoretical mass difference of only 5 Da for the exchange of methionine to azidohomoalanine high precision MALDI with internal calibration was used. The bands for labeled and unlabeled protein are overlapping, but as can be seen in Figure B.2 very accurately corresponding mass values for the unlabeled and labeled case were obtained. If the obtained shift was not exactly as calculated, but in between numbers for labeled and unlabeled protein the ratio was calculated and taken as estimate for labeling efficiency (e.g. a mass with difference 2.5 was measured instead of 5, meaning a labeling efficiency of only 50 % was reached).

CD Spectroscopy. CD spectra were measured with a J-720 spectropolarimeter by Jasco. Data were accumulated in the range from 260 nm to 178 nm with a scanning speed of 200 nm/min. The number of scans was 32. Protein concentrations varied between 1.5 to 2.3 mg/ml, depending on the original sample. Samples were prepared in phosphate buffer (see rest of experimental section) and measured in a measurement cell with CaF2 windows and a spacer thickness of 50µm. As can be seen in Figure B.3 all mutants show a similar secondary structure as can be deduced from the highly overlapping spectra (wild type is shown for comparison). However due to the phosphate buffer data in the region below 195 nm are hard to interpret and disturbed (see [384] for further information).

ITC Measurements. ITC measurements were performed using a VP-ITC microcalorimeter. Samples were prepared from 75–200 µl of frozen protein stock diluted with 50 mM sodium phosphate buffer, pH 6.8 to a final volume of 2 ml and a corresponding concentration of approx. 0.1–0.12 mg/ml. Before injection into the sample chamber, all protein solutions were centrifuged in a micro concentrator (Vivaspin, 5 kDa cut-off) and degassed for 15 min. The final volume was adjusted to 2.2 ml after preparation, corresponding to a final concentration of approx. 0.2 mM. For the analysis the stoichiometry of the binding reaction was set to n=1. As a ligand acNYKQTSV was used in a
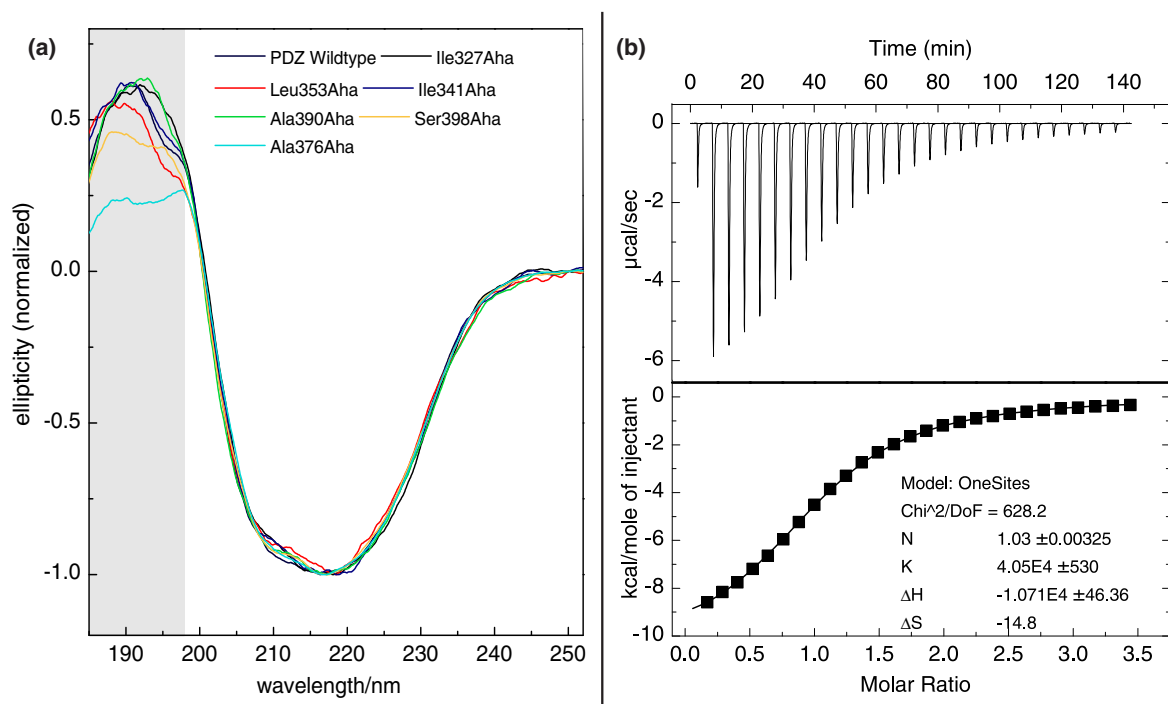
Figure B.3: a) CD spectra of the PDZ mutants investigated in this thesis and the wild type. b) example of ITC results for Ile327Aha. Binding kinetics studied for the native ligand ac- NYKQTSV; comparable results with Sato et al. [320] and Petit et al. [188]; CD spectra for all studied mutants with WT for comparison. Data are normalized to better visualize the similarity, samples were prepared in 50 mM Na_2HPO_4 buffer with pH 6.8. Perturbations in the spectrum below 200 nm are caused by the phosphate buffer [384]. The corresponding High Voltage trace shows the increase (not plotted).The area disturbed by phosphate is indicated by a gray background.

concentration of 0.88 mg in 500 μl sodium phosphate buffer, leading to a final concentration of 2 mM. Measurements were done at 25 °C with a total number of 28 injections, the first with 5 μl, all following with 10 μl. Data were analyzed with the accompanying software.

FTIR Measurements. All FTIR measurements of labelled PDZ domain mutants were performed in aqueous phosphate buffer (H_2O), pH 6.8 with no additional salts. The sample cell consists of two CaF_2 windows (see [296]) with a spacer thickness of 100 μm. Protein concentrations varied between 3–4 mM. Measurements with the native CRIPT peptide acNYKQTSV as ligand were performed the same way with 1.5–2 fold excess of ligand to obtain maximum binding and repeated to ensure they are reproductive. All data were measured against phosphate buffer as background. Data were further corrected for background signals from the H_2O combination band at 2000–2300 cm^{-1} by fitting a polynomial function of 5th order to the background, while leaving the interval with data points (approx. 2080–2180 cm^{-1}) out for fitting using baseline correction in *OriginPro 8.5*. All measurements were performed using a Bruker Tensor FTIR spectrometer equipped with liquid nitrogen-cooled MCT detector. An additional long pass filter with a cut-off at 4 μm was used. The mirror speed was set to 20 kHz and values for aperture and amplification to use the full linear range of the detector were chosen.

B.3 Overview of Sample Sources

Sample	Source
N3A: boc-Azidohomoalanine	Marx Group, Uni Konstanz
fmoc-Aha: Fmoc-Azidohomoalanine	Iris-Biotech
Aha: Azidohomoalanine	Iris-Biotech
N3P: boc-Azidophenylalanine	bachem
N3A: boc-Cyanoalanine	bachem
CNP: boc-Cyanophenylalanine	bachem
AzuA: Azulenyl-Alanine	Budisa Group, TU Berlin
acAzuA: Acetylated Azulenyl-Alanine	Budisa Group, TU Berlin
AzuCa: Azulene-1-yl-acetic-acid	Schwarzer Group, MPI bpc Göttingen
Azulene-Azidohomoalanine Dipeptide	Budisa Group, TU Berlin
AzuP: Azu-Tyr-Asn-Aha-Gly	synthesized by M. Anders-Maurer, Uni Frankfurt
CRIPT: acNYKQTSV	synthesized by M. Anders-Maurer, Uni Frankfurt
Azu-QTSV	synthesized by M. Anders-Maurer, Uni Frankfurt
Azu-KQTSV	synthesized by M. Anders-Maurer, Uni Frankfurt
PDZ-WT	residues 302-401, purified by S. Oesteritz
PDZ Ile327Aha	residues 302-401, purified by S. Oesteritz
PDZ Ile341 Aha	residues 302-401, purified by S. Oesteritz
PDZ Ala376Aha	residues 302-401, purified by S. Oesteritz
PDZ Ala390Aha	residues 302-401, purified by S. Oesteritz
PDZ Leu353Aha	residues 302-401, purified by S. Oesteritz
PDZ Ser398Aha	residues 302-401, purified by S. Oesteritz

Table B.2: Overview on Samples studied in this thesis.

C Computational Methods

C.1 Docking/Bioinformatics

The Molecular Docking was mainly performed by Martin Essig during his Bachelor Thesis [362] and afterwards as a student assistant supervised by the author. This Appendix gives only a brief overview on the main experiments. The visualisation of Docking results was performed by the author.

For all investigated mutants molecular docking of the CRIPT peptide (as heptamer, acNYKQTSV) into the known structure of PDZ3 holoprotein (1be9, crystal structure from protein ligand complex) using AutoDock 4.2 [316, 317] was performed.

The pdb file was modified introducing a *in silico* mutation using UCSF Chimera [202] before usage as receptor file in the docking. Simulations were additionally performed with Aha as flexible side chain. Resulting pdb data from simulations with flexible Aha were used to visualize the orientation of the azide moiety in the investigated mutants using PyMol. The surface of surrounding residues in the proximity of Aha was colored according to the free energy of the amino acid side chain for the transition from cyclohexane to H_2O in the gas phase (values obtained from [318]). For this a gradient was applied to show different degrees of hydrophobic or polar environment with three steps for polar (dark blue to light blue), three steps for hydrophobic (dark red to light red) and white for non-polar residues. The figure shows the surrounding surface of the Aha with the azide as center point and Aha shown as sticks. To produce this view, the surface volume of aha was removed from the whole protein volume.

***In silico* Mutation.**   Chimera 1.5.2 [202] was used for visualization and modification of the PDB-data set (1be9, [203]) of the PDZ domain. To accomplish an *in silico* mutation, the unnatural amino acid azidohomoalanine was constructed by adding additional atoms to an amino acid backbone. Bond lengths and torsion angles were adjusted to match a prior DFT calculation (as reported in Chapter 4). The mutation sites in the PDZ domain were identified and selected in the PDB data set. The corresponding side chain was deleted and replaced with the constructed azidohomoalanine. Prior side chain orientation was matched if possible, but in some cases (i.e. alanine mutations) some of the side chain torsions had to be changed due to steric hindering. To correct this further each docking session was done with a flexible azidohomoalanine side chain, as described below.

Molecular Docking.   MGLTools 1.5.4 and its subprograms AutoGrid 4.2 and AutoDock 4.2 [316, 317] were used for docking preparation, execution and analysis. Preparation of the mutated receptors involved converting the .pdb-files to the .pdbqt format used by AutoDock and therefore assigning a reasonable charge to the azide group. Since the algorithm used to assign Gasteiger charges to the receptor can not predict the special properties of the azide functional group, the charges were changed to resemble those obtained by previous DFT calculations of free Aha ($N_1 : -0.128$, $N_2 : 0.11$, $N_3 : -0.11$). This leaves the system at a non integer charge, but the deficit was small enough to be negligible. The size of the grid box was chosen to include the Aha residue (different for each mutant), and always included the binding pocket and the important residues within it, while leaving enough

space for the ligand. Grid spacing was set to 0.375 Å for all dockings. The search parameters were mostly left at their standard values, except for the rate of gene mutation which was increased from 2% to 5%. The maximum number of energy evaluation was set to "long" $(2.5 \cdot 10^7)$ and a docking session includes 50 docking runs (except for the wild type docking with only 40 runs). To analyze if the results are reproducible, the best docked ligand conformations of each run were compared and sorted into clusters, based on their RMSD. (clustering algorithm of MGLTools) A cluster with multiple conformations shows that very similar docked conformations are reached by multiple, independent docking runs, which raises the probability of a *native-like* docked state.

Visualization in PyMol.   Resulting pdb data from simulations with flexible Aha were used to visualize the orientation of the azide moiety in the investigated mutants using PyMol. The surface of surrounding residues in the proximity of Aha was colored according to the free energy of the amino acid side chain for the transition from cyclohexane to H_2O in the gas phase (values obtained from [318]). For this a gradient was applied to show different degrees of hydrophobic or polar environment with three steps for polar (dark blue to light blue), three steps for hydrophobic (dark red to light red) and white for non-polar residues. Figure 4 in the main paper shows the surrounding surface of Aha with the azide as center point and Aha shown as sticks. To produce this view, the surface volume of Aha was removed from the whole protein volume. Figure 5.5 shows the azide group for all positions in PDZ with its surrounding surface colored by the relative polarity.

C.2 Quantum Chemistry/DFT Calculations

All computations reported in Chapter 4 and Chapter 7 were performed with the Gaussian09 suite of programs, [297] using density functional theory (DFT). All calculations have been performed on the CSC (Center for Scientific Computing, Frankfurt). For the calculations reported in Chapter 4 the functional B3LYP in conjunction with the $6-311G(d,p)$ basis set was chosen. This functional is regularly used for the calculation of vibrational modes (see [252]). Because of the discrepancy in assignment for the modes in the amide II region in the molecules CNP and N3P (see Chapter 7 for details) from experiment versus calculations, a higher basis set $(6-311G(d,p))$ was chosen. Overall the calculations for the three amino acids Aha, CNP and N3P have been performed with several different basis sets in conjunction with the B3LYP functional. (not all data reported)

For the computations reported in Chapter 7 Truhlar's hybrid functional M06 [332] in conjunction with the $6-31+G(d,p)$ basis set was chosen, as it reached very good agreement with the experimental results on molecular structure, vibrational frequencies, and on transition dipole moment orientations, which are very sensitive to the localization of vibrations in previous studies [99]. The B97D functional by Grimme [333] in conjunction with the $6-31+G(d,p)$ basis set has been chosen for comparison because the computation resulted in a different order of the investigated modes. The influence of the solvent was taken into account by the self-consistent reaction field (SC RF) method using the polarizable continuum model (PCM). For creating the solvent cavity, the Gaussian09 default UFF radii [385] and the van der Waals radii of Bondi [386] were employed, both with the default scaling of 1.1 and explicit hydrogen atoms [387].

The computed normal modes, as derived by either using the M06 or the B97D functional, in the region between 1450 cm^{-1} to 2200 cm^{-1} have been visualized using a Mathematica script. The script plots the atomic coordinates and colors the atoms corresponding to their relative vibrational energy, which is calculated as potential energy derived from the displacement.

Center Number	Atomic Number	Atomic Type	Coordinates (Å)		
			X	Y	Z
1	7	0	−1.903 049	0.825 097	−0.187 084
2	1	0	−2.171 475	1.558 820	−0.830 164
3	6	0	−0.506 721	0.709 449	0.190 190
4	1	0	−0.450 401	0.135 738	1.116 174
5	6	0	0.322 551	−0.016 202	−0.917 460
6	6	0	0.036 424	2.110 984	0.440 005
7	1	0	−0.205 857	−0.955 559	−1.109 383
8	1	0	0.269 043	0.584 347	−1.831 396
9	6	0	1.764 135	−0.303 167	−0.561 580
10	8	0	−0.287 989	3.093 959	−0.204 040
11	6	0	2.092 855	−1.352 989	0.312 328
12	6	0	2.810 429	0.460 079	−1.099 214
13	1	0	1.302 576	−1.967 289	0.735 837
14	6	0	3.417 352	−1.629 257	0.643 785
15	6	0	4.144 028	0.197 649	−0.779 116
16	1	0	2.584 310	1.271 767	−1.785 766
17	1	0	3.664 135	−2.444 377	1.316 490
18	6	0	4.447 918	−0.852 182	0.097 573
19	1	0	4.933 384	0.803 152	−1.214 574
20	6	0	−2.835 680	−0.098 934	0.173 143
21	8	0	−2.605 846	−1.064 502	0.900 793
22	8	0	−4.028 264	0.213 203	−0.377 841
23	6	0	−5.255 551	−0.587 337	−0.130 590
24	7	0	5.771 766	−1.207 644	0.485 357
25	7	0	6.718 512	−0.556 749	0.031 696
26	7	0	7.676 431	−0.041 196	−0.311 439
27	8	0	0.942 140	2.142 654	1.427 410
28	1	0	1.296 062	3.048 583	1.502 740
29	6	0	−5.602 425	−0.563 286	1.360 349
30	1	0	−6.579 401	−1.035 199	1.506 819
31	1	0	−4.863 254	−1.103 549	1.953 469
32	1	0	−5.664 971	0.468 493	1.720 997
33	6	0	−5.072 854	−2.007 298	−0.672 838
34	1	0	−6.029 019	−2.536 845	−0.610 248
35	1	0	−4.767 344	−1.978 171	−1.723 774
36	1	0	−4.329 655	−2.564 147	−0.100 446
37	6	0	−6.307 881	0.170 766	−0.942 926
38	1	0	−7.277 639	−0.324 533	−0.838 159
39	1	0	−6.403 948	1.201 111	−0.586 970
40	1	0	−6.039 988	0.188 931	−2.003 822

Table C.1: Atomic coordinates as derived from DFT calculations for visualization of calculated normal modes in N3P using the B97D functional.

Center	Atomic	Atomic	Coordinates (Å)		
Number	Number	Type	X	Y	Z
1	7	0	−1.893 566	0.938 732	−0.016 997
2	1	0	−2.152 667	1.723 641	−0.602 517
3	6	0	−0.499 284	0.742 637	0.301 639
4	1	0	−0.427 547	0.205 782	1.254 876
5	6	0	0.223 217	−0.064 226	−0.801 082
6	6	0	0.147 106	2.101 559	0.438 735
7	1	0	−0.340 670	−0.999 468	−0.909 537
8	1	0	0.126 862	0.491 560	−1.744 014
9	6	0	1.664 338	−0.351 591	−0.500 773
10	8	0	−0.110 805	3.043 269	−0.280 170
11	6	0	2.010 599	−1.320 335	0.447 074
12	6	0	2.687 210	0.359 890	−1.130 185
13	1	0	1.224 086	−1.888 189	0.943 786
14	6	0	3.338 213	−1.572 503	0.760 347
15	6	0	4.023 859	0.118 636	−0.830 621
16	1	0	2.436 215	1.116 393	−1.873 256
17	1	0	3.611 394	−2.327 265	1.493 327
18	6	0	4.346 507	−0.851 015	0.119 095
19	1	0	4.804 869	0.681 651	−1.338 215
20	6	0	−2.803 928	−0.048 376	0.208 875
21	8	0	−2.540 866	−1.091 326	0.787 346
22	8	0	−3.998 540	0.309 611	−0.280 517
23	6	0	−5.169 536	−0.569 972	−0.167 189
24	7	0	5.678 469	−1.174 830	0.492 431
25	7	0	6.594 861	−0.564 776	−0.054 567
26	7	0	7.522 481	−0.068 231	−0.492 027
27	8	0	1.065 678	2.135 555	1.404 121
28	1	0	1.486 982	3.012 340	1.398 361
29	6	0	−5.511 511	−0.799 970	1.294 552
30	1	0	−6.467 785	−1.332 838	1.358 037
31	1	0	−4.747 990	−1.395 405	1.801 236
32	1	0	−5.621 844	0.158 757	1.815 031
33	6	0	−4.921 557	−1.865 962	−0.919 475
34	1	0	−5.849 013	−2.450 418	−0.943 251
35	1	0	−4.626 987	−1.655 704	−1.954 588
36	1	0	−4.144 386	−2.468 366	−0.441 976
37	6	0	−6.258 896	0.240 089	−0.846 710
38	1	0	−7.200 307	−0.320 392	−0.833 769
39	1	0	−6.414 863	1.192 726	−0.327 960
40	1	0	−5.993 828	0.448 882	−1.889 388

Table C.2: Atomic coordinates as derived from DFT calculations for visualization of calculated normal modes in N3P using the M06 functional.

Frequencies		1450.9957			1467.4895			1491.2880		
Red. masses		1.0527			1.0567			2.3742		
Frc consts		1.3059			1.3407			3.1109		
IR Intensity		3.0121			10.6260			273.5761		
Atom	AN	X	Y	Z	X	Y	Z	X	Y	Z
1	7	0.00	0.00	0.00	0.01	0.00	0.00	0.03	0.02	0.00
2	1	0.00	0.00	0.00	−0.06	−0.02	0.00	−0.19	−0.06	−0.01
3	6	0.00	0.00	0.00	−0.01	−0.01	0.00	−0.01	−0.02	0.00
4	1	0.00	0.00	0.00	0.04	0.01	0.01	0.09	0.02	0.01
5	6	0.00	0.00	0.00	0.00	0.00	0.00	0.04	0.00	0.01
6	6	0.00	0.00	0.00	0.00	0.00	0.00	0.01	0.01	0.00
7	1	0.00	0.00	0.00	−0.01	0.00	0.01	0.01	0.02	−0.01
8	1	0.00	0.00	0.00	0.00	0.00	0.00	−0.01	−0.03	0.00
9	6	0.00	0.00	0.00	0.00	0.00	0.00	−0.14	0.02	−0.02
10	8	0.00	0.00	0.00	0.00	0.00	0.00	0.00	0.00	0.00
11	6	0.00	0.00	0.00	0.00	0.00	0.00	0.03	−0.07	0.07
12	6	0.00	0.00	0.00	0.00	0.00	0.00	0.10	0.06	−0.05
13	1	0.00	0.00	0.00	0.00	0.00	0.00	−0.33	0.19	−0.19
14	6	0.00	0.00	0.00	0.00	0.00	0.00	0.14	0.05	−0.04
15	6	0.00	0.00	0.00	0.00	0.00	0.00	0.08	−0.09	0.09
16	1	0.00	0.00	0.00	0.00	0.00	0.00	−0.43	−0.03	0.01
17	1	0.00	0.00	0.00	0.00	0.00	0.00	−0.47	−0.06	0.04
18	6	0.00	0.00	0.00	0.00	0.00	0.00	−0.15	0.03	−0.03
19	1	0.00	0.00	0.00	0.00	0.00	0.00	−0.36	0.22	−0.23
20	6	0.00	0.00	0.00	0.00	0.01	0.00	−0.02	−0.01	0.00
21	8	0.00	0.00	0.00	0.00	0.00	0.00	0.00	0.00	0.00
22	8	0.00	0.00	0.00	0.00	0.00	0.00	0.00	0.00	0.00
23	6	0.01	−0.02	−0.04	−0.03	−0.03	0.01	0.01	0.00	0.00
24	7	0.00	0.00	0.00	0.00	0.00	0.00	0.04	0.00	0.00
25	7	0.00	0.00	0.00	0.00	0.00	0.00	0.00	0.00	0.00
26	7	0.00	0.00	0.00	0.00	0.00	0.00	−0.01	0.00	0.00
27	8	0.00	0.00	0.00	0.00	0.00	0.00	0.00	0.00	0.00
28	1	0.00	0.00	0.00	−0.01	0.00	−0.01	−0.01	0.00	−0.01
29	6	−0.02	−0.03	0.00	−0.02	−0.02	−0.02	0.00	0.00	0.00
30	1	−0.13	0.17	−0.20	−0.06	0.05	−0.22	0.00	0.00	0.01
31	1	0.20	0.35	0.09	0.11	0.36	0.19	0.00	−0.01	−0.01
32	1	0.13	−0.11	0.23	0.26	−0.10	0.26	−0.01	0.00	−0.01
33	6	0.02	0.02	−0.02	−0.03	0.00	0.02	0.00	0.00	0.00
34	1	0.16	−0.23	0.15	−0.13	0.18	0.02	0.00	−0.01	−0.01
35	1	−0.14	0.22	−0.02	0.30	−0.20	0.08	−0.01	0.00	0.00
36	1	−0.30	−0.20	0.20	0.26	0.08	−0.31	0.00	0.00	0.01
37	6	0.01	−0.01	−0.02	−0.01	−0.02	0.01	0.00	0.00	0.00
38	1	−0.10	0.19	0.32	0.08	−0.15	0.09	0.00	0.01	0.00
39	1	−0.29	−0.06	−0.01	0.12	0.14	−0.29	0.00	0.00	0.01
40	1	0.26	0.05	0.06	0.00	0.33	0.06	0.00	−0.01	0.00

(a)

Table C.3: Displacement per atom for normal modes in N3P as derived from DFT calculations using the B97D functional.

Frequencies		1504.2563			1566.1930			1600.2382		
Red. masses			1.7467			6.3479			5.7760		
Frc consts			2.3287			9.1742			8.7146		
IR Intensity			365.8979			10.6930			27.5265		
Atom	AN	X	Y	Z	X	Y	Z	X	Y	Z
1	7	−0.16	−0.08	0.02	0.00	0.00	0.00	−0.01	0.00	0.00
2	1	0.82	0.26	0.03	−0.02	0.00	0.00	0.03	0.01	0.00
3	6	0.07	0.06	−0.02	0.00	−0.01	0.00	0.01	0.00	−0.01
4	1	−0.37	−0.07	−0.06	0.01	0.01	0.01	−0.02	0.01	0.00
5	6	0.01	−0.01	0.01	−0.01	−0.03	0.03	0.03	0.00	0.01
6	6	−0.03	−0.02	−0.02	0.00	0.00	0.00	0.00	0.00	0.00
7	1	0.03	−0.01	−0.06	−0.16	0.07	0.00	0.04	−0.01	−0.03
8	1	−0.05	0.01	0.02	0.24	−0.05	−0.01	−0.05	−0.02	0.01
9	6	−0.02	0.00	0.00	0.07	0.26	−0.24	−0.23	0.01	−0.02
10	8	0.00	0.00	0.00	0.00	0.00	0.00	0.00	0.00	0.00
11	6	0.00	−0.01	0.01	0.08	−0.19	0.18	0.26	−0.10	0.11
12	6	0.01	0.01	−0.01	−0.11	−0.13	0.11	0.33	0.02	−0.01
13	1	−0.05	0.03	−0.03	−0.36	0.12	−0.13	−0.20	0.25	−0.25
14	6	0.03	0.01	−0.01	0.12	0.14	−0.12	−0.30	−0.01	−0.01
15	6	0.02	−0.01	0.01	−0.06	0.18	−0.17	−0.23	0.07	−0.07
16	1	−0.05	0.00	0.00	0.24	−0.07	0.08	−0.42	−0.12	0.09
17	1	−0.08	−0.01	0.01	−0.26	0.08	−0.09	0.31	0.12	−0.09
18	6	−0.03	0.00	0.00	−0.09	−0.25	0.23	0.15	0.01	0.00
19	1	−0.05	0.04	−0.04	0.31	−0.08	0.09	0.10	−0.19	0.19
20	6	0.11	0.05	0.02	0.00	0.00	0.00	0.01	0.00	0.00
21	8	−0.01	0.00	0.00	0.00	0.00	0.00	0.00	0.00	0.00
22	8	−0.01	0.00	0.00	0.00	0.00	0.00	0.00	0.00	0.00
23	6	−0.02	0.00	0.00	0.00	0.00	0.00	0.00	0.00	0.00
24	7	0.01	0.00	0.00	−0.01	0.02	−0.02	0.01	0.00	0.00
25	7	0.00	0.00	0.00	0.00	−0.01	0.01	0.01	0.00	0.00
26	7	0.00	0.00	0.00	0.01	0.01	−0.01	−0.02	−0.01	0.01
27	8	0.01	0.01	0.01	0.00	0.00	0.00	0.00	0.00	0.00
28	1	0.03	−0.01	0.04	0.00	0.00	0.00	0.00	0.00	0.00
29	6	0.00	0.00	0.00	0.00	0.00	0.00	0.00	0.00	0.00
30	1	0.00	−0.01	−0.05	0.00	0.00	0.00	0.00	0.00	0.00
31	1	0.00	0.03	0.03	0.00	0.00	0.00	0.00	0.00	0.00
32	1	0.03	0.00	0.02	0.00	0.00	0.00	0.00	0.00	0.00
33	6	0.00	0.00	0.00	0.00	0.00	0.00	0.00	0.00	0.00
34	1	−0.02	0.03	0.03	0.00	0.00	0.00	0.00	0.00	0.00
35	1	0.04	−0.01	0.01	0.00	0.00	0.00	0.00	0.00	0.00
36	1	0.02	−0.01	−0.03	0.00	0.00	0.00	0.00	0.00	0.00
37	6	0.00	0.00	0.00	0.00	0.00	0.00	0.00	0.00	0.00
38	1	0.01	−0.02	0.01	0.00	0.00	0.00	0.00	0.00	0.00
39	1	0.01	0.01	−0.02	0.00	0.00	0.00	0.00	0.00	0.00
40	1	0.00	0.03	0.00	0.00	0.00	0.00	0.00	0.00	0.00

(b) continued from page 147

Table C.3

Frequencies		1665.0458			1714.9490			2173.1119		
Red. masses		10.5176			9.6163			13.9807		
Frc consts		17.1798			16.6633			38.8995		
IR Intensity		726.9133			415.5353			1720.4352		
Atom	AN	X	Y	Z	X	Y	Z	X	Y	Z
1	7	−0.02	−0.09	0.05	0.00	0.02	−0.01	0.00	0.00	0.00
2	1	−0.28	−0.24	−0.03	0.11	0.08	0.01	0.00	0.00	0.00
3	6	−0.02	0.00	−0.01	−0.02	−0.06	0.02	0.00	0.00	0.00
4	1	0.07	0.00	−0.04	−0.10	−0.21	−0.06	0.00	0.00	0.00
5	6	0.01	0.00	0.01	0.01	−0.01	−0.01	0.00	0.00	0.00
6	6	−0.02	0.09	−0.06	−0.11	0.58	−0.38	0.00	0.00	0.00
7	1	0.00	0.01	−0.02	−0.05	0.01	0.09	0.01	−0.01	0.00
8	1	−0.04	0.00	0.01	0.00	0.05	0.02	0.01	0.00	0.00
9	6	−0.01	0.00	0.00	0.00	0.00	0.00	0.00	0.00	0.00
10	8	0.02	−0.06	0.04	0.09	−0.35	0.25	0.00	0.00	0.00
11	6	0.00	0.00	0.00	0.00	0.00	0.00	0.00	0.00	0.00
12	6	0.01	0.00	0.00	0.00	0.00	0.00	0.00	0.00	0.00
13	1	0.00	0.00	0.00	0.00	0.00	0.00	−0.01	0.00	0.00
14	6	0.00	0.00	0.00	0.00	0.00	0.00	0.01	0.01	−0.01
15	6	0.00	0.00	0.00	0.00	0.00	0.00	0.01	0.00	0.00
16	1	−0.01	0.00	0.00	0.00	0.00	0.00	0.01	0.01	−0.01
17	1	0.01	0.00	0.00	0.00	0.00	0.00	−0.01	0.00	0.00
18	6	0.00	0.00	0.00	0.00	0.00	0.00	−0.04	−0.03	0.02
19	1	0.00	0.00	0.00	0.00	0.00	0.00	0.01	0.02	−0.01
20	6	−0.09	0.64	−0.39	0.01	−0.10	0.06	0.00	0.00	0.00
21	8	0.08	−0.36	0.22	−0.01	0.05	−0.03	0.00	0.00	0.00
22	8	0.02	−0.05	0.03	0.00	0.01	0.00	0.00	0.00	0.00
23	6	0.01	0.04	−0.02	0.00	−0.01	0.00	0.00	0.00	0.00
24	7	0.00	0.00	0.00	0.00	0.00	0.00	−0.18	−0.07	0.06
25	7	0.00	0.00	0.00	0.00	0.00	0.00	0.68	0.32	−0.26
26	7	0.00	0.00	0.00	0.00	0.00	0.00	−0.48	−0.23	0.19
27	8	0.01	0.00	0.01	0.02	−0.05	0.04	0.00	0.00	0.00
28	1	−0.04	0.02	−0.05	−0.27	0.10	−0.34	0.00	0.00	0.00
29	6	0.00	0.00	0.00	0.00	0.00	0.00	0.00	0.00	0.00
30	1	0.04	−0.06	0.09	0.00	0.01	−0.01	0.00	0.00	0.00
31	1	−0.09	−0.05	0.06	0.01	0.00	−0.01	0.00	0.00	0.00
32	1	0.02	0.01	−0.02	0.00	0.00	0.00	0.00	0.00	0.00
33	6	0.00	0.00	0.00	0.00	0.00	0.00	0.00	0.00	0.00
34	1	0.05	−0.09	0.03	−0.01	0.01	0.00	0.00	0.00	0.00
35	1	0.01	0.03	0.01	0.00	0.00	0.00	0.00	0.00	0.00
36	1	−0.06	−0.09	−0.03	0.01	0.01	0.00	0.00	0.00	0.00
37	6	0.00	−0.01	0.00	0.00	0.00	0.00	0.00	0.00	0.00
38	1	−0.03	0.05	−0.03	0.01	−0.01	0.01	0.00	0.00	0.00
39	1	0.01	−0.01	0.01	0.00	0.00	0.00	0.00	0.00	0.00
40	1	0.01	−0.02	0.01	0.00	0.00	0.00	0.00	0.00	0.00

(c) continued from page 148

Table C.3

Frequencies		1465.7775			1484.3199			1523.3900		
Red. masses		1.0760			1.0691			2.5764		
Frc consts		1.3621			1.3877			3.5228		
IR Intensity		5.4370			7.5908			834.2472		
Atom	AN	X	Y	Z	X	Y	Z	X	Y	Z
1	7	0.00	0.00	0.00	0.02	0.01	0.00	0.21	0.11	−0.01
2	1	0.01	0.00	0.00	−0.07	−0.02	0.00	−0.76	−0.23	−0.04
3	6	0.00	0.00	0.00	−0.01	−0.01	0.00	−0.11	−0.07	0.01
4	1	−0.01	0.00	0.00	0.05	0.01	0.01	0.33	0.07	0.06
5	6	0.00	0.00	0.00	0.00	0.00	0.00	0.01	0.01	0.00
6	6	0.00	0.00	0.00	0.01	0.01	0.01	0.05	0.03	0.04
7	1	0.00	0.00	−0.01	−0.01	0.01	0.01	−0.04	0.02	0.07
8	1	0.00	0.00	0.00	0.01	0.00	0.00	0.05	−0.01	−0.01
9	6	0.00	0.00	0.00	0.00	0.00	0.00	−0.04	0.01	−0.01
10	8	0.00	0.00	0.00	0.00	0.00	0.00	−0.01	0.00	−0.01
11	6	0.00	0.00	0.00	0.00	0.00	0.00	0.02	−0.02	0.02
12	6	0.00	0.00	0.00	0.00	0.00	0.00	0.03	0.02	−0.01
13	1	0.00	0.00	0.00	0.00	0.00	0.00	−0.09	0.05	−0.05
14	6	0.00	0.00	0.00	0.00	0.00	0.00	0.03	0.02	−0.01
15	6	0.00	0.00	0.00	0.00	0.00	0.00	0.02	−0.03	0.03
16	1	0.00	0.00	0.00	0.00	0.00	0.00	−0.12	−0.01	0.00
17	1	0.00	0.00	0.00	0.00	0.00	0.00	−0.10	−0.01	0.00
18	6	0.00	0.00	0.00	0.00	0.00	0.00	−0.04	0.01	−0.01
19	1	0.00	0.00	0.00	0.00	0.00	0.00	−0.11	0.06	−0.07
20	6	0.00	0.00	0.00	−0.01	0.00	0.00	−0.19	−0.06	−0.03
21	8	0.00	0.00	0.00	0.00	0.00	0.00	0.02	−0.01	0.01
22	8	0.00	0.00	0.00	0.00	0.00	0.00	0.02	0.00	0.01
23	6	0.03	−0.04	−0.04	−0.04	−0.03	0.01	0.04	0.01	0.01
24	7	0.00	0.00	0.00	0.00	0.00	0.00	0.01	0.00	0.00
25	7	0.00	0.00	0.00	0.00	0.00	0.00	0.00	0.00	0.00
26	7	0.00	0.00	0.00	0.00	0.00	0.00	0.00	0.00	0.00
27	8	0.00	0.00	0.00	0.00	0.00	0.00	−0.02	−0.01	−0.01
28	1	0.00	0.00	0.00	−0.01	0.00	−0.01	−0.05	0.01	−0.06
29	6	−0.01	−0.03	0.02	−0.01	−0.01	−0.02	−0.01	0.00	0.00
30	1	−0.23	0.35	−0.20	−0.05	0.05	−0.19	−0.01	0.01	0.07
31	1	0.34	0.36	−0.05	0.10	0.31	0.19	0.01	−0.04	−0.06
32	1	−0.03	−0.14	0.22	0.24	−0.11	0.22	−0.05	0.01	−0.04
33	6	0.01	0.02	0.00	−0.03	0.01	0.02	0.00	0.00	0.00
34	1	0.13	−0.17	0.00	−0.13	0.18	0.05	0.03	−0.05	−0.05
35	1	−0.18	0.13	−0.03	0.32	−0.22	0.06	−0.06	0.03	−0.01
36	1	−0.21	−0.12	0.18	0.26	0.09	−0.34	−0.03	0.01	0.07
37	6	0.00	0.00	−0.02	0.00	−0.02	0.01	−0.01	0.00	0.00
38	1	−0.07	0.12	0.33	0.08	−0.16	0.09	−0.03	0.03	−0.02
39	1	−0.24	−0.03	−0.03	0.11	0.16	−0.29	−0.01	−0.03	0.05
40	1	0.28	0.06	0.07	0.00	0.34	0.08	0.02	−0.06	−0.01

(a)

Table C.4: Displacement per atom for normal modes in N3P as derived from DFT calculations using the M06 functional.

Frequencies		1536.2043			1633.9572			1667.0588		
Red. masses		2.8578			7.1566			6.7145		
Frc consts		3.9736			11.2573			10.9943		
IR Intensity		62.3145			6.9664			37.3803		
Atom	AN	X	Y	Z	X	Y	Z	X	Y	Z
1	7	0.06	0.03	0.00	0.00	0.00	0.00	−0.01	0.00	0.00
2	1	−0.21	−0.07	−0.01	−0.01	0.00	0.00	0.02	0.01	0.00
3	6	−0.03	−0.02	0.00	0.00	−0.01	0.00	0.01	0.00	0.00
4	1	0.08	0.02	0.02	0.01	0.00	0.00	−0.02	0.01	0.00
5	6	−0.05	0.01	−0.01	−0.01	−0.02	0.03	0.04	0.00	0.01
6	6	0.01	0.01	0.01	0.00	0.00	0.00	0.00	0.00	0.00
7	1	−0.03	−0.01	0.02	−0.14	0.06	0.00	0.05	−0.01	−0.01
8	1	0.02	0.00	−0.02	0.22	−0.04	−0.01	−0.03	0.00	0.01
9	6	0.17	−0.03	0.03	0.08	0.27	−0.25	−0.25	0.01	−0.01
10	8	0.00	0.00	0.00	0.00	0.00	0.00	0.00	0.00	0.00
11	6	−0.05	0.09	−0.09	0.08	−0.19	0.19	0.28	−0.10	0.11
12	6	−0.09	−0.06	0.05	−0.12	−0.14	0.12	0.35	0.03	−0.01
13	1	0.34	−0.18	0.19	−0.31	0.08	−0.09	−0.16	0.23	−0.23
14	6	−0.14	−0.06	0.05	0.11	0.14	−0.13	−0.34	−0.02	0.00
15	6	−0.09	0.09	−0.10	−0.08	0.19	−0.19	−0.26	0.08	−0.09
16	1	0.39	0.02	−0.01	0.23	−0.08	0.09	−0.36	−0.11	0.09
17	1	0.40	0.04	−0.01	−0.20	0.10	−0.10	0.28	0.12	−0.09
18	6	0.18	−0.02	0.02	−0.08	−0.28	0.27	0.17	0.01	0.00
19	1	0.39	−0.24	0.25	0.34	−0.08	0.10	0.12	−0.20	0.20
20	6	−0.06	−0.02	−0.01	0.00	0.00	0.00	0.01	0.00	0.00
21	8	0.01	0.00	0.00	0.00	0.00	0.00	0.00	0.00	0.00
22	8	0.01	0.00	0.00	0.00	0.00	0.00	0.00	0.00	0.00
23	6	0.01	0.00	0.00	0.00	0.00	0.00	0.00	0.00	0.00
24	7	−0.06	−0.01	0.00	−0.01	0.02	−0.02	0.00	0.00	0.00
25	7	0.00	0.01	−0.01	0.00	−0.01	0.01	0.01	0.00	0.00
26	7	0.01	0.01	−0.01	0.01	0.01	−0.01	−0.02	−0.01	0.01
27	8	−0.01	0.00	0.00	0.00	0.00	0.00	0.00	0.00	0.00
28	1	−0.01	0.00	−0.02	0.00	0.00	0.00	0.00	0.00	0.00
29	6	0.00	0.00	0.00	0.00	0.00	0.00	0.00	0.00	0.00
30	1	0.00	0.00	0.02	0.00	0.00	0.00	0.00	0.00	0.00
31	1	0.00	−0.01	−0.01	0.00	0.00	0.00	0.00	0.00	0.00
32	1	−0.01	0.00	−0.01	0.00	0.00	0.00	0.00	0.00	0.00
33	6	0.00	0.00	0.00	0.00	0.00	0.00	0.00	0.00	0.00
34	1	0.01	−0.01	−0.01	0.00	0.00	0.00	0.00	0.00	0.00
35	1	−0.01	0.01	0.00	0.00	0.00	0.00	0.00	0.00	0.00
36	1	−0.01	0.00	0.01	0.00	0.00	0.00	0.00	0.00	0.00
37	6	0.00	0.00	0.00	0.00	0.00	0.00	0.00	0.00	0.00
38	1	−0.01	0.01	0.00	0.00	0.00	0.00	0.00	0.00	0.00
39	1	0.00	−0.01	0.01	0.00	0.00	0.00	0.00	0.00	0.00
40	1	0.00	−0.01	0.00	0.00	0.00	0.00	0.00	0.00	0.00

(b) continued from page 150

Table C.4

Frequencies		1777.9745			1830.1448			2273.9380		
Red. masses		11.6022			10.7286			13.9837		
Frc consts		21.6093			21.1721			42.6021		
IR Intensity		633.8339			420.3064			1584.3492		
Atom	AN	X	Y	Z	X	Y	Z	X	Y	Z
1	7	−0.03	−0.09	0.04	0.01	0.02	−0.01	0.00	0.00	0.00
2	1	−0.19	−0.17	−0.01	0.08	0.06	0.01	0.00	0.00	0.00
3	6	−0.02	0.01	−0.01	−0.02	−0.07	0.02	0.00	0.00	0.00
4	1	0.06	0.01	−0.04	−0.07	−0.18	−0.05	0.00	0.00	0.00
5	6	0.01	0.00	0.00	0.01	0.00	−0.01	0.00	0.00	0.00
6	6	−0.02	0.07	−0.06	−0.12	0.61	−0.42	0.00	0.00	0.00
7	1	0.01	0.01	−0.03	−0.04	0.01	0.07	0.01	−0.01	0.00
8	1	−0.04	0.00	0.01	0.00	0.04	0.01	0.00	0.00	−0.01
9	6	0.00	0.00	0.00	0.00	0.00	0.00	0.00	0.00	0.00
10	8	0.01	−0.05	0.04	0.09	−0.37	0.27	0.00	0.00	0.00
11	6	0.00	0.00	0.00	0.00	0.00	0.00	0.00	0.00	0.00
12	6	0.00	0.00	0.00	0.00	0.00	0.00	0.00	0.00	0.00
13	1	0.00	0.00	0.00	0.00	0.00	0.00	−0.01	0.00	0.00
14	6	0.00	0.00	0.00	0.00	0.00	0.00	0.01	0.01	−0.01
15	6	0.00	0.00	0.00	0.00	0.00	0.00	0.01	0.00	0.00
16	1	0.00	0.00	0.00	0.00	0.00	0.00	0.01	0.01	−0.01
17	1	0.00	0.00	0.00	0.00	0.00	0.00	−0.01	0.00	0.00
18	6	0.00	0.00	0.00	0.00	0.00	0.00	−0.04	−0.02	0.02
19	1	0.00	0.00	0.00	0.00	0.00	0.00	0.01	0.01	−0.01
20	6	−0.12	0.69	−0.37	0.01	−0.08	0.05	0.00	0.00	0.00
21	8	0.09	−0.40	0.22	−0.01	0.04	−0.02	0.00	0.00	0.00
22	8	0.03	−0.05	0.03	0.00	0.01	0.00	0.00	0.00	0.00
23	6	0.01	0.04	−0.02	0.00	−0.01	0.00	0.00	0.00	0.00
24	7	0.00	0.00	0.00	0.00	0.00	0.00	−0.17	−0.08	0.07
25	7	0.00	0.00	0.00	0.00	0.00	0.00	0.65	0.34	−0.30
26	7	0.00	0.00	0.00	0.00	0.00	0.00	−0.47	−0.25	0.22
27	8	0.01	0.00	0.01	0.02	−0.04	0.04	0.00	0.00	0.00
28	1	−0.03	0.02	−0.03	−0.23	0.09	−0.28	0.00	0.00	0.00
29	6	0.00	0.00	0.00	0.00	0.00	0.00	0.00	0.00	0.00
30	1	0.03	−0.06	0.07	0.00	0.01	−0.01	0.00	0.00	0.00
31	1	−0.08	−0.04	0.06	0.01	0.00	−0.01	0.00	0.00	0.00
32	1	0.02	0.01	−0.02	0.00	0.00	0.00	0.00	0.00	0.00
33	6	0.00	0.00	0.00	0.00	0.00	0.00	0.00	0.00	0.00
34	1	0.05	−0.08	0.02	0.00	0.01	0.00	0.00	0.00	0.00
35	1	0.01	0.02	0.01	0.00	0.00	0.00	0.00	0.00	0.00
36	1	−0.05	−0.08	−0.04	0.00	0.01	0.00	0.00	0.00	0.00
37	6	−0.01	−0.01	0.00	0.00	0.00	0.00	0.00	0.00	0.00
38	1	−0.03	0.04	−0.02	0.00	−0.01	0.00	0.00	0.00	0.00
39	1	0.01	−0.01	0.01	0.00	0.00	0.00	0.00	0.00	0.00
40	1	0.01	−0.01	0.01	0.00	0.00	0.00	0.00	0.00	0.00

Table C.4

Zusammenfassung

Proteine sind hochspezialisierte, komplexe Maschinen deren vielfältige Funktionen biochemische Katalyse, Signalverarbeitung, Transport und Strukturbildung umfassen. Für ein umfassendes Verständnis der spezialisierten Funktion von Proteinen und ihres komplexen Zusammenspiels, sind Standbilder allein jedoch nicht ausreichend: Zeitaufgelöste Beobachtungen sind nötig, da (Bio)chemie dynamisch ist. Biochemische Prozesse erstrecken sich über eine Zeitskala vom sub-pikosekunden-Bereich bis zum Minutenbereich und länger. Die ersten Schritte (bio)chemischer Reaktionen spielen sich auf den kürzesten Zeitskalen im Femtosekunden bis Pikosekunden-Bereich ab, ebenso wie erste funktionell relevante Strukturveränderungen, die sehr gut in Molekulardynamik-Simulationen behandelt werden können. Die experimentelle Beobachtung dieser ultraschnellen Prozesse in Proteinen allerdings ist schwierig (insbesondere mit hoher räumlicher Auflösung) und noch in der Entwicklung, viele Erkenntnisse sind insbesondere durch optische Spektroskopie zugänglich.

Eine wichtige Methode mit hoher Zeitauflösung und möglicher Strukturauflösung ist die zweidimensionale oder allgemeiner mehrdimensionale Infrarotspektroskopie (2D-IR), ein konzeptionelles Pendant zur mehrdimensionalen NMR Spektroskopie im Infraroten mit einer Zeitauflösung im Femtosekundenbereich. Schwingungsmoden erlauben Einblicke in ultraschnelle Prozesse in Echtzeit. (eine Schwingungsperiode einer typischen Amid-Bande bei 1600 cm^{-1} hat eine Dauer von ca. 20 fs) Die 2D-IR Spektroskopie erlaubt die direkte Untersuchung struktureller Dynamik spezifischer funktioneller Gruppen innerhalb eines Experiments. Einerseits ist die Beobachtung der Dynamik im Gleichgewicht möglich, andererseits kann mittels transienter 2D-IR Spektroskopie ähnlich wie in anderen Anreg-Abtast-Experimenten auch über einen Zeitbereich bis zu Nanosekunden und länger gemessen werden, um Nichtgleichgewichtsprozesse zu beobachten.

Die ultraschnelle Dynamik von kleinen Molekülen lässt sich so im Detail sehr genau studieren und sogar Strukturaufklärung ist möglich. Für Messungen an biologischen Makromolekülen, im speziellen an Proteinen, stößt die 2D-IR Spektroskopie jedoch an dieselben Grenzen wie klassische FTIR Spektroskopie. Infrarot Spektroskopie ist sensitiv für alle infrarotaktiven Schwingungsmoden und durch die Wiederholung von funktionellen Gruppen wie der Peptidbindung sind IR Spektren eine Überlagerung der Signale einzelner Gruppen, die nicht mehr unterschieden werden können. So ist zwar eine Messung von Sekundärstrukturänderungen und der Dynamik des Proteinrückgrats möglich, aber nicht eine Analyse der lokalen Dynamik einzelner Seitenketten. Nur in Ausnahmefällen, z.B. wenn das Protein einen Liganden oder Chromophor besitzt, der in einem separierten Spektralbereich absorbiert, sind zeitaufgelöste ortsspezifische Messungen möglich. Hier setzt die vorliegende Dissertation mit dem Titel **Unnatural Amino Acids as Novel Probes for Ultrafast 2D-IR Spectroscopy of Proteins** - deutsch: **Unnatürliche Aminosäuren als neue Schwingungssonden für die mehrdimensionale Infrarotspektroskopie an Proteinen** an. Sie verbindet das junge Forschungsgebiet der mehrdimensionalen zeitaufgelösten Infrarotspektroskopie mit neuen Methoden aus der chemischen Biologie. Ziel ist es, neue spezifische Schwingungsmarker zu charakterisieren und diese auf ihre Anwendbarkeit in Proteinen zu testen, um so das Anwendungsgebiet der 2D-IR Spektroskopie zu erweitern.

Die Arbeit gliedert sich in vier Teile:

- Teil 1: Einleitung und theoretischer Hintergrund.

- Teil 2: Experimentelle Charakterisierung neuer Schwingungsmarker für die 2D-IR.

- Teil 3: Anwendungsbeispiel 1: Ortsspezifische Untersuchung konformationeller Änderungen und lokaler Dynamik.

- Teil 4: Anwendungsbeispiel 2: Echtzeitmessung von Schwingungsenergietransport.

Teil 1: Einleitung und theoretischer Hintergrund. Dieser Teil erklärt die physikalischen und technischen Grundlagen der 2D-IR Spektroskopie und stellt das untersuchte Modellprotein, die dritte PDZ-Domäne des Multidomänenproteinkomplexes PSD-95 vor.

In Kapitel 1 werden die Konzepte und Methoden der mehrdimensionalen Infrarotspektroskopie erklärt. Dabei handelt es sich um eine Ultrakurzzeitmethode mit Subpikosekunden-Zeitauflösung. Die Spektren, mit zwei Frequenzachsen (oder mehr, bisher wurden maximal drei demonstriert), ähnlich wie bei mehrdimensionaler NMR-Spektroskopie, erlauben die direkte Analyse von Schwingungsmoden bezüglich verschiedenster Parameter wie Anharmonizität, Lebensdauer oder spektraler Diffusion aus den Signalen auf der Diagonale. Ebenso ist es möglich Kreuzsignale zwischen Schwingungsmoden zu messen, die Aufschluss über Kopplungen zwischen den beteiligten Oszillatoren oder Populationstransfer sowie Schwingungsenergietransferprozesse erlauben.

Kapitel 2 stellt das untersuchte Modellprotein PDZ3 und das Konzept von Energietransferwegen in Proteinen, von denen angenommen wird, dass sie für Allosterie wichtig sind, vor. Allosterie ist ein grundlegendes Konzept der Biochemie, hiermit ist im allgemeinen eine Veränderung von Protein-Eigenschaften durch einen Effektor an einer entfernten Wechselwirkungsstelle gemeint. PDZ3 ist ein Modellsystem für Allosterie ohne konformationelle Änderungen, hier sind spezifische Energietransferwege von gekoppelten Aminosäure-Seitenketten u.a. mittels Molekulardynamiksimulationen prognostiziert worden. Über solche Energietransferwege könnte Information (z.B. über den Status von Ligandenbindung) von einer Seite des Proteins zur anderen vermittelt werden. Die Simulationen schlagen eine spezifische, anisotrope Wärmeleitung durchs Protein vor, die auf Pikosekundenzeitskala abläft. Dieser Prozess könnte durch Nutzung der in dieser Doktorarbeit entwickelten methodischen Ansätze erstmals im Experiment untersucht werden.

Teil 2: Definition und Charakterisierung neuer Observablen. Besonders aussichtsreiche Kandidaten für die Nutzung als neuartige ortsspezifische Schwingungssonden sind unnatürliche Aminosäuren. In den letzten Jahren wurden neuartige Ansätze in der chemischen Biologie entwickelt um funktionalisierte Aminosäuren mit nicht proteinogenen Seitenketten ortsspezifisch co-translational einzubauen. Die beiden Hauptansätze hierfür sind entweder die Nutzung eines zusätzlichen, künstlichen Codons und damit die Erweiterung des genetischen Codes (bekannt als *stop codon suppression oder genetic code expansion*) oder aber die Substitution einer proteinogenen Aminosäure durch ein Strukturanalogon. (bekannt als *supplementation based incorporation*)

In Kapitel 3 werden diese Methoden erklärt, sowie weitere Möglichkeiten für neuartige Schwingungssonden diskutiert. Neben dem ortsspezifischen und co-translationalen Einbau unnatürlicher Aminosäuren mit funktionellen Gruppen (wie z.B. Azid- oder Nitrilgruppen, deren Absorption bei $2100\,\mathrm{cm}^{-1}$ bzw. $2200\,\mathrm{cm}^{-1}$ liegt) in der Seitenkette, deren Infrarotabsorptionsbanden im Bereich zwischen $1800\,\mathrm{cm}^{-1}$ und $3000\,\mathrm{cm}^{-1}$ und damit im "biologisch freien Fensterliegen, ist für Peptide

	Cyanophenylalanin	Azidophenylalanin	Azidohomoalanin
Einbau:	Stop Codon Suppression	Stop Codon Suppression	Einbau als Met Analogon
IR:	$\bar{\nu} = 2251$ cm^{-1} $\epsilon = 194\ M^{-1}cm^{-1}$ $\tau = 1.07$ ps/4.64 ps	$\bar{\nu} = 2114$ cm^{-1} $\epsilon = 736\ M^{-1}cm^{-1}$ $\tau = 0.542$ ps/4.607 ps	$\bar{\nu} = 2099$ cm^{-1} $\epsilon = 506\ M^{-1}cm^{-1}$ $\tau = 0.83$ ps/4.89 ps
2D-IR:	hohe Anharmonizität, wenig spektrale Diffusion	Komplexes 2D-IR Spektrum aufgrund von Fermi Resonanz	ausgeprägte spektrale Diffusion, klare Linienform

Tabelle 5: Übersicht der (spektroskopischen) Eigenschaften der untersuchten unnatürlichen Aminosäuren in Bezug auf ihre Anwendbarkeit in Proteinen. Alle Werte sind für Messungen im Lösungsmittel Tetrahydrofuran, das als Referenz für Polarität im Proteininneren verwendet wird, gemessen.

und kleine Proteine auch eine Synthese möglich. Hier besteht dann die Möglichkeit von ortsspezifischer Isotopenmarkierung z.B. der Carbonylgruppe in der Peptidbindung oder aber auch der Einbau deuterierter Seitenketten. Eine weitere Alternative ist die post-translationale, chemische Modifikation eines Proteins. Ein Beispiel hierfür ist die Umwandlung des Thiols einer Cystein-Seitenkette in ein Thiocyanat, das auch im freien Fenster bei 2150 cm^{-1} absorbiert. Ein Nachteil dieses Ansatzes gegenüber dem co-translationalen Einbau ist der geringere Markierungsgrad einer Probe.

Im experimentellen in Kapitel 4 liegt der Fokus auf der Untersuchung von Azid- und Nitril-markierten Derivaten der Aminosäuren Phenylalanin und Alanin bezüglich ihrer Eignung als neuartige Schwingungsmarker in Proteinen. Ein neuer Schwingungsmarker sollte wichtige Voraussetzungen erfüllen. Einerseits muss der Extinktionskoeffizient der Absorptionsbande groß sein, um Signale von Proteinproben mit geringer Konzentration messen zu können. Des weiteren sollte das Absorptionsmaximum im freien Fenster von Biomolekülen zwischen 1800 cm^{-1} und 3000 cm^{-1} liegen und idealerweise nicht von Schwingungsmoden von H$_2$O oder D$_2$O überlagert sein. Außerdem sollte ein möglichst vielfältige einsetzbarer Marker auch photostabil im sichtbaren Spektralbereich sein, um Untersuchungen von Nichtgleichgewichtsprozessen mittels transienter 2D-IR Spektroskopie zu erlauben. Die Aminosäuren Azidophenylalanin, Azidohomoalanin, Cyanophenylalanin und Cyanoalanin sind auf diese Eigenschaften hin mittels FTIR und UV/Vis Spektroskopie untersucht worden. Um Informationen über strukturelle Dynamik und lokale Änderungen der Umgebung im Protein zu erhalten, sind Messungen der spektralen Diffusion mit 2D-IR erforderlich. Deswegen sollte ein neuer Schwingungsmarker selbst keine komplizierte Bandenform im 2D-IR zeigen, muss aber auflösbare spektrale Diffusion zeigen. Ein weiteres Kriterium ist die Schwingungslebensdauer, die bestimmt, welches Zeitfenster tatsächlich beobachtet werden kann. Schließlich ist es auch von Vorteil, wenn es möglich ist, Kreuzsignale zu anderen funktionellen Gruppen zu messen, dies kann z.B. in Untersuchungen zur Strukturaufklärung oder zur Messung von Schwingungsenergietransfer (der direkt Aufschluss über Wärmeleitung erlaubt) genutzt werden. Diese Eigenschaften sind mittels Breitband IR-Anreg-IR-Abtast-Spektroskopie sowie 2D-IR und 2-Farben-2D-IR untersucht worden. Eine Übersicht über die Ergebnisse ist in Tabelle 5 zu finden.

Aus den Experimenten ergibt sich, dass Azidohomoalanin der aussichtsreichste Kandidat für eine Nutzung in Proteinen ist. Diese Aminosäure kann als Methionin-Analogon in Proteine eingebaut werden, hat ein Absorptionsmaximum bei 2119 cm^{-1} (in Wasser) und ist damit sowohl in H$_2$O als auch D$_2$O nutzbar. Die Absorptionsbande hat eine klare Linienform (im Gegensatz zu Azidophenylalanin) und der Extinktionskoeffizient ist mit ca. 500 M^{-1}cm^{-1} ausreichend hoch. Die Azidbande ist im sichtbaren Spektralbereich photostabil und mit ca. 6 ps Schwingungslebensdauer sollte eine

Untersuchung des Zeitfensters zwischen 1 ps und 10 ps möglich sein. In den beiden folgenden Teilen der Doktorarbeit wurde Azidohomoalanin in verschiedenen Anwendungen genutzt.

Teil 3: Ortsspezifische Untersuchung von Protein-Mikroumgebung und lokaler Dynamik.
In Kapitel 5 wird am Beispiel der Ligandenbindung in der PDZ Domäne demonstriert, wie ein neuer Schwingungsmarker bereits in statischen FTIR Spektren eine Untersuchung ungeklärter biophysikalischer Fragestellungen erlaubt. Die Absorptionsbande des Azids der Azidohomoalanin-Seitenkette ist sensitiv für die Polarität ihrer Umgebung und wird außerdem durch die Bildung von Wasserstoffbrücken beeinflusst. Damit ist zwar keine direkte Messung des elektrischen Feldes möglich, aber dennoch kann die direkte Umgebung qualitativ untersucht werden. An sechs ausgewählten Positionen in PDZ, sowohl in der Bindungstasche, als auch im Inneren des Proteins sowie an der Oberfläche ist Azidohomoalanin eingebaut worden. Ein Vergleich mit bekannten Strukturdaten zeigt eine eindeutige Korrelation zwischen der Hydrophobizität der umliegenden Aminosäuren und dem Absorptionsmaximum. Außerdem ist die Ligandenbindung untersucht worden. Es ist möglich für direkt an der Bindung beteiligte bzw. der Bindetasche benachbarte Seitenketten eine Änderung der Hydrophobizität durch Ausschluss von Wasser aus der Bindetasche zu zeigen (Beispiel Mutante Ala376Aha). Außerdem konnten auch kleine konformationelle Änderungen durch die Peptidbindung beobachtet werden, allerdings nur für die drei Mutanten, die Teil des von Ota und Agard prognostizierten Transferweges sind. Für zwei andere Kontrollpositionen wurde keine Änderung der lokalen Umgebung gemessen. Dies ist ein erster experimenteller Hinweis auf die Existenz des prognostizierten Transferweges und zeigt wie die Nutzung neuer Schwingungslabel hilft um auch langreichweitige Effekte in Proteinen zu messen, die mit anderen Methoden wie Röntgenkristallographie oder NMR Spektroskopie bisher nicht beobachtet wurden.

Kapitel 6 zeigt erste 2D-IR Spektren von PDZ, das mit Azidohomoalanin markiert ist. Zwei Mutanten, PDZ-Ile327Aha und PDZ-Ala390Aha sind untersucht worden und es konnte gezeigt werden, dass es technisch möglich ist, 2D-IR Spektren dieser Proben in der Frequenzdomäne in Anreg-Abtast-Geometrie zu messen. Hierbei ist besonders zu beachten, dass die Proben in H_2O vorliegen, das bei 2125 cm^{-1}, also genau unter der Azid-Absorption eine Kombinationsschwingung hat und damit einerseits die optische Dichte der Proben so erhöht, dass Messungen nur mit Schichtdicken bis 50 μm möglich sind und andererseits ein zeitabhängiger Lösungsmittelhintergrund durch Wärmetransfer in den Spektren vorhanden ist. Die Korrektur der Spektren ist aber möglich, so dass aus den gemessen Daten Aufschlüsse über die lokale Dynamik gezogen werden können. Die Mutante PDZ-Ile327Aha ist sowohl ohne Ligand als auch im Komplex mit ihrem nativen Bindungspartner, dem CRIPT-Peptid in seiner Form als Heptamer gemessen worden. Die 2D-IR Spektren bestätigen die Tendenz aus den FTIR-Spektren derselben Mutante, dass eine bereits im ungebundenen Zustand vorliegende Proteinkonformation (von zwei anhand ihrer Azid-Absorption unterscheidbaren Konformationen) den Liganden bindet und scheinbar keine große konformationelle Änderung passiert. Dieses Ergebnis bestärkt die Vorhersage von Steiner und Caflish, die aus Moleklardynamik-Simulationen derselben PDZ-Domäne schließen, dass der Bindungsmechanismus konformationeller Selektion vorliegt. Die Mutante PDZ-Ala390Aha hat im FTIR die beiden am stärksten getrennten Sub-Ensemble gezeigt, auch im 2D-IR Spektrum lassen sich zwei Peaks unterscheiden, wobei die spektrale Auflösung nicht für eine detaillierte Analyse der spektralen Diffusion ausreicht. Aus der Analyse der zeitabhängigen Signalintensität für die zwei Maxima zeigt sich, dass eine der beiden Konformationen eine deutlich polarere Umgebung hat (da hier das Absorptionsmaximum bei höherer Wellenzahl vorliegt und die Relaxation ähnlich wie in reinem H_2O schneller ist) und die zweite Konformation eine unpolarere Umgebung hat. Ein weitergehendes

Experiment mit höherer spektraler Auflösung könnte hier Aufschluss über Seitenkettendynamik im Pikosekundenbereich geben.

Teil 4: Untersuchung von Energiefluss in Proteinen in Echtzeit. Schwingungsenergietransfer innerhalb von kleinen Molekülen ist ein gut studiertes Phänomen in der physikalischen Chemie. 2D-IR lässt sich gut für die Untersuchung von gerichtetem Schwingungsenergietransfer (VET) bzw. die Ausbreitung von Wärme durch niederfrequente Moden innerhalb eines Systems nutzen. Aber nicht nur in kleinen Systemen scheint dieser Mechanismus stattzufinden, sondern auch für Proteine sind Schwingungsenergietransferwege oder Netzwerke zwischen einzelnen Moden prognostiziert bzw. modelliert worden. Die in dieser Arbeit untersuchte PDZ Domäne ist eines der bekanntesten Beispiele. Das bereits zuvor beschriebene Netzwerk gekoppelter Aminosäurereste, das vermutlich eine Funktionalität für langreichweitige Kommunikation oder Allosterie im Protein besitzt, hat sich in einer Simulation mittels Wärmeleitung nachweisen lassen und auch für viele andere Proteine sind bereits ähnliche Transferwege simuliert worden. Jedoch fehlen experimentelle Ansätze um gerichtete Wärmeleitung in Proteinen ortsspezifisch zu messen. Der vierte Teil dieser Doktorarbeit beschäftigt sich mit dem experimentellen Nachweis und Anwendungsmöglichkeiten von Schwingungsenergietransfer in Systemen unterschiedlicher Größe mit dem Ziel einen experimentellen Ansatz für den Nachweis von Transferwegen in Proteinen zu entwickeln und zu testen.

Zunächst ist am Beispiel von Azidophenylalanin demonstriert worden, dass sich innerhalb einzelner unnatürlicher Aminosäuren Energietransfer zwischen einzelnen funktionellen Gruppen mittels 2Farben-2D-IR direkt verfolgen lässt. In Kapitel 7 werden die experimentell ermittelten Energietransferzeiten zur eindeutigen Zuordnung von FTIR-Absorptionsbanden genutzt und im Vergleich mit quantenchemischen Rechnungen zeigt sich hier eine interessante Anwendung dieser Technik für die Analytik.

Um gezielt Transferwege in komplexeren Systemen zu untersuchen ist die Verwendung spezifischer Marker, wie sie bereits in Teil 2 vorgeschlagen wurden, notwendig. Kapitel 8 diskutiert einen Lösungsansatz für dieses Problem. Aminosäuren mit Azid in der Seitenkette sind hervorragende Kandidaten für die Beobachtung von Energietransfer am Endpunkt eines Transferweges, jedoch ist eine initial größtmögliche Wärmeinjektion in das zu untersuchende System wünschenswert, um auch auf wenig effizienten Transferwegen, wie z.B. dem prognostizierten Weg in PDZ3, einen Schwingungsenergietransfer zu beobachten. Hierfür bedarf es eines anderen Chromophors der als Donor fungiert. Ein guter Kandidat ist Azulen, das bei 600 nm seinen ersten elektronischen Übergang von S_0 nach S_1 hat und die Absorptionsenergie mittels interner Konversion strahlungslos im elektronischen Grundzustand in angeregte Schwingungszustände umwandelt. So lässt sich innerhalb der Relaxationszeit von 1 ps ca. 10 mal mehr Schwingungsenergie am Startpunkt des Transferwegs deponieren als bei Nutzung eines Infrarot-Chromophors. Das vorgeschlagene Donor-Akzeptor-Paar für die Untersuchung von Schwingungsenergietransfer in Proteinen aus Azulenyl-Alanin und Azidohomoalanin ist in mehreren Modellpeptiden untersucht worden. Bei einem Abstand von ca. 2 nm in Bindungslängen ist immer noch ein ausreichendes Transfersignal für die Azidschwingung zu beobachten und weitere Experimente in verschiedenen Lösungsmitteln zeigen die Anwendbarkeit in Wasser.

Das abschließende Kapitel 9 dieser Doktorarbeit vereint die vorherigen Arbeiten, um erste Experimente auf dem Weg zur direkten zeitaufgelösten Messung des vorhergesagten Energietransferwegs in PDZ3 durchzuführen. Da der gleichzeitige Einbau verschiedener unnatürlicher Aminosäuren in ein Protein kompliziert und noch ineffizient ist, wurde ein anderer Ansatz gewählt um ein Mo-

dellsystem zu designen, dass sowohl Azulen als Donor als auch Azidohomoalanin als Akzeptor in PDZ3 enthält. Es wurde ein optimierter Peptidligand, abgeleitet vom nativen CRIPT Peptid, genutzt, der Azulen als c-terminalen Rest in direkter Nähe zum prognostizierten Startpunkt am His372 enthält. An dem Komplex aus PDZ-Ile341Aha und AzuKQTSV sind transiente Infrarotspektren aufgenommen worden und alle technischen Probleme, um diese Art von Proben zu messen, konnten gelöst werden. Allerdings konnte in den Experimenten kein Signal gemessen werden, außer einem Hintergrundsignal der erhitzten Wasserschwingung im gleichen Spektralbereich, das zeigt, dass die Messung technisch erfolgreich war. Somit steht eine abschließende Beurteilung über die Existenz des Energietransferweges weiterhin aus. Dennoch lässt sich ableiten, dass die Nutzung des vorgeschlagenen Donor-Akzeptor-Paares die experimentelle Untersuchung der lange vorhergesagten Theorie über Wärmeleitung im Protein ermöglicht.

Insgesamt konnte in dieser Doktorarbeit demonstriert werden, wie sich unnatürliche Aminosäuren als neuartige Schwingungsmarker für die zeitaufgelöste 2D-IR Spektroskopie und FTIR-Spektroskopie verwenden lassen und welche vielfältigen biophysikalischen Fragestellungen mit diesem Ansatz untersucht werden können. Im Rahmen dieser Arbeit sind viele weitere Ideen entwickelt worden, die im abschließenden Ausblick kurz vorgestellt werden.

References

[1] Villy Sundström. *Femtobiology.* Annu. Rev. Phys. Chem., 59:53–77, 2008 [1]

[2] Marten H. Vos and Jean-Louis L Martin. *Femtosecond processes in proteins.* Biochim. Biophys. Acta, 1411(1):1–20, 1999 [1]

[3] Katherine Henzler-Wildman and Dorothee Kern. *Dynamic personalities of proteins.* Nature, 450(7172):964–72, 2007 [1, 17, 20]

[4] Hans Frauenfelder, Benjamin H. McMahon, and Paul W. Fenimore. *Myoglobin: the hydrogen atom of biology and a paradigm of complexity.* Proc. Natl. Acad. Sci. U. S. A., 100(15):8615–7, 2003 [1, 43]

[5] Krzysztof Palczewski. *G protein-coupled receptor rhodopsin.* Annu. Rev. Biochem., 75:743–67, 2006 [1]

[6] Hyotcherl Ihee, Sudarshan Rajagopal, Vukica Šrajer, Reinhard Pahl, Spencer Anderson, Marius Schmidt, Friedrich Schotte, Philip A. Anfinrud, Michael Wulff, and Keith Moffat. *Visualizing reaction pathways in photoactive yellow protein from nanoseconds to seconds.* Proc. Natl. Acad. Sci. U. S. A., 102(20):7145–7150, 2005 [1]

[7] Eunjoon Kim and Morgan Sheng. *PDZ domain proteins of synapses.* Nat. Rev. Neurosci., 5(10):771–81, 2004 [1, 20]

[8] Wei Feng and Mingjie Zhang. *Organization and dynamics of PDZ-domain-related supramodules in the postsynaptic density.* Nat. Rev. Neurosci., 10(2):87–99, 2009 [1, 20]

[9] Rama Ranganathan and Steve W Lockless. *Evolutionarily Conserved Pathways of Energetic Connectivity in Protein Families.* Science, 286(5438):295–299, 1999 [1, 4, 17, 18, 20, 22, 60, 61, 70, 77, 113, 114, 115, 126, 127]

[10] Nobuyuki Ota and David A. Agard. *Intramolecular signaling pathways revealed by modeling anisotropic thermal diffusion.* J. Mol. Biol., 351(2):345–54, 2005 [1, 4, 17, 18, 19, 20, 22, 23, 59, 60, 61, 69, 70, 71, 74, 77, 82, 100, 113, 115, 116, 123, 124, 126, 127, 129]

[11] Marten H Vos. *Ultrafast dynamics of ligands within heme proteins.* Biochim. Biophys. Acta, 1777(1):15–31, 2008 [1]

[12] Andrea Nagy, Valentyn Prokhorenko, and R J Dwayne Miller. *Do we live in a quantum world? Advances in multidimensional coherent spectroscopies refine our understanding of quantum coherences and structural dynamics of biological systems.* Curr. Opin. Struct. Biol., 16(5):654–63, 2006 [1]

[13] Elspeth F Garman. *Developments in x-ray crystallographic structure determination of biological macromolecules.* Science, 343(6175):1102–8, 2014 [1]

[14] David S Goodsell, Stephen K Burley, and Helen M Berman. *Revealing structural views of biology.* Biopolymers, 99(11):817–24, 2013 [1]

[15] Research Collaboratory for Structural Bioinformatics. *PDB: Annual Report.* 2013 [1]

[16] Richard Phillips Feynman, Robert B Leighton, and Matthew L Sands. *The Feynman Lectures on Physics*, volume 1. Addison-Wesley, 1963. ISBN 0-201-02010-6 [1]

[17] Ron O. Dror, Robert M. Dirks, J. P. Grossman, Huafeng Xu, and David E. Shaw. *Biomolecular simulation: a computational microscope for molecular biology.* Annu. Rev. Biophys., 41:429–52, 2012 [1, 3]

[18] Martin Karplus and J Andrew McCammon. *Molecular dynamics simulations of biomolecules.* Nat. Struct. Biol., 9(9):646–52, 2002 [1, 3]

[19] John L Klepeis, Kresten Lindorff-Larsen, Ron O Dror, and David E Shaw. *Long-timescale molecular dynamics simulations of protein structure and function.* Curr. Opin. Struct. Biol., 19(2):120–7, 2009 [1, 3]

[20] Michael Levitt. *Nobel Lecture: Birth & Future of Multi-Scale Modeling of Biological Macromolecules.* Nobelprize.org. Nobel Media AB 2014., 2013 [1, 3]

[21] Britton Chance. *The stopped-flow method and chemical intermediates in enzyme reactions — a personal essay.* In J. Thomas Beatty, Howard Gest, and John F. Allen (editors), *Discov. Photosynth. Adv. Photosynth. Respir.*, volume 20 of *Advances in Photosynthesis and Respiration*, pp. 621–632. Springer-Verlag, Berlin/Heidelberg, 2005. ISBN 1-4020-3323-0 [1]

[22] Andrew J Baldwin and Lewis E Kay. *NMR spectroscopy brings invisible protein states into focus.* Nat. Chem. Biol., 5(11):808–14, 2009 [1]

[23] Ashok Sekhar and Lewis E Kay. *NMR paves the way for atomic level descriptions of sparsely populated, transiently formed biomolecular conformers.* Proc. Natl. Acad. Sci. U. S. A., 110(32):12867–74, 2013 [1, 20]

[24] Anthony Mittermaier and Lewis E Kay. *New tools provide new insights in NMR studies of protein dynamics.* Science, 312(5771):224–8, 2006 [1, 20]

[25] Nils A Lakomek, Teresa Carlomagno, Stefan Becker, Christian Griesinger, and Jens Meiler. *A thorough dynamic interpretation of residual dipolar couplings in ubiquitin.* J. Biomol. NMR, 34(2):101–15, 2006 [1]

[26] Judith Klein-Seetharaman, Naveena V K Yanamala, Fathima Javeed, Philip J Reeves, Elena V Getmanova, Michele C Loewen, Harald Schwalbe, and H Gobind Khorana. *Differential dynamics in the G protein-coupled receptor rhodopsin revealed by solution NMR.* Proc. Natl. Acad. Sci. U. S. A., 101(10):3409–13, 2004 [1]

[27] Ian R Kleckner and Mark P Foster. *An introduction to NMR-based approaches for measuring protein dynamics.* Biochim. Biophys. Acta, 1814(8):942–68, 2011 [1]

[28] Robert Silvers, Friederike Sziegat, Hideki Tachibana, Shin ichi Segawa, Sara Whittaker, Ulrich L Günther, Frank Gabel, Jie rong Huang, Martin Blackledge, Julia Wirmer-Bartoschek, and Harald Schwalbe. *Modulation of structure and dynamics by disulfide bond formation in unfolded states.* J. Am. Chem. Soc., 134(15):6846–54, 2012 [1]

[29] Paul J Sapienza and Andrew L Lee. *Using NMR to study fast dynamics in proteins: methods and applications.* Curr. Opin. Pharmacol., 10(6):723–30, 2010 [1]

[30] Jochen Stehle, Robert Silvers, Karla Werner, Deep Chatterjee, Santosh Gande, Frank Scholz, Arpana Dutta, Josef Wachtveitl, Judith Klein-Seetharaman, and Harald Schwalbe. *Characterization of the simultaneous decay kinetics of metarhodopsin states II and III in rhodopsin by solution-state NMR spectroscopy.* Angew. Chem. Int. Ed. Engl., 53(8):2078–84, 2014 [1]

[31] Ulrich K. Genick, Gloria E. O. Borgstahl, Kingman Ng, Zhong Ren, Claude Pradervand, Patrick M. Burke, Vukica Srajer, Tsu-Yi Teng, Wilfried Schildkamp, Duncan E. McRee, Keith Moffat, and Elizabeth D. Getzoff. *Structure of a Protein Photocycle Intermediate by Millisecond Time-Resolved Crystallography.* Science, 275(5305):1471–1475, 1997 [1]

[32] Friedrich Schotte, Manho Lim, Timothy A. Jackson, Aleksandr V. Smirnov, Jayashree Soman, John S. Olson, George N. Phillips, Michael Wulff, and Philip A. Anfinrud. *Watching a protein as it functions with 150-ps time-resolved x-ray crystallography.* Science, 300(5627):1944–7, 2003 [1]

[33] Friedrich Schotte, Hyun Sun, Ville R I Kaila, Hironari Kamikubo, Naranbaatar Dashdorj, Eric R Henry, Hyun Sun Cho, Timothy J Graber, Robert Henning, Michael Wulff, Gerhard Hummer, Mikio Kataoka, and Philip A. Anfinrud. *Watching a signaling protein function in real time via 100-ps time-resolved Laue crystallography.* Proc. Natl. Acad. Sci. U. S. A., 109(47):19256–61, 2012 [1]

[34] A H Zewail. *Laser femtochemistry.* Science, 242(4886):1645–53, 1988 [1]

[35] Ahmed H. Zewail. *Femtochemistry. Past, present, and future.* Pure Appl. Chem., 72(12):2219–2231, 2000 [1]

[36] Erik T. J. Nibbering, Henk Fidder, and Ehud Pines. *Ultrafast chemistry: using time-resolved vibrational spectroscopy for interrogation of structural dynamics.* Annu. Rev. Phys. Chem., 56:337–67, 2005 [1]

[37] Minheang Cho. *Two-Dimensional Optical Spectroscopy.* Boca Raton: CRC press, 2009 [1, 7]

[38] John T M Kennis and Marie-Louise Groot. *Ultrafast spectroscopy of biological photoreceptors.* Curr. Opin. Struct. Biol., 17(5):623–30, 2007 [1, 43]

[39] Marie Louise Groot, Luuk J G W van Wilderen, and Mariangela Di Donato. *Time-resolved methods in biophysics. 5. Femtosecond time-resolved and dispersed infrared spectroscopy on proteins.* Photochem. Photobiol. Sci., 6(5):501–7, 2007 [1, 3]

[40] Robin M Hochstrasser. *Two-dimensional spectroscopy at infrared and optical frequencies.* Proc. Natl. Acad. Sci. U. S. A., 104(36):14190–6, 2007 [2, 7]

[41] W. P. Aue, E. Bartholdi, and Richard R. Ernst. *Two-dimensional spectroscopy. Application to nuclear magnetic resonance.* J. Chem. Phys., 64(5):2229–46, 1976 [2, 9]

[42] Peter Hamm, Manho Lim, and Robin M. Hochstrasser. *Structure of the Amide I Band of Peptides Measured by Femtosecond Nonlinear-Infrared Spectroscopy.* J. Phys. Chem. B, 102(31):6123–6138, 1998 [2, 9, 10, 36, 134]

[43] Peter Hamm, Manho Lim, and Robin M. Hochstrasser. *Vibrational energy relaxation of the cyanide ion in water.* J. Chem. Phys., 107(24):10523, 1997 [2, 35]

[44] Peter Hamm and Martin T. Zanni. *Concepts and methods of 2D infrared spectroscopy.* Cambridge: Cambridge University Press, 2011 [2, 7, 10]

[45] Bredenbeck J Hamm P. Helbing J. *Two-dimensional Infrared Spectroscopy of Photoswitchable Peptides.* Annu. Rev. Phys. Chem., 59:291–317, 2008 [2]

[46] Jens Bredenbeck. *Transient 2D-IR Spectroscopy — Towards Ultrafast Structural Dynamics of Peptides and Proteins.* Diss. Univ. Zürich, 2005 [2, 9, 33, 36]

[47] Jens Bredenbeck, Jan Helbing, Karin Nienhaus, G. Ulrich Nienhaus, and Peter Hamm. *Protein ligand migration mapped by nonequilibrium 2D-IR exchange spectroscopy.* Proc. Natl. Acad. Sci. U. S. A., 104(36):14243–8, 2007 [2, 3, 9, 14, 36, 38, 43]

[48] Feng Ding and Martin T. Zanni. *Heterodyned 3D IR spectroscopy.* Chem. Phys., 341(1-3):95–105, 2007 [2]

[49] Neil T Hunt. *2D-IR spectroscopy: ultrafast insights into biomolecule structure and function.* Chem. Soc. Rev., 38(7):1837–48, 2009 [2, 9]

[50] Katrin Adamczyk, Marco Candelaresi, Kirsty Robb, Andrea Gumiero, Martin a Walsh, Anthony W Parker, Paul a Hoskisson, Nicholas P Tucker, and Neil T Hunt. *Measuring protein dynamics with ultrafast two-dimensional infrared spectroscopy.* Meas. Sci. Technol., 23(6):062001, 2012 [2, 7, 12]

[51] M. D. Fayer. *Dynamics of liquids, molecules, and proteins measured with ultrafast 2D IR vibrational echo chemical exchange spectroscopy.* Annu. Rev. Phys. Chem., 60:21–38, 2009 [2, 9]

[52] Yung Sam Kim and Robin M Hochstrasser. *Applications of 2D IR spectroscopy to peptides, proteins, and hydrogen-bond dynamics.* J. Phys. Chem. B, 113(24):8231–51, 2009 [2, 36, 42]

[53] John D. Hybl, Allison W. Albrecht, S M Gallagher Faeder, David M. Jonas, and Sarah M. Gallagher Faeder. *Two-dimensional electronic spectroscopy.* Chem. Phys. Lett., 297(3):307–313, 1998 [2, 9]

[54] David M Jonas. *Two-dimensional femtosecond spectroscopy.* Annu. Rev. Phys. Chem., 54:425–63, 2003 [2, 9]

[55] Jennifer P. Ogilvie and Kevin J. Kubarych. *Advances in Atomic Molecular and Optical Physics*, volume 57 of *Advances In Atomic, Molecular, and Optical Physics.* Elsevier, 2009. ISBN 9780-12-374799-0 [2, 9]

[56] Cristina Consani, Gerald Auböck, Frank van Mourik, and Majed Chergui. *Ultrafast tryptophan-to-heme electron transfer in myoglobins revealed by UV 2D spectroscopy.* Science, 339(6127):1586–9, 2013 [2, 9]

[57] Stefan Ruetzel, Meike Diekmann, Patrick Nuernberger, Christof Walter, Bernd Engels, and Tobias Brixner. *Multidimensional spectroscopy of photoreactivity.* Proc. Natl. Acad. Sci. U. S. A., 111(13):4764–9, 2014 [2, 9]

[58] Jens Bredenbeck, Avishek Ghosh, Marc Smits, and Mischa Bonn. *Ultrafast two dimensional-infrared spectroscopy of a molecular monolayer.* J. Am. Chem. Soc., 130(7):2152–3, 2008 [2, 9]

[59] Luuk J G W van Wilderen, Andreas T Messmer, and Jens Bredenbeck. *Mixed IR/Vis two-dimensional spectroscopy: chemical exchange beyond the vibrational lifetime and sub-ensemble selective photochemistry.* Angew. Chem. Int. Ed. Engl., 53(10):2667–72, 2014 [2, 9]

[60] Thomas A A Oliver, Nicholas H C Lewis, and Graham R Fleming. *Correlating the motion of electrons and nuclei with two-dimensional electronic-vibrational spectroscopy.* Proc. Natl. Acad. Sci. U. S. A., 111(28):10061–10066, 2014 [2, 9]

[61] Friedrich Siebert and Peter Hildebrandt. *Vibrational spectroscopy in life science.* Weinheim: Wiley-VCH, 2008. ISBN 9783-527-6213-5-4 [2, 8]

[62] Andreas Barth and Christian Zscherp. *What vibrations tell about proteins.* Q. Rev. Biophys., 35(4):369–430, 2002 [2, 7, 8, 33, 51]

[63] Andreas Barth. *Infrared spectroscopy of proteins.* Biochim. Biophys. Acta, 1767(9):1073–101, 2007 [2, 8, 33]

[64] Ronald Brudler, Robin Rammelsberg, Tammy T. Woo, Elizabeth D. Getzoff, and Klaus Gerwert. *Structure of the I1 early intermediate of photoactive yellow protein by FTIR spectroscopy.* Nat Struct Mol Biol, 8(3):265–270, 2001 [3]

[65] Klaus Gerwert, Benno Hess, Jörg Soppa, and Dieter Oesterhelt. *Role of aspartate-96 in proton translocation by bacteriorhodopsin.* Proc. Natl. Acad. Sci. U. S. A., 86(13):4943–7, 1989 [3]

[66] Florian Garczarek and Klaus Gerwert. *Functional waters in intraprotein proton transfer monitored by FTIR difference spectroscopy.* Nature, 439(7072):109–12, 2006 [3, 92]

[67] Kenichi Ataka, Tilman Kottke, and Joachim Heberle. *Thinner, smaller, faster: IR techniques to probe the functionality of biological and biomimetic systems.* Angew. Chemie, Int. Ed. English, 49(32):5416–24, 2010 [3, 92]

[68] Thomas Friedrich, Sven Geibel, Rolf Kalmbach, Igor Chizhov, Kenichi Ataka, Joachim Heberle, Martin Engelhard, and Ernst Bamberg. *Proteorhodopsin is a Light-driven Proton Pump with Variable Vectoriality.* J. Mol. Biol., 321(5):821–838, 2002 [3, 38]

[69] Karin Hauser, Carsten Krejtschi, Rong Huang, Ling Wu, and Timothy A Keiderling. *Site-specific relaxation kinetics of a tryptophan zipper hairpin peptide using temperature-jump IR spectroscopy and isotopic labeling.* J. Am. Chem. Soc., 130(10):2984–92, 2008 [3, 33]

[70] Petra Hellwig, Borries Rost, Ulrike Kaiser, Christian Ostermeier, Hartmut Michel, and Werner Mäntele. *Carboxyl group protonation upon reduction of the Paracoccus denitrificans cytochrome c oxidase: direct evidence by FTIR spectroscopy.* FEBS Lett., 385(1-2):53–57, 1996 [3]

[71] Ayanjeet Ghosh, Matthew J Tucker, and Robin M Hochstrasser. *Identification of arginine residues in peptides by 2D-IR echo spectroscopy.* J. Phys. Chem. A, 115(34):9731–8, 2011 [3]

References

[72] Ayanjeet Ghosh, Jade Qiu, William F DeGrado, and Robin M Hochstrasser. *Tidal surge in the M2 proton channel, sensed by 2D IR spectroscopy.* Proc. Natl. Acad. Sci. U. S. A., 108(15):6115–20, 2011 [3]

[73] Manho Lim, Timothy A Jackson, and Philip A Anfinrud. *Orientational distribution of CO before and after photolysis of MbCO and HbCO: a determination using time-resolved polarized Mid-IR spectroscopy.* J. Am. Chem. Soc., 126(25):7946–57, 2004 [3]

[74] Manho H Lim, Timothy A Jackson, and Philip A Anfinrud. *Ultrafast rotation and trapping of carbon monoxide dissociated from myoglobin.* Nature, 4(3):209–214, 1997 [3]

[75] Heejae Kim and Minhaeng Cho. *Infrared Probes for Studying the Structure and Dynamics of Biomolecules.* Chem. Rev., 2013 [4, 32, 35, 36, 60, 125]

[76] Matthias M. Waegele, Robert M Culik, and Feng Gai. *Site-Specific Spectroscopic Reporters of the Local Electric Field, Hydration, Structure, and Dynamics of Biomolecules.* J. Phys. Chem. Lett., 2(20):2598–2609, 2011 [4, 32, 34, 35, 36, 62, 93, 125]

[77] Zhaohui Wang, Andrei Pakoulev, and Dana D. Dlott. *Watching vibrational energy transfer in liquids with atomic spatial resolution.* Science, 296(5576):2201–3, 2002 [4, 27, 93, 100, 106, 128]

[78] Lei Wang and Peter G Schultz. *Expanding the genetic code.* Angew. Chemie, Int. Ed. English, 44(1):34–66, 2004 [4, 27, 32, 101]

[79] Kathryn C. Schultz, Lubica Supekova, Youngha Ryu, Jianming Xie, Roshan Perera, and Peter G. Schultz. *A genetically encoded infrared probe.* J. Am. Chem. Soc., 128(43):13984–5, 2006 [4, 27, 31, 32, 35, 55, 130]

[80] Michael Georg Hoesl and Nediljko Budisa. *Recent advances in genetic code engineering in Escherichia coli.* Curr. Opin. Biotechnol., 23(5):751–7, 2012 [4, 27, 28, 29, 101]

[81] Sandra Lepthien, Lars Merkel, and Nediljko Budisa. *In vivo double and triple labeling of proteins using synthetic amino acids.* Angew. Chemie, Int. Ed. English, 49(32):5446–50, 2010 [4, 27, 115]

[82] Shixin Ye, Thomas Huber, Reiner Vogel, and Thomas P Sakmar. *FTIR analysis of GPCR activation using azido probes.* Nat. Chem. Biol., 5(6):397–9, 2009 [4, 32, 36, 55, 59, 60, 93, 125, 127, 129]

[83] Shixin Ye, Ekaterina Zaitseva, Gianluigi Caltabiano, Gebhard F X Schertler, Thomas P Sakmar, Xavier Deupi, and Reiner Vogel. *Tracking G-protein-coupled receptor activation using genetically encoded infrared probes.* Nature, 464(7293):1386–9, 2010 [4, 32, 36, 55, 60, 127, 129]

[84] Santosh Kumar Jha, Minbiao Ji, Kelly J Gaffney, and Steven G Boxer. *Site-specific measurement of water dynamics in the substrate pocket of ketosteroid isomerase using time-resolved vibrational spectroscopy.* J. Phys. Chem. B, 116(37):11414–21, 2012 [4, 34, 36, 130]

[85] David M Leitner. *Frequency-resolved communication maps for proteins and other nanoscale materials.* J. Chem. Phys., 130(19):195101, 2009 [4, 19, 100, 124]

164

[86] Jens Bredenbeck, Jan Helbing, Christoph Kolano, and Peter Hamm. *Ultrafast 2D-IR spectroscopy of transient species.* ChemPhysChem, 8(12):1747–56, 2007 [7, 9, 33, 79]

[87] Shaul Mukamel. *Principles of Nonlinear Optical Spectroscopy (Oxford Series on Optical and Imaging Sciences).* Oxford University Press, Oxford, 1999 [7]

[88] Martina Wolpert and Petra Hellwig. *Infrared spectra and molar absorption coefficients of the 20 alpha amino acids in aqueous solutions in the spectral range from 1800 to 500 cm(-1).* Spectrochim. Acta. A. Mol. Biomol. Spectrosc., 64(4):987–1001, 2006 [8, 105]

[89] Andreas Barth. *The infrared absorption of amino acid side chains.* Prog. Biophys. Mol. Biol., 74(3-5):141–73, 2000 [8, 105]

[90] John B. Asbury, Tobias Steinel, C. Stromberg, S. A. Corcelli, C. P. Lawrence, J. L. Skinner, and M. D. Fayer. *Water Dynamics: Vibrational Echo Correlation Spectroscopy and Comparison to Molecular Dynamics Simulations.* J. Phys. Chem. A, 108(7):1107–1119, 2004 [9]

[91] D Kraemer, M L Cowan, A Paarmann, N Huse, E T J Nibbering, T Elsaesser, and R J Dwayne Miller. *Temperature dependence of the two-dimensional infrared spectrum of liquid H2O.* Proc. Natl. Acad. Sci. U. S. A., 105(2):437–42, 2008 [9]

[92] A Paarmann, T Hayashi, S Mukamel, and R J D Miller. *Probing intermolecular couplings in liquid water with two-dimensional infrared photon echo spectroscopy.* J. Chem. Phys., 128(19):191103, 2008 [9]

[93] H J Bakker and J L Skinner. *Vibrational spectroscopy as a probe of structure and dynamics in liquid water.* Chem. Rev., 110(3):1498–517, 2010 [9]

[94] Sander Woutersen and Peter Hamm. *Structure Determination of Trialanine in Water Using Polarization Sensitive Two-Dimensional Vibrational Spectroscopy.* J. Phys. Chem. B, 104(47):11316–11320, 2000 [9, 14]

[95] Sander Woutersen and Peter Hamm. *Nonlinear two-dimensional vibrational spectroscopy of peptides.* J. Phys. Condens. Matter, 14(39):R1035–R1062, 2002 [9, 14, 36]

[96] Peter Hamm and Robin M Hochstrasser. *Structure and dynamics of proteins and peptides: Femtosecond two-dimensional infrared spectroscopy in "Ultrafast Infrared and Raman Spectroscopy".* In Michael D Fayer (editor), *Ultrafast Infrared Raman Spectrosc.* Marcel Dekker, New York, 2001 [9]

[97] A. I. Stewart, I. P. Clark, M. Towrie, S. K. Ibrahim, A. W. Parker, C. J. Pickett, and N. T. Hunt. *Structure and vibrational dynamics of model compounds of the [FeFe]-hydrogenase enzyme system via ultrafast two-dimensional infrared spectroscopy.* J. Phys. Chem. B, 112(32):10023–32, 2008 [9]

[98] Andreas T Messmer, Katharina M Lippert, Peter R Schreiner, and Jens Bredenbeck. *Structure analysis of substrate catalyst complexes in mixtures with ultrafast two-dimensional infrared spectroscopy.* Phys. Chem. Chem. Phys., 15(5):1509–17, 2013 [9, 14]

[99] Andreas T. Messmer, Katharina M. Lippert, Sabrina Steinwand, Eliza-Beth W. Lerch, Kira Hof, David Ley, Dennis Gerbig, Heike Hausmann, Peter R. Schreiner, and Jens Bredenbeck.

Two-dimensional infrared spectroscopy reveals the structure of an Evans auxiliary derivative and its SnCl4 Lewis acid complex. Chem. - A Eur. J., 18(47):14989–95, 2012 [9, 14, 80, 128, 144]

[100] Junrong Zheng, Kyungwon Kwak, John Asbury, Xin Chen, Ivan R Piletic, and M D Fayer. *Ultrafast dynamics of solute-solvent complexation observed at thermal equilibrium in real time.* Science, 309(5739):1338–43, 2005 [9, 14]

[101] Kyungwon Kwak, Junrong Zheng, Hu Cang, and M D Fayer. *Ultrafast two-dimensional infrared vibrational echo chemical exchange experiments and theory.* J. Phys. Chem. B, 110(40):19998–20013, 2006 [9]

[102] Junrong Zheng, Kyungwon Kwak, and M D Fayer. *Ultrafast 2D IR vibrational echo spectroscopy.* Acc. Chem. Res., 40(1):75–83, 2007 [9]

[103] Haruto Ishikawa, Kyungwon Kwak, Jean K Chung, Seongheun Kim, and Michael D Fayer. *Direct observation of fast protein conformational switching.* Proc. Natl. Acad. Sci. U. S. A., 105(25):8619–24, 2008 [9]

[104] Dmitry V. Kurochkin, Sri Ram G. Naraharisetty, and Igor V. Rubtsov. *A relaxation-assisted 2D IR spectroscopy method.* Proc. Natl. Acad. Sci. U. S. A., 104(36):14209–14, 2007 [9, 15, 48, 49, 93, 106]

[105] Dmitry V. Kurochkin, Sri Ram G. Naraharisetty, and Igor V. Rubtsov. *Dual-Frequency 2D IR on Interaction of Weak and Strong IR Modes.* J. Phys. Chem. A, 109(48):10799–10802, 2005 [9]

[106] Igor V. Rubtsov. *Relaxation-assisted two-dimensional infrared (RA 2DIR) method: accessing distances over 10 A and measuring bond connectivity patterns.* Acc. Chem. Res., 42(9):1385–94, 2009 [9, 100, 105]

[107] Ellen H G Backus, Robbert Bloem, Rolf Pfister, Alessandro Moretto, Marco Crisma, Claudio Toniolo, and Peter Hamm. *Dynamical transition in a small helical peptide and its implication for vibrational energy transport.* J. Phys. Chem. B, 113(40):13405–9, 2009 [9]

[108] Marco Schade, Alessandro Moretto, Marco Crisma, Claudio Toniolo, and Peter Hamm. *Vibrational energy transport in peptide helices after excitation of C-D modes in Leu-d10.* J. Phys. Chem. B, 113(40):13393–7, 2009 [9, 33, 100, 107, 125]

[109] Ellen H G Backus, Phuong H Nguyen, Virgiliu Botan, Rolf Pfister, Alessandro Moretto, Marco Crisma, Claudio Toniolo, Gerhard Stock, and Peter Hamm. *Energy transport in peptide helices: a comparison between high- and low-energy excitations.* J. Phys. Chem. B, 112(30):9091–9, 2008 [9, 15, 20, 128]

[110] Ellen H G Backus, Phuong H Nguyen, Virgiliu Botan, Alessandro Moretto, Marco Crisma, Claudio Toniolo, Oliver Zerbe, Gerhard Stock, and Peter Hamm. *Structural Flexibility of a Helical Peptide Regulates Vibrational Energy Transport Properties.* Science, pp. 15487–15492, 2008 [9, 15]

[111] Henrike M. Müller-Werkmeister, Yun-Liang Li, Eliza-Beth W. Lerch, Damien Bigourd, and Jens Bredenbeck. *Ultrafast hopping from band to band: assigning infrared spectra based on vibrational energy transfer.* Angew. Chem. Int. Ed. Engl., 52(24):6214–7, 2013 [9, 15, 91, 92, 94, 95, 96, 100, 105, 107]

[112] Henrike M. Müller-Werkmeister and Jens Bredenbeck. *A donor-acceptor pair for the real time study of vibrational energy transfer in proteins.* Phys. Chem. Chem. Phys., 16(7):3261–6, 2014 [9, 20, 29, 99, 100, 102, 103, 104, 105, 106, 107, 115, 128]

[113] Lauren P. DeFlores, Ziad Ganim, Rebecca A. Nicodemus, and Andrei Tokmakoff. *Amide I'-II' 2D IR Spectroscopy Provides Enhanced Protein Secondary Structural Sensitivity.* J. Am. Chem. Soc., 131(9):3385–3391, 2009 [9, 36]

[114] Prabuddha Mukherjee, Itamar Kass, Isaiah T. Arkin, and Martin T. Zanni. *Picosecond dynamics of a membrane protein revealed by 2D IR.* Proc. Natl. Acad. Sci. U. S. A., 103(10):3528–33, 2006 [9, 33]

[115] Martin Gruebele, Chris T. Middleton, Ann Marie Woys, Sudipta S. Mukherjee, and Martin T. Zanni. *Residue-specific structural kinetics of proteins through the union of isotope labeling, mid-IR pulse shaping, and coherent 2D IR spectroscopy.* Methods, 52(1):12–22, 2010 [9]

[116] Ayanjeet Ghosh, Matthew J Tucker, and Feng Gai. *2D IR Spectroscopy of Histidine: Probing Side-Chain Structure and Dynamics via Backbone Amide Vibrations.* J. Phys. Chem. B, 118(28):7799–805, 2014 [9]

[117] Hoi Sung Chung, Ziad Ganim, Kevin C Jones, and Andrei Tokmakoff. *Transient 2D IR spectroscopy of ubiquitin unfolding dynamics.* Proc. Natl. Acad. Sci. U. S. A., 104(36):14237–42, 2007 [9, 36, 130]

[118] Ilya J Finkelstein, Haruto Ishikawa, Seongheun Kim, Aaron M Massari, and M D Fayer. *Substrate binding and protein conformational dynamics measured by 2D-IR vibrational echo spectroscopy.* Proc. Natl. Acad. Sci. U. S. A., 104(8):2637–42, 2007 [9, 79, 86]

[119] Tobias Brixner, Jens Stenger, Harsha M. Vaswani, Minhaeng Cho, Robert E. Blankenship, and Graham R. Fleming. *Two-dimensional spectroscopy of electronic couplings in photosynthesis.* Nature, 434(7033):625–628, 2005 [9]

[120] Jens Bredenbeck, Jan Helbing, J Wachtveitl, and Peter Hamm. *Transient 2D-IR Spectroscopy: Towards Measuring Ultrafast Structural Dynamics.* biophys.uni-frankfurt.de, 2004 [9, 33]

[121] Jens Bredenbeck, Jan Helbing, Raymond Behrendt, Christian Renner, Luis Moroder, Josef Wachtveitl, and Peter Hamm. *Transient 2D-IR Spectroscopy: Snapshots of the Nonequilibrium Ensemble during the Picosecond Conformational Transition of a Small Peptide.* J. Phys. Chem. B, 107(33):8654–8660, 2003 [9]

[122] Hoi Sung Chung, Ali Shandiz, Tobin R Sosnick, and Andrei Tokmakoff. *Probing the folding transition state of ubiquitin mutants by temperature-jump-induced downhill unfolding.* Biochemistry, 47(52):13870–7, 2008 [10]

[123] Rebecca A. Nicodemus, Krupa Ramasesha, Sean T. Roberts, and Andrei Tokmakoff. *Hydrogen Bond Rearrangements in Water Probed with Temperature-Dependent 2D IR.* J. Phys. Chem. Lett., 1(7):1068–1072, 2010 [10]

[124] Kevin C Jones, Chunte Sam Peng, and Andrei Tokmakoff. *Folding of a heterogeneous β-hairpin peptide from temperature-jump 2D IR spectroscopy.* Proc. Natl. Acad. Sci. U. S. A., 110(8):2828–33, 2013 [10]

[125] Carlos R. Baiz, Mike Reppert, and Andrei Tokmakoff. *An Introduction to Protein 2D IR Spectroscopy*. In Michael Fayer (editor), *Ultrafast Infrared Vib. Spectrosc.*, chapter 12, pp. 361–404. CRC Press, 2013. ISBN 9781-466-5101-3-5 [10, 130]

[126] Martin T. Zanni, Matthew C. Asplund, and Robin M. Hochstrasser. *Two-dimensional heterodyned and stimulated infrared photon echoes of N-methylacetamide-D.* J. Chem. Phys., 114(10):4579, 2001 [10]

[127] Valentina Cervetto, Jan Helbing, Jens Bredenbeck, and Peter Hamm. *Double-resonance versus pulsed Fourier transform two-dimensional infrared spectroscopy: an experimental and theoretical comparison.* J. Chem. Phys., 121(12):5935–42, 2004 [10, 13, 14]

[128] Lauren P. DeFlores, Rebecca A. Nicodemus, and Andrei Tokmakoff. *Two-dimensional Fourier transform spectroscopy in the pump-probe geometry.* Opt. Lett., 32(20):2966, 2007 [10]

[129] Jan Helbing and Peter Hamm. *Compact implementation of Fourier transform two-dimensional IR spectroscopy without phase ambiguity.* J. Opt. Soc. Am. B, 28(1):171, 2010 [10]

[130] Daniele Brida, Cristian Manzoni, and Giulio Cerullo. *Phase-locked pulses for two-dimensional spectroscopy by a birefringent delay line.* Opt. Lett., 37(15):3027–9, 2012 [10]

[131] Sang-Hee Shim, David B. Strasfeld, Eric C. Fulmer, and Martin T. Zanni. *Femtosecond pulse shaping directly in the mid-IR using acousto-optic modulation.* Opt. Lett., 31(6):838, 2006 [10]

[132] Sang-Hee Shim, David B Strasfeld, Yun L Ling, and Martin T Zanni. *Automated 2D IR spectroscopy using a mid-IR pulse shaper and application of this technology to the human islet amyloid polypeptide.* Proc. Natl. Acad. Sci. U. S. A., 104(36):14197–202, 2007 [10]

[133] Sang-Hee Shim and Martin T Zanni. *How to turn your pump-probe instrument into a multidimensional spectrometer: 2D IR and Vis spectroscopies via pulse shaping.* Phys. Chem. Chem. Phys., 11(5):748–61, 2009 [10]

[134] Peter Hamm, Robert A. Kaindl, and Jens Stenger. *Noise suppression in femtosecond midinfrared light sources.* Opt. Lett., 25(24):1798–800, 2000 [10, 16, 133]

[135] Kusai a. Merchant, W. G. Noid, David E. Thompson, Ryo Akiyama, Roger F. Loring, and M. D. Fayer. *Structural Assignments and Dynamics of the A Substates of MbCO: Spectrally Resolved Vibrational Echo Experiments and Molecular Dynamics Simulations.* J. Phys. Chem. B, 107(1):4–7, 2003 [12]

[136] Megan C Thielges and Michael D Fayer. *Protein dynamics studied with ultrafast two-dimensional infrared vibrational echo spectroscopy.* Acc. Chem. Res., 45(11):1866–74, 2012 [12, 32, 87]

[137] John T King, Evan J Arthur, Charles L Brooks, and Kevin J Kubarych. *Site-specific hydration dynamics of globular proteins and the role of constrained water in solvent exchange with amphiphilic cosolvents.* J. Phys. Chem. B, 116(19):5604–11, 2012 [12, 33, 87, 125, 127]

[138] John T King and Kevin J Kubarych. *Site-specific coupling of hydration water and protein flexibility studied in solution with ultrafast 2D-IR spectroscopy.* J. Am. Chem. Soc., 134(45):18705–12, 2012 [12, 33, 125]

[139] Robbert Bloem, Klemens Koziol, Steven A Waldauer, Brigitte Buchli, Reto Walser, Brighton Samatanga, Ilian Jelesarov, and Peter Hamm. *Ligand binding studied by 2D IR spectroscopy using the azidohomoalanine label.* J. Phys. Chem. B, 116(46):13705–12, 2012 [12, 40, 53, 54, 56, 62, 77, 86, 87, 125]

[140] Sayan Bagchi, Steven G Boxer, and Michael D Fayer. *Ribonuclease S dynamics measured using a nitrile label with 2D IR vibrational echo spectroscopy.* J. Phys. Chem. B, 116(13):4034–42, 2012 [12, 55, 130]

[141] Andreas T. Messmer. *Shedding Light on Reaction Mechanisms- Structure Determination of Reactive Intermediates and Investigation of Protein Structural Dynamics Using 2D-IR Spectroscopy.* Ph.D. thesis, Frankfurt, 2012 [14, 133]

[142] Munira Khalil, Nurettin Demirdöven, and Andrei Tokmakoff. *Coherent 2D IR Spectroscopy: Molecular Structure and Dynamics in Solution.* J. Phys. Chem. A, 107(27):5258–5279, 2003 [14, 33]

[143] James F Cahoon, Karma R Sawyer, Jacob P Schlegel, and Charles B Harris. *Determining transition-state geometries in liquids using 2D-IR.* Science, 319(5871):1820–3, 2008 [14]

[144] Zhiwei Lin and Igor V Rubtsov. *Constant-speed vibrational signaling along polyethyleneglycol chain up to 60-Ådistance.* Proc. Natl. Acad. Sci. U. S. A., 109(5):1413–8, 2012 [15, 93, 106, 107, 124, 128]

[145] D. Schwarzer, P. Kutne, C. Schröder, and J. Troe. *Intramolecular vibrational energy redistribution in bridged azulene-anthracene compounds: ballistic energy transport through molecular chains.* J. Chem. Phys., 121(4):1754–64, 2004 [15, 20, 93, 102, 107]

[146] David M. Leitner. *Thermal boundary conductance and thermal rectification in molecules.* J. Phys. Chem. B, 117(42):12820–8, 2013 [15, 19, 102]

[147] Xin Yu and David M. Leitner. *Anomalous diffusion of vibrational energy in proteins.* J. Chem. Phys., 119(23):12673, 2003 [15, 100, 124, 129]

[148] David M Leitner. *Energy flow in proteins.* Annu. Rev. Phys. Chem., 59(1):233–59, 2008 [15, 17, 19, 93, 100, 113, 124, 129]

[149] Marco Schade and Peter Hamm. *Transition from IVR limited vibrational energy transport to bulk heat transport.* Chem. Phys., 393(1):46–50, 2012 [15, 124]

[150] D. Schwarzer, C. Hanisch, P. Kutne, and J. Troe. *Vibrational Energy Transfer in Highly Excited Bridged Azulene-Aryl Compounds: Direct Observation of Energy Flow through Aliphatic Chains and into the Solvent.* J. Phys. Chem. A, 106(35):8019–8028, 2002 [15, 20, 101, 102, 107]

[151] Sri Ram G Naraharisetty, Valeriy M Kasyanenko, and Igor V Rubtsov. *Bond connectivity measured via relaxation-assisted two-dimensional infrared spectroscopy.* J. Chem. Phys., 128(May 2011):104502, 2008 [15]

[152] Virgiliu Botan, Ellen H G Backus, Rolf Pfister, Alessandro Moretto, Marco Crisma, Claudio Toniolo, Phuong H Nguyen, Gerhard Stock, and Peter Hamm. *Energy transport in peptide helices.* Proc. Natl. Acad. Sci. U. S. A., 104(31):12749–54, 2007 [15, 20, 100, 102, 124, 128]

References

[153] Igor V. Rubtsov, Jianping Wang, and Robin M. Hochstrasser. *Dual-frequency 2D-IR spectroscopy heterodyned photon echo of the peptide bond.* Proc. Natl. Acad. Sci. U. S. A., 100(10):5601–6, 2003 [16, 48, 49]

[154] Hongtao Bian, Jiebo Li, Xiewen Wen, Zhigang Sun, Jian Song, Wei Zhuang, and Junrong Zheng. *Mapping molecular conformations with multiple-mode two-dimensional infrared spectroscopy.* J. Phys. Chem. A, 115(15):3357–65, 2011 [16]

[155] ed. David M. Leitner and John E. Straub. *Proteins: Energy, Heat and Signal Flow (Computations in Chemistry).* CRC Press, Boca Raton, US, 1st edition, 2009 [17, 19, 100, 124, 129]

[156] Hiroshi Fujisaki and John E Straub. *Vibrational energy relaxation in proteins.* Proc. Natl. Acad. Sci. U. S. A., 102(19):6726–31, 2005 [17, 19, 100, 124, 129]

[157] Anne Dhulesia, Joerg Gsponer, and Michele Vendruscolo. *Mapping of two networks of residues that exhibit structural and dynamical changes upon binding in a PDZ domain protein.* J. Am. Chem. Soc., 130(28):8931–9, 2008 [17, 21, 23]

[158] Pavel I Zhuravlev and Garegin a Papoian. *Protein functional landscapes, dynamics, allostery: a tortuous path towards a universal theoretical framework.* Q. Rev. Biophys., 43(3):295–332, 2010 [17, 19]

[159] Gürol M Süel, Steve W Lockless, Mark a Wall, and Rama Ranganathan. *Evolutionarily conserved networks of residues mediate allosteric communication in proteins.* Nat. Struct. Biol., 10(1):59–69, 2003 [17, 113]

[160] Yao Xu and David M Leitner. *Communication Maps of Vibrational Energy Transport Through Photoactive Yellow Protein.* J. Phys. Chem. A, 2014 [17, 23, 113, 129]

[161] Yao Xu and David M Leitner. *Vibrational Energy Flow through the Green Fluorescent Protein-Water Interface: Communication Maps and Thermal Boundary Conductance.* J. Phys. Chem. B, 2014 [17, 113, 129]

[162] Qiang Cui and Martin Karplus. *Allostery and cooperativity revisited.* Protein Sci., 17(8):1295–307, 2008 [17, 18]

[163] Vincent J. Hilser, James O. Wrabl, and Hesam N. Motlagh. *Structural and energetic basis of allostery.* Annu. Rev. Biophys., 41:585–609, 2012 [17]

[164] Shiou-Ru Tzeng and Charalampos G Kalodimos. *Protein dynamics and allostery: an NMR view.* Curr. Opin. Struct. Biol., 21(1):62–7, 2011 [17, 20]

[165] Joanna F Swain and Lila M Gierasch. *The changing landscape of protein allostery.* Curr. Opin. Struct. Biol., 16(1):102–108, 2006 [17, 18, 19]

[166] Nina M Goodey and Stephen J Benkovic. *Allosteric regulation and catalysis emerge via a common route.* Nat. Chem. Biol., 4(8):474–82, 2008 [17, 18, 19]

[167] Kim Sharp and John J Skinner. *Pump-Probe Molecular Dynamics as a Tool for Studying Protein Motion and Long Range Coupling.* Bioinformatics, 361(April):347–361, 2006 [17, 20, 23, 100, 113]

[168] Yifei Kong and Martin Karplus. *Signaling pathways of PDZ2 domain: a molecular dynamics interaction correlation analysis.* Proteins, 74(1):145–54, 2009 [17, 20, 23, 113]

[169] Hesam N Motlagh, James O Wrabl, Jing Li, and Vincent J Hilser. *The ensemble nature of allostery.* Nature, 508(7496):331–9, 2014 [17, 18]

[170] Jacques Monod, Jeffries Wyman, and Jean-Pierre Changeux. *On the nature of allosteric transitions: a plausible model.* J. Mol. Biol., 12:88–118, 1965 [17]

[171] Jean-Pierre Changeux. *Allostery and the Monod-Wyman-Changeux model after 50 years.* Annu. Rev. Biophys., 41:103–33, 2012 [17]

[172] Jeremy M. Berg, John L. Tymoczko, and Lubert Stryer. *Biochemistry 5th edition.* New York: W H Freeman, 2002. ISBN 0-7167-3051-0 [17]

[173] Robert G Smock and Lila M Gierasch. *Sending signals dynamically.* Science, 324(5924):198–203, 2009 [18, 19, 73]

[174] A. Cooper and D. T. F. Dryden. *Allostery without conformational change.* Eur. Biophys. J., 11(2):103–109, 1984 [18]

[175] Dennis Bray and Thomas Duke. *Conformational spread: the propagation of allosteric states in large multiprotein complexes.* Annu. Rev. Biophys. Biomol. Struct., 33:53–73, 2004 [18]

[176] Jean-Pierre Changeux and Stuart J Edelstein. *Allosteric mechanisms of signal transduction.* Science, 308(5727):1424–8, 2005 [18]

[177] H Frauenfelder, S. Sligar, and P. Wolynes. *The energy landscapes and motions of proteins.* Science, 254(5038):1598–1603, 1991 [19]

[178] Xin Yu and David M. Leitner. *Vibrational Energy Transfer and Heat Conduction in a Protein.* J. Phys. Chem. B, 107(7):1698–1707, 2003 [19, 129]

[179] Thomas L. Rodgers, Philip D. Townsend, David Burnell, Matthew L. Jones, Shane A. Richards, Tom C. B. McLeish, Ehmke Pohl, Mark R. Wilson, and Martin J. Cann. *Modulation of global low-frequency motions underlies allosteric regulation: demonstration in CRP/FNR family transcription factors.* PLoS Biol., 11(9):e1001651, 2013 [19]

[180] Diane E. Sagnella and John E. Straub. *Directed Energy "Funneling" Mechanism for Heme Cooling Following Ligand Photolysis or Direct Excitation in Solvated Carbonmonoxy Myoglobin.* J. Phys. Chem. B, 105(29):7057–7063, 2001 [19, 100]

[181] Yasuhisa Mizutani and Teizo Kitagawa. *Direct Observation of Cooling of Heme Upon Photodissociation of Carbonmonoxy Myoglobin.* Science, 278(5337):443–446, 1997 [20, 101]

[182] Diane E Sagnella, John E Straub, Timothy A Jackson, Manho Lim, and Philip A Anfinrud. *Vibrational population relaxation of carbon monoxide in the heme pocket of photolyzed carbonmonoxy myoglobin: comparison of time-resolved mid-IR absorbance experiments and molecular dynamics simulations.* Proc. Natl. Acad. Sci. U. S. A., 96(25):14324–9, 1999 [20]

[183] Wolfgang J Schreier, Tobias Aumüller, Karin Haiser, Florian O Koller, Markus Löweneck, Hans-Jürgen Musiol, Tobias E Schrader, Thomas Kiefhaber, Luis Moroder, and Wolfgang Zinth. *Following the energy transfer in and out of a polyproline-peptide.* Biopolymers, 100(1):38–50, 2013 [20, 100]

[184] Naoki Fujii, Misao Mizuno, Haruto Ishikawa, and Yasuhisa Mizutani. *Observing Vibrational Energy Flow in a Protein with the Spatial Resolution of a Single Amino Acid Residue.* J. Phys. Chem. Lett., p. 140905164629000, 2014 [20, 101]

[185] Dorothee Kern and Erik RP Zuiderweg. *The role of dynamics in allosteric regulation.* Curr. Opin. Struct. Biol., 13(6):748–57, 2003 [20]

[186] Ernesto J. Fuentes, Channing J. Der, and Andrew L. Lee. *Ligand-dependent Dynamics and Intramolecular Signaling in a PDZ Domain.* J. Mol. Biol., 335(4):1105–1115, 2004 [20, 21, 23]

[187] Celestine N Chi, Anders Bach, Kristian Strømgaard, Stefano Gianni, and Per Jemth. *Ligand binding by PDZ domains.* Biofactors, 38(5):338–48, 2012 [20, 70, 127]

[188] Chad M. Petit, Jun Zhang, Paul J. Sapienza, Ernesto J. Fuentes, and Andrew L. Lee. *Hidden dynamic allostery in a PDZ domain.* Proc. Natl. Acad. Sci. U. S. A., 106(43):18249–54, 2009 [20, 23, 61, 64, 68, 69, 70, 127, 140]

[189] Brigitte Buchli, Steven a Waldauer, Reto Walser, Mateusz L Donten, Rolf Pfister, Nicolas Blöchliger, Sandra Steiner, Amedeo Caflisch, Oliver Zerbe, and Peter Hamm. *Kinetic response of a photoperturbed allosteric protein.* Proc. Natl. Acad. Sci. U. S. A., 110(29):11725–30, 2013 [20, 23]

[190] Per Jemth and Stefano Gianni. *PDZ domains: folding and binding.* Biochemistry, 46(30):8701–8, 2007 [20]

[191] Claire Nourry, Seth G. N. Grant, and Jean-Paul Borg. *PDZ domain proteins: plug and play!* Sci. STKE, 2003(179):RE7, 2003 [20]

[192] Craig C. Garner, Joanne Nash, and Richard L. Huganir. *PDZ domains in synapse assembly and signalling.* Trends Cell Biol., 10(7):274–280, 2000 [20]

[193] Lieke C J van den Berk, Elena Landi, Tine Walma, Geerten W Vuister, Luciana Dente, and Wiljan J a J Hendriks. *An allosteric intramolecular PDZ-PDZ interaction modulates PTP-BL PDZ2 binding specificity.* Biochemistry, 46(47):13629–37, 2007 [20]

[194] Z Songyang, A S Fanning, C Fu, J Xu, S M Marfatia, A H Chishti, A Crompton, A C Chan, J M Anderson, and L C Cantley. *Recognition of unique carboxyl-terminal motifs by distinct PDZ domains.* Science, 275(5296):73–7, 1997 [20]

[195] Tony Pawson and John D. Scott. *Signaling through scaffold, anchoring, and adaptor proteins.* Science, 278(5346):2075–80, 1997 [21]

[196] Ilya Bezprozvanny and Anton Maximov. *PDZ domains: More than just a glue.* Proc. Natl. Acad. Sci. U. S. A., 98(3):787–9, 2001 [21]

[197] Celestine N Chi, Lisa Elfström, Yao Shi, Tord Snäll, Ake Engström, and Per Jemth. *Reassessing a sparse energetic network within a single protein domain.* Proc. Natl. Acad. Sci. U. S. A., 105(12):4679–84, 2008 [21, 23, 70, 126]

[198] Stefano Gianni, Ake Engström, Mårten Larsson, Nicoletta Calosci, Francesco Malatesta, Lars Eklund, Chi Celestine Ngang, Carlo Travaglini-Allocatelli, and Per Jemth. *The kinetics of PDZ domain-ligand interactions and implications for the binding mechanism.* J. Biol. Chem., 280(41):34805–12, 2005 [21]

[199] Celestine N. Chi, Anders Bach, Ake Engström, Huiqun Wang, Kristian Strømgaard, Stefano Gianni, and Per Jemth. *A sequential binding mechanism in a PDZ domain.* Biochemistry, 48(30):7089–97, 2009 [21, 127]

[200] Greta Hultqvist, Søren W Pedersen, Celestine N Chi, Kristian Strømgaard, Stefano Gianni, and Per Jemth. *An expanded view of the protein folding landscape of PDZ domains.* Biochem. Biophys. Res. Commun., 421(3):550–3, 2012 [21]

[201] Stefano Gianni, S Raza Haq, Linda C Montemiglio, Maike C Jürgens, Åke Engström, Celestine N Chi, Maurizio Brunori, and Per Jemth. *Sequence-specific long range networks in PSD-95/discs large/ZO-1 (PDZ) domains tune their binding selectivity.* J. Biol. Chem., 286(31):27167–75, 2011 [21, 23]

[202] Eric F Pettersen, Thomas D Goddard, Conrad C Huang, Gregory S Couch, Daniel M Greenblatt, Elaine C Meng, and Thomas E Ferrin. *UCSF Chimera–a visualization system for exploratory research and analysis.* J. Comput. Chem., 25(13):1605–12, 2004 [21, 143]

[203] Declan A. Doyle, Alice Lee, John Lewis, Eunjoon Kim, Morgan Sheng, and Roderick MacKinnon. *Crystal structures of a complexed and peptide-free membrane protein-binding domain: molecular basis of peptide recognition by PDZ.* Cell, 85(7):1067–76, 1996 [21, 61, 62, 65, 67, 68, 69, 70, 127, 137, 143]

[204] Martin Gruebele and P. G. Wolynes. *Vibrational energy flow and chemical reactions.* Acc. Chem. Res., 37(4):261–7, 2004 [23, 100, 113, 124, 129]

[205] Sofia Burendahl and Lennart Nilsson. *Computational studies of LXR molecular interactions reveal an allosteric communication pathway.* Proteins, 80(1):294–306, 2012 [23, 100]

[206] Takakazu Ishikura and Takahisa Yamato. *Energy transfer pathways relevant for long-range intramolecular signaling of photosensory protein revealed by microscopic energy conductivity analysis.* Chem. Phys. Lett., 432(4-6):533–537, 2006 [23, 100, 124]

[207] Celestine N Chi, S Raza Haq, Serena Rinaldo, Jakob Dogan, Francesca Cutruzzolà, Åke Engström, Stefano Gianni, Patrik Lundström, and Per Jemth. *Interactions outside the boundaries of the canonical binding groove of a PDZ domain influence ligand binding.* Biochemistry, 51(44):8971–9, 2012 [23, 61, 69, 127]

[208] Sandra Steiner and Amedeo Caflisch. *Peptide binding to the PDZ3 domain by conformational selection.* Proteins, 80(11):2562–72, 2012 [23, 70, 73, 128]

[209] Chang C Liu and Peter G Schultz. *Adding new chemistries to the genetic code.* Annu. Rev. Biochem., 79:413–44, 2010 [27, 31, 32]

[210] Lei Wang, Ansgar Brock, Brad Herberich, and Peter G. Schultz. *Expanding the genetic code of Escherichia coli.* Science, 292(5516):498–500, 2001 [27, 32, 101]

References

[211] Michael Georg Hoesl and Nediljko Budisa. *In vivo incorporation of multiple noncanonical amino acids into proteins.* Angew. Chemie, Int. Ed. English, 50(13):2896–902, 2011 [27, 115]

[212] Nediljko Budisa. *Prolegomena to future experimental efforts on genetic code engineering by expanding its amino acid repertoire.* Angew. Chemie, Int. Ed. English, 43(47):6426–63, 2004 [27, 29, 30, 101, 115]

[213] Lei Wang, Jianming Xie, and Peter G Schultz. *Expanding the genetic code.* Annu. Rev. Biophys. Biomol. Struct., 35:225–49, 2006 [27, 32]

[214] Kaihang Wang, Wolfgang H Schmied, and Jason W Chin. *Reprogramming the genetic code: from triplet to quadruplet codes.* Angew. Chemie, Int. Ed. English, 51(10):2288–97, 2012 [27, 32, 114, 115]

[215] Ellen M Sletten and Carolyn R Bertozzi. *Bioorthogonal chemistry: fishing for selectivity in a sea of functionality.* Angew. Chemie, Int. Ed. English, 48(38):6974–98, 2009 [27]

[216] Tomasz Fekner and Michael K Chan. *The pyrrolysine translational machinery as a genetic-code expansion tool.* Curr. Opin. Chem. Biol., 15(3):387–91, 2011 [27, 32]

[217] Jason W. Chin, Stephen W. Santoro, Andrew B. Martin, David S. King, Lei Wang, and Peter G. Schultz. *Addition of p-Azido-l-phenylalanine to the Genetic Code of Escherichia coli.* J. Am. Chem. Soc., 124(31):9026–9027, 2002 [27, 32, 35]

[218] Kristi L. Kiick, Eliana Saxon, David A. Tirrell, and Carolyn R. Bertozzi. *Incorporation of azides into recombinant proteins for chemoselective modification by the Staudinger ligation.* Proc. Natl. Acad. Sci. U. S. A., 99(1):19–24, 2002 [27, 29, 35, 36, 56, 60, 101, 137]

[219] Kimberly E. Beatty and David A. Tirrell. *Two-color labeling of temporally defined protein populations in mammalian cells.* Bioorg. Med. Chem. Lett., 18(22):5995–9, 2008 [27, 34]

[220] Silvia Eger, Martin Scheffner, Andreas Marx, and Marina Rubini. *Synthesis of defined ubiquitin dimers.* J. Am. Chem. Soc., 132(46):16337–9, 2010 [27, 29, 34, 42, 137]

[221] Ying Ma, Hernán Biava, Roberto Contestabile, Nediljko Budisa, and Martino Luigi di Salvo. *Coupling bioorthogonal chemistries with artificial metabolism: intracellular biosynthesis of azidohomoalanine and its incorporation into recombinant proteins.* Molecules, 19(1):1004–22, 2014 [27, 29]

[222] Nediljko Budisa and Prajna Paramita Pal. *Designing novel spectral classes of proteins with a tryptophan-expanded genetic code.* Biol. Chem., 385(10):893–904, 2004 [27]

[223] Sandra Lepthien, Michael G. Hoesl, Lars Merkel, and Nediljko Budisa. *Azatryptophans endow proteins with intrinsic blue fluorescence.* Proc. Natl. Acad. Sci. U. S. A., 105(42):16095–100, 2008 [27, 29]

[224] Michael Georg Hoesl, Maud Larregola, Haissi Cui, and Nediljko Budisa. *Azatryptophans as tools to study polarity requirements for folding of green fluorescent protein.* J. Pept. Sci., 16(10):589–95, 2010 [27]

[225] Mark R Fleissner, Eric M Brustad, Tamás Kálai, Christian Altenbach, Duilio Cascio, Francis B Peters, Kálmán Hideg, Sebastian Peuker, Peter G Schultz, and Wayne L Hubbell. *Site-directed spin labeling of a genetically encoded unnatural amino acid.* Proc. Natl. Acad. Sci. U. S. A., 106(51):21637–42, 2009 [27]

[226] Moritz J Schmidt, Julia Borbas, Malte Drescher, and Daniel Summerer. *A genetically encoded spin label for electron paramagnetic resonance distance measurements.* J. Am. Chem. Soc., 136(4):1238–41, 2014 [27]

[227] Nediljko Budisa, Boris Steipe, Pascal Demange, Christoph Eckerskorn, Josef Kellermann, and Robert Huber. *High-level biosynthetic substitution of methionine in proteins by its analogs 2-aminohexanoic acid, selenomethionine, telluromethionine and ethionine in Escherichia coli.* Eur. J. Biochem., 230(2):788–96, 1995 [29]

[228] Lars Merkel, Michael G. Hoesl, Marcel Albrecht, Andreas Schmidt, and Nediljko Budisa. *Blue fluorescent amino acids as in vivo building blocks for proteins.* Chembiochem, 11(3):305–14, 2010 [29]

[229] A. James Link and David A. Tirrell. *Reassignment of sense codons in vivo.* Methods, 36(3):291–8, 2005 [29]

[230] A James Link, Mandy K S Vink, and David A Tirrell. *Preparation of the functionalizable methionine surrogate azidohomoalanine via copper-catalyzed diazo transfer.* Nat. Protoc., 2(8):1879–83, 2007 [29]

[231] A James Link, Mandy K S Vink, and David A Tirrell. *Synthesis of the functionalizable methionine surrogate azidohomoalanine using Boc-homoserine as precursor.* Nat. Protoc., 2(8):1884–7, 2007 [29]

[232] Stefanie Roth, William C Drewe, and Neil R Thomas. *A concise and scalable route to L-azidohomoalanine.* Nat. Protoc., 5(12):1967–73, 2010 [29]

[233] Yurii S. Moroz, Wolfgang Binder, Patrik Nygren, Gregory A. Caputo, and Ivan V. Korendovych. *Painting proteins blue: β-(1-azulenyl)-L-alanine as a probe for studying protein-protein interactions.* Chem. Commun. (Camb)., 49(5):490–2, 2013 [29, 102]

[234] Nediljko Budisa. *personal communication* [29, 101, 115]

[235] Rolf Furter. *Expansion of the genetic code: site-directed p-fluoro-phenylalanine incorporation in Escherichia coli.* Protein Sci., 7(2):419–26, 1998 [31]

[236] Jiantao Guo, Charles E. Melançon, Hyun Soo Lee, Dan Groff, and Peter G. Schultz. *Evolution of amber suppressor tRNAs for efficient bacterial production of proteins containing nonnatural amino acids.* Angew. Chemie, Int. Ed. English, 48(48):9148–51, 2009 [32]

[237] Travis S. Young, Insha Ahmad, Jun A. Yin, and Peter G. Schultz. *An enhanced system for unnatural amino acid mutagenesis in E. coli.* J. Mol. Biol., 395(2):361–74, 2010 [32, 115]

[238] J Christopher Anderson, Ning Wu, Stephen W Santoro, Vishva Lakshman, David S King, and Peter G Schultz. *An expanded genetic code with a functional quadruplet codon.* Proc. Natl. Acad. Sci. U. S. A., 101(20):7566–71, 2004 [32]

[239] Heinz Neumann, Kaihang Wang, Lloyd Davis, Maria Garcia-Alai, and Jason W Chin. *Encoding multiple unnatural amino acids via evolution of a quadruplet-decoding ribosome.* Nature, 464(7287):441–4, 2010 [32, 114, 115]

[240] Kayo Nozawa, Patrick O'Donoghue, Sarath Gundllapalli, Yuhei Araiso, Ryuichiro Ishitani, Takuya Umehara, Dieter Söll, and Osamu Nureki. *Pyrrolysyl-tRNA synthetase-tRNA(Pyl) structure reveals the molecular basis of orthogonality.* Nature, 457(7233):1163–7, 2009 [32]

[241] Susan M Hancock, Rajendra Uprety, Alexander Deiters, and Jason W Chin. *Expanding the genetic code of yeast for incorporation of diverse unnatural amino acids via a pyrrolysyl-tRNA synthetase/tRNA pair.* J. Am. Chem. Soc., 132(42):14819–24, 2010 [32]

[242] Vanessa K. Lacey, Gordon V. Louie, Joseph P. Noel, and Lei Wang. *Expanding the library and substrate diversity of the pyrrolysyl-tRNA synthetase to incorporate unnatural amino acids containing conjugated rings.* ChemBioChem, 14(16):2100–5, 2013 [32]

[243] Ryan A Mehl, J Christopher Anderson, Stephen W Santoro, Lei Wang, Andrew B Martin, David S King, David M Horn, and Peter G Schultz. *Generation of a bacterium with a 21 amino acid genetic code.* J. Am. Chem. Soc., 125(4):935–9, 2003 [32]

[244] Wei Niu, Peter G Schultz, and Jiantao Guo. *An Expanded Genetic Code in Mammalian Cells with a Functional Quadruplet Codon.* ACS Chem. Biol., 8(7):1640–1645, 2013 [32]

[245] Peter Marek, Ruchi Gupta, and Daniel P. Raleigh. *The fluorescent amino acid p-cyanophenylalanine provides an intrinsic probe of amyloid formation.* ChemBioChem, 9(9):1372–4, 2008 [32]

[246] Peter Marek, Sudipta Mukherjee, Martin T Zanni, and Daniel P Raleigh. *Residue-specific, real-time characterization of lag-phase species and fibril growth during amyloid formation: a combined fluorescence and IR study of p-cyanophenylalanine analogs of islet amyloid polypeptide.* J. Mol. Biol., 400(4):878–88, 2010 [32, 55]

[247] Christopher G Bazewicz, Jacob S Lipkin, Emily E Smith, Melanie T Liskov, and Scott H Brewer. *Expanding the utility of 4-cyano-L-phenylalanine as a vibrational reporter of protein environments.* J. Phys. Chem. B, 116(35):10824–31, 2012 [32]

[248] Diana C Urbanek, Dmitriy Yu Vorobyev, Arnaldo L Serrano, Feng Gai, and Robin M Hochstrasser. *The Two Dimensional Vibrational Echo of a Nitrile Probe of the Villin HP35 Protein.* J. Phys. Chem. Lett., 1(23):3311–3315, 2010 [32, 36]

[249] Megan C Thielges, Jun Y Axup, Daryl Wong, Hyun Soo Lee, Jean K Chung, Peter G Schultz, and Michael D Fayer. *Two-dimensional IR spectroscopy of protein dynamics using two vibrational labels: a site-specific genetically encoded unnatural amino acid and an active site ligand.* J. Phys. Chem. B, 115(38):11294–304, 2011 [32, 42, 86, 87]

[250] Ziad Ganim, Hoi Sung Chung, Adam W. Smith, Lauren P. DeFlores, Kevin C. Jones, and Andrei Tokmakoff. *Amide I two-dimensional infrared spectroscopy of proteins.* Acc. Chem. Res., 41(3):432–41, 2008 [33]

[251] Laura B Sagle, Jörg Zimmermann, Philip E. Dawson, and Floyd E. Romesberg. *A high-resolution probe of protein folding.* J. Am. Chem. Soc., 126(11):3384–5, 2004 [33, 125]

[252] Sri Ram G. Naraharisetty, Valeriy M. Kasyanenko, Jörg Zimmermann, Megan C. Thielges, Floyd E. Romesberg, and Igor V. Rubtsov. *C-D modes of deuterated side chain of leucine as structural reporters via dual-frequency two-dimensional infrared spectroscopy.* J. Phys. Chem. B, 113(14):4940–6, 2009 [33, 125, 144]

[253] Jörg Zimmermann, Megan C. Thielges, Wayne Yu, Philip E. Dawson, and Floyd E. Romesberg. *Carbon-Deuterium Bonds as Site-Specific and Nonperturbative Probes for Time-Resolved Studies of Protein Dynamics and Folding.* J. Phys. Chem. Lett., 2(5):412–416, 2011 [33, 125]

[254] Ramkrishna Adhikary, Jörg Zimmermann, Jian Liu, Philip E. Dawson, and Floyd E. Romesberg. *Experimental characterization of electrostatic and conformational heterogeneity in an SH3 domain.* J. Phys. Chem. B, 117(42):13082–9, 2013 [33, 42, 125]

[255] Ramkrishna Adhikary, Jörg Zimmermann, Philip E Dawson, and Floyd E Romesberg. *IR probes of protein microenvironments: utility and potential for perturbation.* Chemphyschem, 15(5):849–53, 2014 [33, 56]

[256] Milan Delor, Igor V Sazanovich, Michael Towrie, Steven J P Spall, Theo Keane, Alexander J Blake, Claire Wilson, Anthony J H M Meijer, and Julia A Weinstein. *Dynamics of Ground and Excited State Vibrational Relaxation and Energy Transfer in Transition Metal Carbonyls.* J. Phys. Chem. B, 2014 [33]

[257] Ann Marie Woys, Sudipta S Mukherjee, David R Skoff, Sean Douglas Moran, and Martin T Zanni. *A strongly absorbing class of non-natural labels for probing protein electrostatics and solvation with FTIR and 2D IR spectroscopies.* J. Phys. Chem. B, 117(17):5009–18, 2013 [33, 87, 125]

[258] Aaron T. Fafarman, Lauren J. Webb, Jessica I. Chuang, and Steven G. Boxer. *Site-specific conversion of cysteine thiols into thiocyanate creates an IR probe for electric fields in proteins.* J. Am. Chem. Soc., 128(41):13356–7, 2006 [34, 60, 125, 128, 130]

[259] Heather A. McMahon, Katherine N. Alfieri, Katherine A. A. Clark, and Casey H. Londergan. *Cyanylated Cysteine: A Covalently Attached Vibrational Probe of Protein-Lipid Contacts.* J. Phys. Chem. Lett., 1(5):850–855, 2010 [34]

[260] Luuk J. G. W. van Wilderen, Daniela Kern-Michler, Henrike M. Müller-Werkmeister, and Jens Bredenbeck. *Vibrational dynamics and solvatochromism of the label SCN in various solvents and hemoglobin by time dependent IR and 2D-IR spectroscopy.* Phys. Chem. Chem. Phys., 16(36):19643–53, 2014 [34, 46, 125, 128, 130]

[261] Aaron T. Fafarman, Paul A. Sigala, Daniel Herschlag, and Steven G. Boxer. *Decomposition of vibrational shifts of nitriles into electrostatic and hydrogen-bonding effects.* J. Am. Chem. Soc., 132(37):12811–3, 2010 [34]

[262] Santosh Kumar Jha, Minbiao Ji, Kelly J Gaffney, and Steven G Boxer. *Direct measurement of the protein response to an electrostatic perturbation that mimics the catalytic cycle in ketosteroid isomerase.* Proc. Natl. Acad. Sci. U. S. A., 108(40):16612–7, 2011 [34]

[263] Sayan Bagchi, Stephen D Fried, and Steven G Boxer. *A solvatochromic model calibrates nitriles vibrational frequencies to electrostatic fields.* J. Am. Chem. Soc., 134(25):10373–6, 2012 [34, 55, 60, 62, 125]

[264] Aaron T Fafarman, Paul A Sigala, Jason P Schwans, Timothy D Fenn, Daniel Herschlag, and Steven G Boxer. *Quantitative, directional measurement of electric field heterogeneity in the active site of ketosteroid isomerase.* Proc. Natl. Acad. Sci. U. S. A., 109(6):E299–308, 2012 [34, 60, 62, 130]

[265] Daniela Kern-Michler. *Introduction of the thiocyanate label into PDZ.* Bachelor Thesis, Goethe-University, Frankfurt, 2012 [34, 128, 130]

[266] Jan C. M. van Hest, Kristi L. Kiick, and David A. Tirrell. *Efficient Incorporation of Unsaturated Methionine Analogues into Proteins in Vivo.* J. Am. Chem. Soc., 122(7):1282–1288, 2000 [34]

[267] Kristi L. Kiick and David A. Tirrell. *Protein Engineering by In Vivo Incorporation of Non-Natural Amino Acids: Control of Incorporation of Methionine Analogues by Methionyl-tRNA Synthetase.* Tetrahedron, 56(48):9487–9493, 2000 [34]

[268] Matthew J. Tucker, Yung Sam Kim, and Robin M. Hochstrasser. *2D IR photon echo study of the anharmonic coupling in the OCN region of phenyl cyanate.* Chem. Phys. Lett., 470(1-3):80–84, 2009 [34]

[269] M. Koziński, S. Garrett-Roe, and Peter Hamm. *2D-IR spectroscopy of the sulfhydryl band of cysteines in the hydrophobic core of proteins.* J. Phys. Chem. B, 112(25):7645–50, 2008 [34]

[270] Henrike M. Müller-Werkmeister. *Investigation of Protein-Ligand-Interactions by time-resolved 2D-IR Spectroscopy.* Diploma thesis, Johann-Wolfgang-Goethe Universität, Frankfurt, 2008 [35, 133]

[271] Zelleka Getahun, Cheng-Yen Huang, Ting Wang, Brenda De León, William F. DeGrado, and Feng Gai. *Using nitrile-derivatized amino acids as infrared probes of local environment.* J. Am. Chem. Soc., 125(2):405–11, 2003 [35, 36, 38, 40, 125]

[272] M. Li, J. Owrutsky, M. Sarisky, J. P. Culver, A. Yodh, and Robin M. Hochstrasser. *Vibrational and rotational relaxation times of solvated molecular ions.* J. Chem. Phys., 98(7):5499, 1993 [35]

[273] Helmut Günzler and Hans-Ulrich Gremlich. *IR Spectroscopy: An Introduction.* Wiley-VCH, 2002. ISBN 3-527-28896-1 [35, 93, 95]

[274] Kwang-Im Oh, Joo-Hyun Lee, Cheonik Joo, Hogyu Han, and Minhaeng Cho. *Beta-azidoalanine as an IR probe: application to amyloid Abeta(16-22) aggregation.* J. Phys. Chem. B, 112(33):10352–7, 2008 [36, 60, 62, 125]

[275] Jun-Ho Choi and Minhaeng Cho. *Vibrational solvatochromism and electrochromism of infrared probe molecules containing C=O, C≡N, C=O, or C-F vibrational chromophore.* J. Chem. Phys., 134(15):154513, 2011 [36, 42, 62, 66, 71, 130]

[276] Jun-Ho Choi, Kwang-Im Oh, and Minhaeng Cho. *Azido-derivatized compounds as IR probes of local electrostatic environment: Theoretical studies.* J. Chem. Phys., 129(17):174512, 2008 [36, 62, 66, 71, 125, 130]

[277] Jun-Ho Choi, Kwang-Im Oh, Hochan Lee, Chewook Lee, and Minhaeng Cho. *Nitrile and thiocyanate IR probes: quantum chemistry calculation studies and multivariate least-square fitting analysis.* J. Chem. Phys., 128(13):134506, 2008 [36]

[278] Jun-Ho Choi, Daniel Raleigh, and Minhaeng Cho. *Azido Homoalanine is a Useful Infrared Probe for Monitoring Local Electrostatistics and Sidechain Solvation in Proteins.* J. Phys. Chem. Lett., 2(17):2158–2162, 2011 [36, 60, 66, 67]

[279] Marta P Wolfshorndl, Rachel Baskin, Ishita Dhawan, and Casey H Londergan. *Covalently bound azido groups are very specific water sensors, even in hydrogen-bonding environments.* J. Phys. Chem. B, 116(3):1172–9, 2012 [36, 42, 55, 56, 66, 71, 79, 125]

[280] Jeffrey R. Reimers, J. Zeng, and N. S. Hush. *Vibrational Stark Spectroscopy. 2. Application to the CN Stretch in HCN and Acetonitrile.* J. Phys. Chem., 100(5):1498–1504, 1996 [36]

[281] Beth A. Lindquist, Kristina E. Furse, and Steven A. Corcelli. *Nitrile groups as vibrational probes of biomolecular structure and dynamics: an overview.* Phys. Chem. Chem. Phys., 11(37):8119–32, 2009 [36, 42, 125]

[282] Steven S. Andrews and Steven G. Boxer. *Vibrational Stark Effects of Nitriles I. Methods and Experimental Results.* J. Phys. Chem. A, 104(51):11853–11863, 2000 [36]

[283] Ian T Suydam and Steven G Boxer. *Vibrational Stark effects calibrate the sensitivity of vibrational probes for electric fields in proteins.* Biochemistry, 42(41):12050–5, 2003 [36, 130]

[284] Steven G. Boxer. *Stark Realities.* J. Phys. Chem. B, 113(10):2972–2983, 2009 [36]

[285] Nicholas M Levinson, Stephen D Fried, and Steven G Boxer. *Solvent-induced infrared frequency shifts in aromatic nitriles are quantitatively described by the vibrational Stark effect.* J. Phys. Chem. B, 116(35):10470–6, 2012 [36, 130]

[286] Ayanjeet Ghosh, Amanda Remorino, Matthew J. Tucker, and Robin M. Hochstrasser. *2D IR photon echo spectroscopy reveals hydrogen bond dynamics of aromatic nitriles.* Chem. Phys. Lett., 469(4-6):325–330, 2009 [36, 42]

[287] Chong Fang, Joseph D Bauman, Kalyan Das, Amanda Remorino, Eddy Arnold, and Robin M Hochstrasser. *Two-dimensional infrared spectra reveal relaxation of the nonnucleoside inhibitor TMC278 complexed with HIV-1 reverse transcriptase.* Proc. Natl. Acad. Sci. U. S. A., 105(5):1472–7, 2008 [36, 55]

[288] Daniel G Kuroda, Joseph D Bauman, J Reddy Challa, Disha Patel, Thomas Troxler, Kalyan Das, Eddy Arnold, and Robin M Hochstrasser. *Snapshot of the equilibrium dynamics of a drug bound to HIV-1 reverse transcriptase.* Nat. Chem., 5(3):174–81, 2013 [36, 55, 130]

[289] Humeyra Taskent-Sezgin, Juah Chung, Partha S. Banerjee, Sureshbabu Nagarajan, R. Brian Dyer, Isaac Carrico, and Daniel P. Raleigh. *Azidohomoalanine: a conformationally sensitive IR probe of protein folding, protein structure, and electrostatics.* Angew. Chem. Int. Ed. Engl., 49(41):7473–5, 2010 [36, 40, 42, 56, 59, 62, 125]

[290] Kyung-Koo Lee, Kwang-Hee Park, Cheonik Joo, Hyeok-Jun Kwon, Jonggu Jeon, Hyeon-Il Jung, Sungnam Park, Hogyu Han, and Minhaeng Cho. *Infrared probing of 4-azidoproline conformations modulated by azido configurations.* J. Phys. Chem. B, 116(17):5097–110, 2012 [36, 125]

[291] M. Khalil, N. Demirdöven, and Andrei Tokmakoff. *Vibrational coherence transfer characterized with Fourier-transform 2D IR spectroscopy.* J. Chem. Phys., 121(1):362–73, 2004 [36]

[292] Sander Woutersen, Yuguang Mu, Gerhard Stock, and Peter Hamm. *Subpicosecond conformational dynamics of small peptides probed by two-dimensional vibrational spectroscopy.* Proc. Natl. Acad. Sci. U. S. A., 98(20):11254–8, 2001 [36]

[293] Michael A. van der Horst, W. Laan, S. Yeremenko, A. Wende, P. Palm, D. Oesterhelt, and K. J. Hellingwerf. *From primary photochemistry to biological function in the blue-light photoreceptors PYP and AppA.* Photochem. Photobiol. Sci., 4(9):688–93, 2005 [38]

[294] Emanuel Escher and Robert Schwyzer. *p-nitrophenylalanine, p-azidophenylalanine, m-azidophenylalanine, and o-nitro-p-azido-phenylalanine as photoaffinity labels.* FEBS Lett., 46(1-2):347–350, 1974 [38, 42]

[295] F Fahrenholz, G Tóth, P Crause, P Eggena, and I L Schwartz. *[1,6-alpha-aminosuberic acid, 3-(p-azidophenylalanine), 8-arginine] vasopressin: a new photoaffinity label for hydroosmotic hormone receptors. Characterization of the ligand and irreversible stimulation of hydroosmotic water flow in toad bladder by photoa.* J. Biol. Chem., 258(24):14861–14867, 1983 [38]

[296] Jens Bredenbeck and Peter Hamm. *Versatile small volume closed-cycle flow cell system for transient spectroscopy at high repetition rates.* Rev. Sci. Instrum., 74(6):3188, 2003 [40, 74, 104, 121, 140]

[297] M. J. Frisch, G. W. Trucks, H. B. Schlegel, G. E. Scuseria, M. A. Robb, J. R. Cheeseman, G. Scalmani, V. Barone, B. Mennucci, G. A. Petersson, H. Nakatsuji, M. Caricato, X. Li, H. P. Hratchian, A. F. Izmaylov, J. Bloino, G. Zheng, J. L. Sonnenberg, M. Hada, M. Ehara, K. Toyota, R. Fukuda, J. Hasegawa, M. Ishida, T. Nakajima, Y. Honda, O. Kitao, H. Nakai, T. Vreven, J. A. Montgomery, J. E. Peralta, F. Ogliaro, M. Bearpark, J. J. Heyd, E. Brothers, K. N. Kudin, V. N. Staroverov, R. Kobayashi, J. Normand, K. Raghavachari, A. Rendell, J. C. Burant, S. S. Iyengar, J. Tomasi, M. Cossi, N. Rega, M. J. Millam, M. Klene, J. E. Knox, J. B. Cross, V. Bakken, C. Adamo, J. Jaramillo, R. Gomperts, R. E. Stratmann, O. Yazyev, A. J. Austin, R. Cammi, C. Pomelli, J. W. Ochterski, R. L. Martin, K. Morokuma, V. G. Zakrzewski, G. A. Voth, P. Salvador, J. J. Dannenberg, S. Dapprich, A. D. Daniels, Ö. Farkas, J. B. Foresman, J. V. Ortiz, J. Cioslowski, and D. J. Fox. *Gaussian 09, Revision B.01*, 2010 [40, 144]

[298] Martin P. Andersson and P. Uvdal. *New scale factors for harmonic vibrational frequencies using the B3LYP density functional method with the triple-zeta basis set 6-311+G(d,p).* J. Phys. Chem. A, 109(12):2937–41, 2005 [40]

[299] Katharina Eberl. *Biophysikalische Charakterisierung verschiedener Azid-gelabelter Mutanten der PDZ-Domäne.* Bachelor Thesis, Goethe-University, Frankfurt, 2011 [40, 59, 137]

[300] Eugene Lieber, C. N. R. Rao, A. E. Thomas, E. Oftedahl, R. Minnis, and C. V. N. Nambury. *Infrared spectra of acid azides, carbamyl azides and other azido derivatives: Anomalous splittings of the N3 stretching bands.* Spectrochim. Acta, 19(7):1135–1144, 1963 [41, 50, 55]

[301] L. Lešetický, R. Barth, I. Nêmec, M. Štícha, and I. Tišlerová. *Synthesis and spectra of N-15 labelled phenylazides.* Czechoslov. J. Phys., 53(S1):A777–A782, 2003 [41, 48, 50, 55, 93]

[302] M. Jurzak, R. Boer, G. Fritzsch, E. Kojro, and F. Fahrenholz. *Monoclonal antibodies against different epitopes of peptide hormones. Use of photoreactive analogues in studies on vasopressin.* Eur. J. Biochem., 190(1):45–52, 1990 [42]

[303] Tamás Kálai, Mark R. Fleissner, József Jekő, Wayne L. Hubbell, and Kálmán Hideg. *Synthesis of new spin labels for Cu-free click conjugation.* Tetrahedron Lett., 52(21):2747–2749, 2011 [42]

[304] Vsevolod V. Rostovtsev, Luke G. Green, Valery V. Fokin, and K. Barry Sharpless. *A Stepwise Huisgen Cycloaddition Process: Copper(I)-Catalyzed Regioselective "Ligation" of Azides and Terminal Alkynes.* Angew. Chemie, 114(14):2708–2711, 2002 [42]

[305] David Robinette, Nouri Neamati, Kenneth B Tomer, and Christoph H Borchers. *Photoaffinity labeling combined with mass spectrometric approaches as a tool for structural proteomics.* Expert Rev. Proteomics, 3(4):399–408, 2006 [42]

[306] R. A. Mathies, W. T. Pollard, C. H. Brito Cruz, and C. V. Shank. *Direct observation of the femtosecond excited-state cis-trans isomerization in bacteriorhodopsin.* Science, 240(4853):777–9, 1988 [43]

[307] Manho Lim, Timothy a. Jackson, and Philip A. Anfinrud. *Mid-infrared vibrational spectrum of CO after photodissociation from heme: Evidence for a ligand docking site in the heme pocket of hemoglobin and myoglobin.* J. Chem. Phys., 102(11):4355, 1995 [43]

[308] S. Devanathan, S. Lin, M. A. Cusanovich, N. Woodbury, and G. Tollin. *Early photocycle kinetic behavior of the E46A and Y42F mutants of photoactive yellow protein: femtosecond spectroscopy.* Biophys. J., 81(4):2314–9, 2001 [43]

[309] Luuk J. G. W. van Wilderen, Michael A. van der Horst, I. H. M. van Stokkum, K. J. Hellingwerf, R. van Grondelle, and M. L. Groot. *Ultrafast infrared spectroscopy reveals a key step for successful entry into the photocycle for photoactive yellow protein.* Proc. Natl. Acad. Sci. U. S. A., 103(41):15050–15055, 2006 [43]

[310] Christian Greve, Erik T J Nibbering, and Henk Fidder. *Hydrogen-bonding-induced enhancement of Fermi resonances: a linear IR and nonlinear 2D-IR study of aniline-d5.* J. Phys. Chem. B, 117(49):15843–55, 2013 [50]

[311] Arnaldo L Serrano, Thomas Troxler, Matthew J Tucker, and Feng Gai. *Photophysics of a Fluorescent Non-natural Amino Acid: p-Cyanophenylalanine.* Chem. Phys. Lett., 487(4-6):303–306, 2010 [55]

[312] Sureshbabu Nagarajan, Humeyra Taskent-Sezgin, Dzmitry Parul, Isaac Carrico, Daniel P Raleigh, and R Brian Dyer. *Differential ordering of the protein backbone and side chains during protein folding revealed by site-specific recombinant infrared probes.* J. Am. Chem. Soc., 133(50):20335–40, 2011 [56]

[313] Kwang-Im Oh, Woosung Kim, Cheonik Joo, Dong-Geun Yoo, Hogyu Han, Geum-Sook Hwang, and Minhaeng Cho. *Azido gauche effect on the backbone conformation of β-azidoalanine peptides.* J. Phys. Chem. B, 114(40):13021–9, 2010 [60, 66]

[314] Xin Sonia Gai, Basil A. Coutifaris, Scott H. Brewer, and Edward E. Fenlon. *A direct comparison of azide and nitrile vibrational probes.* Phys. Chem. Chem. Phys., 13(13):5926–30, 2011 [62, 125]

[315] Frank E. Critchfield, John A. Gibson, and James L. Hall. *Dielectric Constant and Refractive Index from 20 to 35º and Density at 25º for the System Tetrahydrofuran—Water.* J. Am. Chem. Soc., 75(23):6044–6045, 1953 [62]

[316] Garrett M Morris, Ruth Huey, and Arthur J Olson. *Using AutoDock for ligand-receptor docking.* Curr. Protoc. Bioinforma., Chapter 8(December):Unit 8.14, 2008 [65, 143]

[317] Garrett M Morris, Ruth Huey, William Lindstrom, Michel F Sanner, Richard K Belew, David S Goodsell, and Arthur J Olson. *AutoDock4 and AutoDockTools4: Automated docking with selective receptor flexibility.* J. Comput. Chem., 30(16):2785–91, 2009 [65, 143]

[318] Anna Radzicka and Richard Wolfenden. *Comparing the polarities of the amino acids: side-chain distribution coefficients between the vapor phase, cyclohexane, 1-octanol, and neutral aqueous solution.* Biochemistry, 27(5):1664–1670, 1988 [65, 143, 144]

[319] Schrödinger, LLC. *The PyMOL Molecular Graphics System, Version~1.3r1*, 2010 [65]

[320] Dorina Saro, Tao Li, Chamila Rupasinghe, Azrael Paredes, Nicole Caspers, and Mark R. Spaller. *A thermodynamic ligand binding study of the third PDZ domain (PDZ3) from the mammalian neuronal protein PSD-95.* Biochemistry, 46(21):6340–52, 2007 [68, 116, 140]

[321] Jean-Joseph Max and Camille Chapados. *Isotope effects in liquid water by infrared spectroscopy. III. H2O and D2O spectra from 6000 to 0 cm(-1).* J. Chem. Phys., 131(18):184505, 2009 [74, 75]

[322] Jean K Chung, Megan C Thielges, and Michael D Fayer. *Dynamics of the folded and unfolded villin headpiece (HP35) measured with ultrafast 2D IR vibrational echo spectroscopy.* Proc. Natl. Acad. Sci. U. S. A., 108(9):3578–83, 2011 [87, 125]

[323] Julia Kuligowski, Guillermo Quintás, Miguel de la Guardia, and Bernhard Lendl. *Analytical potential of mid-infrared detection in capillary electrophoresis and liquid chromatography: a review.* Anal. Chim. Acta, 679(1-2):31–42, 2010 [92]

[324] John M Chalmers and Peter R Griffiths (editors). *Handbook of Vibrational Spectroscopy*, volume 1-5. John Wiley & Sons, Ltd, Chichester, UK, 2006. ISBN 0-471-98847-2 [92]

[325] Katrin Adamczyk, Mirabelle Prémont-Schwarz, Dina Pines, Ehud Pines, and Erik T. J. Nibbering. *Real-time observation of carbonic acid formation in aqueous solution.* Science, 326(5960):1690–4, 2009 [92]

[326] Frédéric Thibault-Starzyk, Etienne Seguin, Sébastien Thomas, Marco Daturi, Heike Arnolds, and David A King. *Real-time infrared detection of cyanide flip on silver-alumina NOx removal catalyst.* Science, 324(5930):1048–51, 2009 [92]

[327] Omar F Mohammed, Dina Pines, Jens Dreyer, Ehud Pines, and Erik T. J. Nibbering. *Sequential proton transfer through water bridges in acid-base reactions.* Science, 310(5745):83–6, 2005 [92]

[328] S E Bromberg. *The Mechanism of a C-H Bond Activation Reaction in Room-Temperature Alkane Solution.* Science, 278(5336):260–263, 1997 [92]

[329] Wolfgang J Schreier, Tobias E Schrader, Florian O Koller, Peter Gilch, Carlos E Crespo-Hernández, Vijay N Swaminathan, Thomas Carell, Wolfgang Zinth, and Bern Kohler. *Thymine dimerization in DNA is an ultrafast photoreaction.* Science, 315(5812):625–9, 2007 [92]

[330] Valeriy M Kasyanenko, Sarah L Tesar, Grigory I Rubtsov, Alexander L Burin, and Igor V Rubtsov. *Structure dependent energy transport: relaxation-assisted 2DIR measurements and theoretical studies.* J. Phys. Chem. B, 115(38):11063–73, 2011 [93, 95]

[331] Peter Hamm, S. M. Ohline, and W. Zinth. *Vibrational cooling after ultrafast photoisomerization of azobenzene measured by femtosecond infrared spectroscopy.* J. Chem. Phys., 106(2):519, 1997 [93, 102]

[332] Yan Zhao and Donald G. Truhlar. *The M06 suite of density functionals for main group thermochemistry, thermochemical kinetics, noncovalent interactions, excited states, and transition elements: two new functionals and systematic testing of four M06-class functionals and 12 other function.* Theor. Chem. Acc., 120(1-3):215–241, 2007 [93, 144]

[333] Stefan Grimme. *Semiempirical GGA-type density functional constructed with a long-range dispersion correction.* J. Comput. Chem., 27(15):1787–99, 2006 [93, 144]

[334] Galina M. Chaban and R. Benny Gerber. *Anharmonic vibrational spectroscopy calculations with electronic structure potentials: comparison of MP2 and DFT for organic molecules.* Theor. Chem. Acc., 120(1-3):273–279, 2007 [97]

[335] Karl K Irikura, Russell D Johnson, and Raghu N Kacker. *Uncertainties in scaling factors for ab initio vibrational frequencies.* J. Phys. Chem. A, 109(37):8430–7, 2005 [97]

[336] Tomica Hrenar, Hans-Joachim Werner, and Guntram Rauhut. *Accurate calculation of anharmonic vibrational frequencies of medium sized molecules using local coupled cluster methods.* J. Chem. Phys., 126(13):134108, 2007 [97]

[337] Guntram Rauhut, Gerald Knizia, and Hans-Joachim Werner. *Accurate calculation of vibrational frequencies using explicitly correlated coupled-cluster theory.* J. Chem. Phys., 130(5):054105, 2009 [97]

[338] Henrike M. Müller-Werkmeister, Martin Essig, Patrick Durkin, Nediljko Budisa, and Jens Bredenbeck. *Towards Direct Measurement of Ultrafast Vibrational Energy Transfer in Proteins.* In *19th Int. Conf. Ultrafast Phenom.*, p. 10.Thu.D.6. OSA, Washington, D.C., 2014. ISBN 1-55752-279-0 [99, 107, 113]

[339] David M Leitner. *Quantum localization and protein-assisted vibrational energy flow in cofactors.* New J. Phys., 12(8):85004, 2010 [100, 124]

[340] Hiroshi Fujisaki, Yong Zhang, and John E Straub. *Time-dependent perturbation theory for vibrational energy relaxation and dephasing in peptides and proteins.* J. Chem. Phys., 124(14):144910, 2006 [100, 124]

[341] Leandro Martinez, Ana C M Figueira, Paul Webb, Igor Polikarpov, and Munir S Skaf. *Mapping the Intramolecular Vibrational Energy Flow in Proteins Reveals Functionally Important Residues.* J. Phys. Chem. Lett., 2(16):2073–2078, 2011 [100, 124, 129]

[342] Maja Kobus, Phuong H Nguyen, and Gerhard Stock. *Coherent vibrational energy transfer along a peptide helix.* J. Chem. Phys., 134(12):124518, 2011 [100, 124]

[343] Hiroshi Fujisaki and John E Straub. *Vibrational energy relaxation of isotopically labeled amide I modes in cytochrome c: theoretical investigation of vibrational energy relaxation rates and pathways.* J. Phys. Chem. B, 111(41):12017–23, 2007 [100]

[344] Burak Erman. *Relationships between ligand binding sites, protein architecture and correlated paths of energy and conformational fluctuations.* Phys. Biol., 8(5):56003, 2011 [100]

References

[345] F. Piazza and Y.-H. Sanejouand. *Energy transfer in nonlinear network models of proteins.* EPL (Europhysics Lett., 88(6):68001, 2009 [100]

[346] Yuriy Kholodenko, Martin Volk, E. Gooding, and Robin M. Hochstrasser. *Energy dissipation and relaxation processes in deoxy myoglobin after photoexcitation in the Soret region.* Chem. Phys., 259(1):71–87, 2000 [101]

[347] P. Li and P. M. Champion. *Investigations of the thermal response of laser-excited biomolecules.* Biophys. J., 66(2):430–436, 1994 [101]

[348] Naoki Fujii, Misao Mizuno, and Yasuhisa Mizutani. *Direct observation of vibrational energy flow in cytochrome c.* J. Phys. Chem. B, 115(44):13057–64, 2011 [101, 129]

[349] Kenta Yamada, Haruto Ishikawa, Misao Mizuno, Naoya Shibayama, and Yasuhisa Mizutani. *Intersubunit communication via changes in hemoglobin quaternary structures revealed by time-resolved resonance Raman spectroscopy: direct observation of the Perutz mechanism.* J. Phys. Chem. B, 117(41):12461–8, 2013 [101, 129]

[350] E. P. Ippen, C. V. Shank, and R. L. Woerner. *Picosecond dynamics of azulene.* Chem. Phys. Lett., 46(1):20–23, 1977 [101, 102]

[351] Takao Itoh. *Fluorescence and phosphorescence from higher excited states of organic molecules.* Chem. Rev., 112(8):4541–68, 2012 [101, 102]

[352] Günther Loidl, H J Musiol, Nediljko Budisa, R Huber, S Poirot, D Fourmy, and L Moroder. *Synthesis of beta-(1-azulenyl)-L-alanine as a potential blue-colored fluorescent tryptophan analog and its use in peptide synthesis.* J. Pept. Sci., 6(3):139–44, 2000 [101]

[353] Yasushi Numata, Satoru Toyoshima, Katsuhiko Okuyama, Masafumi Yasunami, and Isamu Suzuka. *S1-state internal conversion of isolated azulene derivatives.* J. Phys. Chem. A, 113(35):9603–11, 2009 [102]

[354] A. J. Wurzer, T. Wilhelm, J. Piel, and E. Riedle. *Comprehensive measurement of the S1 azulene relaxation dynamics and observation of vibrational wavepacket motion.* Chem. Phys. Lett., 299(3-4):296–302, 1999 [102]

[355] Michael Beer and H. C. Longuet-Higgins. *Anomalous Light Emission of Azulene.* J. Chem. Phys., 23(8):1390, 1955 [102]

[356] Jens Bredenbeck, Jan Helbing, Arne Sieg, Tobias Schrader, Wolfgang Zinth, Christian Renner, Raymond Behrendt, Luis Moroder, Josef Wachtveitl, and Peter Hamm. *Picosecond conformational transition and equilibration of a cyclic peptide.* Proc. Natl. Acad. Sci. U. S. A., 100(11):6452–7, 2003 [102]

[357] Natalia I. Rubtsova and Igor V. Rubtsov. *Ballistic energy transport via perfluoroalkane linkers.* Chem. Phys., 422(null):16–21, 2013 [106, 107, 124, 128]

[358] Rebekka S. von Benten and Bernd Abel. *On the nature of intramolecular vibrational energy transfer in dense molecular environments.* Chem. Phys., 378(1-3):19–26, 2010 [108]

[359] Johnson K. Agbo, Ramachandran Gnanasekaran, and David M. Leitner. *Communication Maps: Exploring Energy Transport through Proteins and Water.* Isr. J. Chem., 54(8-9):1065–1073, 2014 [113, 129]

[360] Heinz Neumann, Adrian L. Slusarczyk, and Jason W. Chin. *De novo generation of mutually orthogonal aminoacyl-tRNA synthetase/tRNA pairs.* J. Am. Chem. Soc., 132(7):2142–4, 2010 [114]

[361] Wei Wan, Ying Huang, Zhiyong Wang, William K Russell, Pei-Jing Pai, David H Russell, and Wenshe R Liu. *A facile system for genetic incorporation of two different noncanonical amino acids into one protein in Escherichia coli.* Angew. Chemie, Int. Ed. English, 49(18):3211–4, 2010 [114, 115]

[362] Martin Essig. *Ligandenoptimierung in silico mittels molekularem Docking.* Bachelor Thesis, Goethe-University, Frankfurt, 2011 [116, 127, 143]

[363] Michael Jackson and Henry H. Mantsch. *Beware of proteins in DMSO.* Biochim. Biophys. Acta - Protein Struct. Mol. Enzymol., 1078(2):231–235, 1991 [118]

[364] Alessandra Giugliarelli, Marco Paolantoni, Assunta Morresi, and Paola Sassi. *Denaturation and preservation of globular proteins: the role of DMSO.* J. Phys. Chem. B, 116(45):13361–13367, 2012 [118]

[365] Tsutomu Arakawa, Yoshiko Kita, and Serge N Timasheff. *Protein precipitation and denaturation by dimethyl sulfoxide.* Biophys. Chem., 131(1-3):62–70, 2007 [118]

[366] National Institute of Standards and Technology. *IR spectrum of Dimethylsulfoxide-D6.* Webbook, Source Ref. Coblentz No. 09974, 1970 [120]

[367] Luuk J G W van Wilderen, Craig N Lincoln, and Jasper J van Thor. *Modelling multi-pulse population dynamics from ultrafast spectroscopy.* PLoS One, 6(3):e17373, 2011 [123]

[368] Qi Wang and Yuan-Ping Pang. *Preference of Small Molecules for Local Minimum Conformations when Binding to Proteins.* PLoS One, 2(9):e820, 2007 [124, 128]

[369] Marco Schade and Peter Hamm. *Vibrational energy transport in the presence of intrasite vibrational energy redistribution.* J. Chem. Phys., 131(4):044511, 2009 [124]

[370] Natalia I Rubtsova, Arkady A Kurnosov, Alexander L Burin, and Igor V Rubtsov. *Temperature Dependence of the Ballistic Energy Transport in Perfluoroalkanes.* J. Phys. Chem. B, 2014 [124]

[371] Martin Essig. *Energy transfer in the WW domain investigated by time-resolved IR spectroscopy.* Master Thesis, Goethe-University, Frankfurt, 2014 [124, 129]

[372] Matthias M. Waegele, Matthew J. Tucker, and Feng Gai. *5-Cyanotryptophan as an Infrared Probe of Local Hydration Status of Proteins.* Chem. Phys. Lett., 478(4):249–253, 2009 [125]

[373] Samrat Dutta, William Rock, Richard J Cook, Amnon Kohen, and Christopher M Cheatum. *Two-dimensional infrared spectroscopy of azido-nicotinamide adenine dinucleotide in water.* J. Chem. Phys., 135(5):055106, 2011 [125]

[374] Michael W Nydegger, Samrat Dutta, and Christopher M Cheatum. *Two-dimensional infrared study of 3-azidopyridine as a potential spectroscopic reporter of protonation state.* J. Chem. Phys., 133(13):134506, 2010 [125]

[375] Matthew J. Tucker, Xin Sonia Gai, Edward E. Fenlon, Scott H. Brewer, and Robin M. Hochstrasser. *2D IR photon echo of azido-probes for biomolecular dynamics.* Phys. Chem. Chem. Phys., 13(6):2237–41, 2011 [125]

[376] Mark G Maienschein-Cline and Casey H Londergan. *The CN stretching band of aliphatic thio-cyanate is sensitive to solvent dynamics and specific solvation.* J. Phys. Chem. A, 111(40):10020–5, 2007 [125]

[377] Feng Liu, Deguo Du, Amelia A Fuller, Jennifer E Davoren, Peter Wipf, Jeffery W Kelly, and Martin Gruebele. *An experimental survey of the transition between two-state and downhill protein folding scenarios.* Proc. Natl. Acad. Sci. U. S. A., 105(7):2369–74, 2008 [129]

[378] David E Shaw, Paul Maragakis, Kresten Lindorff-Larsen, Stefano Piana, Ron O Dror, Michael P Eastwood, Joseph A Bank, John M Jumper, John K Salmon, Yibing Shan, and Willy Wriggers. *Atomic-level characterization of the structural dynamics of proteins.* Science, 330(6002):341–6, 2010 [129]

[379] Najeeb Halabi, Olivier Rivoire, Stanislas Leibler, and Rama Ranganathan. *Protein Sectors: Evolutionary Units of Three-Dimensional Structure.* Cell, 138(4):774–786, 2009 [129]

[380] Larissa Blankenburg. *Etablierung eines Expressionssystems zum Einbau von Azidohomoala-nine in Photoactive Yellow Protein.* Bachelor Thesis, Goethe-University, Frankfurt, 2012 [129, 130]

[381] David B Strasfeld, Yun L Ling, Ruchi Gupta, Daniel P Raleigh, and Martin T Zanni. *Strategies for extracting structural information from 2D IR spectroscopy of amyloid: application to islet amyloid polypeptide.* J. Phys. Chem. B, 113(47):15679–91, 2009 [130]

[382] Ian T Suydam, Christopher D Snow, Vijay S Pande, and Steven G Boxer. *Electric fields at the active site of an enzyme: direct comparison of experiment with theory.* Science, 313(5784):200–4, 2006 [130]

[383] Stephen D. Fried, Sayan Bagchi, and Steven G. Boxer. *Measuring electrostatic fields in both hydrogen-bonding and non-hydrogen-bonding environments using carbonyl vibrational probes.* J. Am. Chem. Soc., 135(30):11181–92, 2013 [130]

[384] Sharon M Kelly, Thomas J Jess, and Nicholas C Price. *How to study proteins by circular dichroism.* Biochim. Biophys. Acta, 1751(2):119–39, 2005 [139, 140]

[385] A. K. Rappe, C. J. Casewit, K. S. Colwell, W. A. Goddard, and W. M. Skiff. *UFF, a full periodic table force field for molecular mechanics and molecular dynamics simulations.* J. Am. Chem. Soc., 114(25):10024–10035, 1992 [144]

[386] A. Bondi. *van der Waals Volumes and Radii.* J. Phys. Chem., 68(3):441–451, 1964 [144]

[387] Jacopo Tomasi, Benedetta Mennucci, and Roberto Cammi. *Quantum mechanical continuum solvation models.* Chem. Rev., 105(8):2999–3093, 2005 [144]

List of Figures

List of Tables

Abbreviations

2C-2D-IR	two-color two-dimensional infrared spectroscopy
2D-IR	two-dimensional infrared spectroscopy
$AgGaS_2$	silver thio galate
Aha	azidohomoalanine
AzuA	β-azulenyl-alanine
AzuCa	azulene-1-yl-acetic-acid
AzuP	model peptide AzuCa- YN-Aha -G
AzuP'	model peptide AzuCa-YG
BBO	β barium borate
B3LYP	functional for DFT calculations
CD	circular dichroism
CLS	center line slope
CNA	boc-cyanoalanine
CNP	boc-cyanophenylalanine
COSY	correlation spectroscopy
CPA	chirped pulse amplification
CRIPT	native ligand for PDZ3 (used as heptamer acNYKQTSV)
CW	continuous wave
DFG	difference frequency generation
DFT	density functional theory
$DMSO/d_6$-DMSO	di-methyl-sulfoxide/deutarated di-methyl-sulfoxide
DTGS	deutarated triglycine sulfate (IR detector)
ESA	excited state absorption
FFCF	frequency-frequency correlation function
FP	Fabry Perot etalon
FRET	Foerster resonance energy transfer
fs	femtosecond
FT	Fourier transform
FTIR	Fourier transform infrared spectroscopy
FWHM	full width at half maximum
GSB	ground state bleach
GVD	group velocity dispersion
IC	internal conversion
ISC	intersystem crossing
ITC	isothermal titration calorimetry
IVR	intramolecular vibrational energy flow
IR	infrared
LO	local oscillator

MA	magic angle
MCT	mercury cadmium telluride (IR detector)
MD	molecular dynamics
MIR	mid-infrared
MWCO	molecular weight cut-off
N3A	boc-azidohomoalanine
N3P	boc-azidophenylalanine
NIR	near-infrared
NOPA	noncollinear optical parametric amlifier
OPA	optical parametric amplifier
PA	polarization anisotropy
PDZ	3rd PDZ domain of PSD-95
ps	picosecond
PSD-95	post-synaptic density protein/zonula occludens/disk-large homologue
PYP	photoactive yellow protein
RA-2D-IR	relaxation assisted 2D-IR
rmsd	root mean square deviation
SE	stimulated emission
SHG	second harmonic generation
SNR	signal to noise ratio
T2D-IR	transient two-dimensional infrared spectroscopy
TDC	transition dipole coupling
THG	third harmonic generation
THF	tetrahydrofuran
TIR	transient IR
Ti:S	Ti:sapphire, titanium-doped sapphire
UAA	unnatural amino acid
UV	ultraviolet
UV/Vis	ultraviolet-visible
VET	vibrational energy transfer
WT	wild type

Acknowledgement

Curriculum Vitae

Henrike Margarete Müller-Werkmeister

* 21.01.1984 in Hannover

Im Mörsewinkel 3
30900 Wedemark

rike.muellerwerkmeister@gmail.com

Research and Professional Activity

since 01/2014	Visiting Scientist/Marie Curie Fellow at University of Toronto, Canada, Physics Department with R. J. Dwayne Miller and Biochemistry Department with Oliver P. Ernst Project: *Towards Femtosecond Electron Diffraction of Proteins*
06/2008 -12/2013	PhD project with Prof. Jens Bredenbeck, Institute for Biophysics, Physics Department, Uni Frankfurt Thesis topic: *Unnatural Amino Acids as Novel Probes for Ultrafast 2D-IR Spectroscopy of Proteins*
08/2007-05/2008	Diploma project with Dr. Jens Bredenbeck, Institute for Biophysics, Physics Department, Uni Frankfurt Thesis topic: *Investigation of Protein-Ligand Interaction by Time-Resolved 2D-IR Spectroscopy*
05/2006 - 08/2006	Industry Internship at Sanofi-Aventis Deutschland GmbH, Discovery Analytics: Structural and Physical Chemistry, supervisor Dr. Herbert Kogler Topic: *Structure Elucidation of New Natural Compounds using NMR Spectroscopy*
02/2006 - 04/2006	Student Research Project at Institute for Biophysical Chemistry, Uni Frankfurt in the group of Prof. Clemens Glaubitz Topic: *Alignment Studies on Proteorhodopsin*
07/2005 - 10/2005	Student Research Project at Umeå University, Sweden, Institute for Biophysical Chemistry with Prof. Gerhard Gröbner Topic: *Prerequisites for Helicobacter Pylori Adherence to Blood Group Antigens*
06/2001	Max-Planck-Institute for Biophysical Chemistry, Göttingen, Internship in the group of Prof. Peter Gruss

Education

08/2008 - 12/2013	PhD student in Physics, Institute of Biophysics, Johann-Wolfgang-Goethe-Universität Frankfurt and Graduate School of the Cluster of Excellence "Marcomolecular Complexes", GRACE
05/2008	Biochemistry Diploma (1.3)
starting 04/2005	Physics studies, Johann-Wolfgang-Goethe-Universität, Frankfurt, first as minor subject, later as Bachelor student
starting 10/2002	Biochemistry studies, Johann-Wolfgang-Goethe-Universität, Frankfurt
06/2002	Abitur, Gymnasium Grossburgwedel

Teaching Experience

2013	Biophysics Seminar A and B
2011- 2013	Supervision of four Bachelor projects (by *Katharina Eberl, Martin Essig, Daniela Kern-Michler, Larissa Blankenburg*) and one Master project (by *Martin Essig*) in Biophysics
2011	Biophysics 1 tutorial
2010-2013	Biophysics advanced practical course
2009-2011	Physics for Medicine students practical course

Awards

12/2013	*Marie Curie International Outgoing Fellowship* by the EU for the project ProteinFED (funding period 04/2014-03/2017), hosts: University of Toronto, Canada and Max-Planck-Institute for Structure and Dynamics of Matter, Hamburg, Germany
05/2012	*hot topic* Poster Award by PCCP and Bunsen-Gesellschaft, Bunsentagung Leipzig
11/2011	Honored as *MINT Ambassador of the Year* for great involvement in scientific outreach activities by MINT-Zukunft schaffen e.V.
12/2010	*Young Einstein Scholarship* by Einstein Foundation Berlin for the conference "Falling Walls 2010"
07/2010	Selected Young Researcher at *60th Nobel Laureate Meeting in Lindau/ 3rd Interdisciplinary Meeting*, supported by Wilhelm-and-Else-Hereaus-Foundation as Hereaus Fellow
09/2009	Poster Award at the International Bunsen Discussion Meeting, Leipzig
2003	special prize for an outstanding technological project of a girl on state level at competition *Jugend forscht*, 1st prize regional level
2002	Abitur prize by DPG (Deutsche Physikalische Gesellschaft)
2001	2nd prize state level & special prize for an outstanding technological project of a girl at competition *Jugend forscht*, 1st prize regional level

Extracurricular Activities

Honorary Positions

since 2010	*Jugend forscht* Judge (Interdisciplinary), state level, Lower Saxony
2008 -2010	Executive committee member of MILSET Europe (Mouvement International pour le Loisir Scientifique et Technique)
2004-2008	President of Deutsches Jungforschernetzwerk - juFORUM e.V.

Event and Project Organsiation (Selection)

2010	Young Scientist Symposium for the occasion of juFORUM's 10th anniversary, Frankfurt, Chair and Moderator of Public Panel Discussion
2009	4th International Summer Science Camp, Munich, Co-Chair
2007	2nd International Summer Science Camp, Darmstadt, Chair
2005	Initiator of "International Summer Science Camp" as multidisciplinary trans-European Summer project for (high school) students together with Swedish and Portuguese Partners, running since 2006 - today, partly funded by EU Youth in Action programme and BMBF
2004	5th Annual Congress of juFORUM e.V., Heidelberg, Co-Chair

Invited Conference Presentations, Non-Scientific (Selection)[1]

2013	Impulse Speaker at Conference "Women in Leadership Positions" at Bundeskanzleramt, Berlin, by invitation of Chancellor Angela Merkel
2011	Guest at Panel Discussion "Mentoring in Science", Uni Bochum
2009	Moderator at "MINT Ambassador Conference", Deutsche Telekom, Berlin
2006	Guest at 18th European Union Contest for Young Scientists, by invitation of Förbundet Unga Forskare and EU
2004	Guest at Opening Panel Discussion at Conference "Germany of Tomorrow", by invitation of Minister of Education and Research, Edelgard Buhlman

Academic Teachers

R. Abele, H. Appelshäuser, W. Assmus, E. Bamberg, J. Bereiter-Hahn, J. Bredenbeck, J. Chen, R. Dörner, V. Dötsch, E. Egert, K.- D. Entian, K. Fendler, J. Feierabend, C. Glaubitz, W. Gnatzy, M. Göbel, A. Gottschalk, U. Günther, K. Hainer, M. Huth, W. Hofstetter, R. Lancaster, B. Ludwig, V. Müller, W. E. Müller, M. Thomson, J. Oehlmann, H. - D. Osiewacz, D. Rischke, H. Roskos, L. Schäfer, R. Schmidt, F. Schrenk, H. Schwalbe, G. Stock, R. Tampé, M. R. Valenti, M. Wagner, H. Zimmermann

---

[1]For Publications and Scientific Presentations at Conferences see Beginning of this Thesis.

I'm coming up on InfraRed · There is no running that can hide you · 'cause I can see in the Dark.

Placebo, *InfraRed*